R-3108-NETH

Verification of a Model of the Eastern Scheldt

Jan J. Leendertse

April 1984

Prepared for
The Netherlands Rijkswaterstaat

PREFACE

More than fifteen years ago, the author introduced the use of two-dimensional computational models into the hydraulic engineering profession for the study of tide and long-wave propagation in relatively shallow coastal waters.[1] At that time these studies could be made only in hydraulic laboratories using hydraulic scale models.

Gradually, modeling techniques for these computational models were developed; hundreds of articles have appeared in the technical and scientific magazines concerning their mathematical and computational aspects. Careful comparisons of model results with field measurements, however, have been limited. In many instances the computational models were used to obtain answers to relatively simple problems, and a thorough analysis of model results was not required.

Together with engineers of The Netherlands Rijkswaterstaat, the author developed modeling techniques for applications of the computational model in engineering studies of great complexity. A few years ago, as noted, only hydraulic models would have been considered for such studies; but now these are being replaced by computational models. Naturally, as with any innovation, many questions were raised about the applicability and accuracy of the computational model. The question of its accuracy compared with that of the hydraulic model can now be answered through the unique opportunity offered by the existence of hydraulic model and computational model verification simulations for the same model area, and for the same simulation period, together with the availability of prototype data. The results of the experiments and their comparisons are contained in this report.

---

[1]Jan J. Leendertse, *Aspects of a Computational Model for Long-Period Water-Wave Propagation*, The Rand Corporation, RM-5294-PR, May 1967.

SUMMARY

This report describes a verification simulation of a model of the Eastern Scheldt. Boundary conditions for a simulation of flows and water levels on 11 January 1982 are obtained from gauging stations in the offshore area of the estuary by use of weighting functions obtained from simulations with other models of conditions of September 1975 in the offshore area. The simulation was made first without taking into account the effects of the varying density in the estuary. By operating the model in this mode a direct comparison with a hydraulic model could be made.

A good agreement between observed and computed transport rates through the Hammen, Schaar, and Roompot are obtained. The agreement is better than that obtained with a comparable simulation with the hydraulic model. The agreement between observed and computed water levels is good and comparable to the agreement between observed water levels and water levels obtained with the hydraulic model.

To investigate the effect of the representation of a narrow channel, called the Eendracht, with the two-dimensional representation of the model, two experiments were made with a part of the model extending eastward from the Zeeland bridge. These experiments indicated that the accuracy of the model in the vicinity of the channel ends can be improved by coupling the two-dimensional model with a one-dimensional representation of this channel.

These experiments also indicated that tide gauge data at existing stations can be used directly as boundary conditions for this part of the model, but only in the vicinity of the model boundary are the flow patterns incorrect during some phase of the tide. Some modification of the input will be required to correct this deficiency.

In the verification simulation, pressures resulting from salinity differences were included in the computation. An average salinity distribution was an input at the start of the simulation.

Simulation results indicated a very good agreement between observed and computed transport rates through the Hammen, Schaar, and Roompot. A good agreement between observed and computed water levels was also obtained. The simulation in which the pressures resulting from salinity were included had a better agreement with observed data than the simulation without the salinity.

An analysis of the different components of the observed and computed waters indicated that, in general, the quarter-diurnal tidal component was the most difficult to reproduce in the model.

ACKNOWLEDGMENTS

CONTENTS

FIGURES

TABLES

I. INTRODUCTION

In this study a model of the Oosterschelde (Eastern Scheldt) is described. This model is being used in engineering studies for the construction of the storm-surge barrier being built across the mouth of this estuary.

Geographically, the Oosterschelde estuary is part of the Delta region of the Netherlands, located southwest of Rotterdam. The land in this region is low and has to be protected against flooding by dikes. To increase safety in the region, dams have been built across most of the estuaries to prevent the high tides and storm-surges from penetrating inland (Fig. 1).

A barrier is being constructed across the mouth of the Eastern Scheldt which will have gates that can be closed during storm-surges. Under normal conditions the barrier gates will be open and the tidal movement will be maintained. Because of the flow restriction at the barrier, the tidal range will be reduced in comparison with the present range.

In support of engineering and environmental studies, a number of models are being used. A large physical scale model of the Oosterschelde with a length scale of 400 and a depth scale of 100 has been in operation for many years together with a one-dimensional numerical model [1].
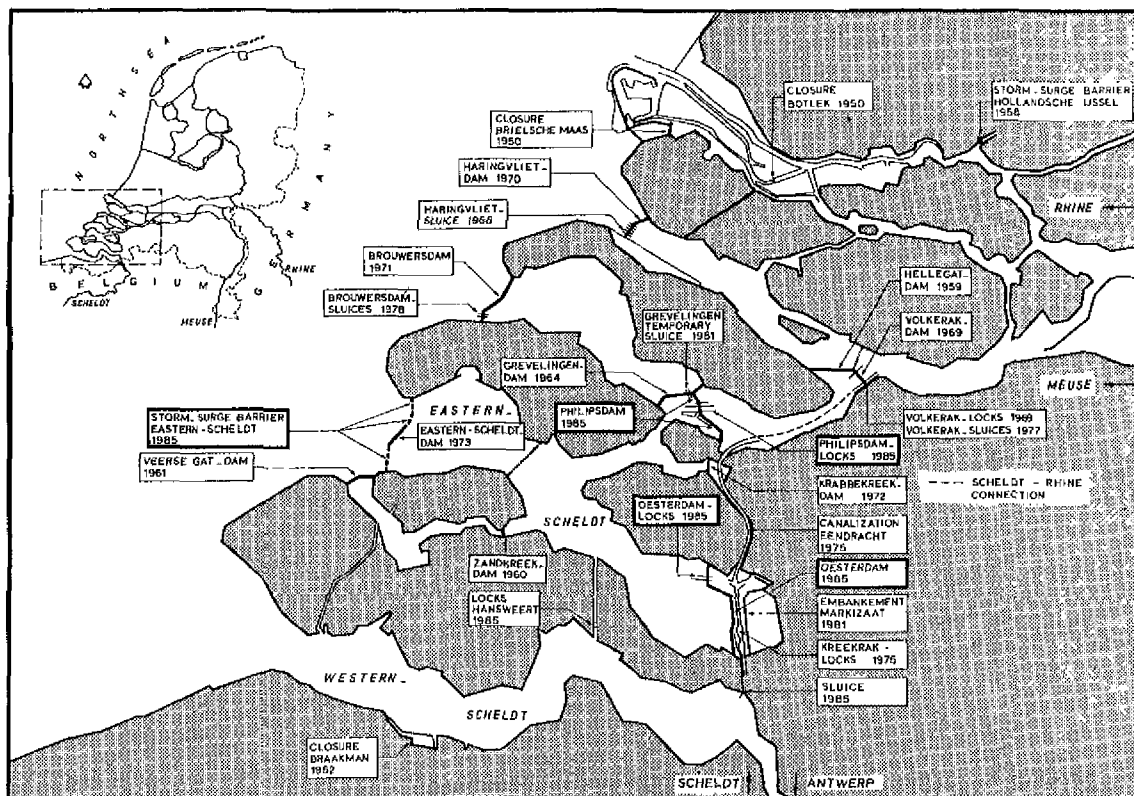
Fig. 1—Construction sequence of protective measures against flooding in the southwestern Netherlands, according to the Delta plan

1

More recently two-dimensional mathematical models have been used in studies, namely, a vertical two-dimensional model to study the effects of vertical circulations [2] and a two-dimensional model based upon homogeneous concentration and velocities over any vertical [3]. This report is concerned with the latter model, which is two-dimensional in plan and is called OOST-II.

Simulation results of the OOST-II model provide inputs to very detailed numerical models of the areas where the barrier is being constructed (Fig. 2). With these detailed submodels, predictions are being made of the time-dependent current distributions near the construction site when the barrier is partially constructed. The current predictions are of great importance as much of the construction operations are possible only during times that the current velocities are below certain intensities. A typical current field of one of these submodels is shown in Fig. 3.

Since errors in the OOST-II model results are directly transferred into errors in the computed flows of the submodels, the OOST-II model has to be validated with data not used for the adjustment of the model. The results of the validation experiment would then give insight into the accuracy of the model. The experiments for the validation are described in this report together with an extensive analysis of the results.

Several verification simulations were made. Since the physical scale model (hydraulic model) is operated with fresh water, the first computations were made with constant density. Thus a direct comparison of the models could be made.

Subsequently, two simulations with variable density were made with part of the Eastern Scheldt model, to investigate the effect of increased resolution in a particular channel (Eendracht). Finally, a verification simulation was made with the model of the whole Eastern Scheldt in which the salinity distribution was also computed and the effect of pressures due to density gradients was accounted for in the computations.
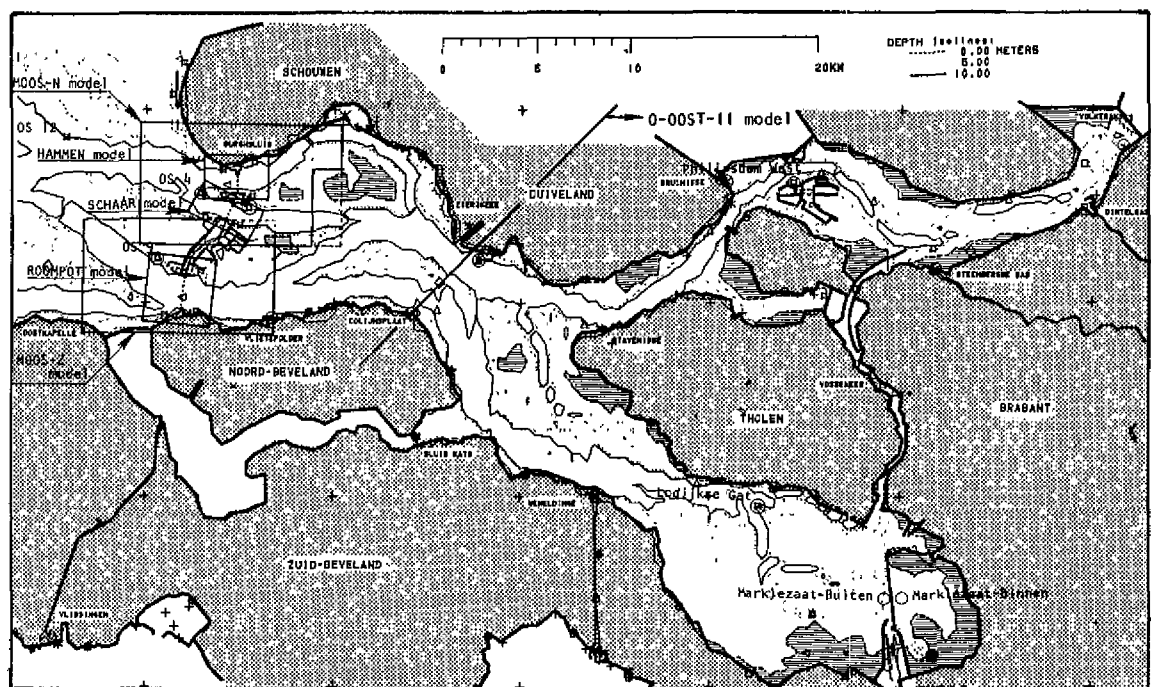
Fig. 2—Bathymetry of the OOST-II model area, with location of the submodels and tide level stations used in the analysis

NOTE: In other graphs of this report the values of the velocity isolines are not indicated, but they can be derived by counting them from the shore. The values at which the isolines are drawn are indicated in the legend of the figures, in this case at the right top.

Fig. 3—One of the submodels of the OOST-II model with a grid size of 90 m. The contour lines are lines of equal velocity with values in m/sec. Note the eddies generated by the flow near the southern shore.

II. THE NUMERICAL MODELING PROCEDURES

The actual simulations for the investigations were made with the SIMSYS2D system[1] installed on an IBM 3032 computer. This system consists of an interlocking set of programs for data processing, two-dimensional simulation, and graphical representation designed particularly for engineering investigations [4].

The input data processor is the first program used for each simulation. Data sets, which are easy to assemble by the model engineer, are reordered by this program in the form suitable for simulation. Simultaneously, checks are made as to consistency of the data, and an annotated report is written for documentation purposes.

The actual simulations are made with a program that computes the vertically integrated equation of motion, the equation of continuity, and transport equations by use of finite differences. The relation between density and salinity is expressed by an equation of state. Two sets of finite difference equations are used alternately, and the sets are solved implicitly for each direction.

The computations are made on a rectangular grid system with variables for the water level ζ and the concentration (P) on points of the grid at integer values. The velocity variables are located between the water level points so that in the computation of the new velocity value the pressure gradient is directly available without averaging. A more detailed description of the basic method used in the system can be found in Leendertse and Gritton [5] (1971), but modifications have been made to obtain a higher order of approximation.

The first set of equations refers to computations centered on time level $n\Delta t$, and can be written as follows:

Momentum Equation in x Direction

$$\delta_t u \;-\; f\bar{\bar{v}} \;+\; A(x) \;+\; g\overline{\delta_x \zeta}^t \;+\; \frac{1}{2}\frac{g}{\rho}(\bar{h}^y + \bar{\zeta}^x)\delta_x \rho \;+\; R(x)\bar{u}^t$$

$$-\; \frac{\theta \rho_a W^2 \sin \psi}{\rho(\bar{h}^y + \bar{\zeta}^x)} \;-\; \delta_x P \;-\; k\nabla^2 u_- \;=\; 0 \quad \text{at } j + \frac{1}{2}, k, n \tag{1}$$

Continuity Equation

$$\delta_{+\frac{1}{2}t}\zeta \;+\; \delta_x[(\bar{h}^y + \bar{\zeta}_f^x)u_+] \;+\; \delta_y[(\bar{h}^x + \bar{\zeta}^y)v] = 0 \tag{2}$$

Transport Equation

$$\delta_{+\frac{1}{2}t}[P_i(\bar{\bar{h}} + \zeta)] \;+\; \delta_x[(\bar{h}^y + \bar{\zeta}_f^x)u_+ \bar{P}_{i_+}^x] \;+\; \delta_y[(\bar{h}^x + \bar{\zeta}^y)v_+ \bar{P}_i^y]$$

$$-\; \delta_x[(\bar{h}^y + \bar{\zeta}_+^x)D_{x_+}\delta_x P_{i_+}] \;-\; \delta_y[(\bar{h}^x + \bar{\zeta}^y)D_y \delta_y P_i]$$

$$+ \sum_{\ell=1}^{i-1} (\bar{\bar{h}} + \zeta_+)K_{i\ell}P_{\ell_+}\alpha_i + \overline{(\bar{\bar{h}} + \zeta)K_{ii}P_i}^{t/2} \tag{3}$$

$$+ \sum_{\ell=i+1}^{\ell_{max}} (\bar{\bar{h}} + \zeta)K_{i\ell}P_\ell\beta_i + S_i = 0 \quad \text{at } j, k, n$$

where
$A(x)$	=	advection term
f	=	Coriolis parameter
g	=	acceleration of gravity
h	=	distance between bottom and reference plane
k	=	horizontal velocity diffusion coefficient
$K_{i\ell}$	=	reaction coefficient between constituent i and ℓ
ℓ_{max}	=	maximum number of constituents
P_i	=	constituent i
P	=	atmospheric pressure
D_x	=	diffusion coefficient in x direction
D_y	=	diffusion coefficient in y direction
$R(x)$	=	bottom stress coefficient
S	=	source or sink of constituent P_i per time unit
u	=	vertically average velocity component in x direction
W	=	wind speed
α_i	=	$\begin{cases} 0 & i = 1 \\ 1 & 1 < i \le \ell_{max} \end{cases}$
β_i	=	$\begin{cases} 0 & i = \ell_{max} \\ 1 & 1 \le i < \ell_{max} \end{cases}$
ζ	=	water level elevation relative to a horizontal reference plane
Θ	=	wind stress coefficient
ρ	=	density of water
ρ_a	=	density of air
ψ	=	angle between wind direction and the positive y direction

Averages and differences are symbolically represented by

$$\bar{F}^x = \frac{1}{2}\left\{ F\left[\left(j + \tfrac{1}{2}\right)\Delta x, k\Delta y, n\Delta t\right] + F\left[\left(j - \tfrac{1}{2}\right)\Delta x, k\Delta y, n\Delta t\right]\right\}$$

$$\delta_x F = \frac{1}{\Delta x}\left\{ F\left[\left(j + \tfrac{1}{2}\right)\Delta x, k\Delta y, n\Delta t\right] - F\left[\left(j - \tfrac{1}{2}\right)\Delta x, k\Delta y, n\Delta t\right]\right\}$$

$$\bar{\bar{F}} = \frac{1}{4}\left\{ F\left[\left(j + \tfrac{1}{2}\right)\Delta x, \left(k + \tfrac{1}{2}\right)\Delta y, n\Delta t\right] + F\left[\left(j + \tfrac{1}{2}\right)\Delta x, \left(k - \tfrac{1}{2}\right)\Delta y, n\Delta t\right]\right.$$

$$\left. + F\left[\left(j - \tfrac{1}{2}\right)\Delta x, \left(k + \tfrac{1}{2}\right)\Delta y, n\Delta t\right] + F\left[\left(j - \tfrac{1}{2}\right)\Delta x, \left(k - \tfrac{1}{2}\right)\Delta y, n\Delta t\right]\right\}$$

These are shown only for x, but are also used for y and t. A special notation is used to indicate shifted time levels:

$$\delta_{+\frac{1}{2}t}F = \frac{2}{\Delta t}\left\{F\left[j\Delta x, k\Delta y, \left(n + \frac{1}{2}\right)\Delta t\right] - F\left(j\Delta x, k\Delta y, n\Delta t\right)\right\}$$

$$F_+ = F\left[j\Delta x, k\Delta y, \left(n + \frac{1}{2}\right)\Delta t\right]$$

$$F_- = F\left[j\Delta x, k\Delta y, \left(n - \frac{1}{2}\right)\Delta t\right]$$

$$\overline{F}^{t/2} = \frac{1}{2}\left\{F\left[j\Delta x, k\Delta y, \left(n + \frac{1}{2}\right)\Delta t\right] + F\left[j\Delta x, k\Delta y, n\Delta t\right]\right\}$$

F_*, F_f = functions at time levels in the range of $\left(n - \frac{1}{2}\right)\Delta t$ to $\left(n + \frac{1}{2}\right)\Delta t$; their value is generally obtained by iteration.

The second set of difference equations are centered around time level $n + \frac{1}{2}$ and are written:

Momentum Equation in y Direction

$$\delta_t v - f\bar{\bar{u}} + A(y) + g\overline{\delta_y \zeta}^t + \frac{1}{2}\frac{g}{\rho}(\bar{h}^x + \bar{\zeta}^y)\delta_y\rho + R(y)\bar{v}^t$$

$$- \frac{\theta\rho_a W^2\cos\psi}{\rho(\bar{h}^x + \bar{\zeta}^y)} - \delta_y P - k\nabla^2 v_- = 0 \quad \text{at } j, k + \frac{1}{2}, n + \frac{1}{2} \tag{4}$$

Continuity Equation

$$\delta_{+\frac{1}{2}t}\zeta + \delta_x[(\bar{h}^y + \bar{\zeta}^x)u]\delta_y + [(\bar{h}^x + \bar{\zeta}^y_f)v_+] = 0 \quad \text{at } j, k + \frac{1}{2}, n + \frac{1}{2} \tag{5}$$

Transport Equation

$$\delta_{+\frac{1}{2}t}[P_i(\bar{\bar{h}} + \zeta)] + \delta_x[(\bar{h}^y + \bar{\zeta}^x)u\bar{P}_i^x] + \delta_y[(\bar{h}^x + \bar{\zeta}^y_+)v_+\bar{P}_{i_+}^y]$$

$$- \delta_x[(\bar{h}^y + \bar{\zeta}^x)D_x\delta_x P_i] - \delta_y[(\bar{h}^x + \bar{\zeta}^y_+)\Gamma_{y_+}\delta_y P_{i_+}]$$

$$+ \sum_{\ell-1}^{\ell-i-1}(h + \zeta)K_{i\ell}P_\ell\alpha_i + \overline{\overline{(\bar{\bar{h}} + \zeta)K_{ii}P_i}}^{t/2}$$

$$+ \sum_{\ell-i+1}^{\ell_{max}}(\bar{\bar{h}} + \zeta_+)K_{i\ell}P_{\ell_+}\beta_i + S_i = 0 \quad \text{at } j, k, n + \frac{1}{2} \tag{6}$$

The investigator can use different options for the advection terms. In the investigation reported here we used

$$A_1(x) = \frac{1}{3}\left\{ \left(\bar{u}\,\overline{x}_{2p}\bar{u}^x_*\right)_x + \overline{\frac{1}{2}\left[u_*(u_* + \Delta^2\nabla^2 u_*)\right]_x}^x + 2\bar{\bar{v}}\,\overline{(u_*)_y}^y + \overline{v^x(u_*)_y}^y \right\} \tag{7}$$

or

$$A_2(x) = u_*\overline{(u_*)_x}^x + \bar{v}\,\overline{(u_*)_y}^y \tag{8}$$

where Δ = grid size in x and y directions

$\nabla^2 u_*$ = $\delta_x^2 u_* + \delta_y^2 u_*$

u_* = averaged value of the velocity u at time n and the computed velocity at time $n + 1$ of the first iteration

Equation (7) is the so-called Arakawa representation of the advection term. This representation of the advection term inhibits the generation of nonlinear instabilities [6].

Equation (8) is a simple representation of the advection term which has been widely used by many investigators. It is particularly suitable for flow with weak contributions of the advection term. $A_1(y)$ and $A_2(y)$ are computed in a similar manner.

For the bottom stress terms $R(x)$ and $R(y)$, the investigator also has options. In this investigation we used

$$R(x) = g\,\frac{[(u_*)^2 + (\bar{v})^2]^{1/2}}{(\bar{h}^y + \bar{\zeta}^x)(\bar{C}^x)^2} \tag{9}$$

From experiments it is found that the Chezy value is not truly a constant, but that it is weakly dependent on the depth. We are introducing the bottom roughness as a Manning's n coefficient and periodically computing the Chezy value by use of

$$C = \frac{1}{n}\bar{\bar{H}}^{1/6} \quad \text{(metric system)} \tag{10}$$

where

$$H = \zeta + \bar{\bar{h}}$$

In addition to the advection of momentum in Eqs. (1) and (4), a term is used to compute the dispersion of momentum. The horizontal momentum diffusion is generally small except when density differences over the vertical are present.

The dispersion coefficient (k) is optionally made a spatial variable to be determined during the adjustment phase of a model investigation.

Strictly speaking, the dispersion term in the semi-momentum equations should have contained the dispersion coefficient in the first derivative, as the dispersion coefficient can be varying in space. Because of the complexity that would result, the more simple expressions are used. This seems justified, as the spatial variability is generally small and the contribution of the term relatively insensitive to the computation results. The dispersion coefficients are obtained experimentally during the adjustment of the model. Experiments described by Leendertse and Liu [7] show that the tidal amplitudes are mainly influenced by the choice of the value of this coefficient, but not the phase. The value of the coefficient in the simulation was 10 m²/sec.

The value of the diffusion coefficients in the transport equations was also found experimentally and will be described in more detail later.

For the simulations described in this report, so-called water level boundaries were used at the seaward extremity of the model. At every point of the grid at the open boundary of the model the water level is specified. The specification of the water levels at every gridpoint of the model for every timestep is a major engineering problem, as generally only very limited data are available to derive these boundary conditions and a considerable effort was made to derive the estimation procedures as described in Chapter IV. From a mathematical point of view, these water level boundary conditions are well posed only if water flows out of the modeled area. During inflow also, information about the velocities should be given to describe the boundary conditions mathematically correctly. In practice these data are not available, and in the computation procedures, the momentum equations for the gridpoints along the boundary are described without the advection terms; with these linearized equations the additional velocity data need not be specified. In a following chapter of this report, the procedures to verify the adequacy of this approach are discussed in more detail.

To solve the finite difference representation of the transport equations, boundary conditions are also required. During outflow the concentrations are computed from the concentration field, but during inflow this concentration on the boundary has to be specified.

Tidal flats and marshes are approximated in the simulation by taking computational points that represent a certain area into the computation when the water level is flooding. When the area is dry the point does not participate in the flow and transport simulation.

The simulation of these areas presented a number of unusual computational problems that resulted in the design of rather extensive computational procedures. A major problem is that the changes are discrete. When a certain area is taken out of the simulation or when the area floods, the sudden change in the flow generates a small wave that propagates from its point of origin. Such a wave can cause flooding or drying of adjacent areas, which in turn generates waves. Stability problems can arise in large simulations with extensive tidal flats. In practice, however, this problem can be alleviated by assessing flooding and drying at larger intervals than the computation step. Waves generated then have time to decay. Nevertheless, at each timestep a check has to be made for consistency in the equation of continuity.

The design of the flooding and drying procedure was severely restrained by the requirements of conservation of water and the mass in the constituent computation. Without these conservation requirements, the computation procedures would have been much simpler.

In the case where the computations are made in the baroclinic mode, the density has to be computed from the salinity. For this computation, the following equation of state described by Eckert [8] is used for each point of the computation field:

$$\rho = \frac{[5890 + 38T - 0.375T^2 + 3s]}{[(1779.5 + 11.25T - 0.0745T^2) - (3.8 + 0.01T)s + 0.698(5890 + 38T - 0.375T^2 + 3s)]} \quad (11)$$

where s = salinity (gr/l)

T = temperature (centigrade)

The density is computed by this equation of state in gr/cm^3. This is inconsistent with the units used in the simulation, but by expressing the reference density ρ_r which appears at the same time also in gr/cm^3, this inconsistency has no effect on the simulation results.

When the effects of the density gradient are included in the computation, then the effect of the salinity gradients on energy dissipation by turbulence must also be included in the computations. As the effect of energy dissipation is computed by means of a bottom stress, the Chezy value is now made a function of the salinity gradient and the direction of the current

according to:

$$C = \frac{\overline{\overline{H}}^{1/6}}{n}\left\{1 + \alpha_1\frac{(\overline{u\delta_x s}^x + \overline{v\delta_y s}^y)}{((\overline{u}^x)^2 + (\overline{v}^y)^2)^{1/2}}\right\} \tag{12}$$

Use of Eq. (12) increases the effects of bottom stress during flood and decreases during ebb. This is in agreement with the considerations presented by Abraham [9]. The use of Eq. (12) lowers the mean water levels in the inland parts of an estuary, whereas use of the coupling between the hydrodynamic equations with the transport equation for salt and the equation of state increases the mean water levels in comparison to computations without this coupling.

III. MODEL DESCRIPTION

Two general models of the Oosterschelde estuary and the adjacent sea area were available: the RANDDELTA-II model with a grid size of 800 m and the SCHELDES model with a grid size of 400 m. Figure 4 shows a computed flow field of the RANDDELTA-II model and Fig. 5 shows a computed flow field of the SCHELDES model. Experiments with the RANDDELTA-II model resulted in good agreement of computed and observed water levels, but the comparison of computed and observed transport rates through the three barrier openings showed somewhat larger computed rates at maximum ebb [3]. As to be expected, the agreement between observed and computed results of the SCHELDES model was better than for the RANDDELTA-II model.

However, computations with the SCHELDES model are expensive and no need existed for the results of the simulation in the Westerschelde. Consequently, only the Oosterschelde part of the SCHELDES model was used and this model was called OOST-II. The open boundary was taken approximately 10 km west of the barrier location, as extensive numerical experiments with the RANDDELTA-II model had shown that the water levels at the location of the boundary are hardly influenced by the barrier construction [10].

The SCHELDES model was based upon survey charts of 1976, the most up-to-date charts available at the time the model was being built; thus the OOST-II model was also based upon 1976 surveys. In the preparation of the depth arrays of the models, extreme care was taken to insure that all cross-sections through the depth points of the model matched the cross-sections of the original survey charts. Thus after completion of the model it could be expected that the transport rates over the sections of 400 m in model and prototype are in close agreement.

For the final adjustment of the OOST-II model we used water levels computed from the RANDDELTA-II model for a condition at the beginning of September 1975. The RANDDELTA-II model was based upon depth data from 1975 and earlier survey data, thus was not completely compatible with the depth schematization of the SCHELDES model and the OOST-II model. Considerable changes in depth do occur in time in the Oosterschelde. For example, it is estimated that a few million cubic meters of sand are moved out of the estuary each year [11]. However, this change was not considered to have much influence on the water levels at the open boundary of the OOST-II model, and we made the final adjustment of the OOST-II model with 1975 tide data even though we have a more recent bathymetry.

For the bottom stress, the Manning's n value was taken to be the same as obtained from the adjusted RANDDELTA-II model and except for modifications in a few small areas, this assumption resulted in good agreement between observed and computed water levels and transport rates. Also, the horizontal momentum exchange coefficient and the diffusion coefficients in the transport equations were taken from the adjusted RANDDELTA-II model and did not need any further adjustment. It is noted here that adjustment of the diffusion coefficients in the northeastern section of the estuary near the Volkerak Locks required several long duration simulations of up to 100 tidal cycles, as described in [3].

For the verification simulation, which is based on the results of measurements taken on 11 January 1982, and which was used for comparison with hydraulic model results, the depth schematization of 1976 is used again, but three major geographic changes in the system were incorporated.
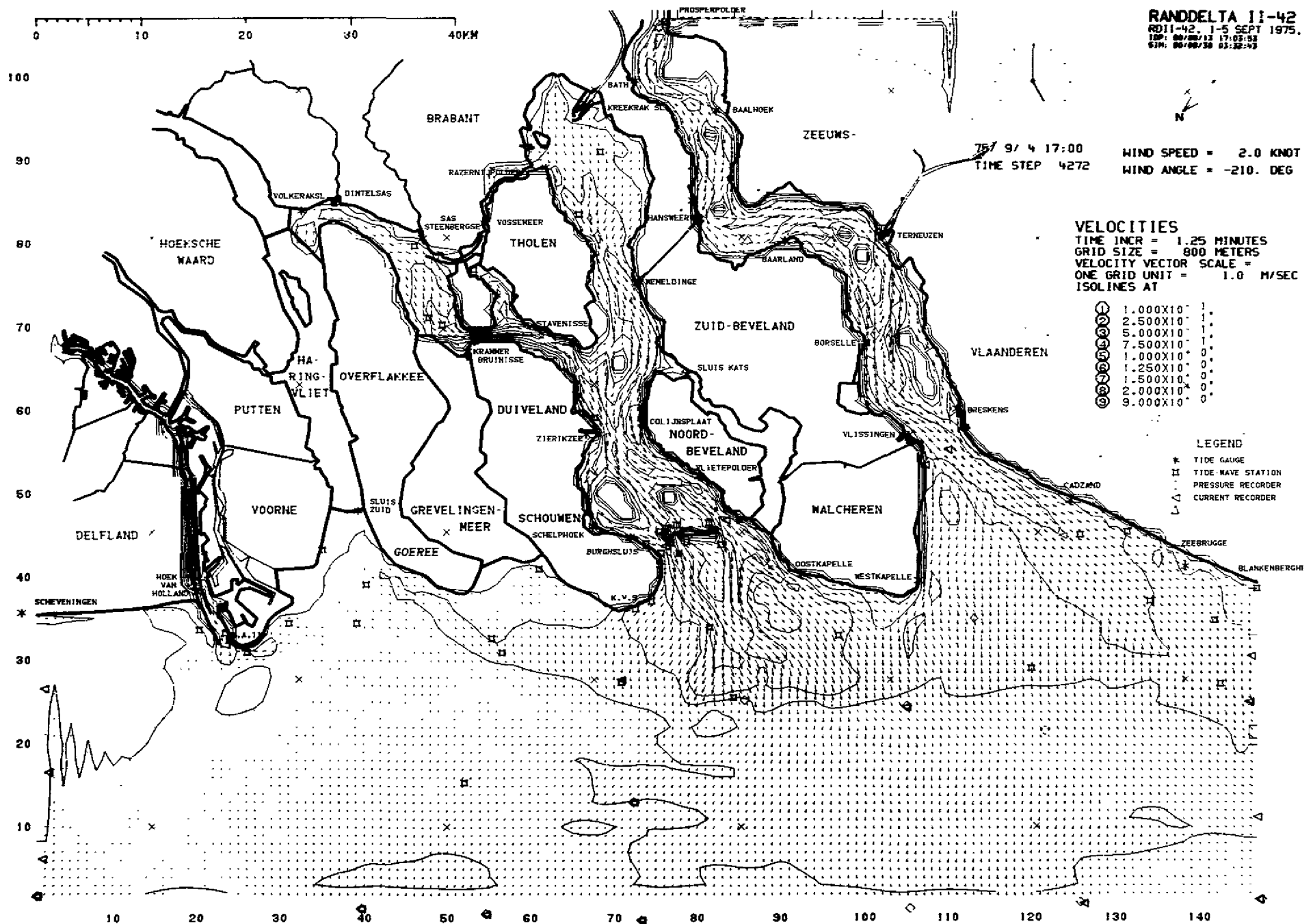
Fig. 4—Computed flow field of the RANDDELTA-II model during maximum ebb at
17:00 hours on 4 September 1975
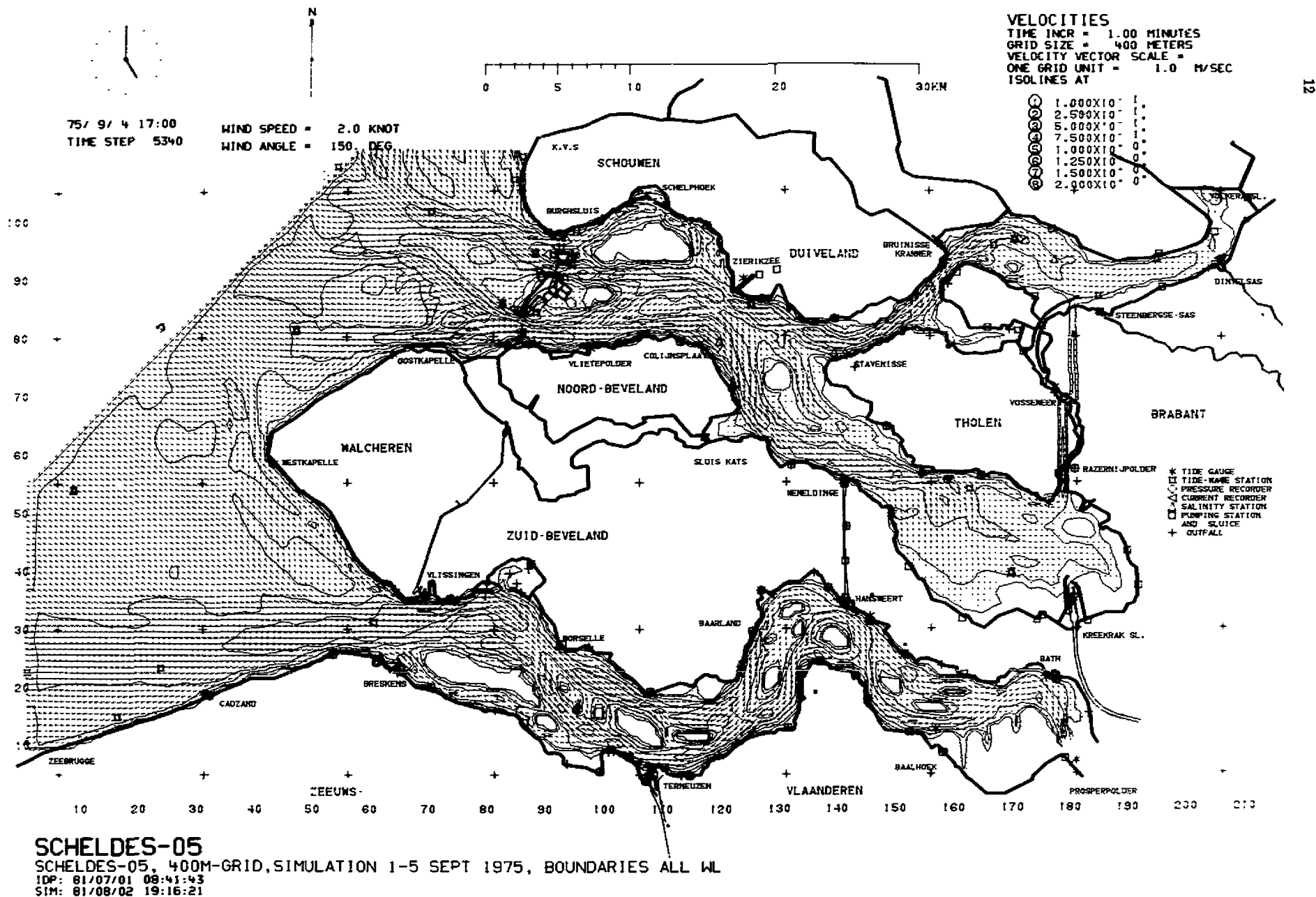
Fig. 5—Computed flow field of the SCHELDES model during maximum ebb at 17:00
hours on 4 September 1975

In January 1982, construction was under way to close the Markiezaatsdam (Fig. 1). This dam would form the eastern embankment of the Schelde-Rijn navigation channel and the area east of the dam would become a fresh water lake. For the time period of the validation simulation it was estimated that the sill of the closure opening was at the reference level (NAP) and the opening was about 400 m wide. The dam and the closure opening could rather easily be incorporated in the model since the WAQUA or SIMSYS2D system, which is designed for engineering studies, has standard features for such modifications.

The second major change in the geography was the construction of an island in the northeastern part of the system, east of Bruinisse and north of St. Philipsland (Fig. 2). This island is the construction site of a large navigation/lock complex which will be situated in a dam. In the model this island was constructed by taking a certain number of gridpoints permanently out of the computation.

The third change was that in the most northern opening of the storm-surge barrier, a short dam had been constructed that would serve as the abutment of the structure in this opening. This abutment was incorporated in the model as well as changes in depth in this channel.

For the final verification simulation the depth in the vicinity of the storm-surge barrier was modified to reflect the conditions of January 1982. This is described in Chapter VIII in more detail.

Boundary information was available from the RANDDELTA-II model for the adjustment simulation, but this was not the case for the validation simulation. An open boundary field survey for the RANDDELTA-II model or the OOST-II model was not made for the period selected for verification; thus boundary data had to be obtained by other means.

Water level data were available at five stations at some distance from the boundary of the OOST-II model for the period of interest. Tide and wave gauges at these stations are recording continuously and transmit data to a central shore station for further processing. The quality of these observations is considered very good. Consequently, a method had to be derived to obtain model boundary conditions directly from these records.

IV. BOUNDARY CONDITION ESTIMATION

On 11 January 1982 from about 10.00 hours to about 23.00 hours, current measurements were made from three to five survey vessels anchored in each of the three channels in which the storm-surge barrier is to be constructed. Consequently, this period is very suitable for the validation of the model.

Since it takes about one and one-half days before the starting transient of the model has effectively disappeared out of a simulation, the time period for which model boundary data had to be prepared was 10 and 11 January.

To construct the boundary data, records of five stations near the locations of the boundary were used, as shown in Fig. 6.
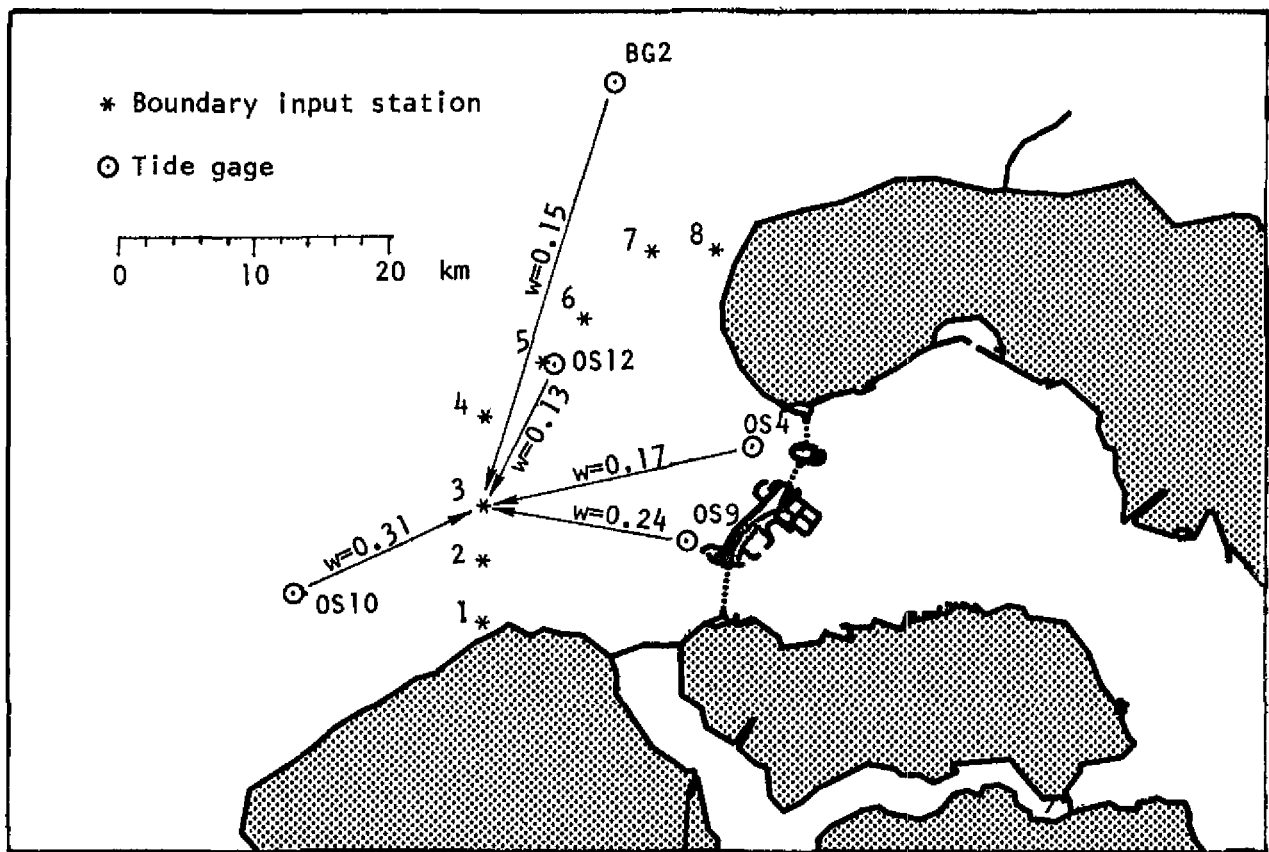
Fig. 6—Location of the water level recording stations in relation to the boundary of the OOST-II model. (For boundary station No. 3, the weights of the transfer functions from the tide gauge stations used in the analysis are also shown.)

Two of the stations are outside the boundary, two inside the boundary, and one very close to the center of the boundary.

The OOST-II model was set up for water level data inputs at eight locations on the boundary (Fig. 6). The amplitudes and phases at particular frequencies were to be supplied for each of these locations, and the simulation program is computing the water levels for the intermediate points at the boundary by linear interpolation of amplitude and phase at each frequency.[1]

No tide level data are available at the location of the eight boundary stations. However, records of tide gauging stations in the vicinity of the model boundary were available, but in general, these stations were at considerable distance from the boundary points. To estimate the tide levels at each of the boundary stations, we assumed that a linear relation exists between the tide level at each boundary station and the tide level at each tide gauging station.

This linear relation can be expressed by transfer or weighting functions. The transfer function determines the relation between amplitudes and phases of the frequency components of the two data series, whereas the weighting function determines the relation in the time domain. As no field data were ever taken at the boundary station, the only way that the transfer and weighting functions could be determined is from simulations with the RANDDELTA-II model and the SCHELDES model. The RANDDELTA-II model covered the boundary stations and all five field stations, but the SCHELDES model has only the boundary stations and three field stations. As the latter model has more resolution and has closer agreement between observed and computed data during the adjustment than the RANDDELTA-II model, we determined the response functions in which OS4, OS9, and OS12 were involved from a simulation with the SCHELDES model (Fig. 6). The transfer and weighting functions of stations BG2 and OS10 to the boundary were determined from a simulation with the RANDDELTA-II model.

The simulation period of the RANDDELTA-II model that could be used for analysis was 100 hours, and the period of the SCHELDES model was 75 hours. Both periods were from a simulation of 1–6 September 1975.

The transfer functions were determined by cross-spectral analysis. With this technique, an optimal estimate of the linear relation between two data series can be found even though the relation is not completely linear. Cross-spectral analysis was used as experience had shown that with this method, a better estimate of the transfer function can be obtained than by a Fourier analysis or harmonic analysis when only short data series are available.

For the first step of the cross-spectral analysis, the cross-covariance functions and the auto-covariance functions were determined from data points with a time interval of one hour apart and with a maximum lag of the intervals of 25. Consequently, the highest frequency for which the transfer function could be determined was 0.5 cycles per hour and the frequency interval of the transfer function was 0.02 cycles per hour. With this interval, the frequencies of the lunar tide and of the overtides nearly coincide with frequencies at which the results of the analysis are obtained. Data were abstracted from the simulation every ten minutes. For the computation of the variances, all data points were used, which resulted in a higher accuracy of the transfer function estimate than when only hourly data were used, as is the usual practice.

---

[1]The accuracy of the boundary data insertion at eight locations together with the omission of the advection terms in the finite difference equations for the momentum near the boundary was determined experimentally by taking water level data at the eight boundary stations out of a simulation with the SCHELDES model, and using those data as inputs for an OOST-II simulation. The computed water levels and current velocities appeared to be virtually the same in both models.

A typical example of the results of an analysis is shown in Fig. 7. This figure shows the amplitude and the phase of the transfer function from station OS4 to boundary station 3 as a function of frequency. In these graphs we also show the 90 percent confidence interval. It will be noted that the amplification from OS4 to station 3 is smaller than unity for the diurnal tide and the tenth-diurnal tide. For all other tidal components the amplification is larger than unity. The confidence interval is quite wide for the higher tidal components, particularly for the tenth-diurnal tide.

From the phase graph it can be seen that the tides at the boundary station precede the tide at OS4 as we would expect. However, the time difference is not the same for all components; thus the tidal wave at OS4 has a different shape than at the boundary station.

Hindcasts at a boundary station can now be made by convoluting the tidal record from the tide gauge station with the weighting function. The weighting function is derived from the transfer function in a manner described by Jenkins and Watts [12] and Liu [13]. In this case, the weighting function extends into the negative time domain as events at the boundary precede those at station OS4. The accuracy of the hindcast depends on the linearity of the relation between the two stations. The coherency is a measure of this, but the coherency is a function of frequency and not very suitable for our analysis. As a measure of accuracy, we used the standard deviation between the tide at the boundary station used for the cross-spectral analysis and the hindcasted tide at that station obtained by use of the weighting functions from the
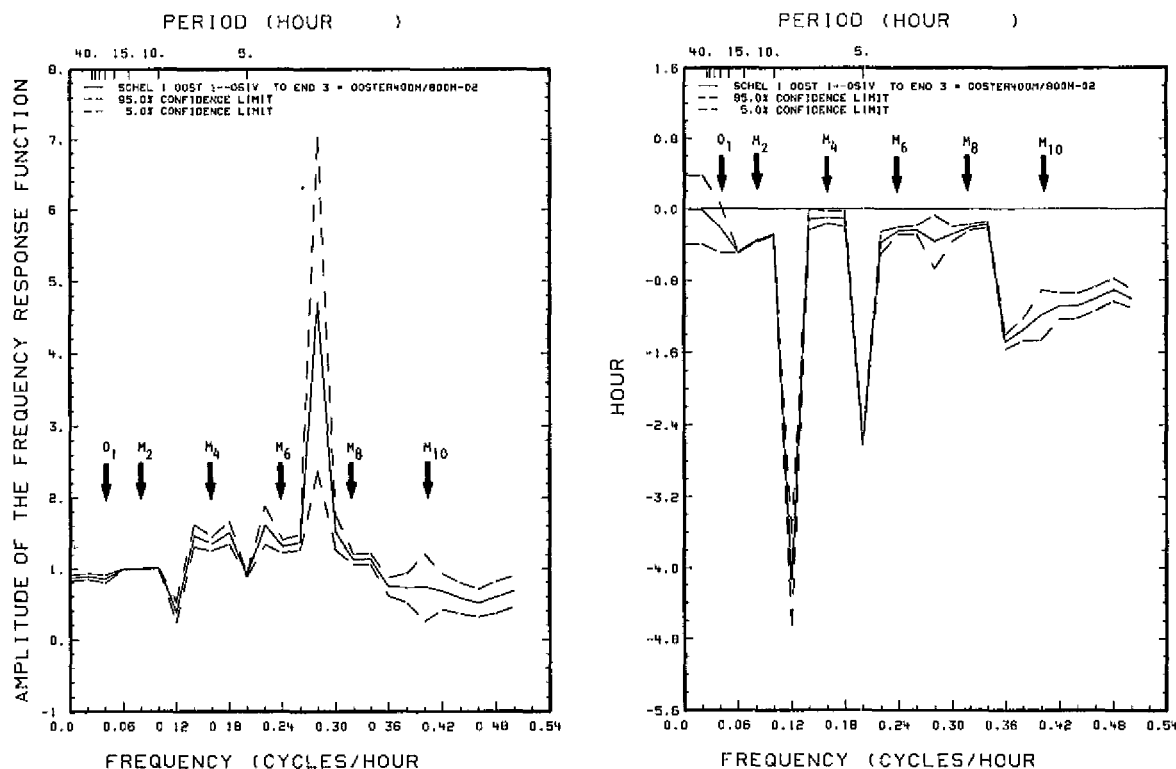
Fig. 7—Transfer function between OS4 and model boundary station 3: (a) amplification versus frequency, (b) phase in hours versus frequency

record of the tide gauge station. For example, the standard deviation at boundary station 3 computed from OS4 appeared to be 0.046 m. In view of the distance of 20 km between the stations this seemed to be a reasonable estimation error. These standard deviations were computed for all cross-spectral relationships, as shown in Table 1.

A careful review of the data in Table 1 reveals that distance is a factor in the accuracy of the prediction, but it is also important that the stations are aligned in the predominant direction of the flows for a good prediction.

To make the hindcast of the boundary conditions of the model on 10 and 11 January, we first made five hindcasts for each boundary station by use of the weighting function from each of the tide gauge stations. Subsequently, each hindcast was weighted according to the inverse of the standard deviations shown in Table 1.

The weights of the hindcasts for boundary station 3 are shown in Fig. 6, as an example. Table 2 shows all the weights.

By combining the estimates obtained for each boundary point from different tide stations, we increased the accuracy considerably. The observation at each tide gauge station naturally

Table 1

STANDARD DEVIATION IN METERS BETWEEN
OBSERVATION AND HINDCAST MADE BY CONVOLUTION

Boundary Station	Reference Station				
	OS4	OS9	OS10	OS12	BG2
1	.050	.035	.021	.091	.060
2	.048	.034	.023	.076	.056
3	.046	.033	.026	.061	.052
4	.038	.027	.033	.032	.049
5	.035	.026	.040	.0004	.049
6	.034	.027	.038	.023	.045
7	.039	.034	.034	.073	.027
8	.033	.029	.041	.098	.038

Table 2

WEIGHTS USED FOR THE HINDCASTS

Boundary Station	Reference Station				
	OS4	OS9	OS10	OS12	BG2
1	.16	.23	.38	.09	.14
2	.17	.24	.35	.10	.14
3	.17	.24	.31	.13	.15
4	.18	.25	.21	.22	.14
5	.00	.00	.00	1.00	.00
6	.19	.23	.17	.27	.14
7	.19	.22	.22	.10	.27
8	.24	.28	.19	.08	.21

has a measurement error and contains some noise from shorter waves and local variations of the density field. These effects are cancelled out to a certain extent by use of the weighted inputs. The more systematic errors induced by wind setup, which is not taken into account in the cross-spectral analysis, are reduced considerably by the fact that the reference stations are outside as well as inside the boundary.

It should be realized that the boundary condition determined in this manner contains errors. These errors will propagate through the system during the simulation and will add to the deviation of model results from the observations. Fortunately, as we will see later, these errors are small, and we can make estimates of their magnitude from a comparison of model data and field data of water level stations close to the boundary.

The development of this boundary estimation technique and the resulting extensive computer programs are important as they permit a direct determination of boundary conditions without going through an extensive effort of finding boundary conditions by trial and error. The main difficulty in obtaining the cross-spectral estimates of the transfer function, and the weighting function, is the proper selection of the variables of the analysis such as the length of the data series, the lag, the time interval, and the window. As with all modeling efforts, the insight of the modeler in setting these variables is a determining factor in the accuracy of the results.

The time series, which were the result of the processes described above, were decomposed into Fourier components. The amplitudes and phases of the components were finally used as input for the validation simulation.

V. SIMULATIONS WITH CONSTANT DENSITY

Two simulations were made without taking the effect of density gradients into account. By making the simulations in this manner a direct comparison with the results of a simulation with the hydraulic model could be made. For the first simulation the boundary conditions, as described in the previous chapter of the report, were used together with wind data for the two days.

The analysis of the results of the first simulation indicated that an error was introduced in the phases of the boundary tide. In the procedures for the abstraction of water level and current data from the model, outputs over a whole timestep are averaged and then assumed to be the value at the end of this timestep. Naturally, a small time shift backward was introduced. To account for this, the phase of each component in the inputs had to be corrected.

Fourier analysis of computed and observed water levels also indicated that the phase of the tenth overtide with a period of 2.5 hours was incorrect. Even though the amplitudes in this frequency band are only a few centimeters, the phase error contributed considerably to the difference between observed and computed tide levels in the estuary and a correction in the phase of this component was made. A review of the cross-spectral analysis for the boundary inputs indicated that the coherency in this frequency between the tide gauge stations and the model boundary is low, which results in a wide confidence interval of the transfer function at that frequency, as can be seen in Fig. 7.

The simulations from which the transfer functions were derived are the conditions of 1975 and 1976; thus the three major changes in geography were not included. Consequently, it is possible that the three major changes in the system have influenced this tide component. The construction of the Markiezaatsdam, in particular, may have caused a change in the co-oscillation of this overtide.

A second simulation was made with the correction of the inputs described above. This second simulation was also required for the abstraction of the boundary conditions for a new submodel that was being constructed (Fig. 3). We added many water level and current stations, and transport rate sections, in OOST-II so that data abstracted from the simulation could readily be used for boundary conditions of this submodel.

Comparison of observed and computed water levels resulting from this second simulation are shown in Fig. 8 for six typical stations in the estuary. In all cases the agreement is good. The standard deviation between observed and computed data for the periods shown on the graphs varies between 0.02 and 0.06 m.

Comparisons of observed and computed water levels for all available stations are also contained in Appendix A.

To obtain a good insight into the differences in behavior between computation and prototype, a Fourier analysis was made for the last 12.5 hours of the simulation. The same analysis was made for the observed data. The amplitudes of the component in the tidal frequencies are shown in Table 3 and the phase lags in Table 4.
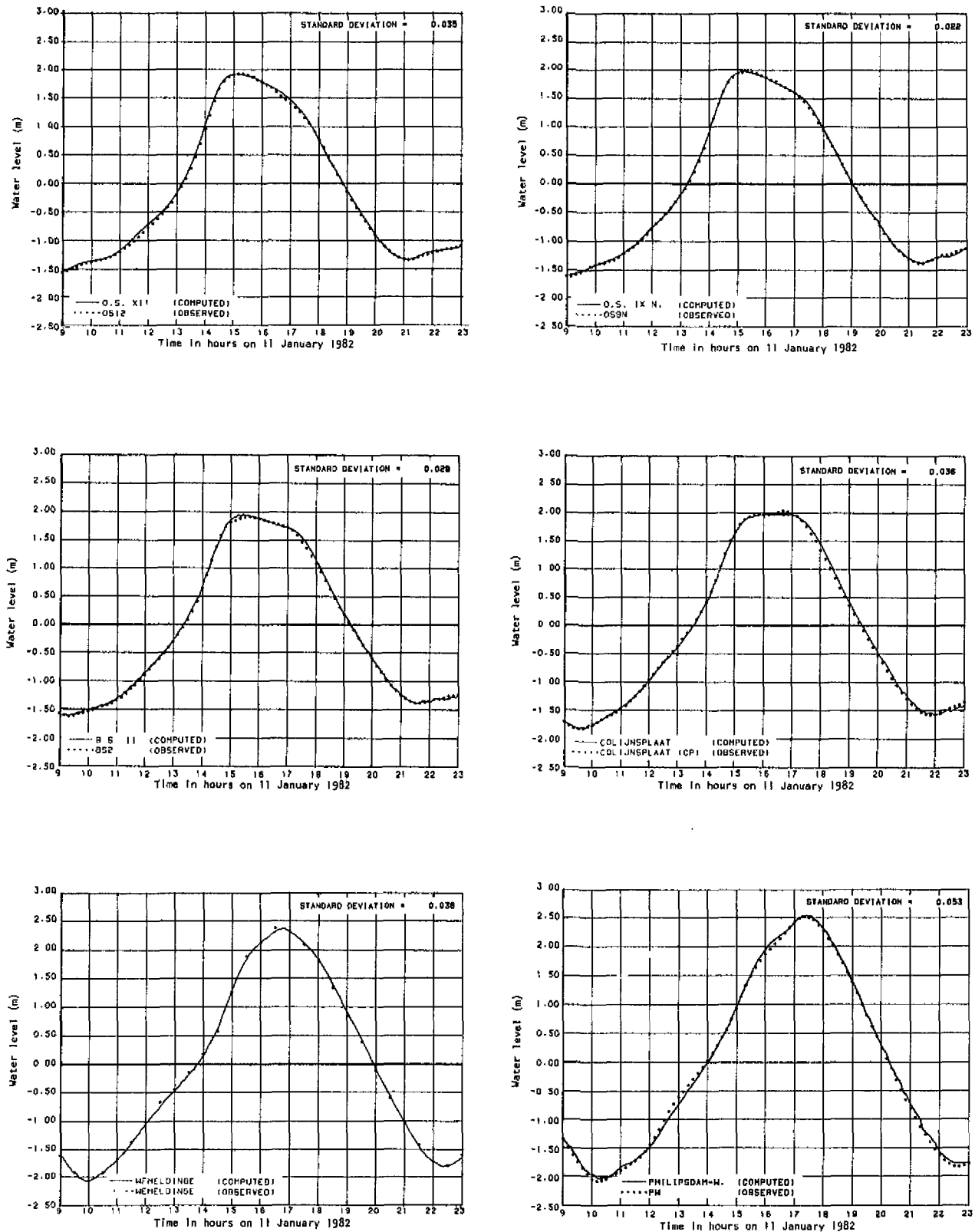
19

20

Fig. 8—Observed and computed water levels at stations in the Eastern Scheldt:
(a) OS12, (b) OS9, (c) BS2, (d) Colijnsplaat, (e) Wemeldinge,
(f) Philipsdam-W (constant density computation)

Table 3

OBSERVED AND COMPUTED MEAN WATER LEVELS AND TIDAL AMPLITUDES
(Constant density simulation)

Station	Mean Obs.	Mean Comp.	M_2 Obs.	M_2 Comp.	M_4 Obs.	M_4 Comp.	M_6 Obs.	M_6 Comp.	M_8 Obs.	M_8 Comp.	M_{10} Obs.	M_{10} Comp.
OS12	0.064	0.085	1.624	1.629	0.288	0.275	0.138	0.133	0.068	0.061	0.076	0.089
OS9	0.108	0.108	1.687	1.690	0.242	0.232	0.128	0.121	0.056	0.064	0.085	0.083
Vlietepolder	0.061	0.114	1.775	1.758	0.204	0.193	0.102	0.091	0.062	0.070	0.097	0.082
Colijnsplaat	0.090	0.098	1.836	1.835	0.214	0.196	0.044	0.049	0.032	0.047	0.085	0.078
Wemeldinge	0.148	0.143	1.998	2.009	0.186	0.178	0.158	0.136	0.046	0.040	0.017	0.019
Markiezaat-Bui	0.146	0.165	2.145	2.120	0.221	0.186	0.277	0.272	0.053	0.059	0.069	0.071
Markiezaat-Bin	1.110	1.059	0.526	0.516	0.128	0.136	0.083	0.062	0.003	0.009	0.014	0.003
Lodijkse Gat	0.140	0.160	2.100	1.091	0.221	0.209	0.212	0.210	0.049	0.044	0.027	0.028
Philipsdam West	0.158	0.171	2.115	2.123	0.206	0.185	0.085	0.072	0.014	0.020	0.038	0.031
Steenbergse Sas	0.205	0.188	2.196	2.229	0.208	0.124	0.148	0.142	0.028	0.036	0.017	0.017
Bruinisse	0.170	0.164	2.053	2.090	0.215	0.184	0.060	0.056	0.017	0.031	0.050	0.043
Zeelandbrug-N	0.124	0.147	1.866	1.857	0.172	0.152	0.057	0.057	0.042	0.053	0.087	0.077
BS2	0.097	0.107	1.705	1.717	0.225	0.213	0.085	0.089	0.049	0.061	0.088	0.086
OS4	0.084	0.112	1.675	1.685	0.240	0.229	0.108	0.108	0.058	0.066	0.088	0.086

Table 4

OBSERVED AND COMPUTED PHASE LAGS
(Constant density simulation)

Station	M_2 Obs.	M_2 Comp.	M_4 Obs.	M_4 Comp.	M_6 Obs.	M_6 Comp.	M_8 Obs.	M_8 Comp.	M_{10} Obs.	M_{10} Comp.
OS12	83.4	81.6	77.7	77.4	3.2	2.0	26.9	22.5	13.2	6.4
OS9	91.3	91.1	84.3	84.4	12.1	10.4	25.9	18.4	17.6	18.8
Vlietepolder	100.3	101.8	96.0	100.8	20.7	20.8	25.5	28.1	19.1	25.4
Colijnsplaat	112.1	114.1	125.4	128.7	54.6	46.7	46.4	35.6	31.5	35.3
Wemeldinge	132.5	133.9	173.5	177.4	110.9	105.4	68.2	60.4	52.9	43.5
Markiezaat-Bui	141.9	150.2	193.4	206.6	116.1	121.0	94.3	86.8	111.6	122.6
Markiezaat-Bin	298.1	294.7	217.8	223.0	190.7	192.0	105.7	85.3	162.6	143.8
Lodijkse Gat	136.2	142.2	182.5	195.0	111.4	112.8	96.4	90.7	105.6	112.8
Philipsdam West	154.0	156.1	213.0	199.6	158.4	154.6	74.7	43.0	50.6	63.2
Steenbergse Sas	166.2	171.2	234.4	208.2	160.1	170.9	112.1	96.8	113.8	136.8
Bruinisse	153.0	150.3	207.8	193.7	151.8	145.8	35.8	36.0	52.7	60.0
Zeelandbrug-N	119.3	121.9	130.7	135.4	54.7	51.7	42.7	36.7	32.9	37.6
BS2	102.3	101.4	92.6	95.0	19.7	17.6	31.6	26.9	22.5	24.1
OS4	97.7	95.7	85.8	85.2	16.4	12.9	31.8	23.5	20.9	20.4

VI. COMPARISON WITH THE HYDRAULIC MODEL

Simulations of the tidal conditions of 11 January 1982 were also made with the hydraulic model [14]. The bathymetry of this model was obtained from a variety of surveys. The Markiezaatsdam, the construction island north of Philipsland, as well as the abutment of the storm-surge barrier were incorporated in the model. The hydraulic model uses water with uniform density; thus the simulations described in previous chapters should be directly comparable with the hydraulic model results as both neglect the influence of density differences.

In the report describing results of the hydraulic model experiments compared with observed data in graphical form, no standard deviation (error) between observed and model results is presented. Consequently, only a subjective comparison between the models can be made by preparing graphical representations of the computation and observations in the same way as presented in the report of the hydraulic model experiment.

Figure 9 presents the transport rates through the three channels in ranges at the location of the storm-surge barrier. The results of the computation as well as the results of the hydraulic model experiments are compared with the data of the field survey. All graphs of this figure are shown in Appendix B on a larger scale.

In general, the computed transport rates are in better agreement with the prototype data than the results of the hydraulic model experiment. In particular, the computed transport rate through the Hammen has a better agreement with prototype than the rate measured in the hydraulic model.

Comparing the distribution of the ebb and flood flow through the three channels as percentages of the total, again it appears that the computation matches better, except for a short period around noon (Figs. 10–12). In these distribution graphs of the computed results, the flow percentage around slack could not be plotted as the total flow is zero or very small, and the percentages then become infinite or very large, as the time of current reversal is not the same in the channels.

The comparisons of the water levels of the models with the observed water levels are shown in Appendix A. A few graphs presented in the report of the hydraulic model experiments could not be compared as the data sets of the observed water levels were not available. However, we could make an additional comparison between observed and computed water levels as we had an observed data set that was apparently not available to the investigators working with the hydraulic model. In general, the accuracy of both models as to reproducing the water levels is about the same when the computational model omits the effects of density.

Reviewing the figures in Appendix A, we note that deviations of both models from the observed data have the same tendencies. It is also apparent that the method of obtaining the model boundaries in the models is different. In the computational model, the agreement between observed and computed data decreases going from the boundary inland. This is to be expected as we made an optimal estimate of the boundary conditions by use of transfer functions and, away from the boundary, the deviation of the water level in the model from the observed water levels increases as the model introduces additional deviations.

The hydraulic model has the best agreement for stations just behind the barrier. The boundary conditions of this model were obtained by successive adjustments of the control gates at the model boundary until agreement was achieved. In a report [15] describing the adjustment of the hydraulic model for another period than the one analyzed here, it was concluded
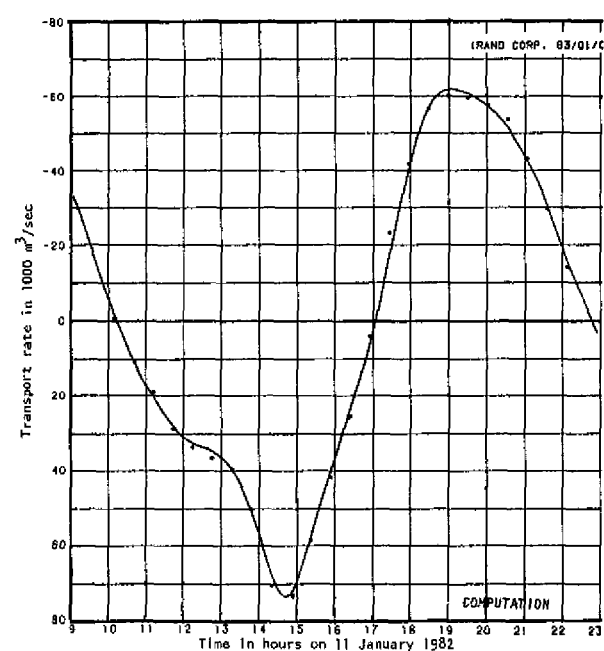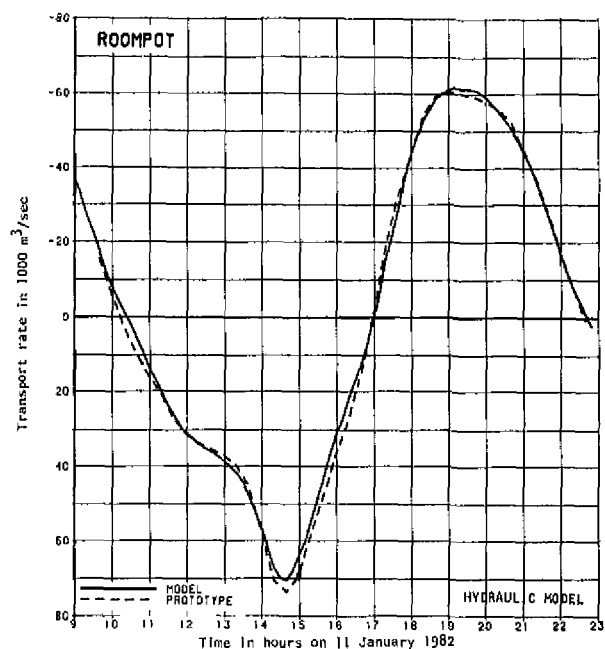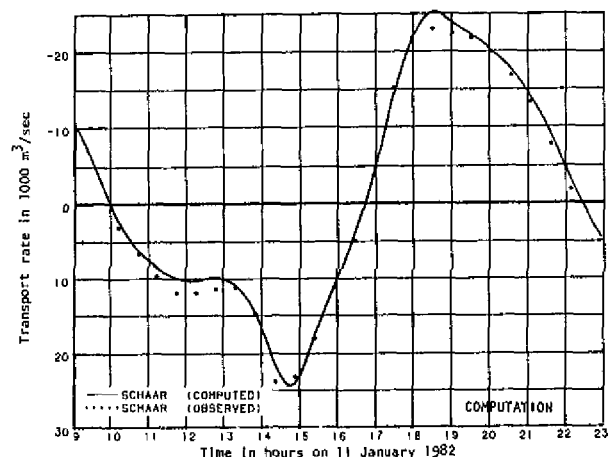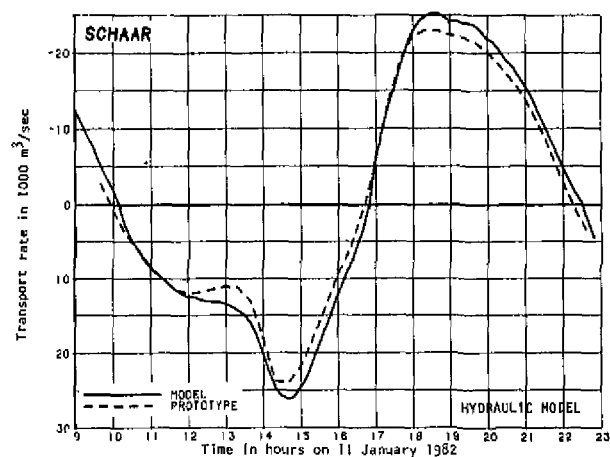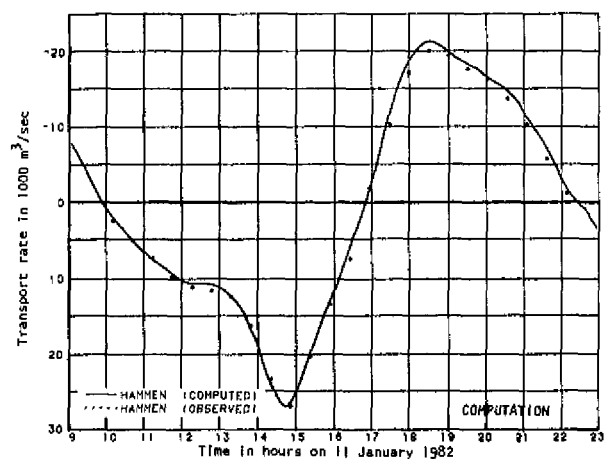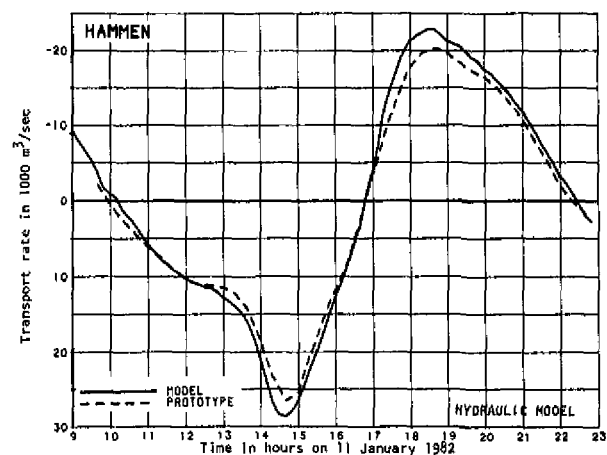
Fig 9—Transport rates through the Hammen, Schaar, and Roompot in the hydraulic
model and the computational model compared to the observed
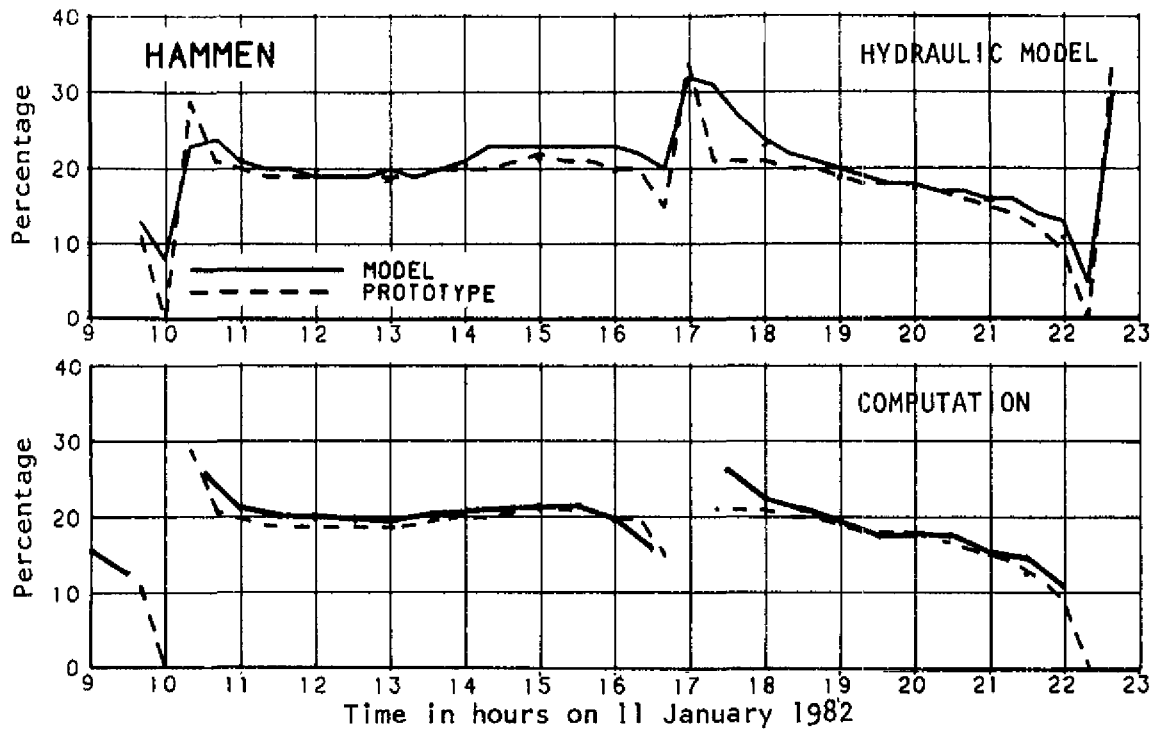transport rates (constant density computation)

Fig. 10—Percentage of the total transport rate for the Hammen in the hydraulic model (top graph) and the computational model (bottom graph) compared to the observed percentage
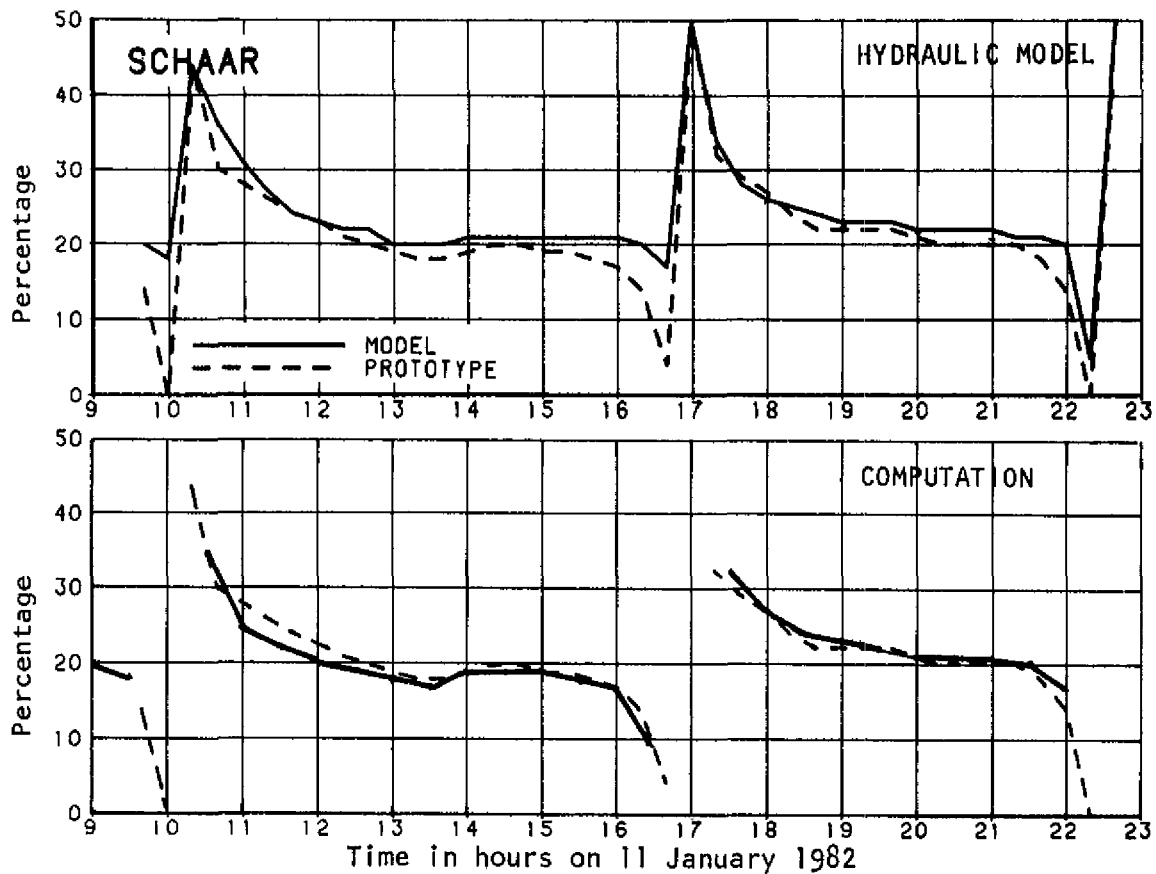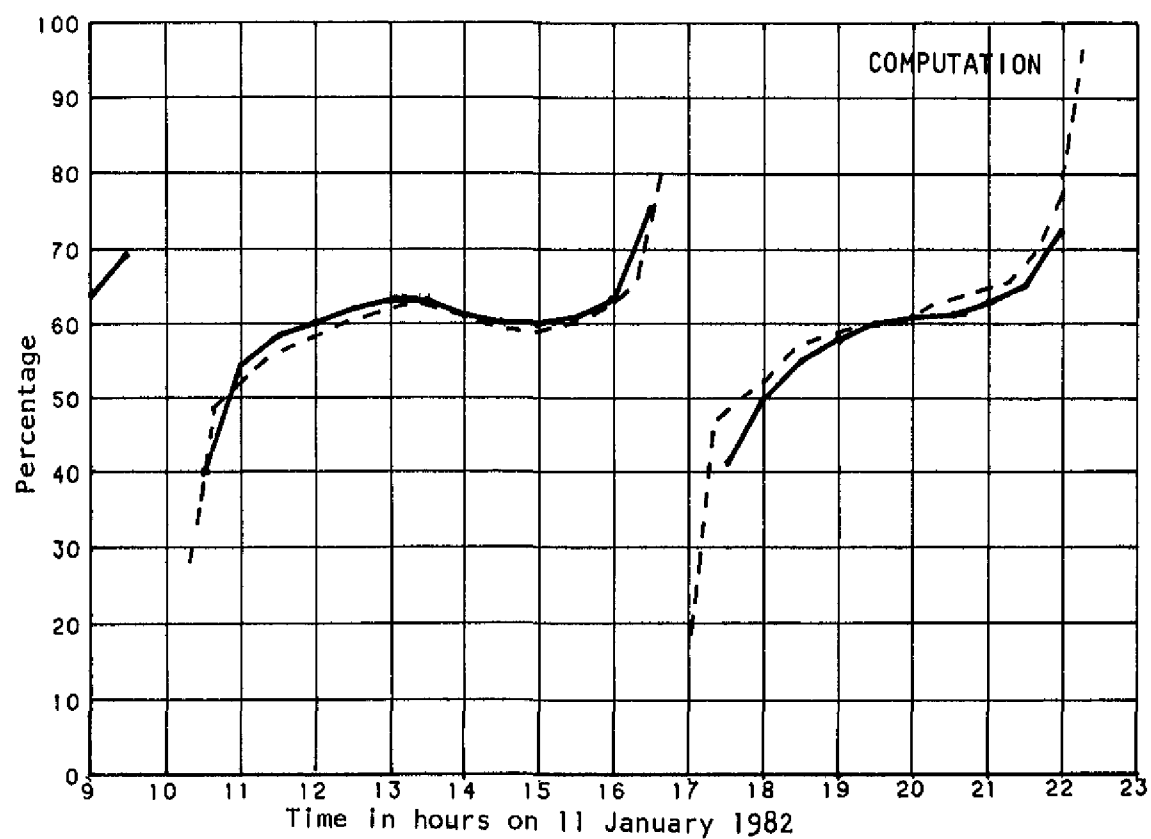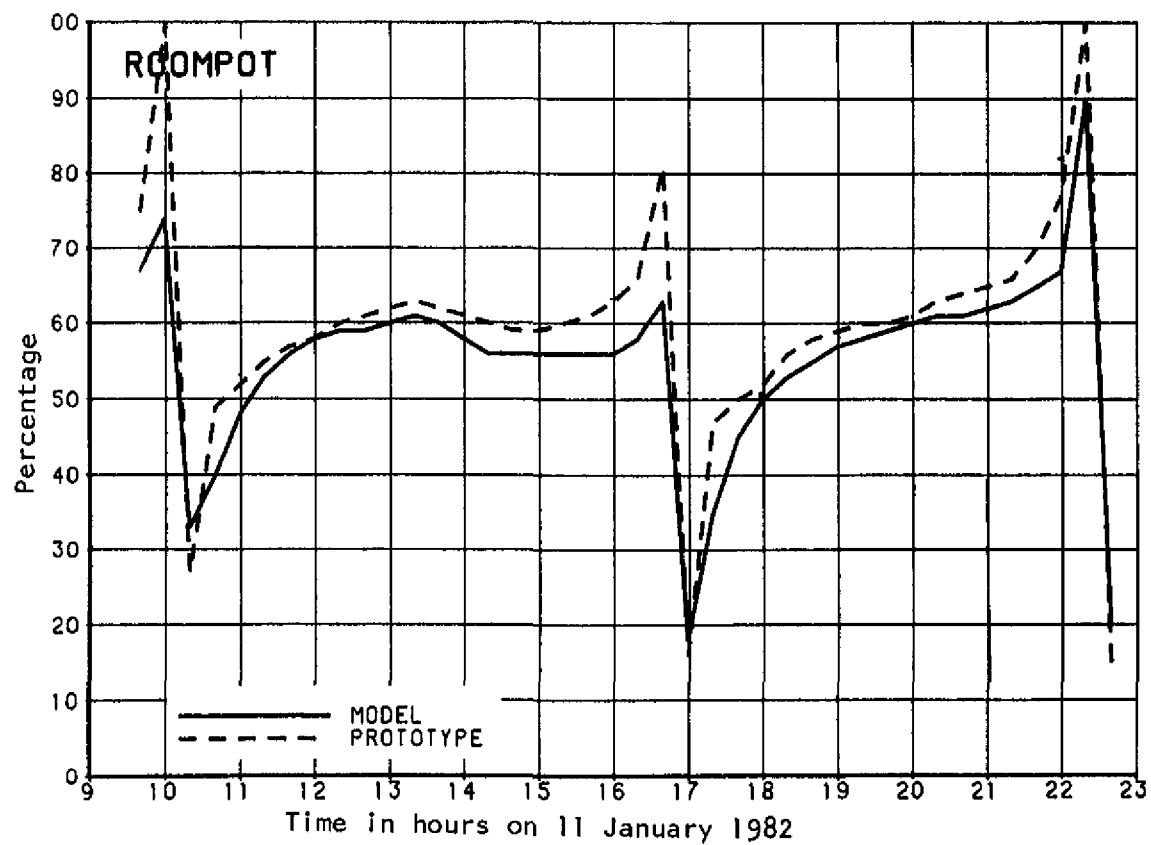

Fig. 11—Percentage of the total transport rate for the Schaar in the hydraulic model (top graph) and the computational model (bottom graph) compared to the observed percentage

Fig. 12—Percentage of the total transport rate for the Roompot in the hydraulic
model (top graph) and the computational model (bottom graph)
compared to the observed percentage

that an approximate linear relation existed between prototype water levels near the model boundary and the water levels in the model near the boundary, but that water levels in the model showed deviations from those in prototype. We conclude from these descriptions that an attempt is made to correct for errors in the tidal wave representation in the offshore area in the adjustment of the boundary conditions.

The approximate linear relation described in the report of the hydraulic model [15] is different from the linear relation with response functions that are used for the computation of the boundary conditions of the computational model. The linear relation noted by the investigators working with the hydraulic model is a relation between water levels at any particular time. Plots of observed water levels at particular times versus the water levels near the control gates of the hydraulic model resulted in a series of points near a straight line that does not go through the origin as a result of the phase differences [15].

It is noted here that the hydraulic model uses cyclic boundary conditions with a period of about 25 hours. A period of only about 13 hours, representing the verification period for which data are available, is used for analysis. This is in contrast with procedures in computational modeling where much longer periods are simulated.

For modelers using computational models, the stability of the simulation is generally of much concern. It is of interest to note here that the water level records of the stations near the hydraulic model boundary show high frequency oscillations (noise) induced by the control system of the model. In contrast, the computation does not show an apparent noise in this region, but some inland stations' records near tidal flats show some noise.

Reviewing the comparisons in Appendix A, we note that the computed tide at Lodijkse Gat is delayed six to eight minutes. This delay in the model is a few minutes larger than the delay in the hydraulic model. However, the tidal amplitudes east of the partially closed Markiezaatsdam at the station Markiezaat-Binnen are much smaller in the hydraulic model than in the computational model. From the hydraulic model results at that station (Fig. A.9), it is apparent that the closure opening is too restricted, which contributes to the closer agreement at Lodijkse-Gat in the hydraulic model.

It can be concluded that the representation of the bathymetry in the eastern part of the Eastern Scheldt is very important in obtaining good agreement between computed and observed water levels in this region. This will be confirmed by the experiments described in the next chapter.

VII. EXPERIMENTS WITH THE O-OOST-II MODEL

Before making the final verification simulation with the OOST-II model in the mode in which the pressure gradient resulting from differences in salinity is computed, simulations were made with a model that covers only the most eastern part of the OOST-II model. This model extends from a line from Colijnsplaat in the northeasterly direction, as indicated in Fig. 2. This model, called O-OOST-II, could be made rather easily as all inputs of the OOST-II model could be processed by a special program that prepares a new submodel of a designated area. Only new boundary conditions needed to be added.

The O-OOST-II model is intended as an investigative tool for studies concerning the construction of the Philipsdam and Oesterdam (Fig. 1). It is a relatively small model and is very economical to use.

The purpose of the few experiments we made with this model was to confirm that boundary conditions derived from tide gauge records at Colijnsplaat and Zeelandbrug-Noord could be used directly. Also, we wanted to investigate the sensitivity of the bathymetry in the eastern part of the Eastern Scheldt upon the tidal wave propagation.

The experiments were made with the observed tides at Colijnsplaat and Zeelandbrug-Noord inserted at the ends of the open boundary. For the intermediate points at the boundary a linear interpolation between the two water levels was used. All other inputs were derived from the OOST-II model except that now the pressure gradients resulting from salinity differences were also computed. In addition, the Chezy coefficient was made a function of the current direction and the salinity gradient as described in Chapter II. With flood the Chezy coefficient has greater values than with ebb for the same temporal depth.

A comparison of observed and computed data at Colijnsplaat and Zeelandbrug-Noord shows small differences (Fig. 13). Even though the observed data at Colijnsplaat were used as
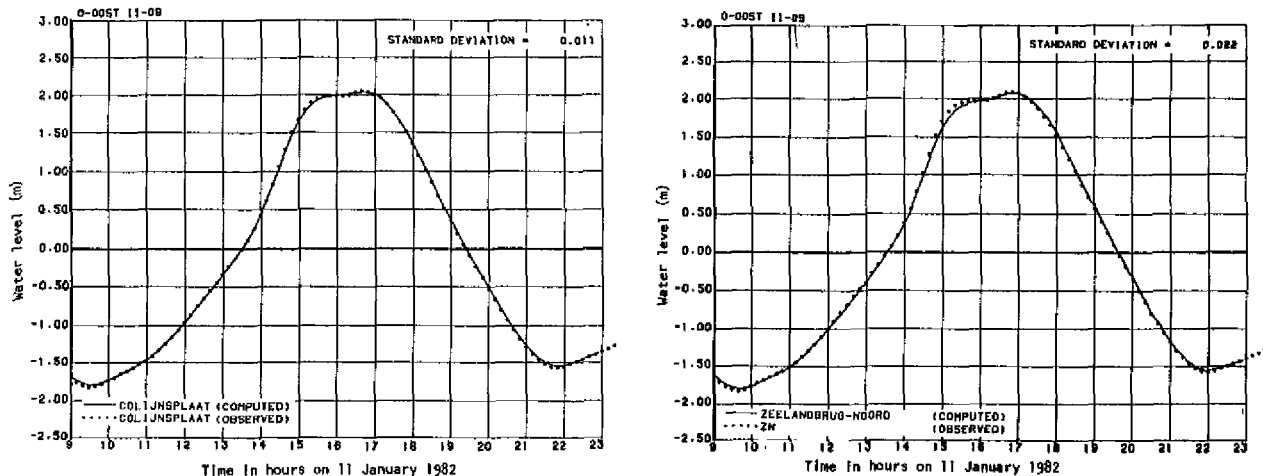

Fig. 13—Observed and computed water levels near the open boundary of the
O-OOST-II model: (a) at Colijnsplaat, (b) at Zeelandbrug-Noord

input, a small phase shift is shown because for each timestep of the computed curve what is plotted is an average value over a timestep.

In the model, the station Zeelandbrug-Noord is not exactly on the boundary as we had assumed for the purpose of boundary data preparation. As a result, the observed tide has a phase shift in addition to the one caused by the averaging procedure, and the standard deviation between observed and computed water levels at Zeelandbrug-Noord is 0.022 m (Fig. 13b).

Several other factors contribute to the errors in the boundary description. Naturally, the trace of the water surface with the vertical boundary plane is not a straight line and the salinity in the model and prototype is not the same. In the model an average salinity distribution was assumed and used as a starting condition. The actual salinity distributions on 11 January 1982 are unknown. The salinity conditions in the prototype are reflected in the observed water level records, and their influence may be considerable as the channels along the northern and southern shore are quite deep.

The recording tide gauges also have errors. Differences in reference levels may exist, and the salinity inside the floatwell may be different from the salinity outside as only a small opening is used near the bottom of the well. If this opening is exposed to currents, then the gauge does not indicate the true water level. In the mechanical recording instrument, as well as in data processing, some errors will be generated.

Even though it is possible to improve the boundary conditions, e.g., by making a correction in the phase, for practical experiments it will be advantageous to use the digitized records directly from Colijnsplaat and Zeelandbrug-Noord. As will be discussed later, agreement between observed and computed water levels at other stations in the model is good, and only in the flow field near the boundary are errors introduced. Sections of the flow field near the boundary are shown in Fig. 14 for hourly intervals. Only near High Water Slack at 17:00 hours does the assumed boundary condition cause obvious errors in the flow field. Comparisons with the flow fields of the OOST-II model, Appendix G, show that the extent of the errors in the flow field as a result of the assumed boundary condition is limited to about 5 km.

The agreement between computed and observed water levels is about the same as for the simulation with the OOST-II model described in Chapter VI of this report. Comparisons of observed and computed water levels for stations near the location of the secondary dams are shown in Fig. 15. The tidal gauge at Steenbergse Sas is in a small harbor near a discharge sluice at a considerable distance from the location in the main body of the tidal water where the model data were abstracted. The long channel across the tidal flat and density differences will contribute considerably to the large standard deviation between observed and computed water levels at Steenbergse Sas.

The phase lag at the station Lodijkse Gat has now been reduced in comparison with the OOST-II simulation described in previous chapters. This is accomplished, in part, by slightly restricting the ebb flow through the opening in the Markiezaatsdam in relation to flood flow. As a result the computed water levels at Markiezaat-Binnen now have a good agreement with the observed water levels, but the computed water level at Markiezaat-Buiten still lags the observed water level.

In the OOST-II model and thus also in the O-OOST-II model, the channel called Eendracht, between Brabant and the island Tholen (Figs. 1, 2) has been modeled with the two-dimensional system as a channel with a width of 400 m. The actual width is about 200 m; thus the tidal prism is too large. The sensitivity of this error in model schematization was investigated by making another simulation, but now with the northern half of the channel closed. From current measurements it is known that currents are nearly always very weak a few

kilometers from the northern extremity of this channel and that the tidal prism is filled mainly from the south. As to tidal prism reduction, the closure as outlined above is a good one, but, naturally, the tidal response in this channel is incorrect as it is too wide.

Results of the simulation with the Eendracht partially closed are shown in Fig. 16. The water levels in the Volkerak are not much influenced, but the agreement between computed and observed water levels improved for the stations at Lodijkse Gat, Markiezaat-Binnen, and Markiezaat-Buiten.

From the results it is concluded that a one-dimensional representation of the Eendracht with the correct cross-sections and stress terms should give further improvement in agreement.

The basic procedures for coupling the two-dimensional computation with the one-dimensional computation are now available [15]. It is recommended that these procedures be implemented before the O-OOST-II model is used for investigations associated with closures of the secondary dams.
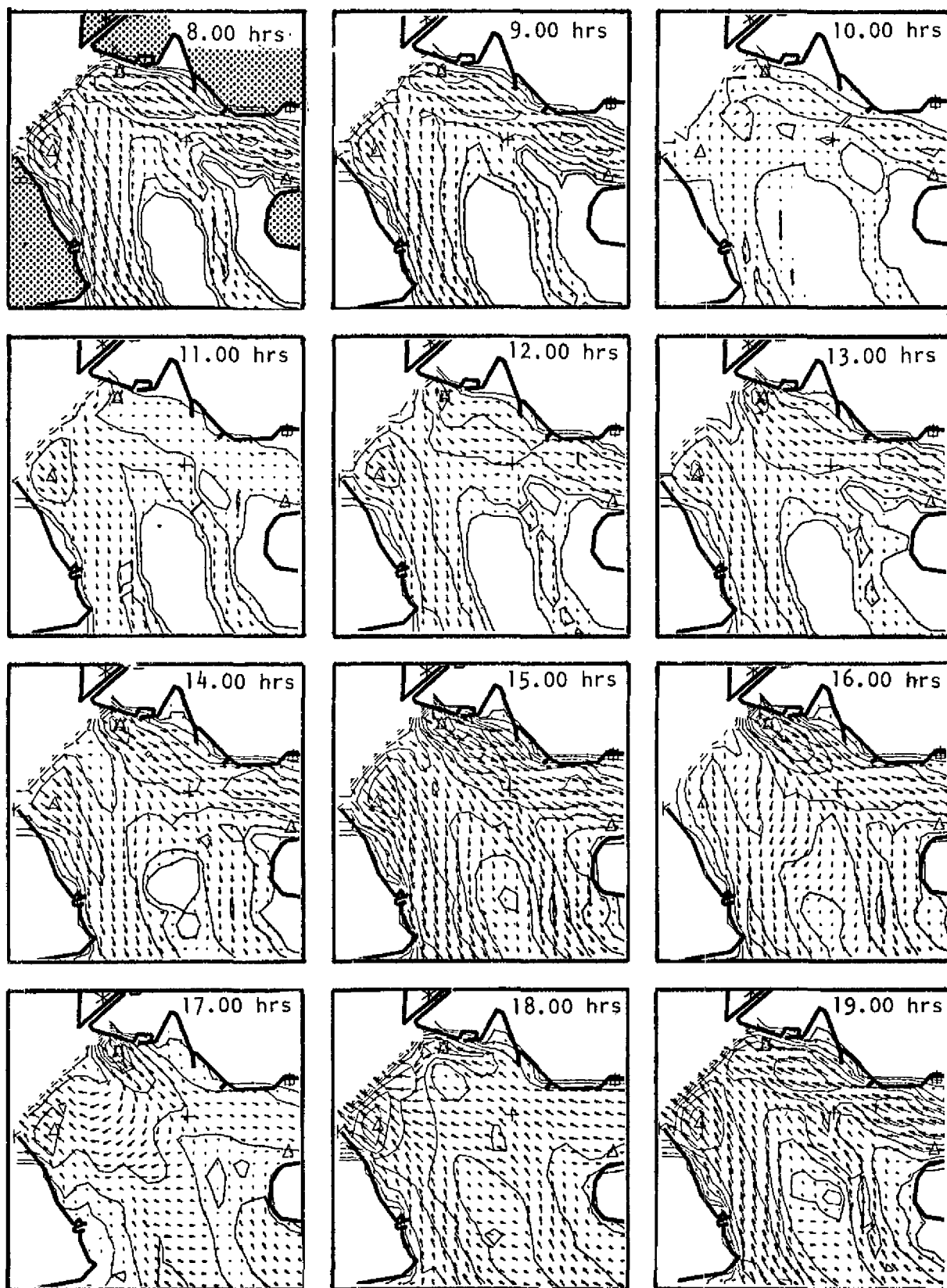
Fig. 14—Computed flow fields near the boundary of the O-OOST-II model at hourly
time intervals on 11 January 1982. (Iso-velocity contours at 0.1,
0.25, 0.50, 0.75, 1.00, and 1.25 m/sec; distance between
vector origins is 400 m.)
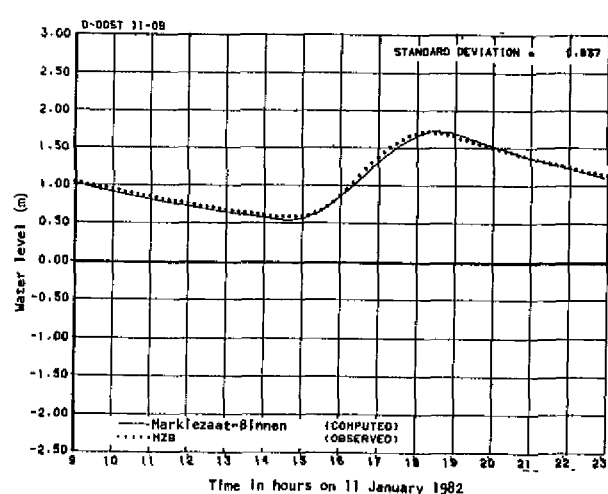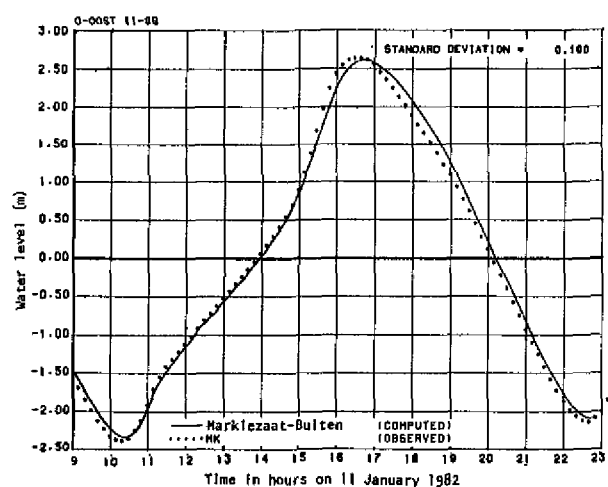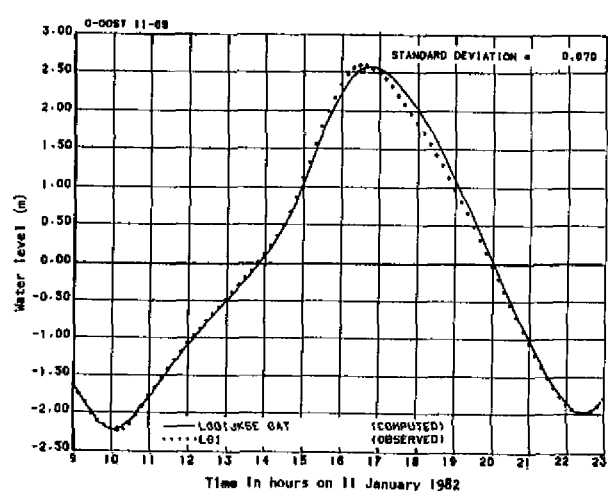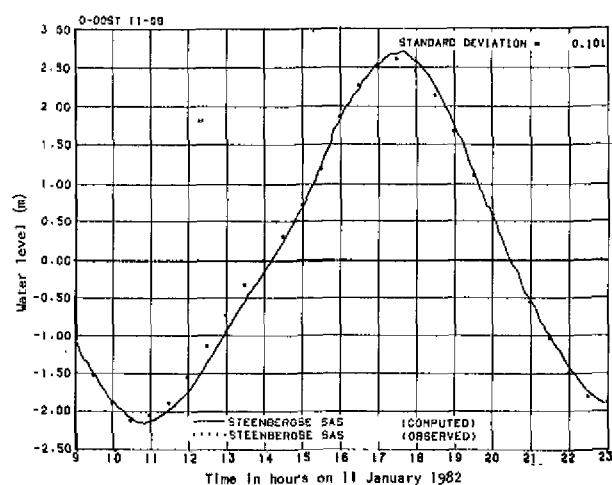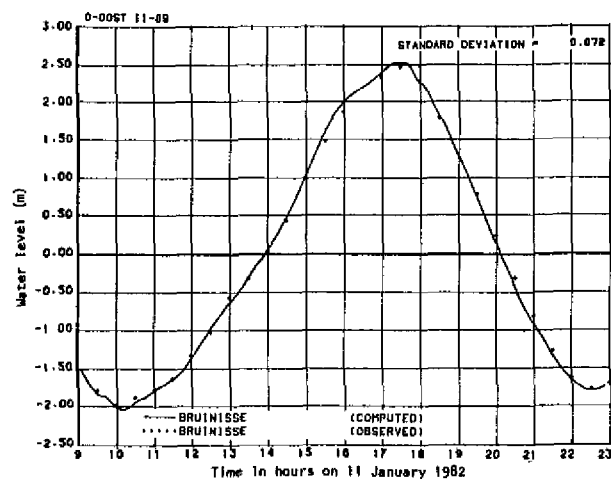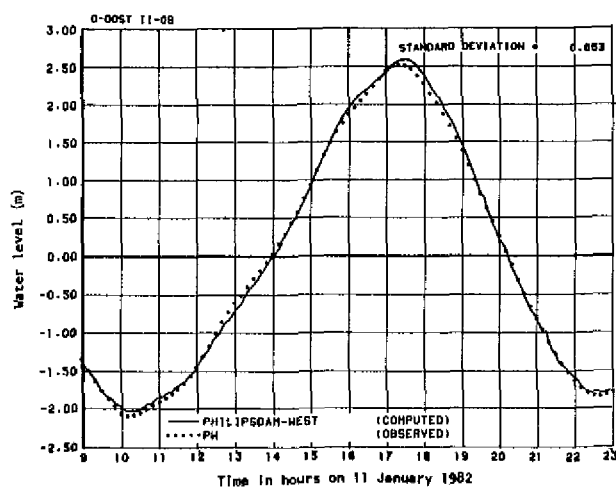
Fig. 15—Observed and computed water levels at stations in the O-OOST-II
model: (a) Philipsdam-West, (b) Bruinisse, (c) Steenbergse Sas,
(d) Lodijkse-Gat, (e) Markiezaat-Buiten, (f) Markiezaat-Binnen

32
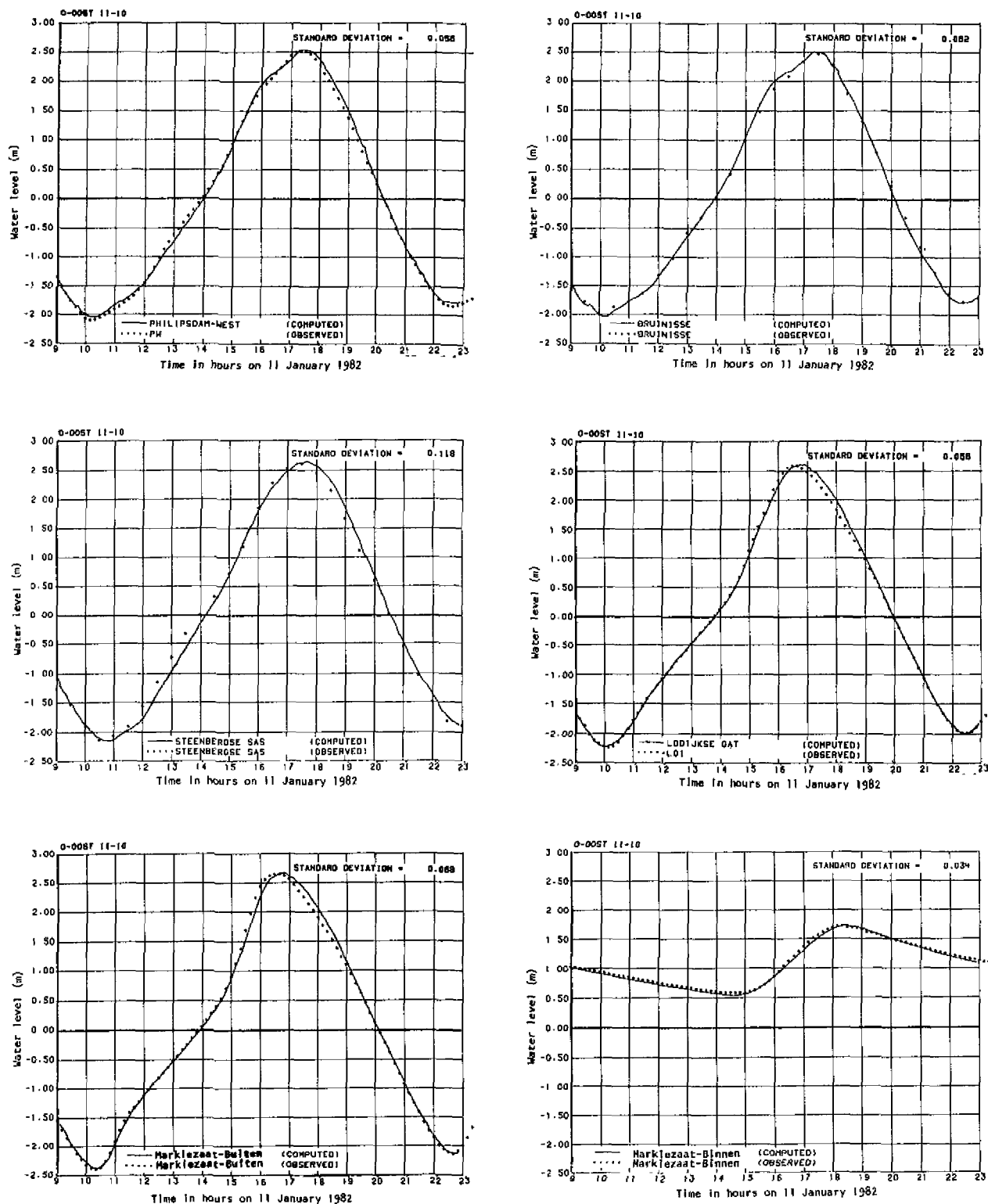
Fig. 16—Observed and computed water levels in the O-OOST-II model with properly
modeled tidal prism of the Eendracht: (a) Philipsdam-West,
(b) Bruinisse, (c) Steenbergse Sas, (d) Lodijkse-Gat,
(e) Markiezaat-Buiten, (f) Markiezaat-Binnen

VIII. VERIFICATION SIMULATION

The verification simulation was made in the baroclinic mode of the computation system; thus the effects of density gradients were taken into account. For the starting condition of the simulation in this mode, a salinity field as input is required. As no field data were available for 11 January 1982, a salinity field was used that represented an average of a large number of surveys. In this verification simulation the bottom stress was also made a function of the salinity gradient according to Eq. (12). The verification simulation used the same open boundary conditions as the simulation described in Chapter V.

The results of the verification simulation are being used to derive boundary conditions for the submodels shown in Fig. 2. These models are representing 1982 conditions; thus for consistency, the OOST-II model should also reflect these conditions for this area.

Thus, the bathymetry of the OOST-II model near the storm-surge barrier was modified from the 1976 condition to the 1982 condition in such a manner that the area of all north/south cross-sections of the models were in agreement with each other.

The agreement between observed and computed water levels is good, as shown in Fig. 17, for six stations. A comparison of observed and computed water levels for all available stations is shown in Appendix C. In general, the agreement between observed and computed is slightly better for this simulation than for the constant density simulation.

The computed mass transport rates in the verification simulation are now in very close agreement with the observations as shown in Fig. 18 and in Appendix D. To analyze the propagation of overtides and their generation in the system, a Fourier analysis was made of observed and computed water levels at all available stations. The results are shown in Tables 5 and 6.

In Appendix E, the observed and computed tides for all stations are shown together with the main tidal components. The observed and computed tides, as well as the semidiurnal tidal components, are shown on a scale of -4.00 m to $+4.00$ m. The fourth, sixth, eighth, and tenth component are shown on a scale 10 times as large. By reviewing these figures, errors in tidal wave propagation and generation of overtides can easily be noted.

It is apparent that, in general, the computed quarter-diurnal tide has the largest deviation from the observed component of all overtides considered. This is to be expected as this component is generated by the nonlinearities of advection and by the exposed water surface area as a function of water level.

The advection is not well represented in the long-wave equations that are being used in the model. In the formulation, it is assumed that the horizontal velocities are uniform in any vertical, which is naturally not the case. The largest deviations from this assumption are in areas with fresh water discharges where the estuary is not well mixed, as in the northeastern part of the system (Volkerak).

The results of the simulation also give considerable insight into the horizontal mixing processes. In Appendix F the hourly salinity distributions are shown. It can be noted by following the iso-contour line for 28 kg/m^2 over the time period from 11:00 hours to 17:00 hours on 11 January 1982 that water with a lower salinity coming out of the Volkerak during ebb is moved during flood toward the southeast until it finally mixes into water of a higher salinity.

In the graphs of Appendix F, the areas that are flooded and participate at that time in the hydrodynamic computations are indicated by a single dot. To give an impression of how
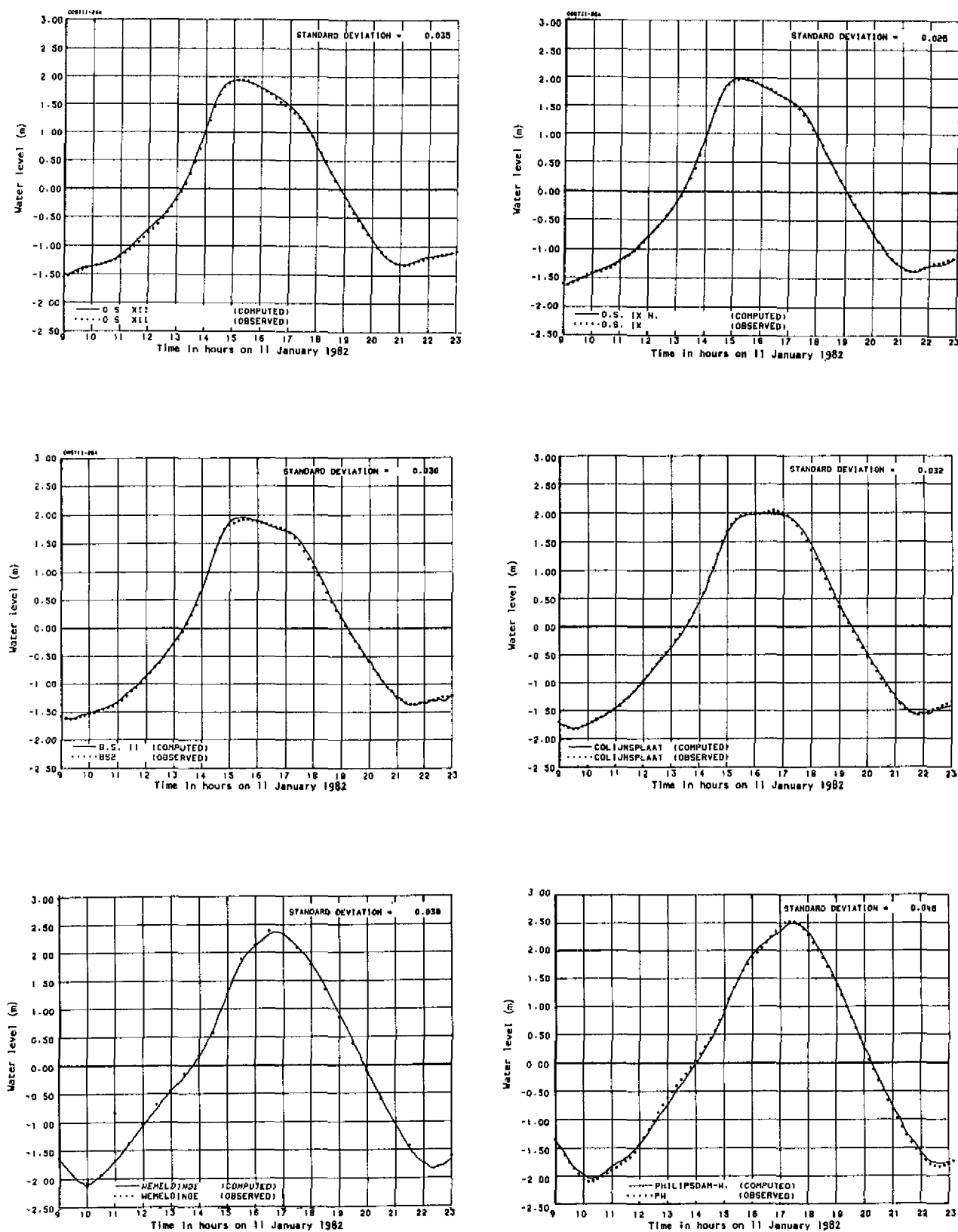
34

Fig. 17—Observed and computed water levels at stations in the Eastern
Scheldt: (a) OS12, (b) OS9, (c) Vlietepolder, (d) Colijnsplaat,
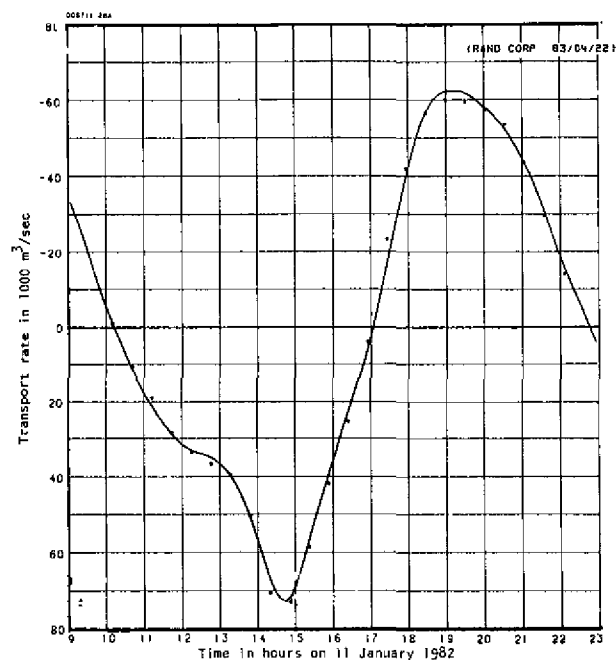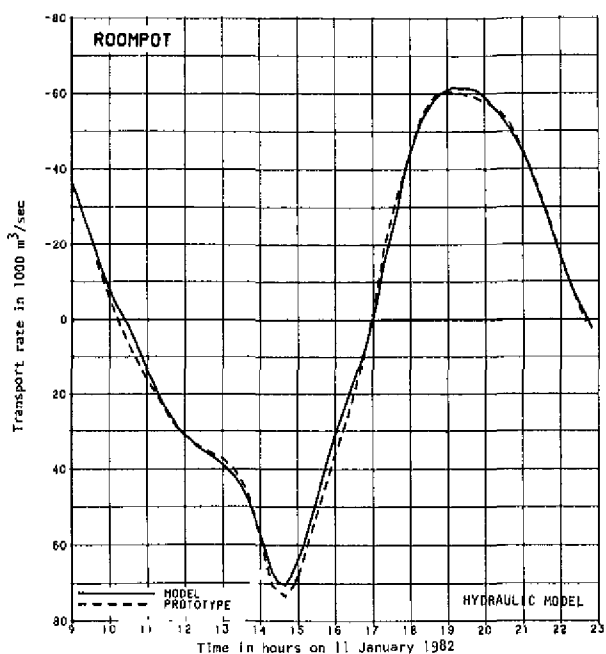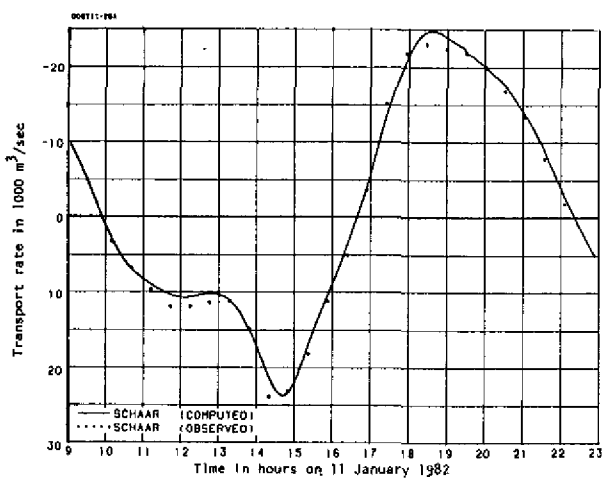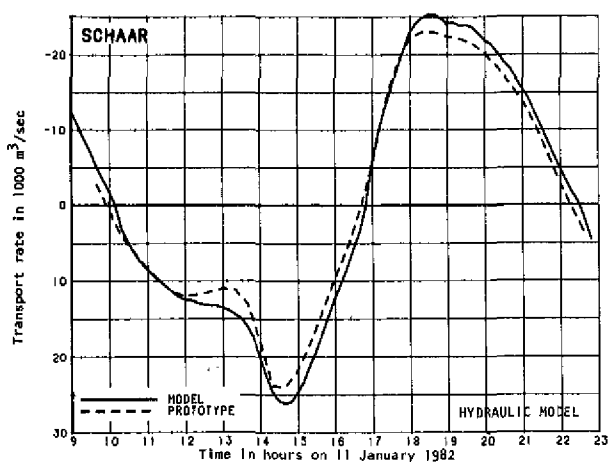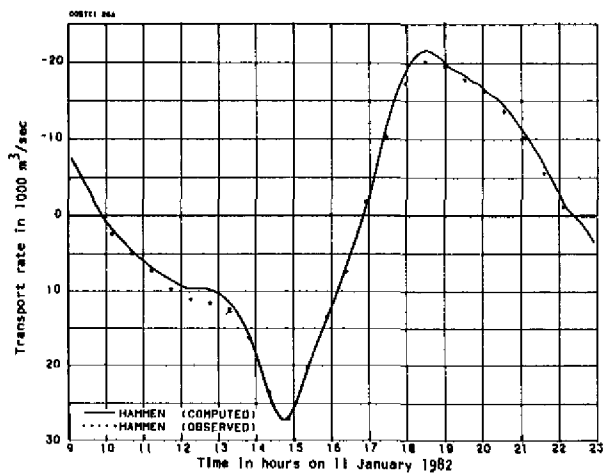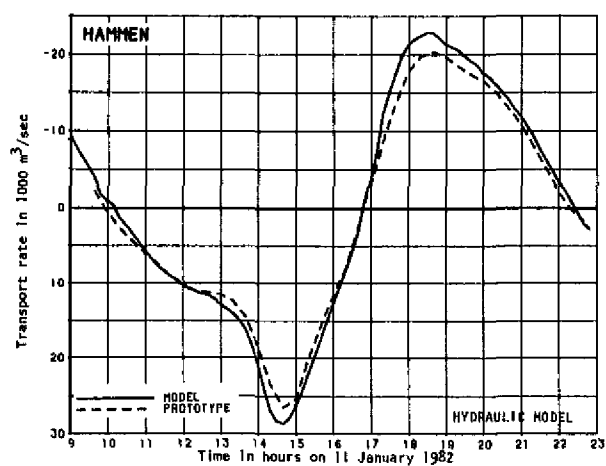(e) Wemeldinge, (f) Philipsdam-W (verification simulation)

Fig. 18—Transport rates through Hammen, Schaar, and Roompot in the hydraulic model
and the computational model compared to the observed transport rates
(verification simulation)

Table 5

OBSERVED AND COMPUTED MEAN WATER LEVELS AND TIDAL AMPLITUDES
(Verification simulation)

Station	Mean		M_2		M_4		M_6		M_8		M_{10}	
	Obs.	Comp.	Obs.	Comp.	Obs.	Comp.	Obs.	Comp.	Obs.	Comp.	Obs.	Comp.
OS12	0.064	0.084	1.624	1.630	0.288	0.274	0.138	0.133	0.068	0.060	0.076	0.089
OS9	0.108	0.108	1.687	1.690	0.242	0.232	0.128	0.126	0.056	0.065	0.085	0.084
Vlietepolder	0.061	0.110	1.775	1.766	0.204	0.197	0.102	0.095	0.062	0.070	0.097	0.081
Colijnsplaat	0.090	0.093	1.836	1.836	0.214	0.194	0.044	0.049	0.032	0.042	0.085	0.080
Wemeldinge	0.148	0.140	1.998	2.011	0.186	0.181	0.158	0.134	0.046	0.036	0.017	0.020
Markiezaat-Bui	0.146	0.162	2.145	2.119	0.221	0.193	0.277	0.272	0.053	0.051	0.069	0.069
Markiezaat-Bin	1.110	1.077	0.526	0.522	0.128	0.122	0.083	0.072	0.003	0.012	0.014	0.007
Lodijkse Gat	0.140	0.155	2.100	2.090	0.221	0.213	0.212	0.209	0.049	0.039	0.027	0.026
Philipsdam West	0.158	0.163	2.115	2.102	0.206	0.202	0.085	0.062	0.014	0.028	0.038	0.035
Steenbergse Sas	0.205	0.163	2.196	2.223	0.208	0.146	0.148	0.131	0.028	0.036	0.017	0.017
Bruinisse	0.170	0.185	2.053	2.073	0.215	0.180	0.060	0.049	0.017	0.049	0.050	0.039
Zeelandbrug-N	0.124	0.140	1.866	1.856	0.172	0.149	0.057	0.060	0.042	0.051	0.087	0.075
BS2	0.097	0.108	1.705	1.718	0.225	0.208	0.085	0.093	0.049	0.061	0.088	0.086
OS4	0.084	0.107	1.675	1.687	0.240	0.226	0.108	0.108	0.058	0.063	0.088	0.083

Table 6

OBSERVED AND COMPUTED PHASE LAGS
(Verification simulation)

Station	M_2		M_4		M_6		M_8		M_{10}	
	Obs.	Comp.	Obs.	Comp.	Obs.	Comp.	Obs.	Comp.	Obs.	Comp.
OS12	83.4	81.7	77.7	77.2	3.2	1.8	26.9	23.1	13.2	6.4
OS9	91.3	90.4	84.3	83.9	12.1	9.8	25.9	17.6	17.6	18.6
Vlietepolder	100.3	100.7	96.0	101.5	20.7	17.3	25.5	29.1	19.1	24.6
Colijnsplaat	112.1	113.6	125.4	129.1	54.6	46.0	46.4	36.5	31.5	34.6
Wemeldinge	132.5	133.4	173.5	178.1	110.9	104.9	68.2	61.6	52.9	42.7
Markiezaat-Bui	141.9	149.5	193.4	209.2	116.1	121.8	94.3	85.9	111.6	122.9
Markiezaat-Bin	298.1	300.4	217.8	223.5	190.7	193 0	105.7	82.5	12.6	11.5
Lodijkse Gat	136.2	141.6	182.5	196.4	111.4	113.3	96.4	91.8	105.6	112.9
Philipsdam West	154.0	155.9	213.0	204.4	158.4	153.3	74.7	51.7	50.6	65.9
Steenbergse Sas	166.2	171.3	234.4	217.1	160.1	171.4	112.1	84.3	113.8	131.1
Bruinisse	153.0	151.0	207.8	203.5	151.8	132.4	35.8	54.3	52.7	61.6
Zeelandbrug-N	119.3	121.5	130.7	137.2	54.7	53.9	42.7	37.5	32.9	40.8
BS2	102.3	101.6	92.6	94.4	19.7	17.2	31.6	29.6	22.5	23.7
OS4	97.7	96.0	85.8	86.5	16.4	12.6	31.8	24.8	20.9	19.3

the water flows at the considered time, velocity vectors are also shown at every other grid point in each direction.

In Appendix G, the computed hourly velocity fields are shown. The contour lines on the graphs of this appendix are contours of equal velocity. As the velocities are zero along shore and the contour values are shown in the right top corner of the figure, the appropriate values for each contour line can easily be established.

IX. DISCUSSION

It has been shown in the simulation with constant density and in the verification simulation that a good agreement between observed and computed water levels can be obtained. The agreement is very comparable with that obtained with the hydraulic model experiments. The computed transport rates through the Hammen, Schaar, and Roompot are in very close agreement with rates obtained from observation. The computed transport rates are in closer agreement with the observed rates than the results of the hydraulic model simulation.

From these results we may conclude that the mathematical formulation, as well as the modeling techniques that were developed, are suitable for engineering studies.

In contrast with the hydraulic model experiments, it was not necessary to determine boundary conditions for the model by trial and error. The cross-spectral method that was used for the determination of boundary conditions appeared to work very effectively. Contributing to its success was undoubtedly the extensive experience with this type of estimating technique that the research and development team obtained over the years.

Even though transport rates and water levels are well in agreement with the prototype, one question as to the application of this boundary determination method is still unresolved, namely, the determination of the mean water level for each boundary station. This level was also found by use of the weighting functions described in Chapter IV. The mean levels of these boundary stations will influence residual flows in the flow channels that run from the model boundary to the three closure openings, but apparently not the total flow through the Hammen, Schaar, and Roompot.

This matter needs further investigation. Naturally, if tide gauge stations closer to the boundary were made available, or if the model boundary were moved closer to existing tide gauge stations, this problem would be reduced or eliminated.

The accuracy of results of the constant density simulation and the verification simulation is comparable, but the verification simulation results with a variable salinity field are slightly better.

For studies involving tidal velocities and water levels it is probably not warranted to compute also the salinity field with the possible exception of water levels in the Volkerak region. It is expected, however, that for studies involving residual currents the inclusion of the pressures resulting from salinity gradients would be required.

As indicated in the previous chapter, the quarter-diurnal tide has, in a few instances, a sizable error in relation to its amplitude. This is likely caused by the approximations made in the advection terms of the vertically averaged momentum equations. Errors in this approximation are particularly important in areas with a large salinity gradient, as occurring in the northeastern part of the system.

X. CONCLUSIONS

With the computational model a good agreement between observed and computed water levels as well as between observed and computed transport rates through the Hammen, Schaar, and Roompot is obtained. The agreement of the water levels in the computation is about the same as obtained with the hydraulic model. The computational model has a better representation of transport rates than the hydraulic model.

If the simulation is made in the baroclinic mode, when the effects of density gradients are taken into account, then the simulation results are slightly better than when a constant density is assumed.

If simulations are made with part of the model extending from the Zeelandbrug eastward, then the tidal records of Colijnsplaat and Zeelandbrug-N can be used directly if the area closer to the model boundary is not important. If this area is important, then corrections on the observed records have to be made.

If the model is to be used for studies related to the closures of the Oesterdam, then it is recommended that a one-dimensional representation of the Eendracht be used.

Appendix A

WATER LEVELS IN THE HYDRAULIC MODEL
AND THE COMPUTATIONAL MODEL
(Constant density computation)

The graphs showing the comparison between the hydraulic model results and the observed water levels are direct copies of the graphs contained in Ref. 10. The graphs showing the comparison of observed and computed water levels are parts of plots made by the SIMSYS2D or WAQUA system [4] to which we added the grid and the scales.

The standard deviations shown in the graphs of the computation results are for the period of 9 hours to 23 hours on 11 January 1982.

The locations of the stations can be found in Fig. 2. The computed water levels are plotted directly from the simulation and are averages over one timestep. No filters have been applied. The results of the hydraulic model were electronically filtered to remove high frequency fluctuations.
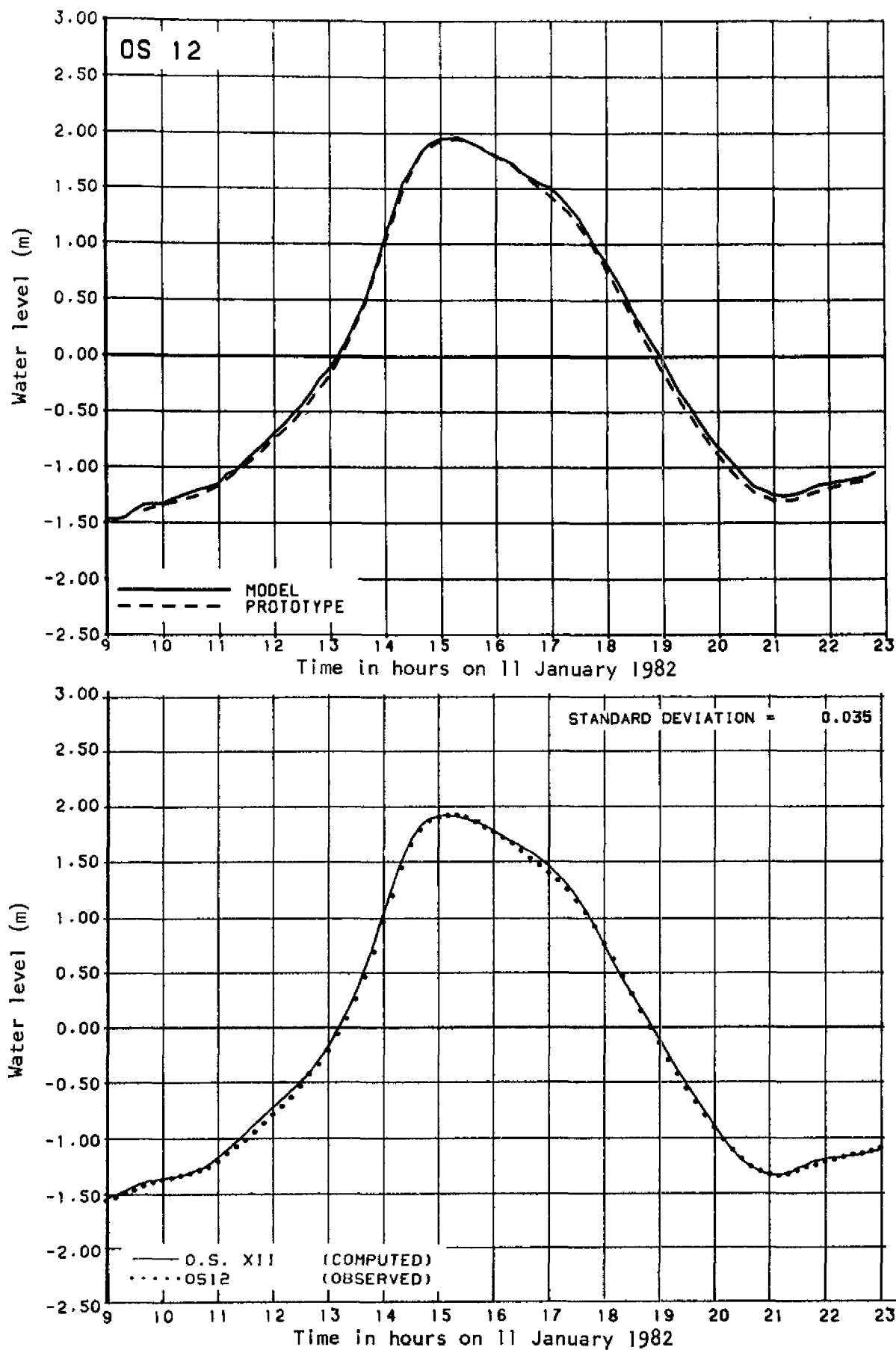
Fig. A.1—Water level at OS12 in the hydraulic model (top graph) and the computational model (bottom graph) compared to the observed water level
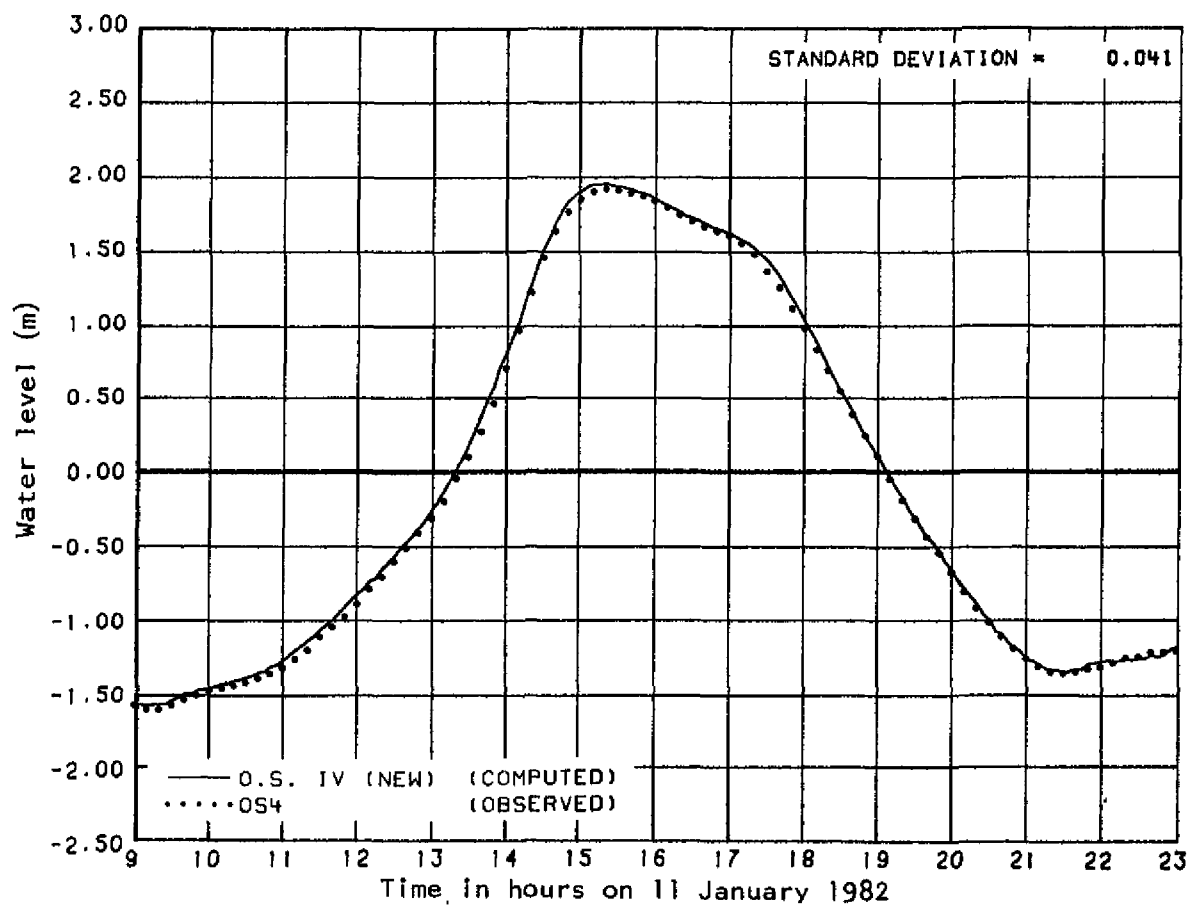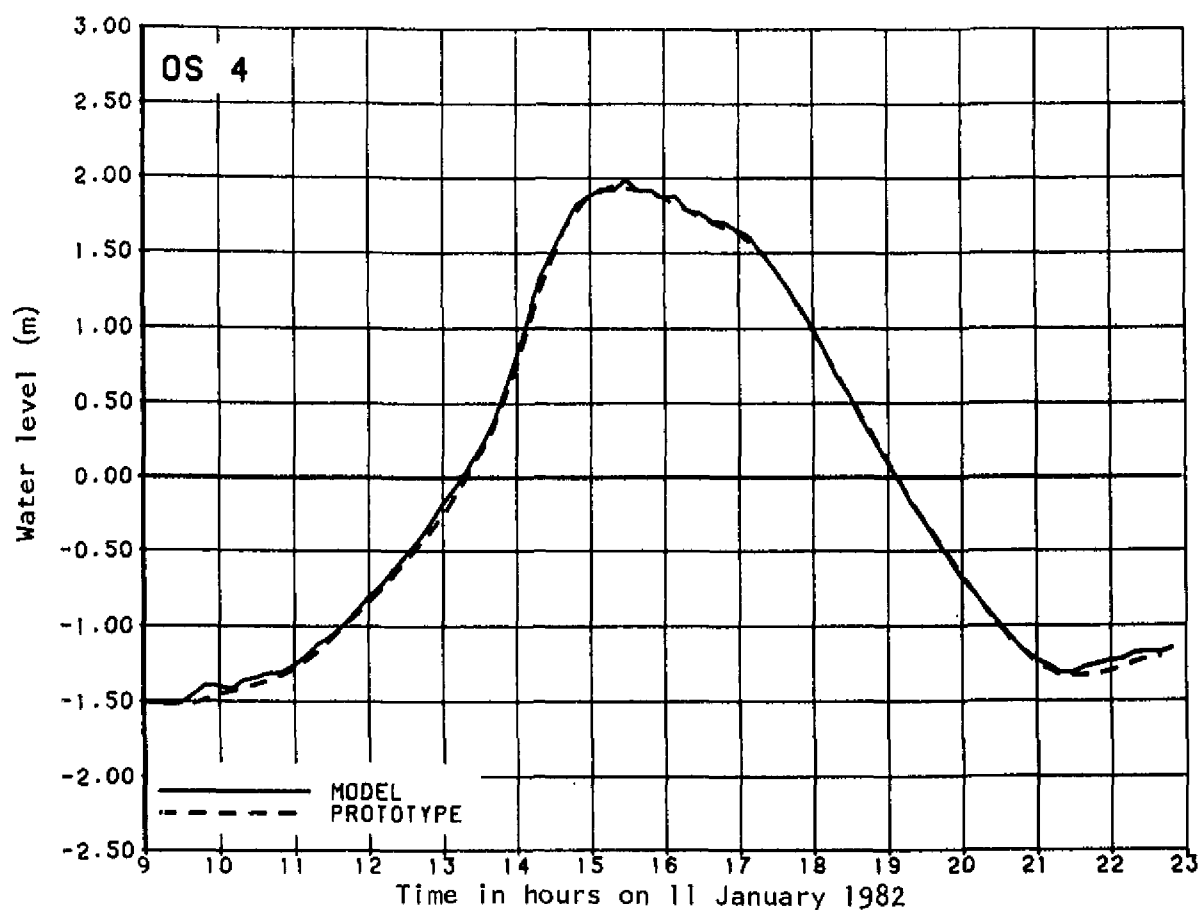
Fig. A.2—Water level at OS4 in the hydraulic model (top graph) and the computational model (bottom graph) compared to the observed water level
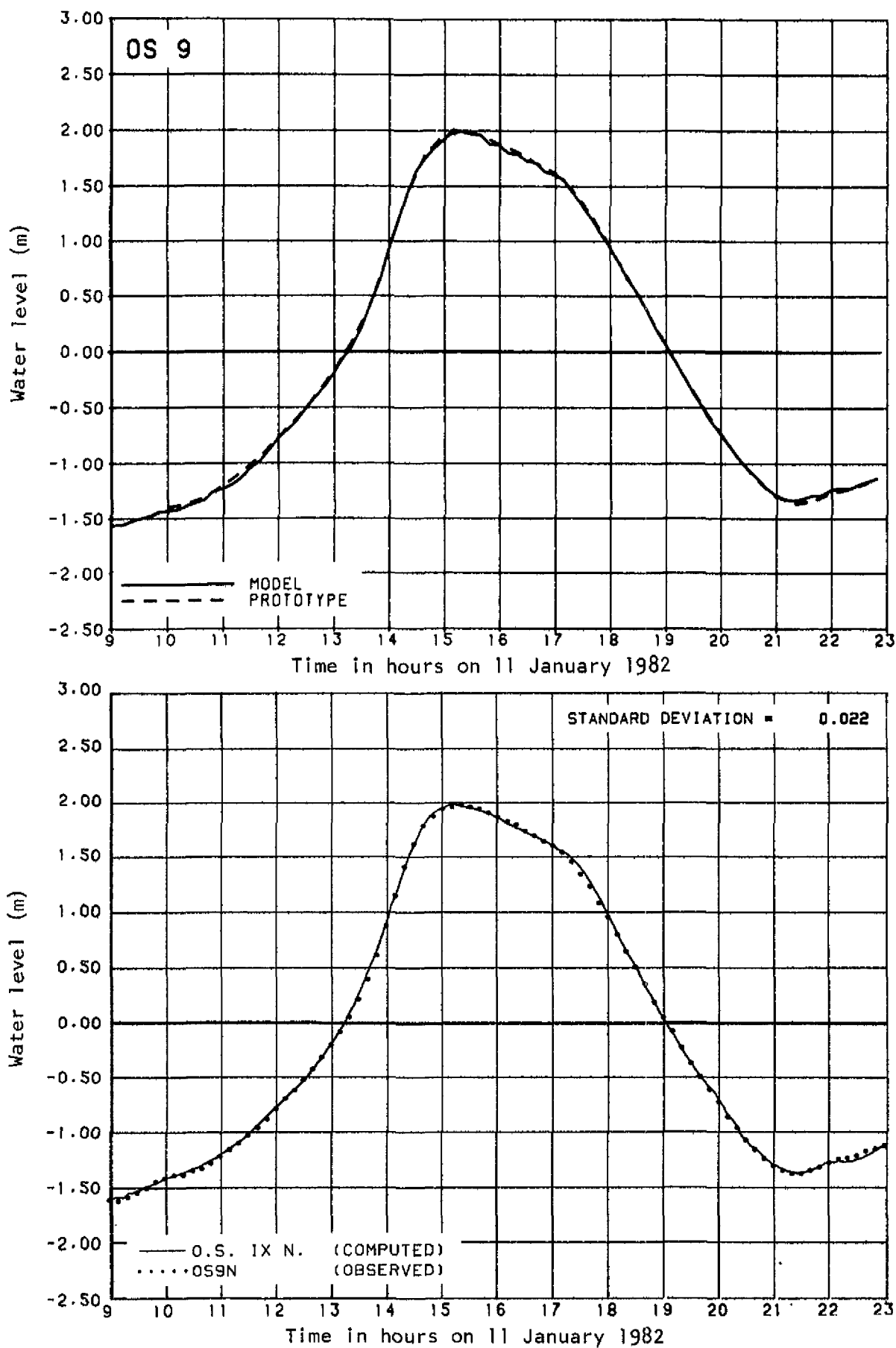
Fig. A.3—Water level at OS9 in the hydraulic model (top graph) and the computational model (bottom graph) compared to the observed water level
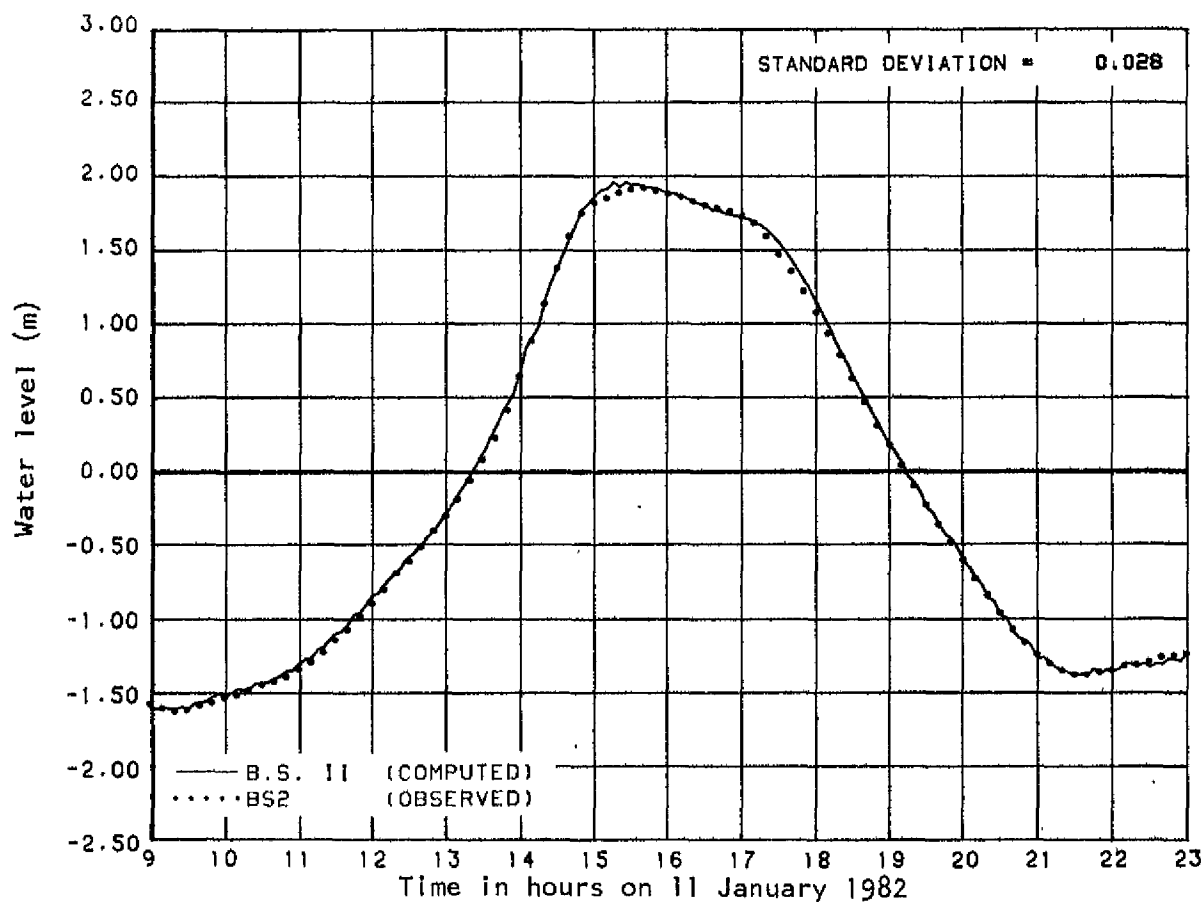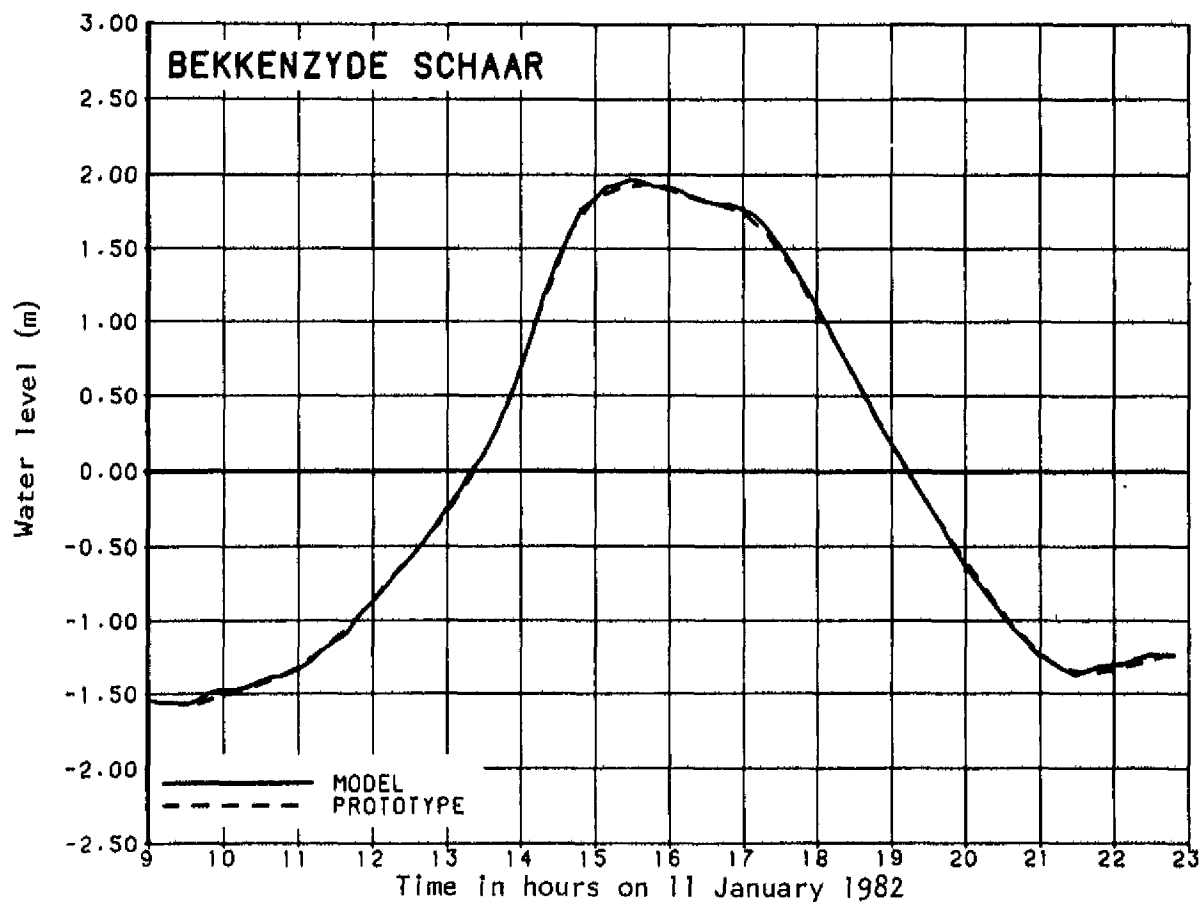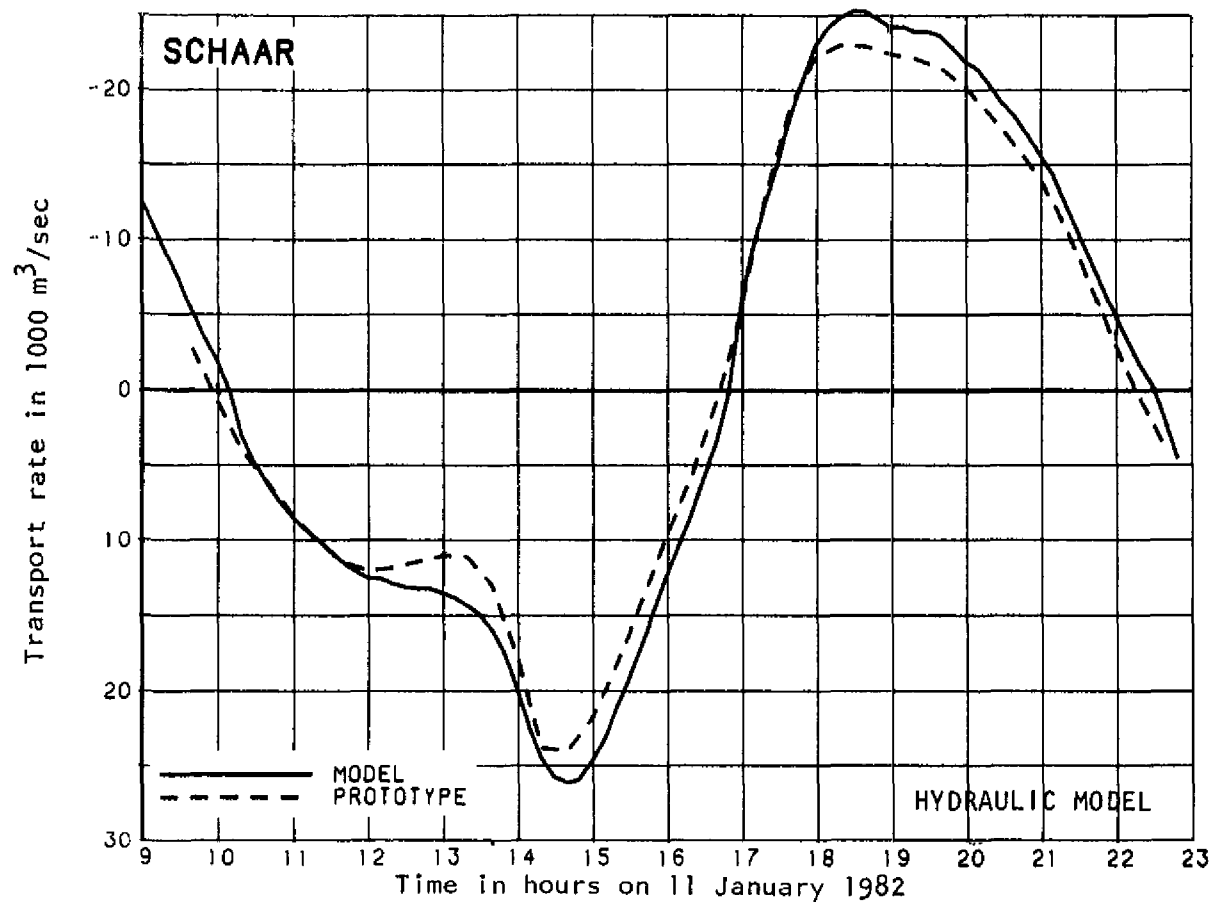
Fig. A.4—Water level at Bekkenzyde Schaar in the hydraulic model (top graph) and the computational model (bottom graph) compared to the observed water level
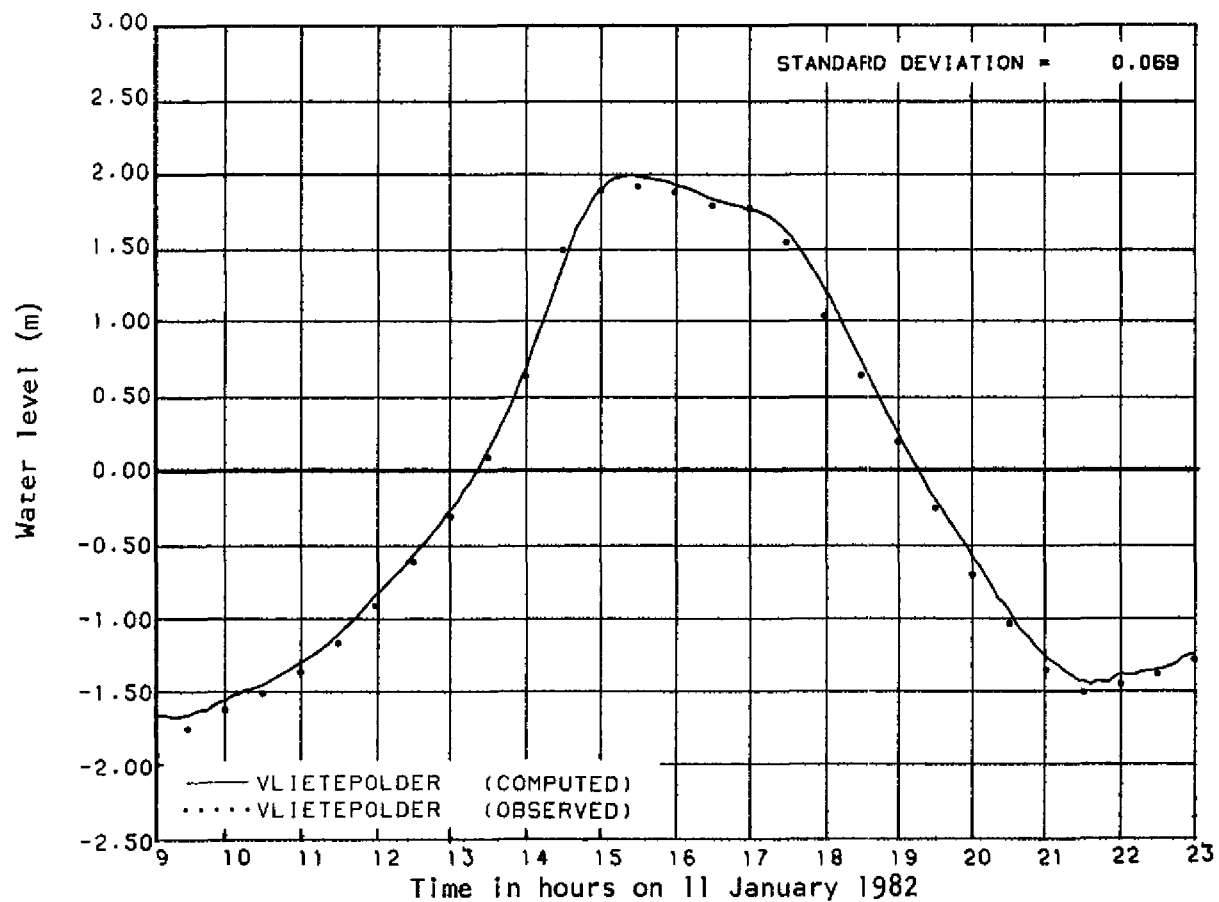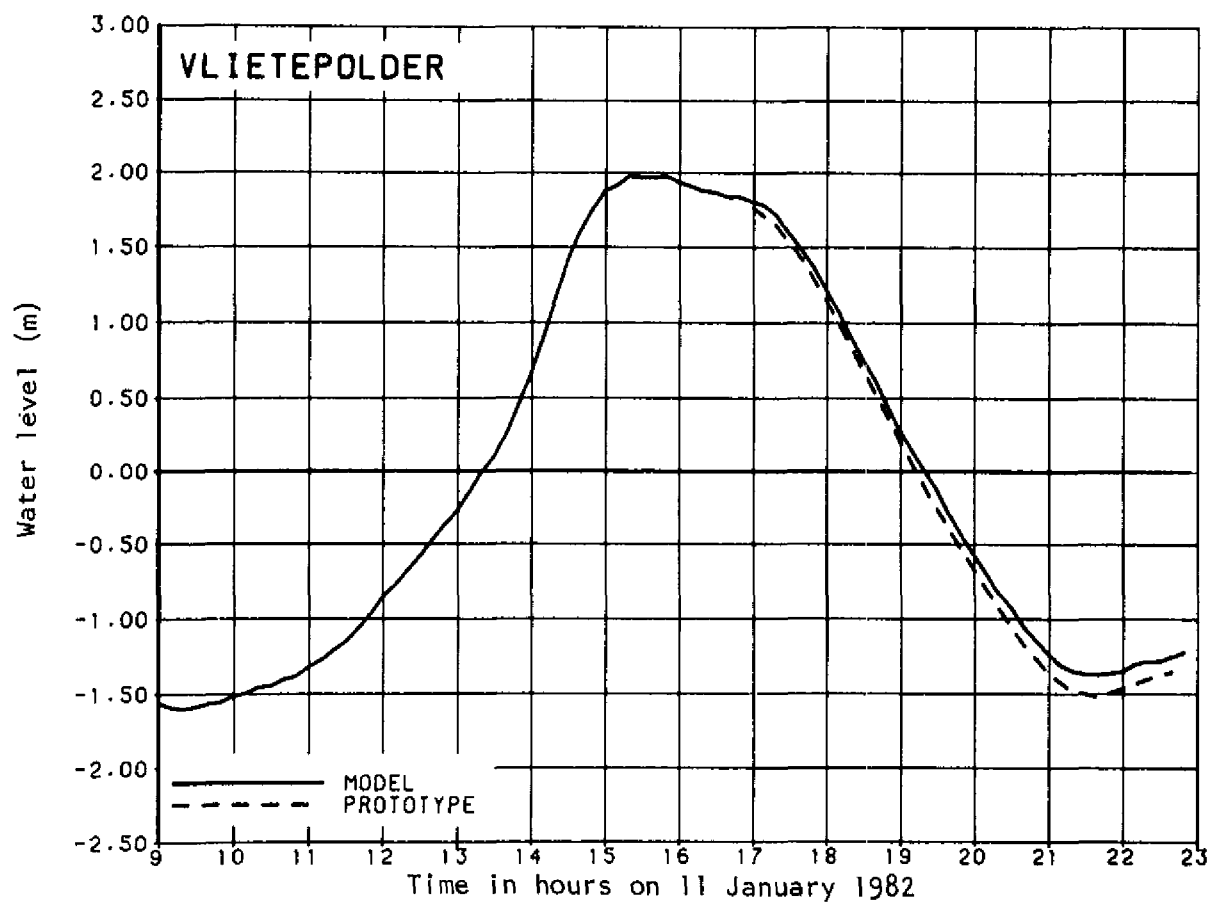
Fig. A.5—Water level at Vlietepolder in the hydraulic model (top graph) and the computational model (bottom graph) compared to the observed water level
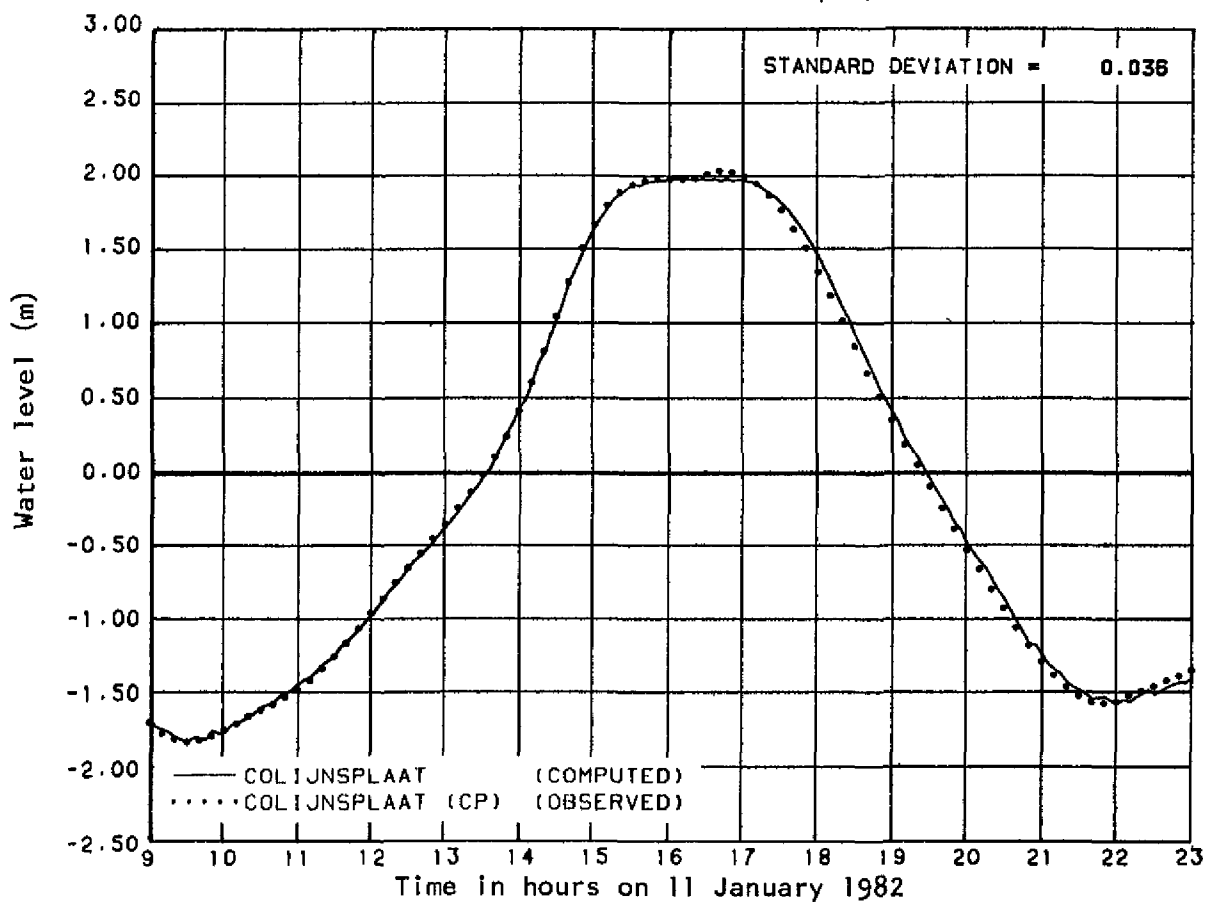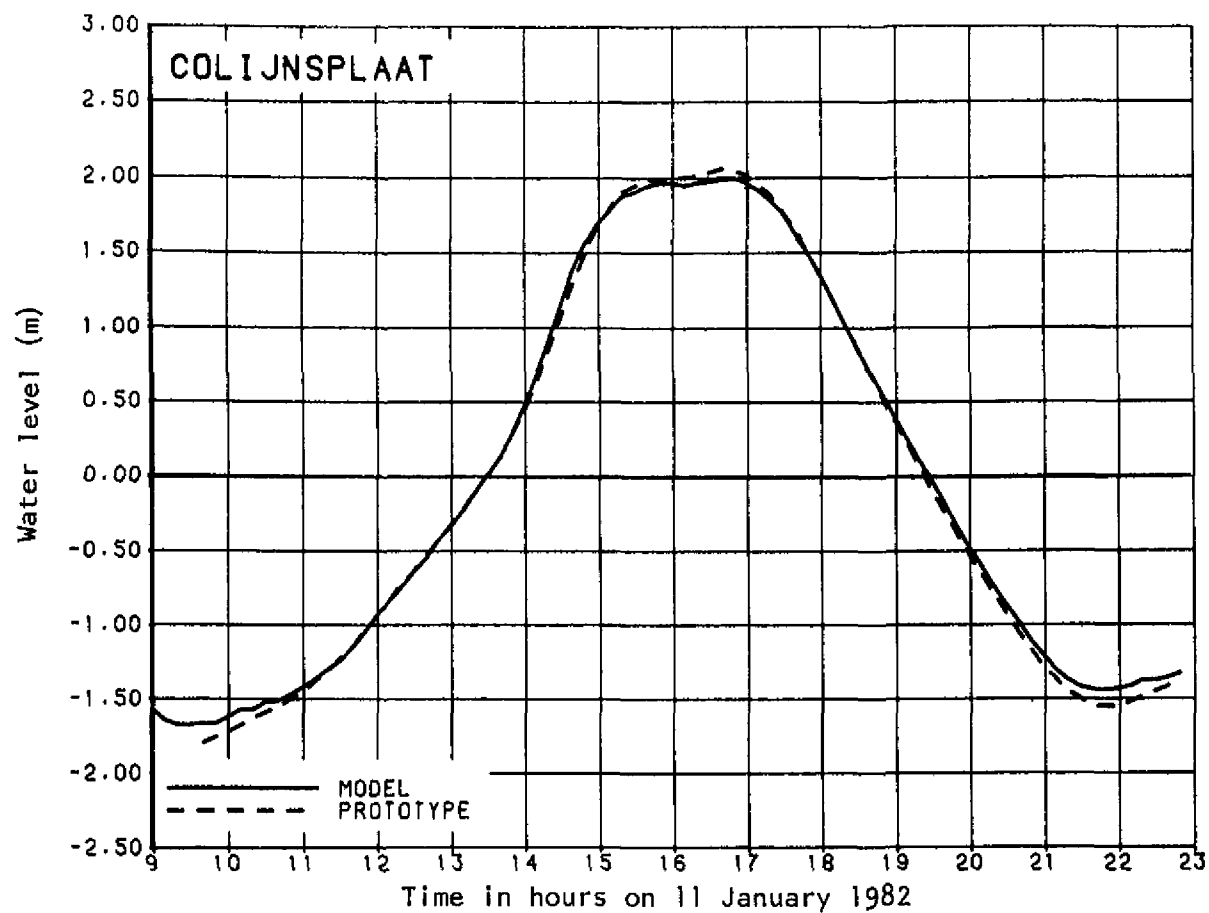
Fig. A.6—Water level at Colijnsplaat in the hydraulic model (top graph) and the computational model (bottom graph) compared to the observed water level
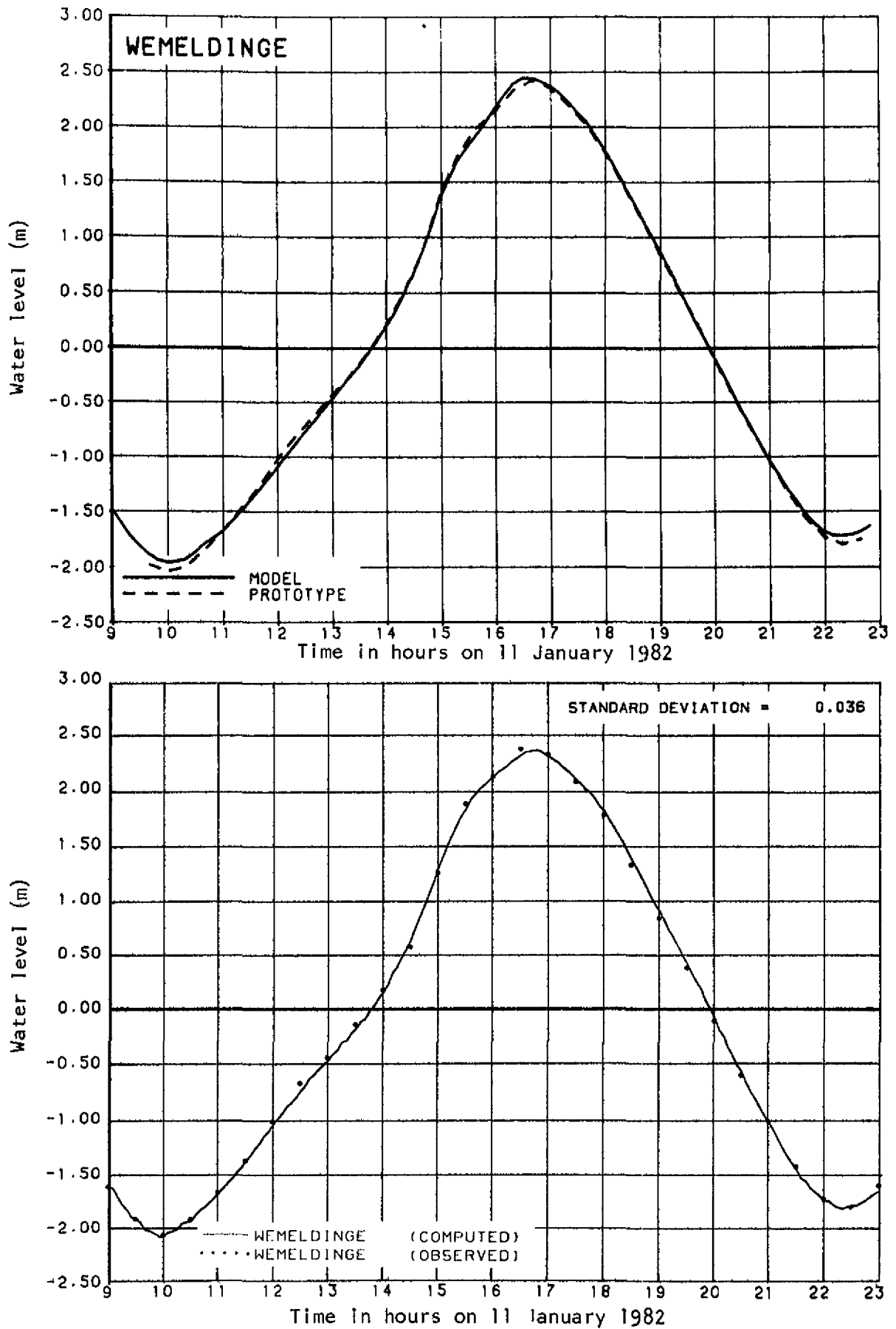
Fig. A.7—Water level at Wemeldinge in the hydraulic model (top graph) and the computational model (bottom graph) compared to the observed water level
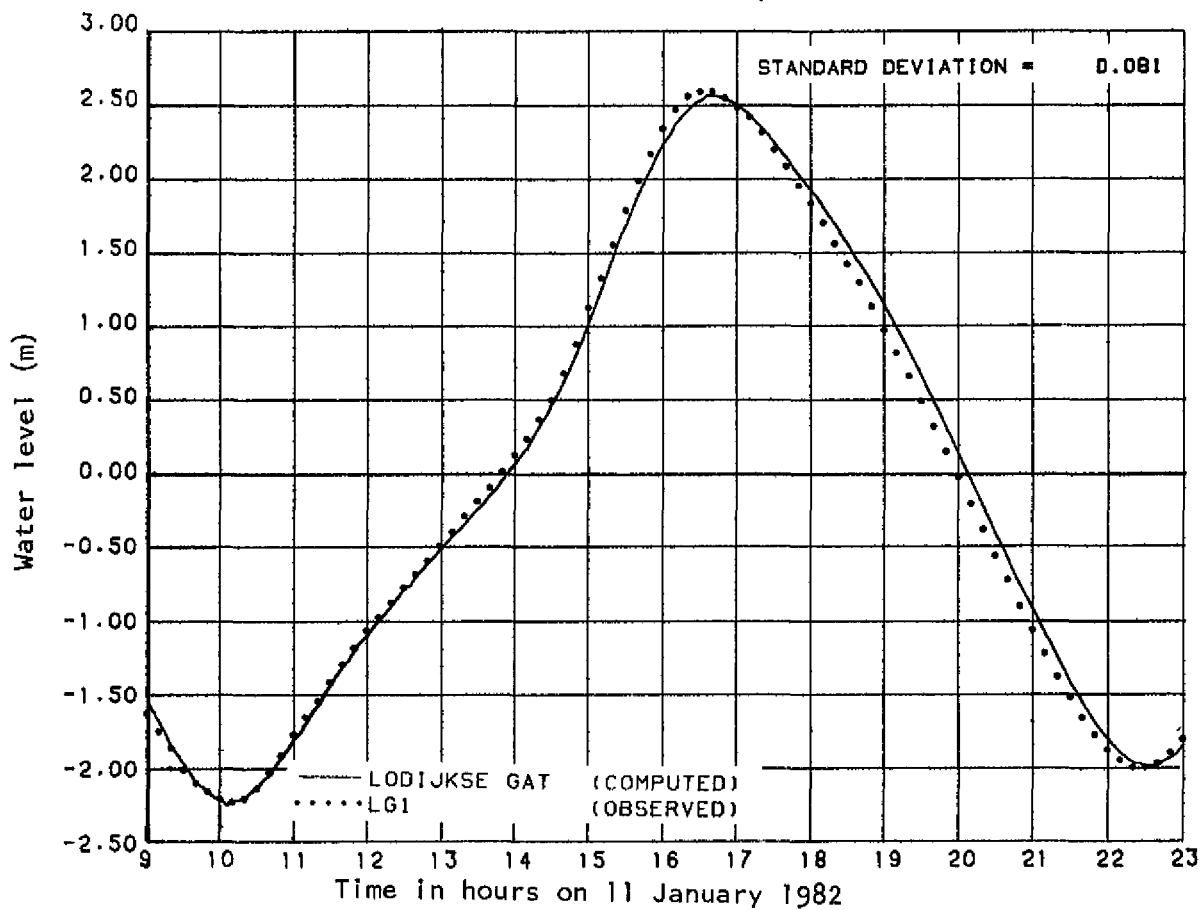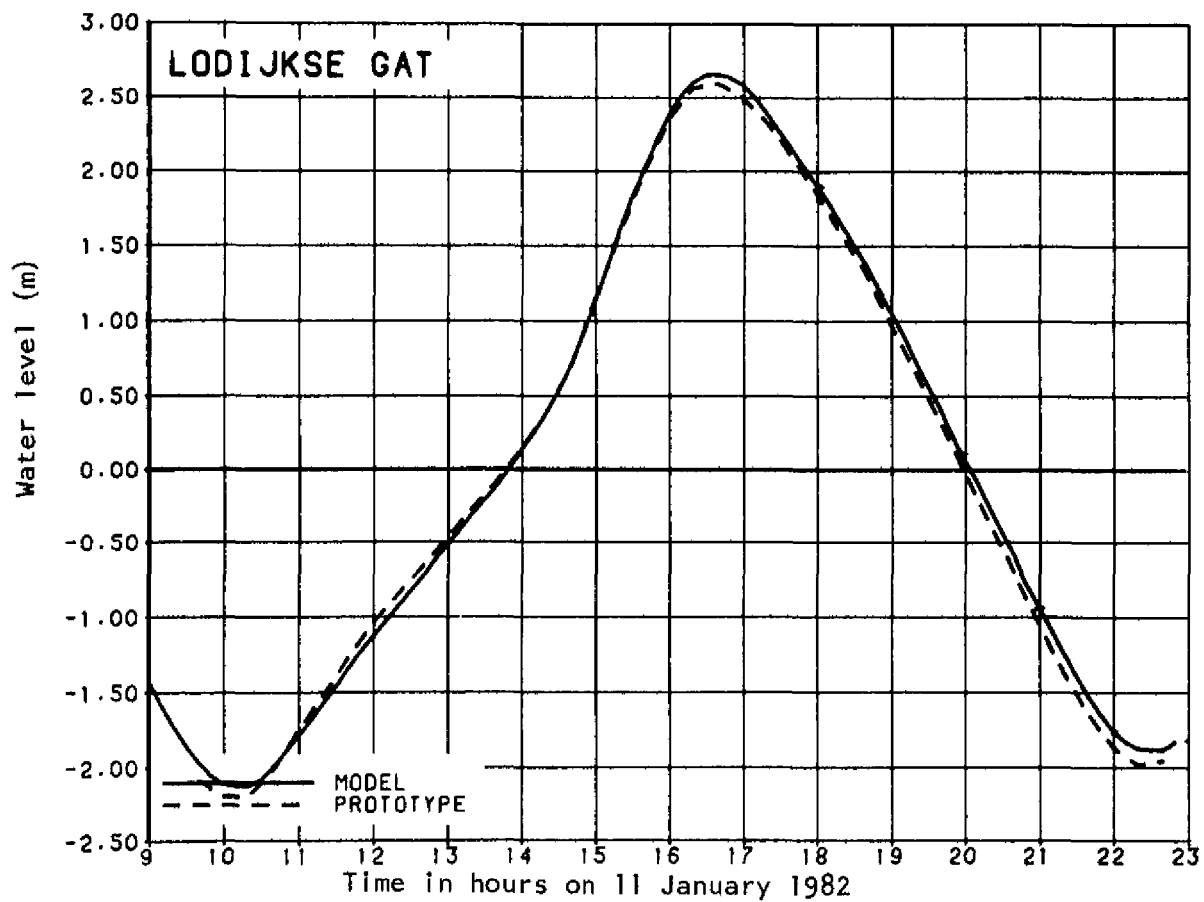
Fig. A.8—Water level at Lodijkse Gat in the hydraulic model (top graph) and the computational model (bottom graph) compared to the observed water level
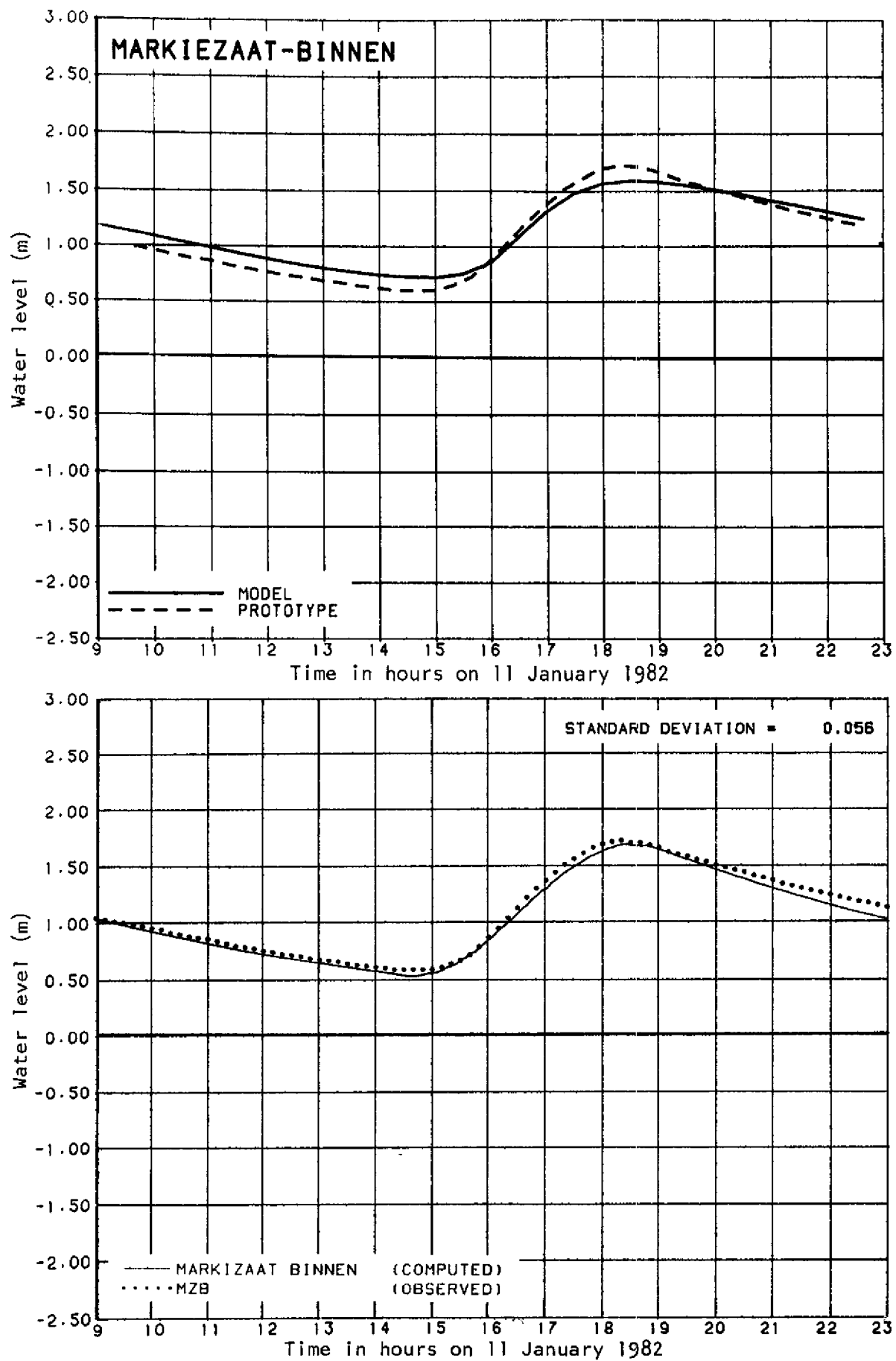
Fig. A.9—Water level at Markiezaat-Binnen in the hydraulic model (top graph) and the computational model (bottom graph) compared to the observed water level
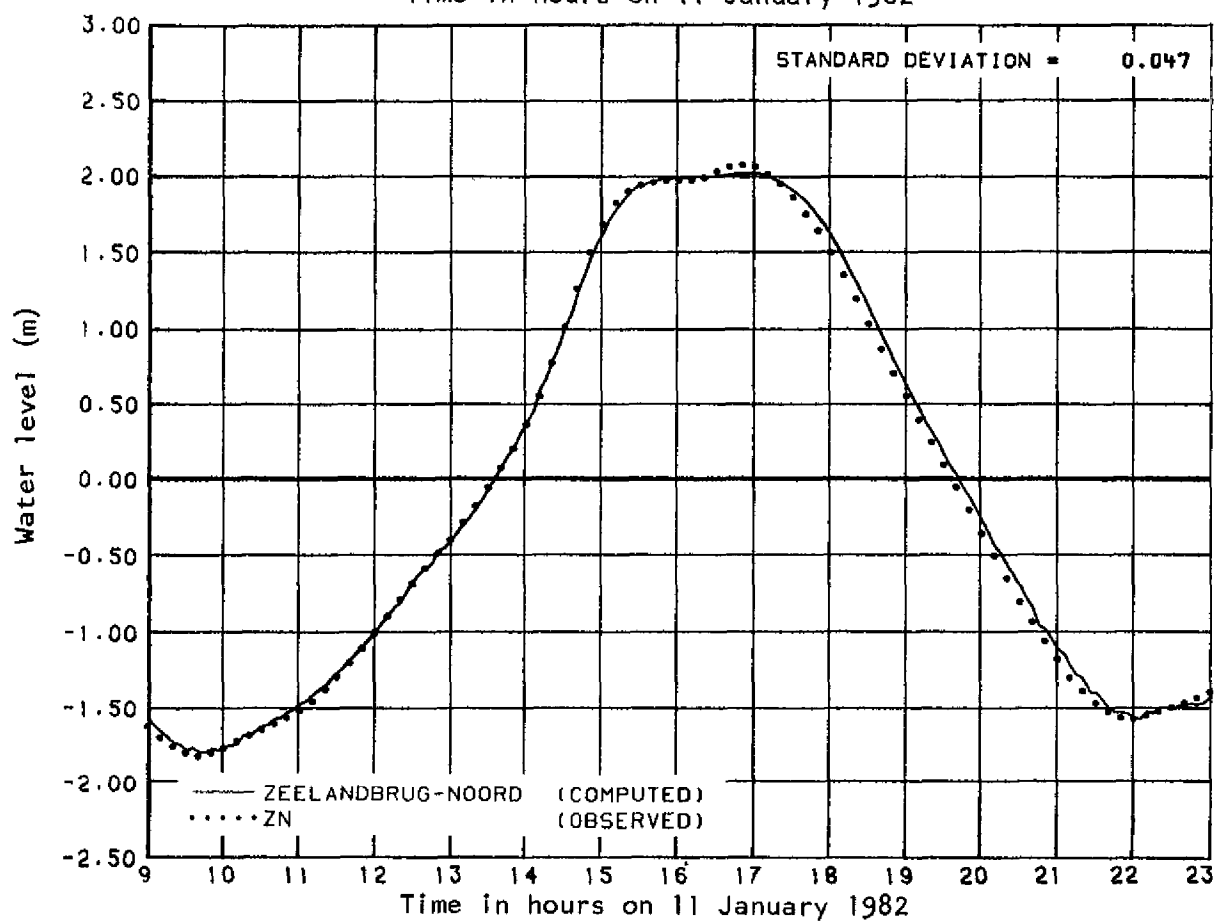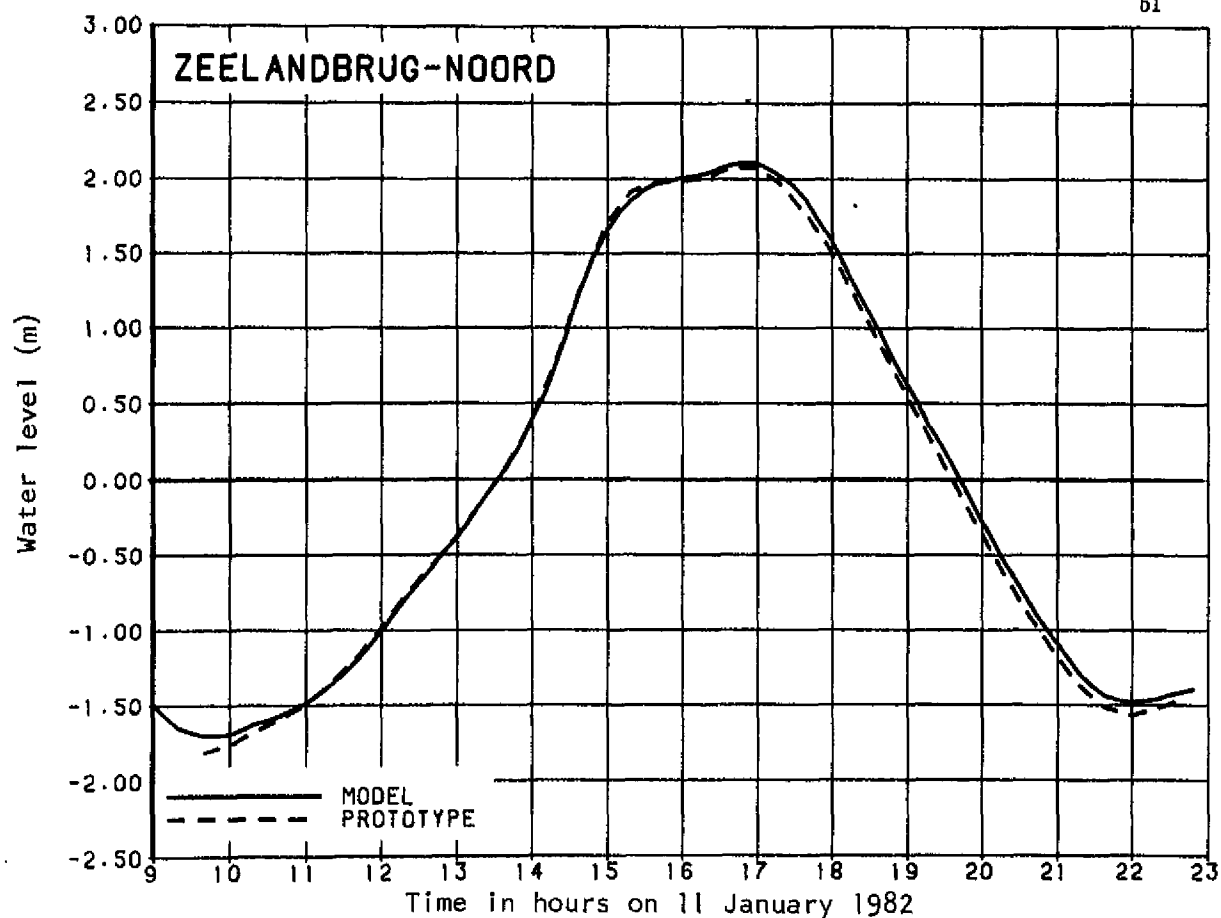
Fig. A.10—Water level at Zeelandbrug-Noord in the hydraulic model (top graph) and the computational model (bottom graph) compared to the observed water level
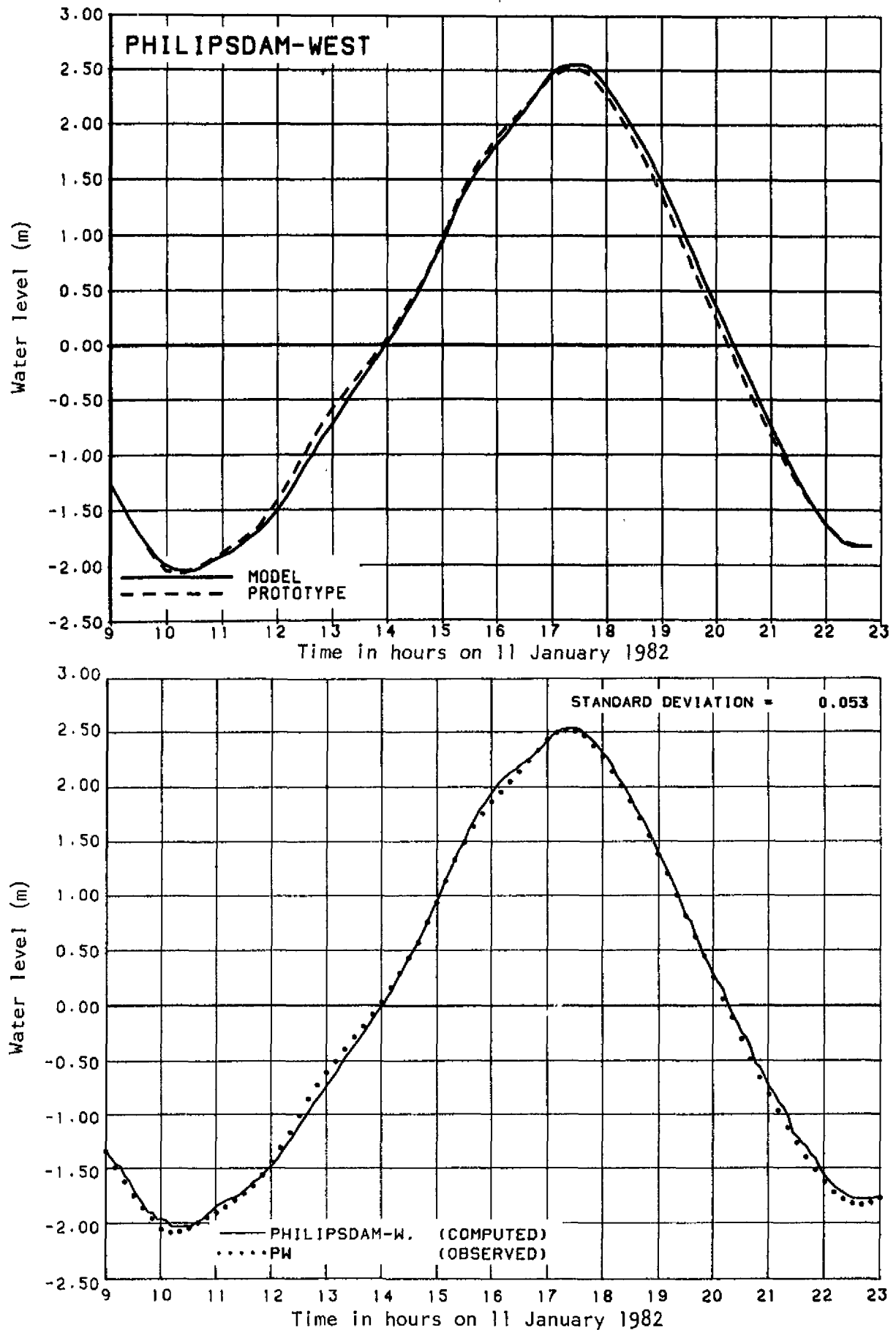
Fig. A.11—Water level at Philipsdam-West in the hydraulic model (top graph) and the computational model (bottom graph) compared to the observed water level
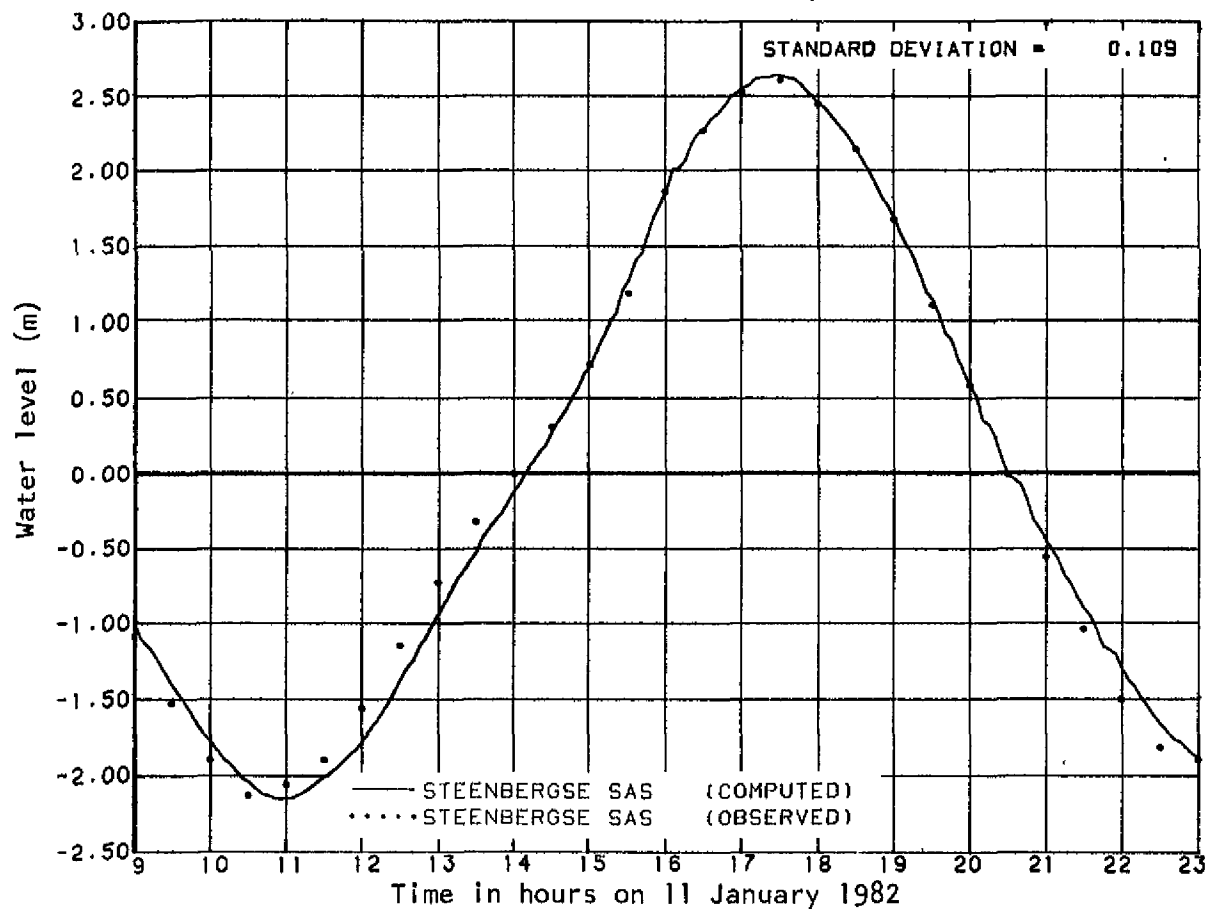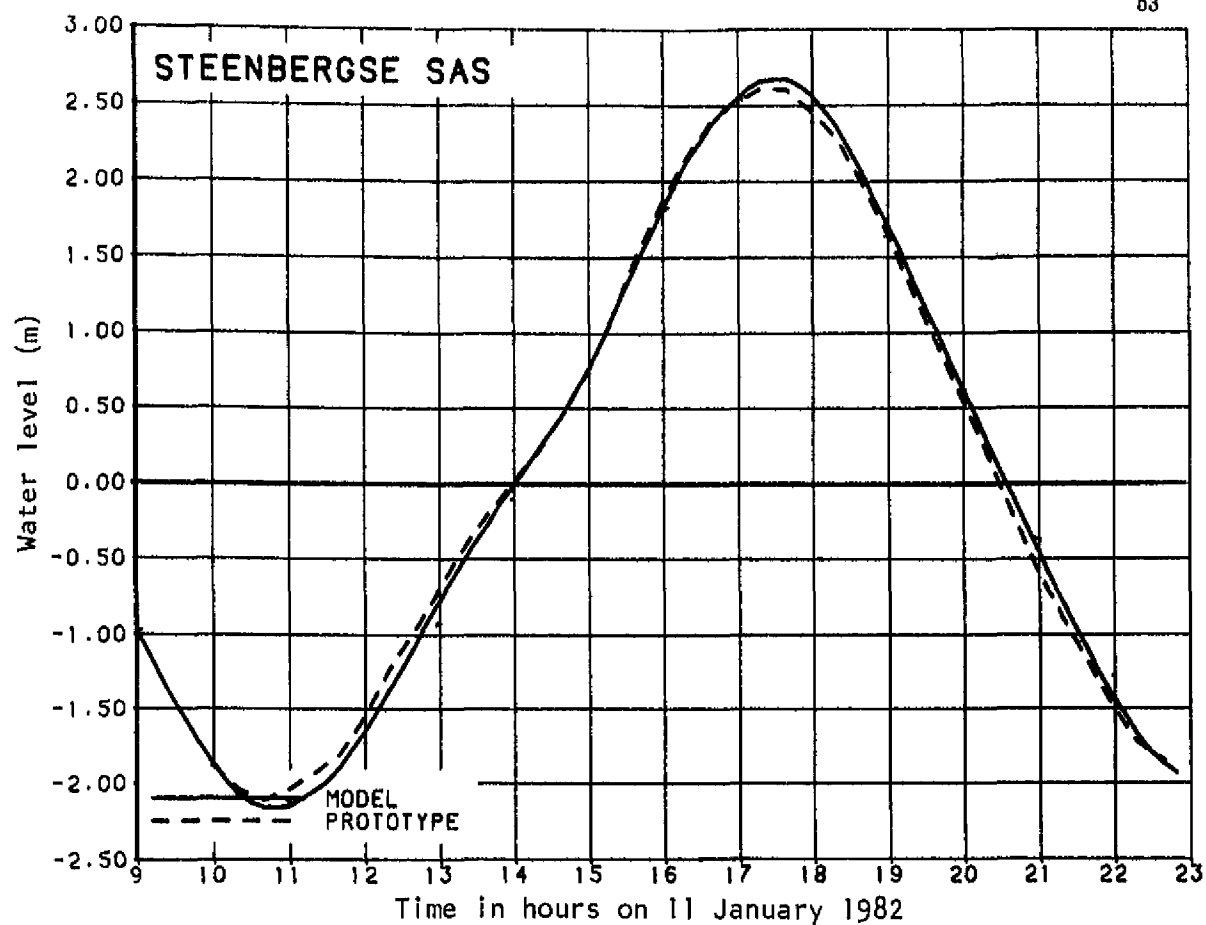
Fig. A.12—Water level at Steenbergse Sas in the hydraulic model (top graph) and the computational model (bottom graph) compared to the observed water level
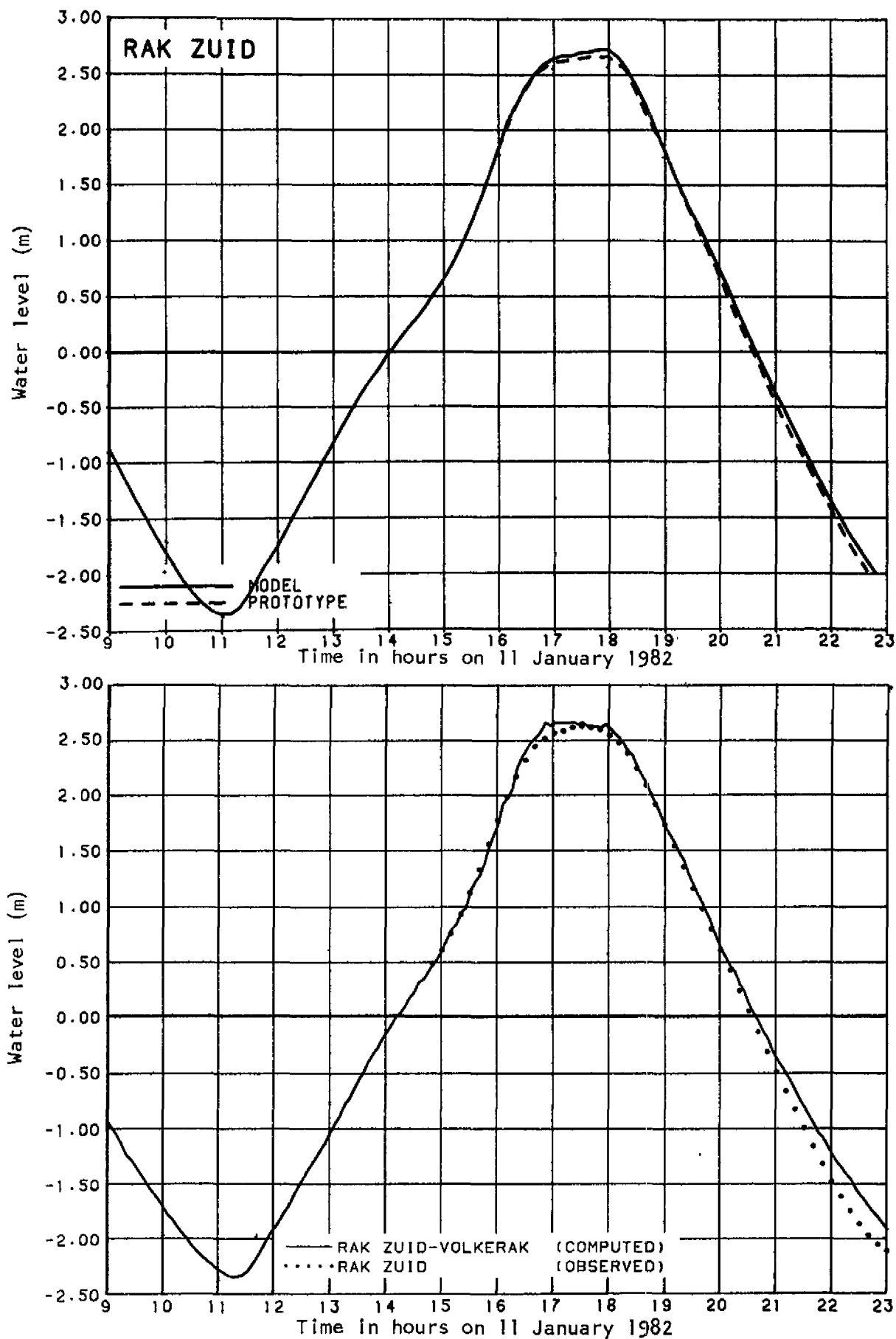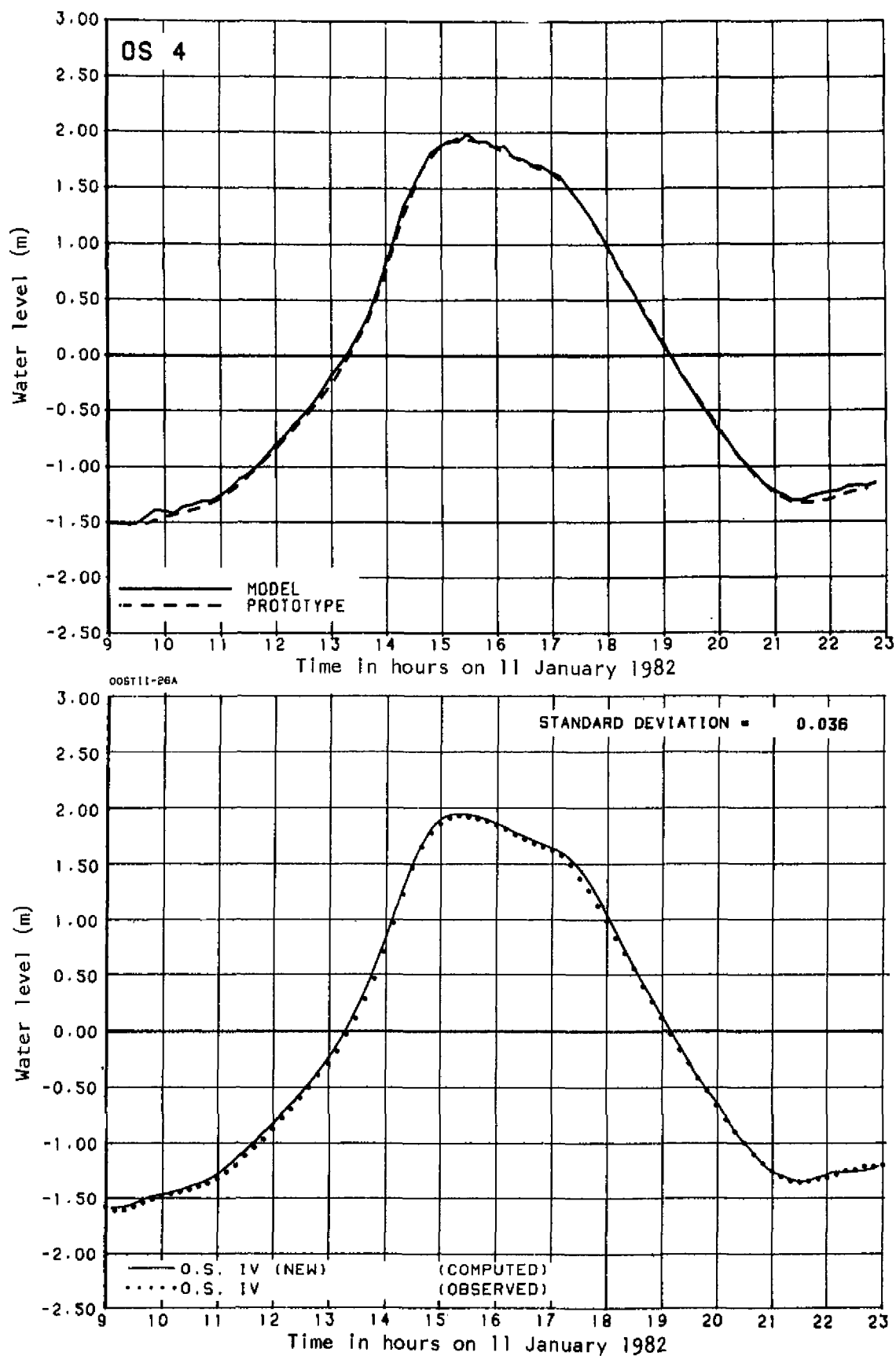
Fig. A.13—Water level at Rak Zuid in the hydraulic model (top graph) and the computational model (bottom graph) compared to the observed water level
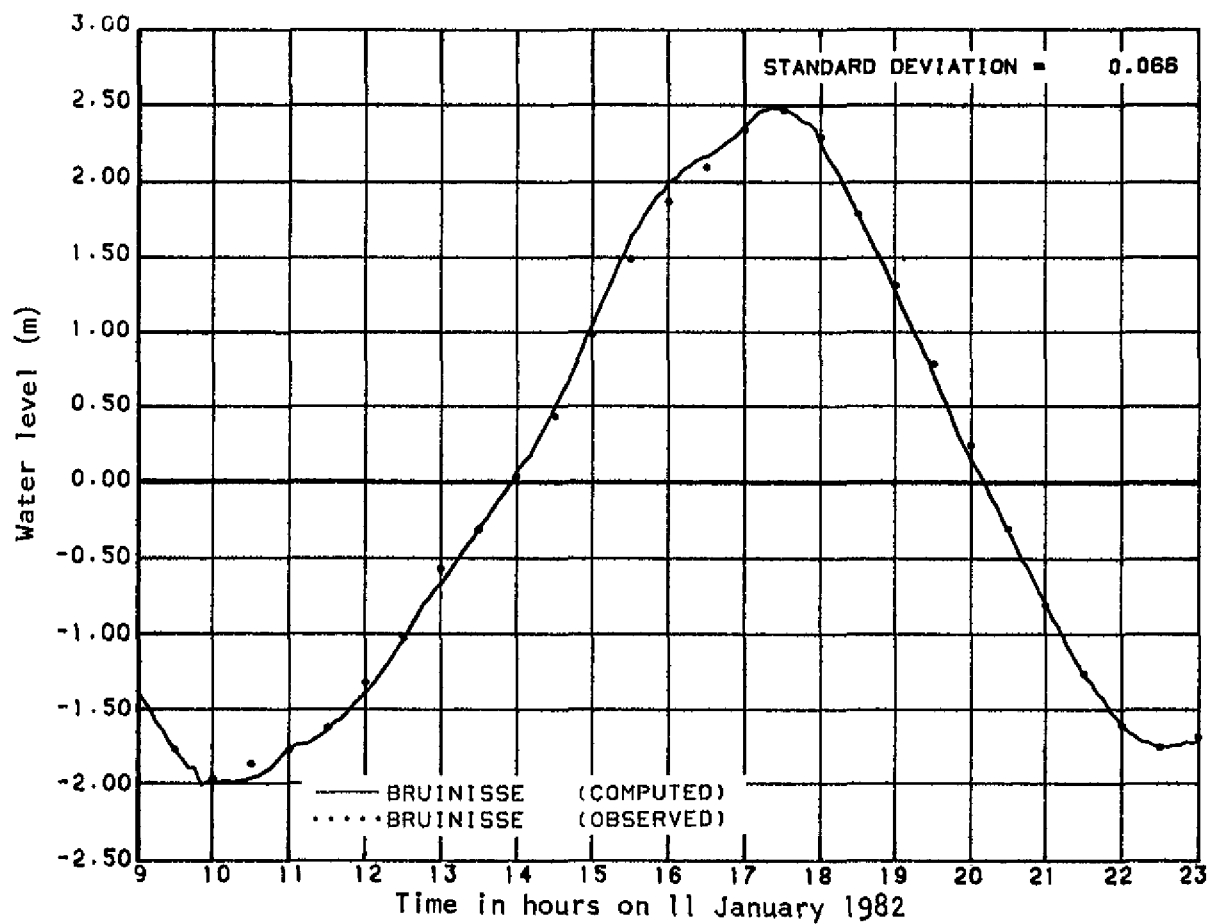
Fig. A.14—Water level at Bruinisse in the computational model compared to the observed
water level

Appendix B

TRANSPORT RATES THROUGH THE
HAMMEN, SCHAAR, AND ROOMPOT
(Constant density computation)

The graphs in this appendix are the same graphs shown in Fig. 9 but are presented on a larger scale. The observed data in the results of the computation are presented at intervals of one-half lunar hour. The data were received in this form from the sponsor.
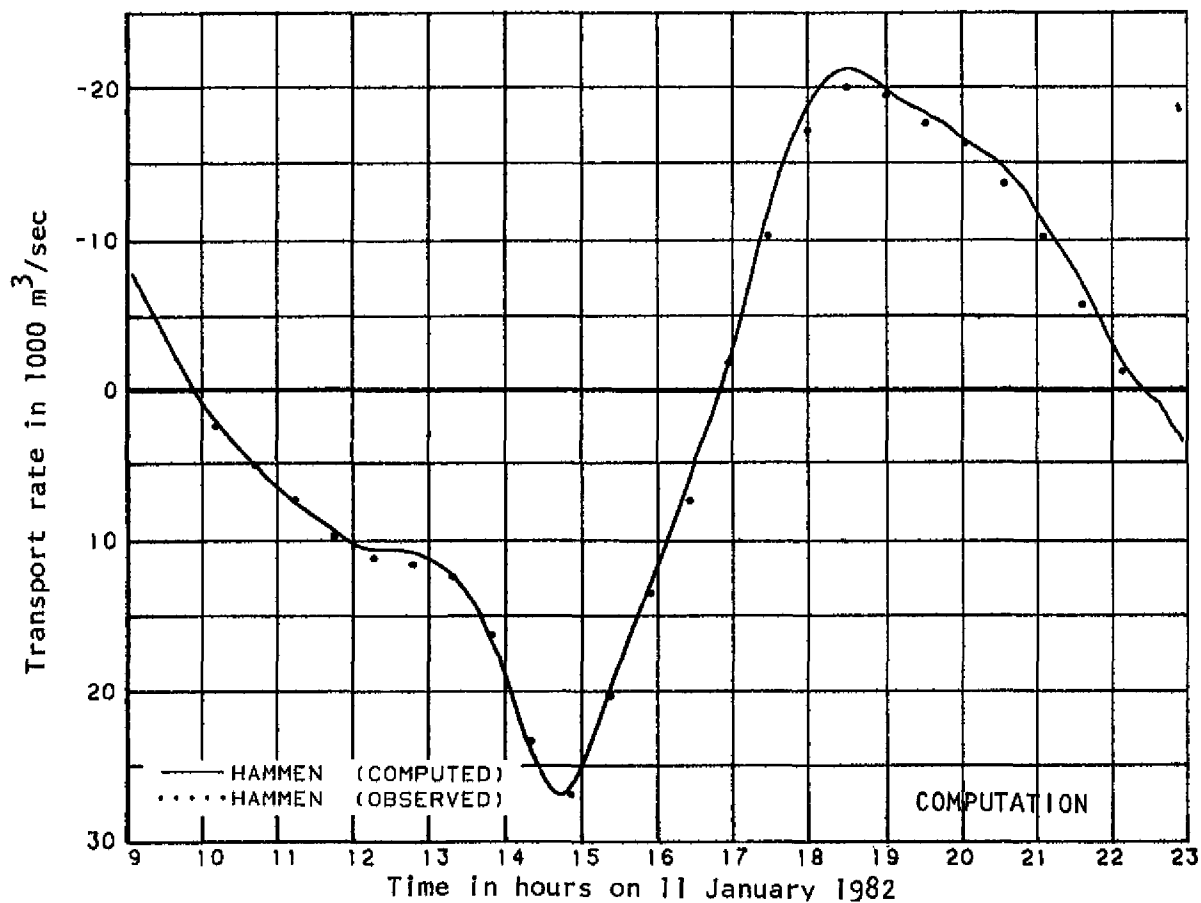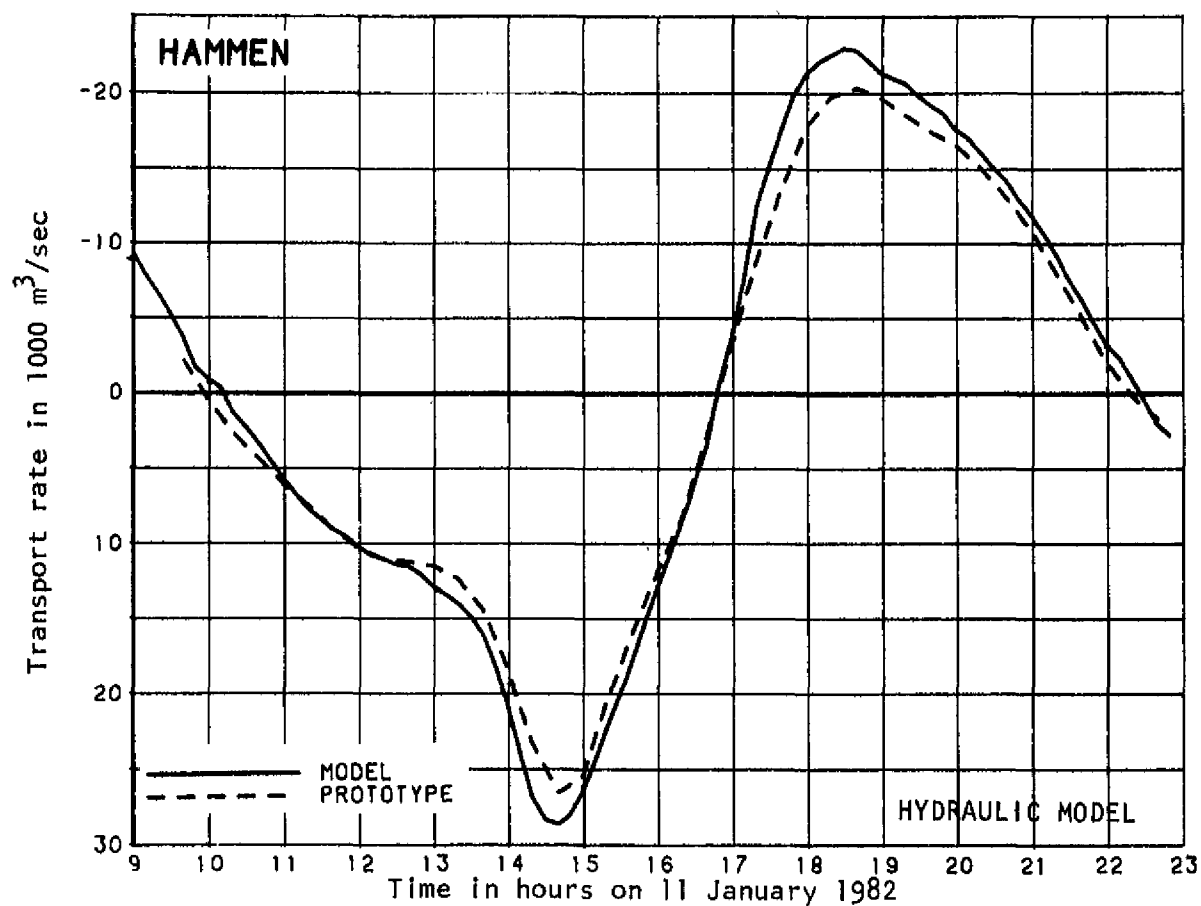
Fig. B.1—Transport rate through the Hammen in the hydraulic model (top graph) and in the computational model (bottom graph) compared to the observed transport rate
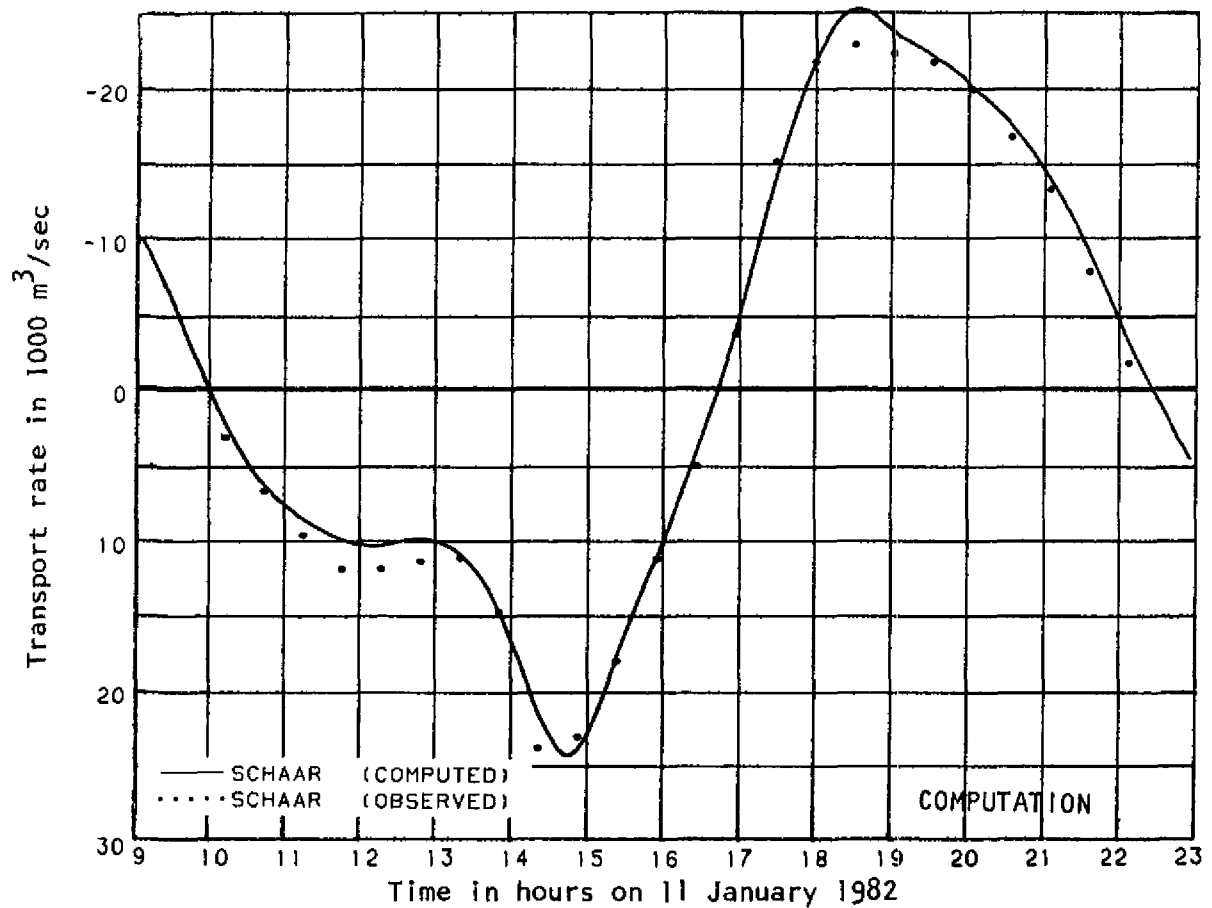
Fig. B.2—Transport rate through the Schaar in the hydraulic model (top graph) and in the computational model (bottom graph) compared to the observed transport rate
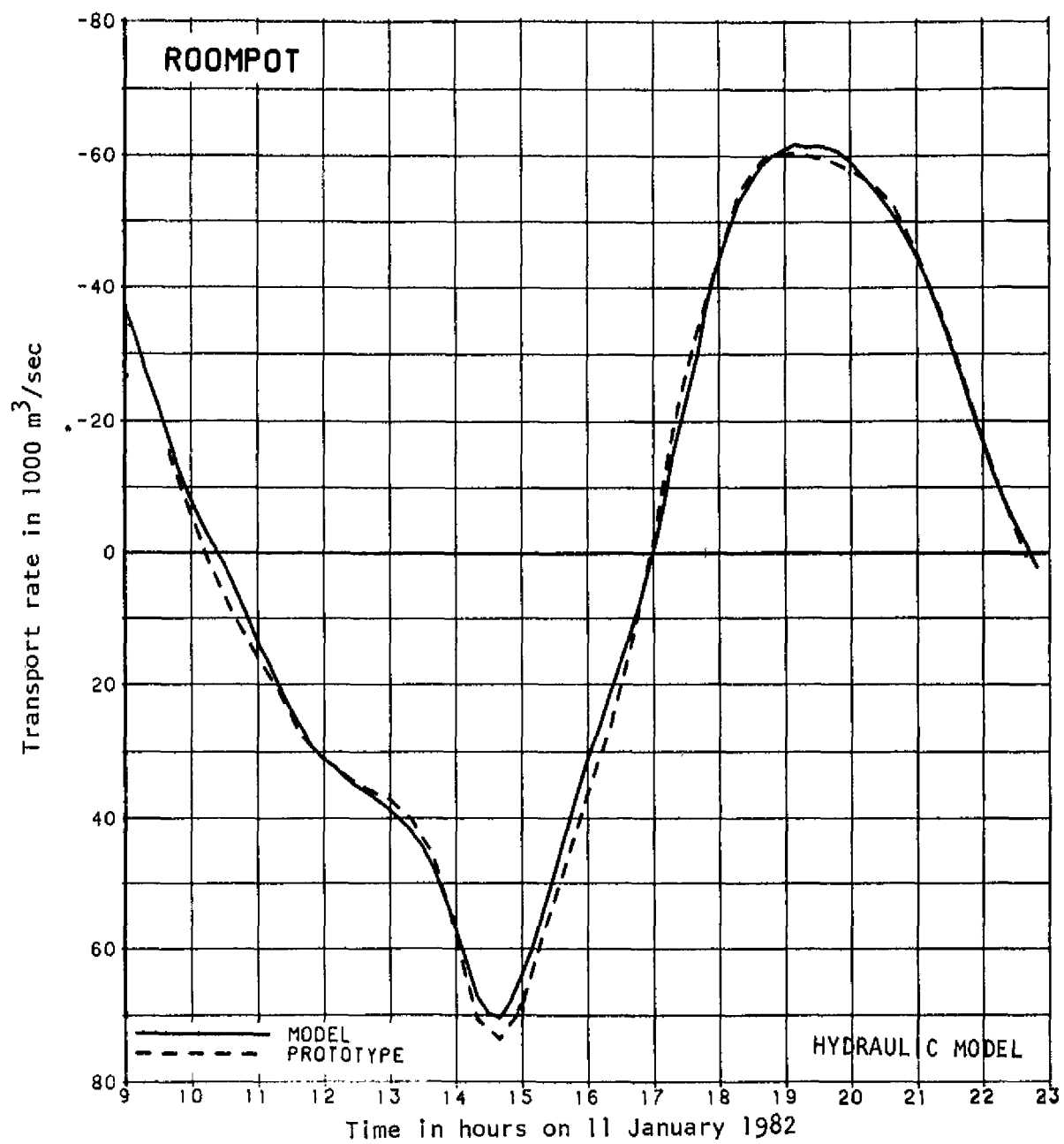
Fig. B.3—Transport rate through the Roompot in the hydraulic model compared to the observed transport rate
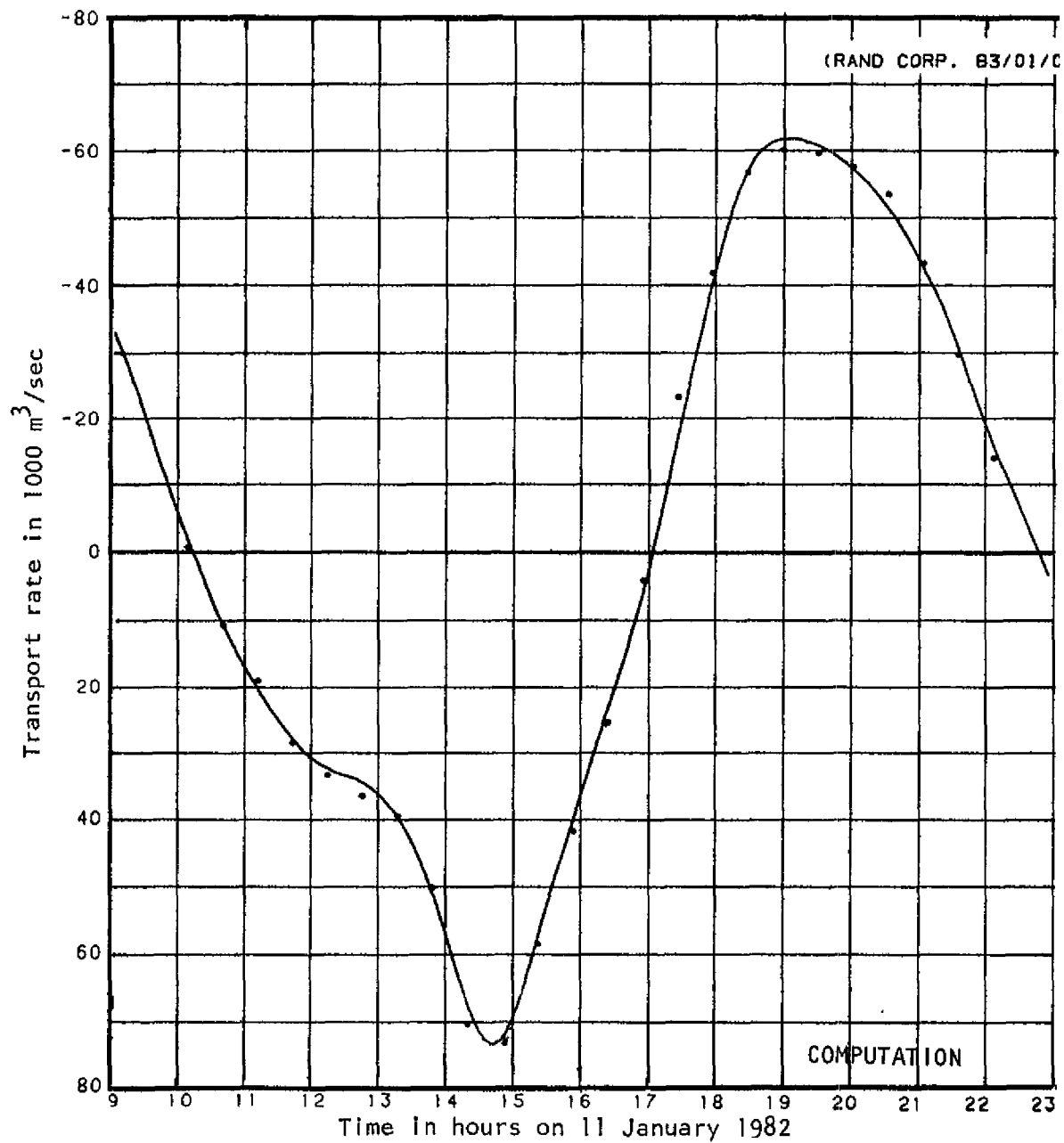
Fig. B.4—Transport rate through the Roompot in the computational model compared to the
observed transport rate

Appendix C

WATER LEVELS IN THE HYDRAULIC MODEL
AND THE COMPUTATIONAL MODEL
(Verification simulation)

The graphs in this appendix show the comparison between the hydraulic model results and the observed water levels, and they are copies of the graphs contained in Ref. 10. The graphs on the bottom part of the pages are parts of plots made by the SIMSYS2D system to which the grid and scales were added to make the graphs similar in appearance to those of the hydraulic model results. The observed data plotted versus the computed data are obtained from digital data files from the Delta Service.

In general the agreement between observed and computed is better for the landward stations than for those found in Appendix A.
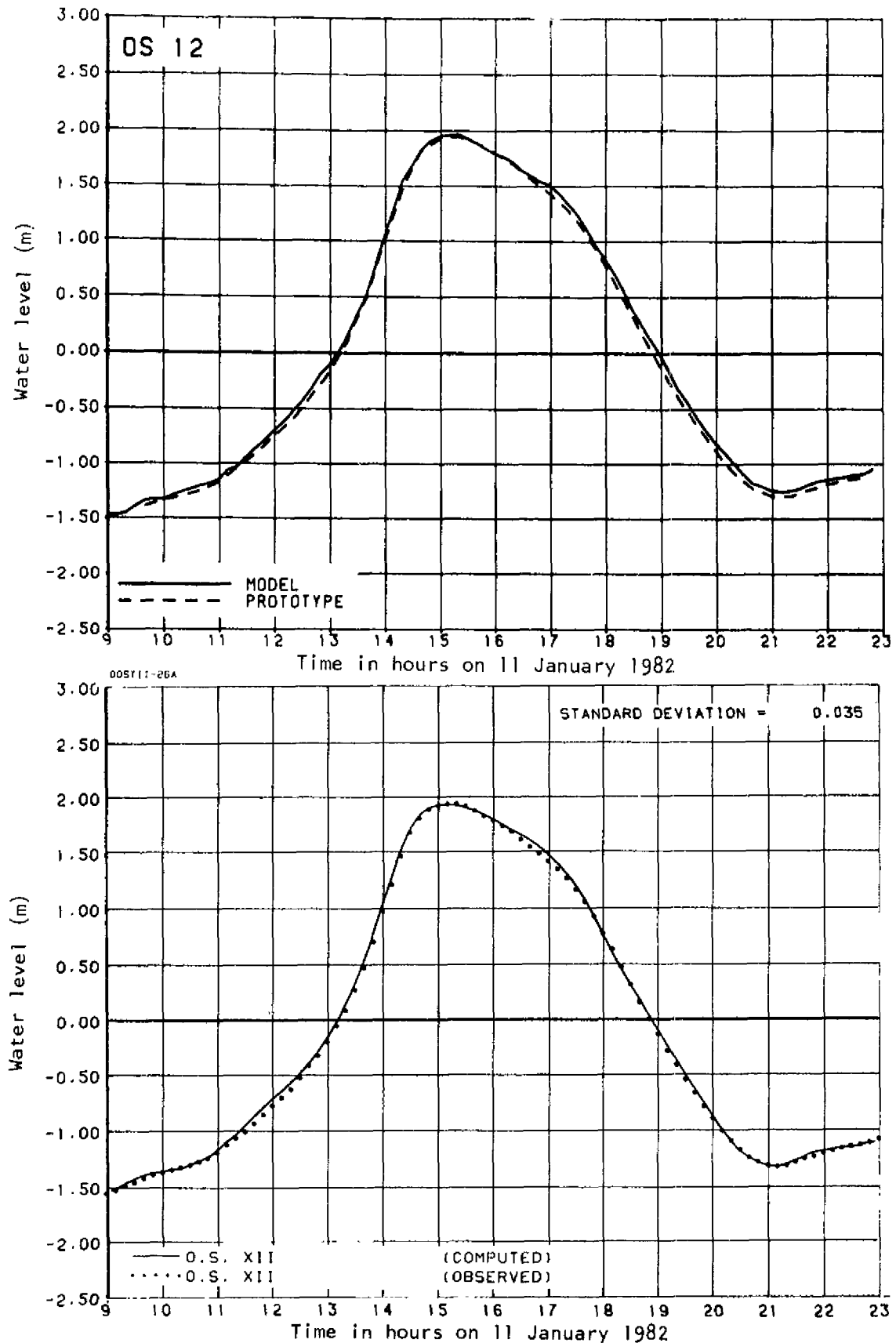
Fig. C.1—Water level at OS12 in the hydraulic model (top graph) and the computational model with variable density (bottom graph) compared to the observed water level

Fig. C.2—Water level at OS4 in the hydraulic model (top graph) and the computational model with variable density (bottom graph) compared to the observed water level
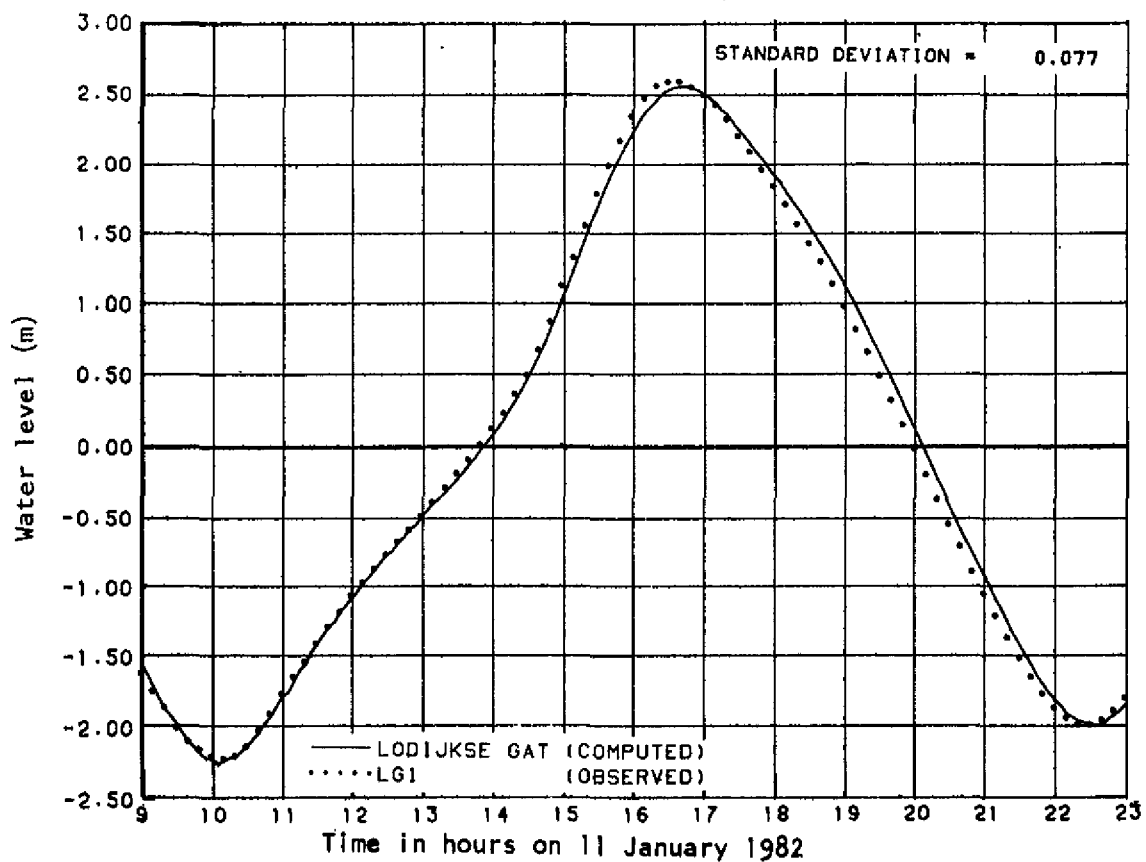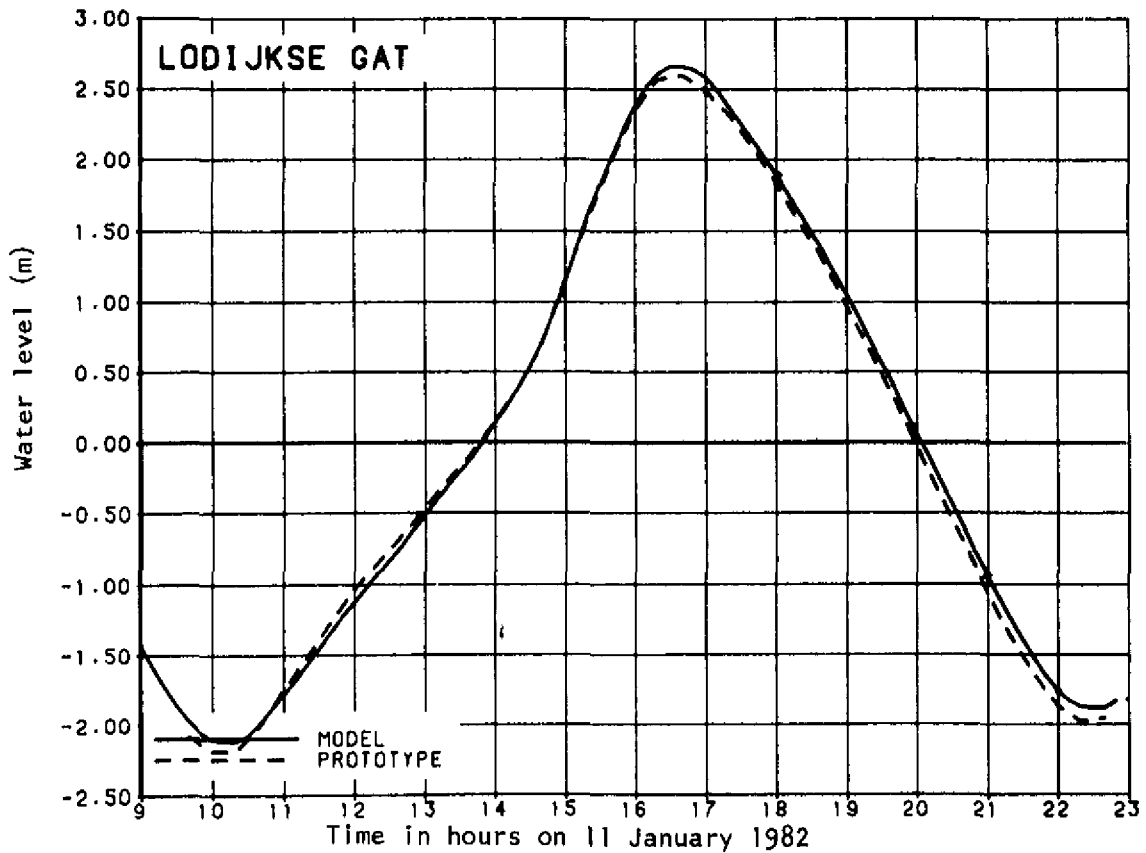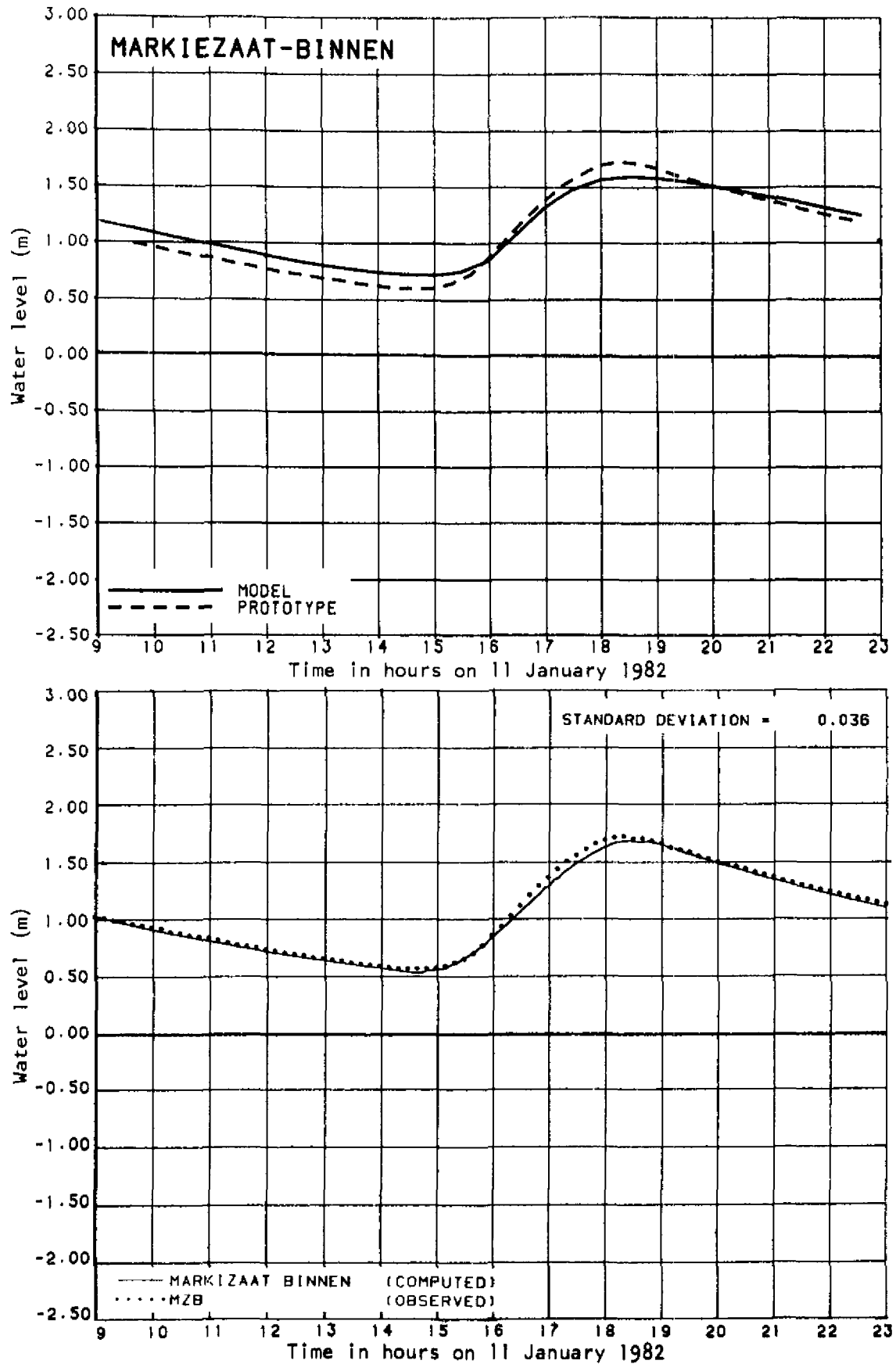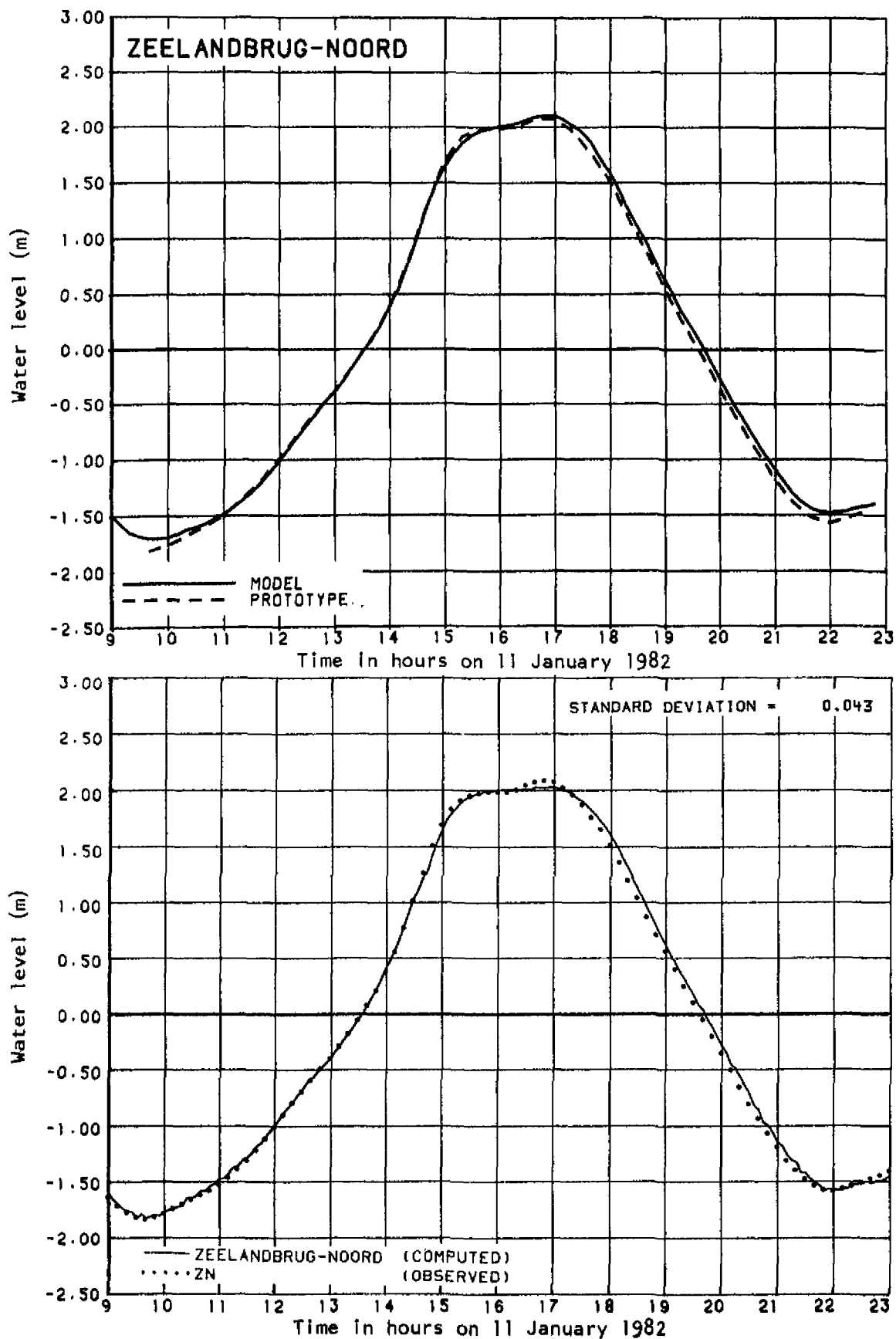
64
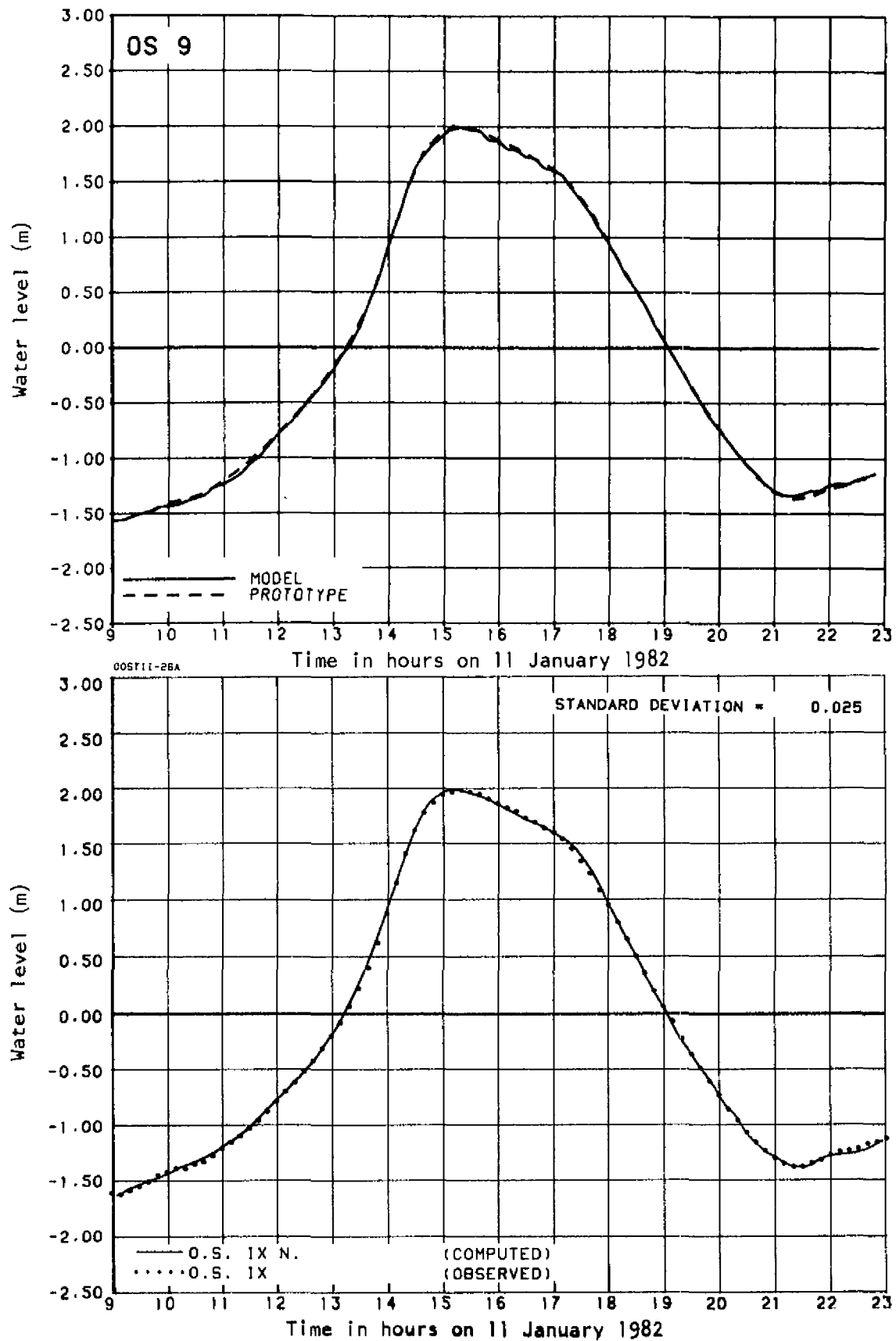
Fig. C.3—Water level at OS9 in the hydraulic model (top graph) and the computational
model with variable density (bottom graph) compared to the observed water level
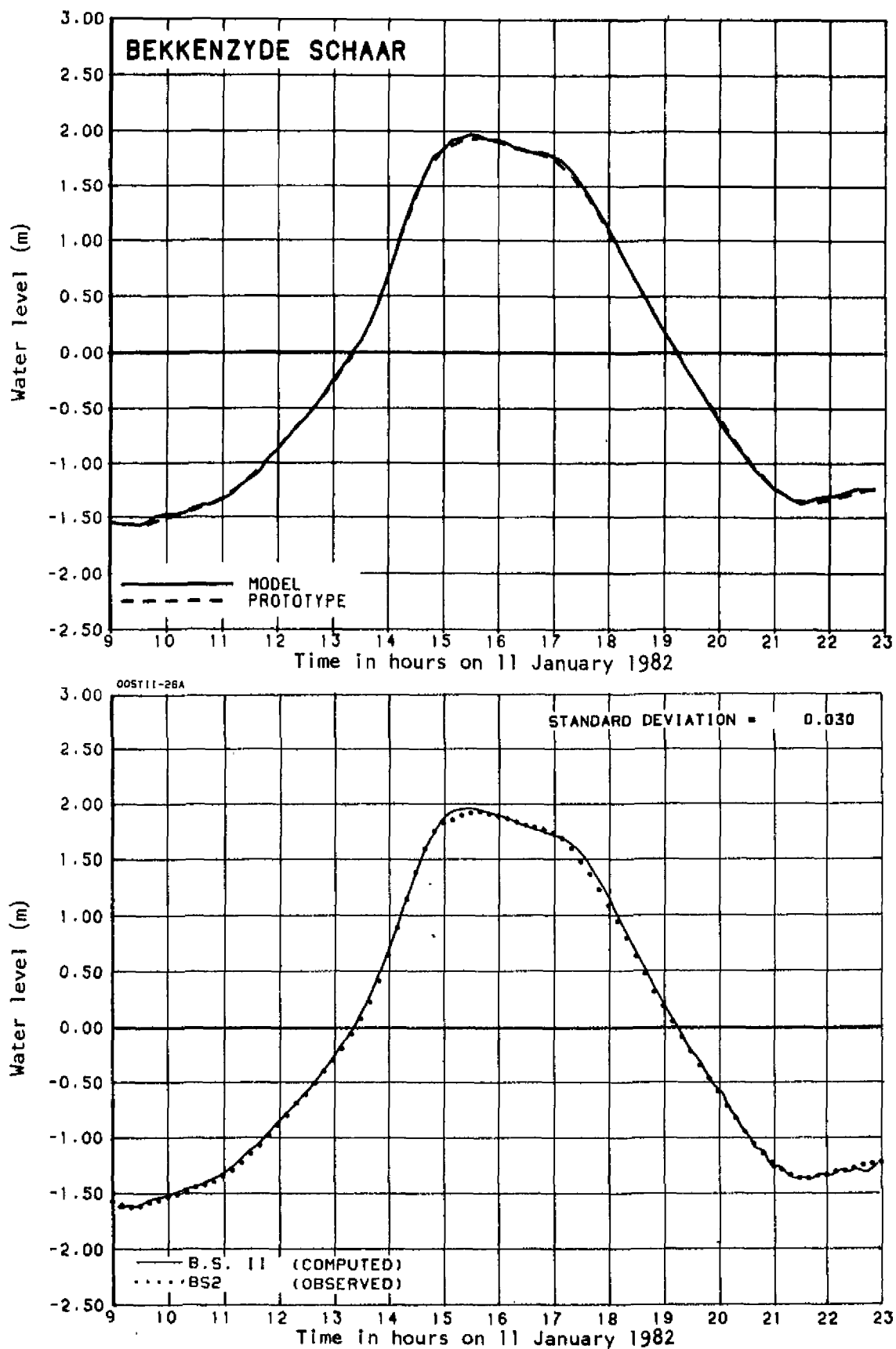
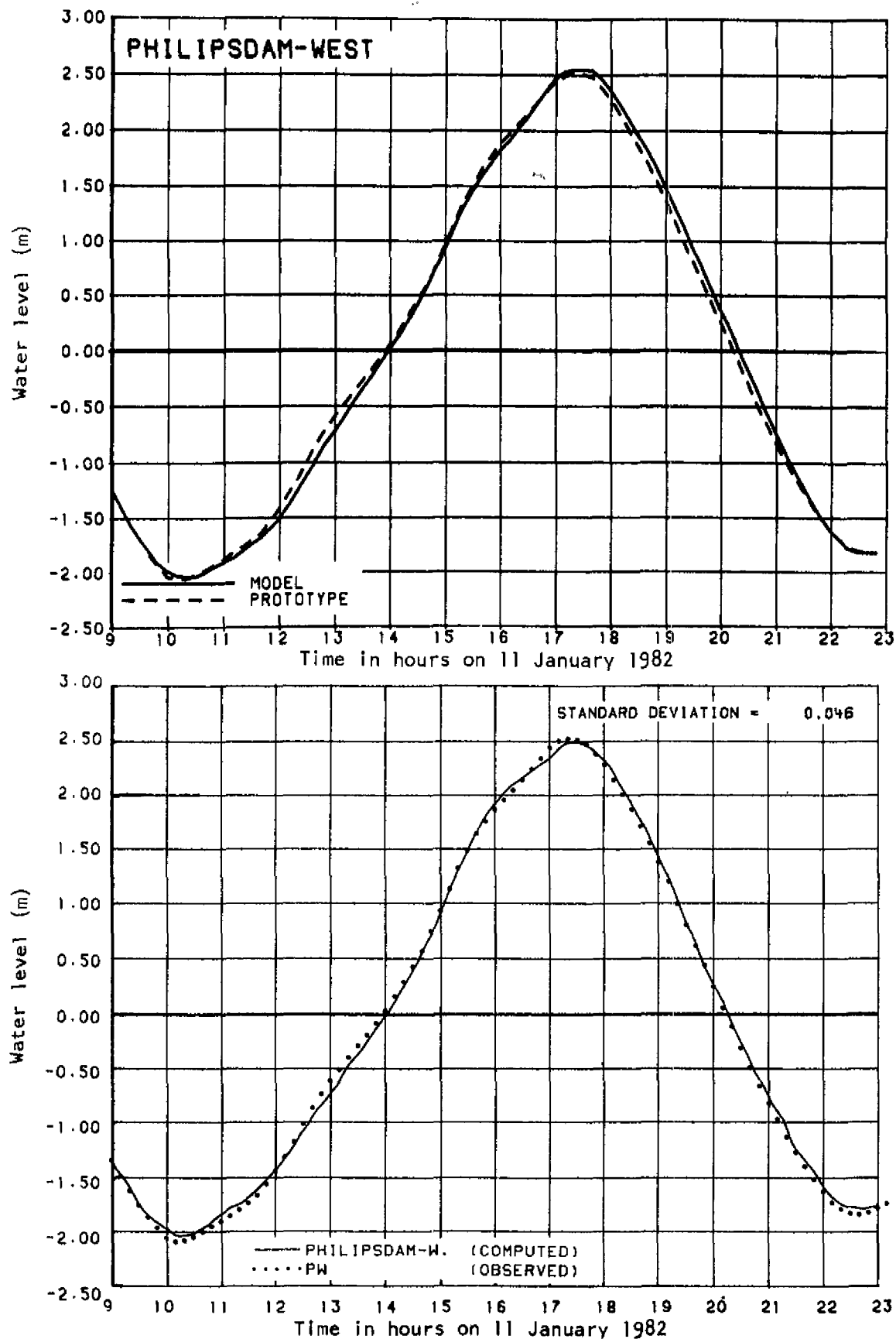Fig. C.4—Water level at Bekkenzyde Schaar in the hydraulic model (top graph) and the computational model with variable density (bottom graph) compared to the observed water level
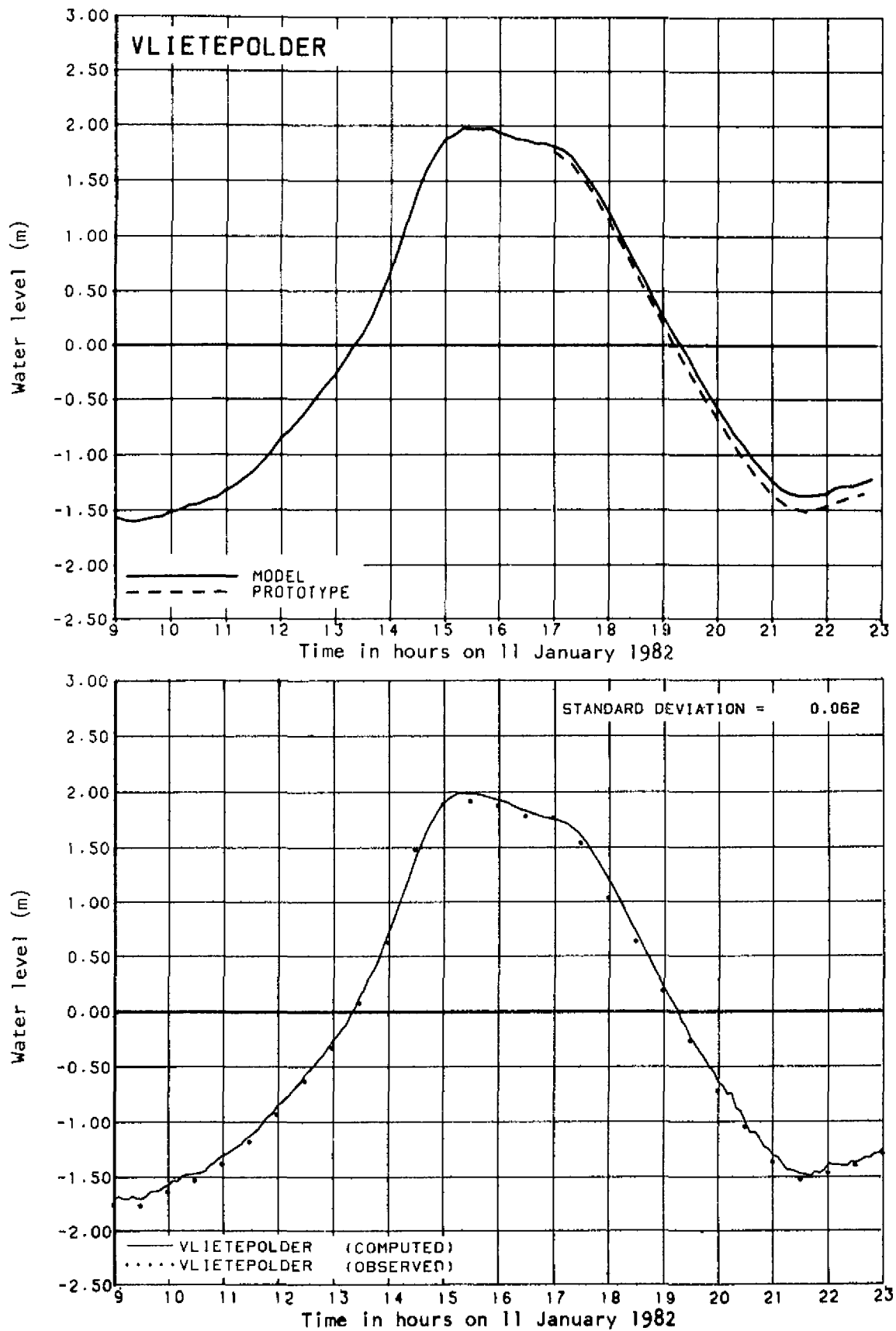
Fig. C.5—Water level at Vlietepolder in the hydraulic model (top graph) and the computational model with variable density (bottom graph) compared to the observed water level
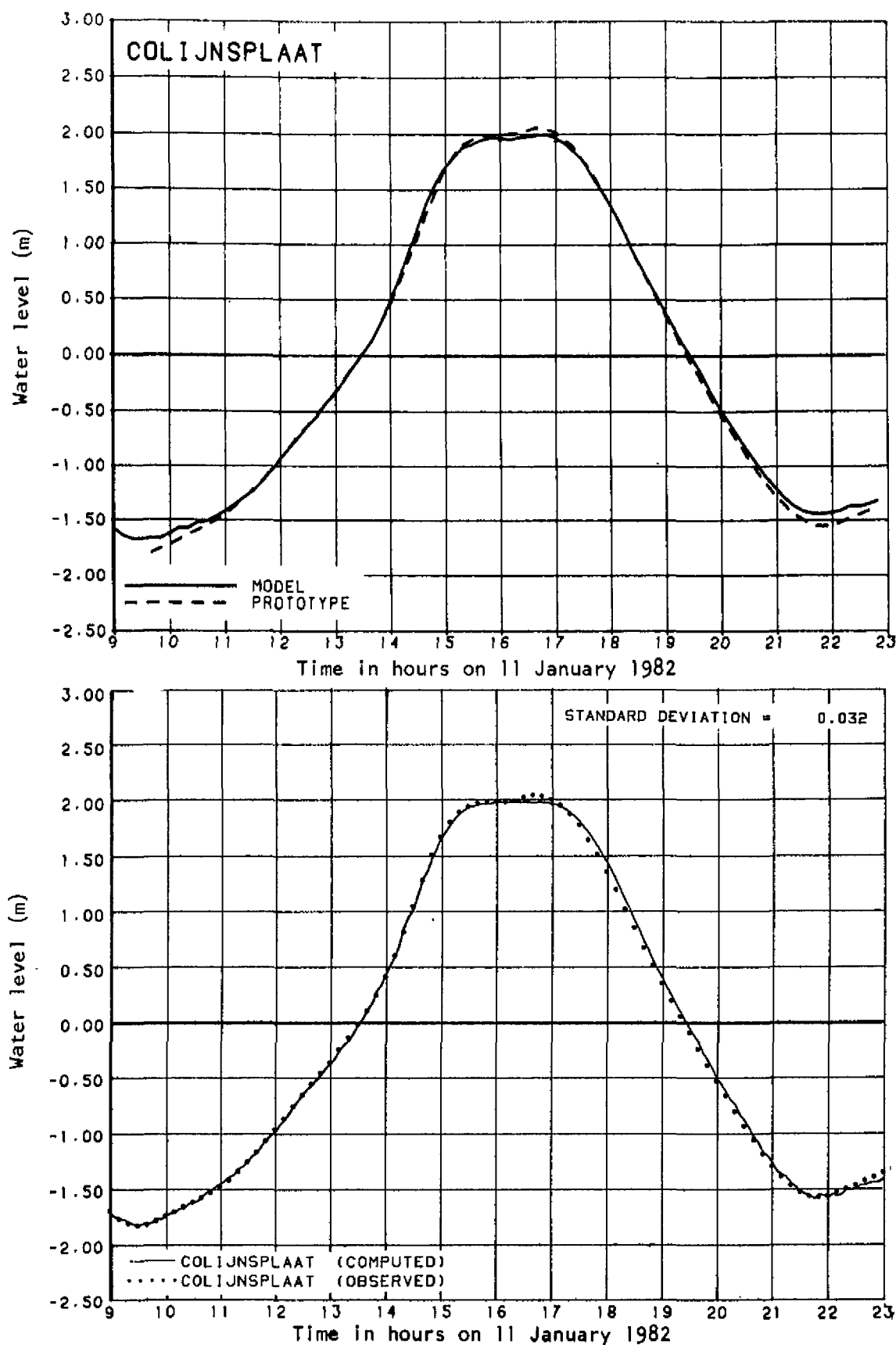
Fig. C.6—Water level at Colijnsplaat in the hydraulic model (top graph) and the computational model with variable density (bottom graph) compared to the observed water level
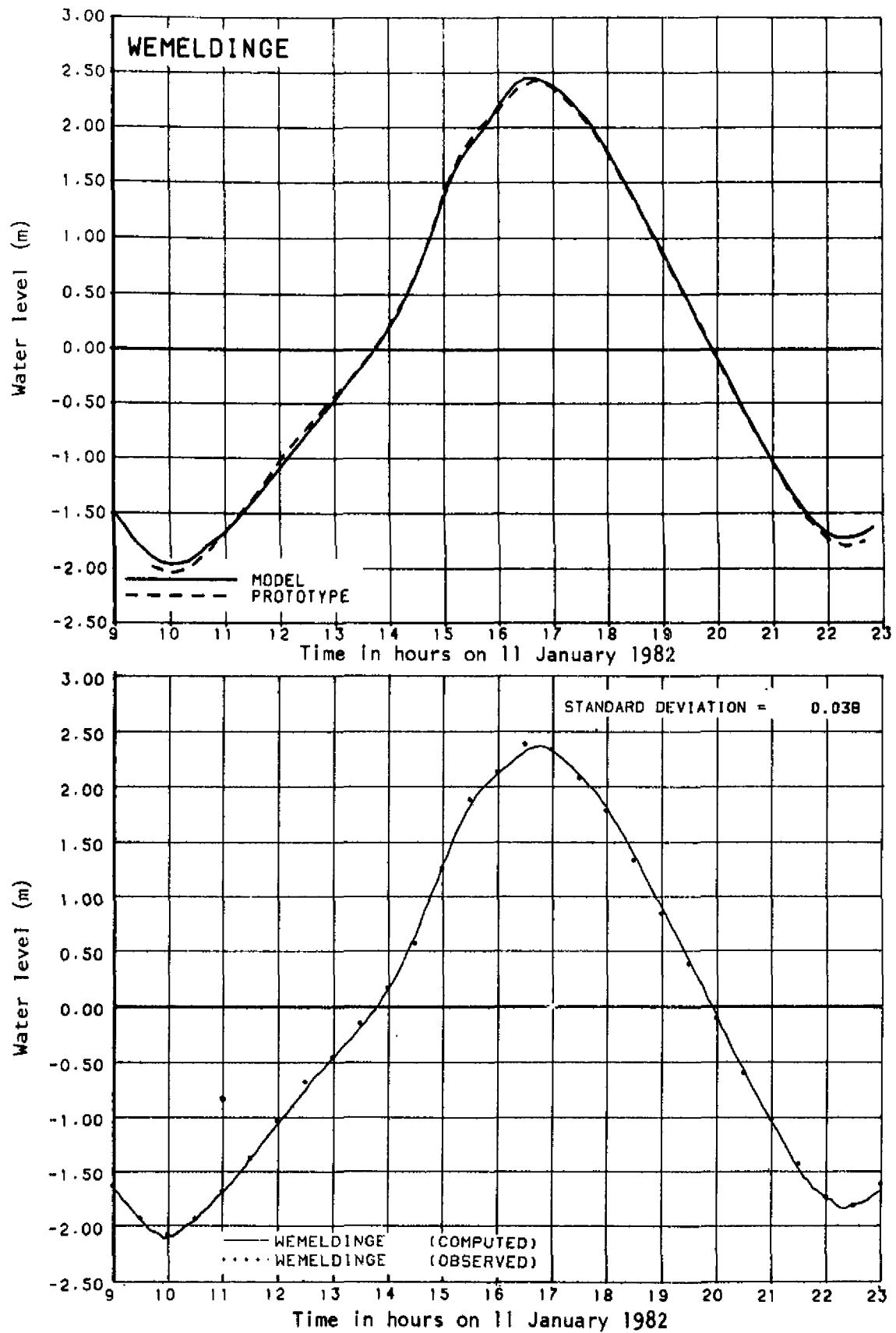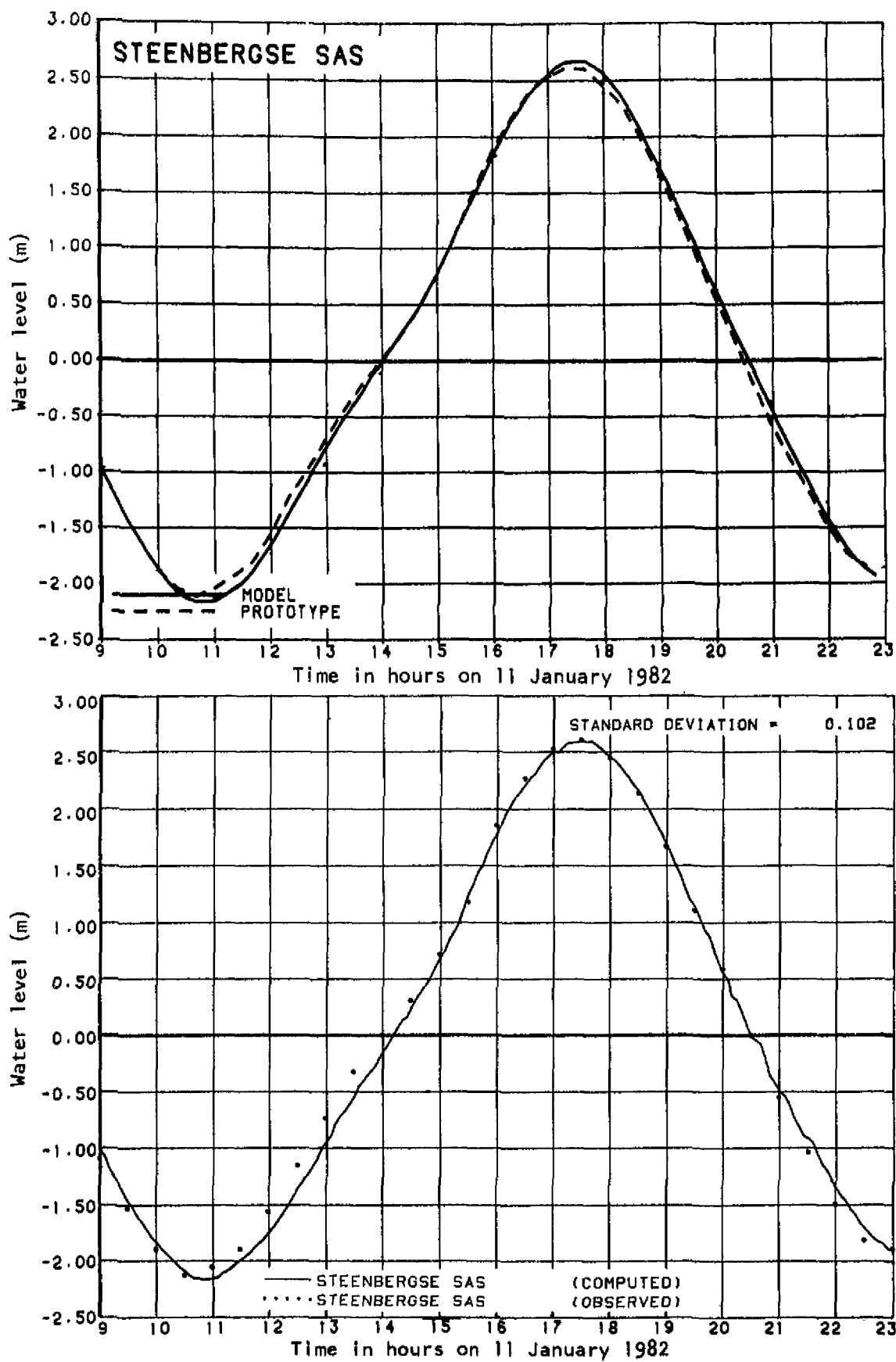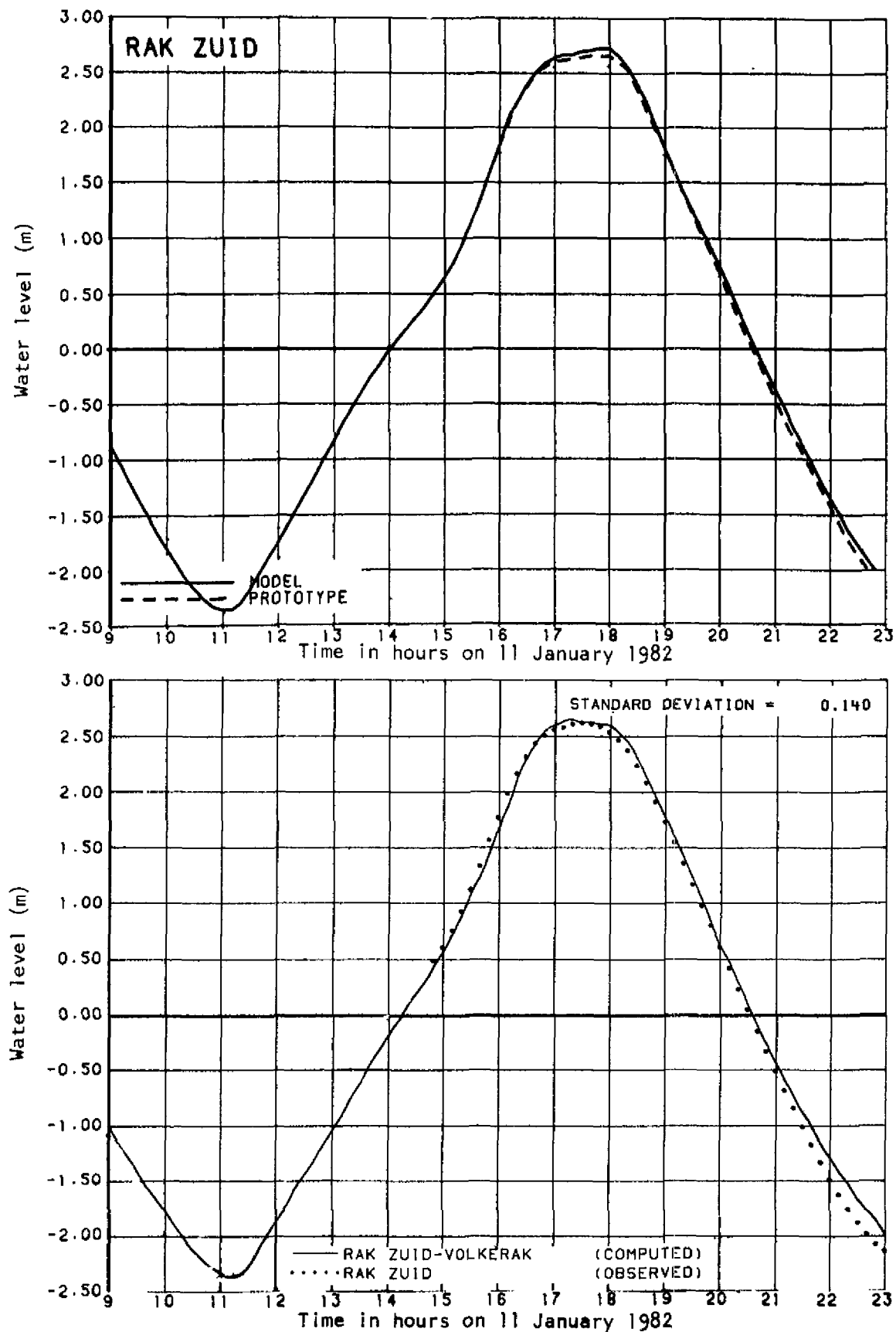
Fig. C.7—Water level at Wemeldinge in the hydraulic model (top graph) and the computational model with variable density (bottom graph) compared to the observed water level

Fig. C.8—Water level at Lodijkse Gat in the hydraulic model (top graph) and the computational model with variable density (bottom graph) compared to the observed water level

Fig. C.9—Water level at Markiezaat-Binnen in the hydraulic model (top graph) and the computational model with variable density (bottom graph) compared to the observed water level

Fig. C.10—Water level at Zeelandbrug-Noord in the hydraulic model (top graph) and the computational model with variable density (bottom graph) compared to the observed water level

Fig. C.11—Water level at Philipsdam-West in the hydraulic model (top graph) and the computational model with variable density (bottom graph) compared to the observed water level

Fig. C.12—Water level at Steenbergse Sas in the hydraulic model (top graph) and the computational model with variable density (bottom graph) compared to the observed water level
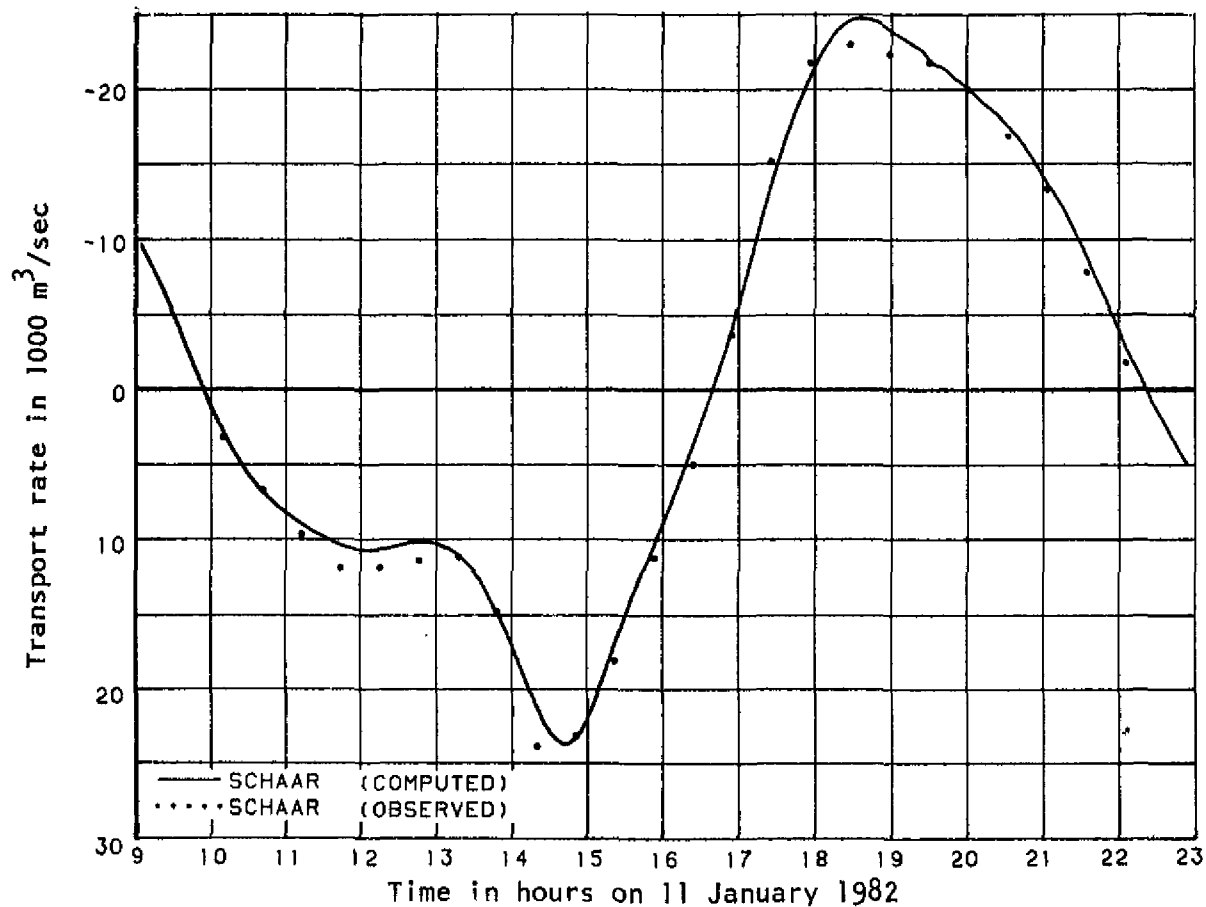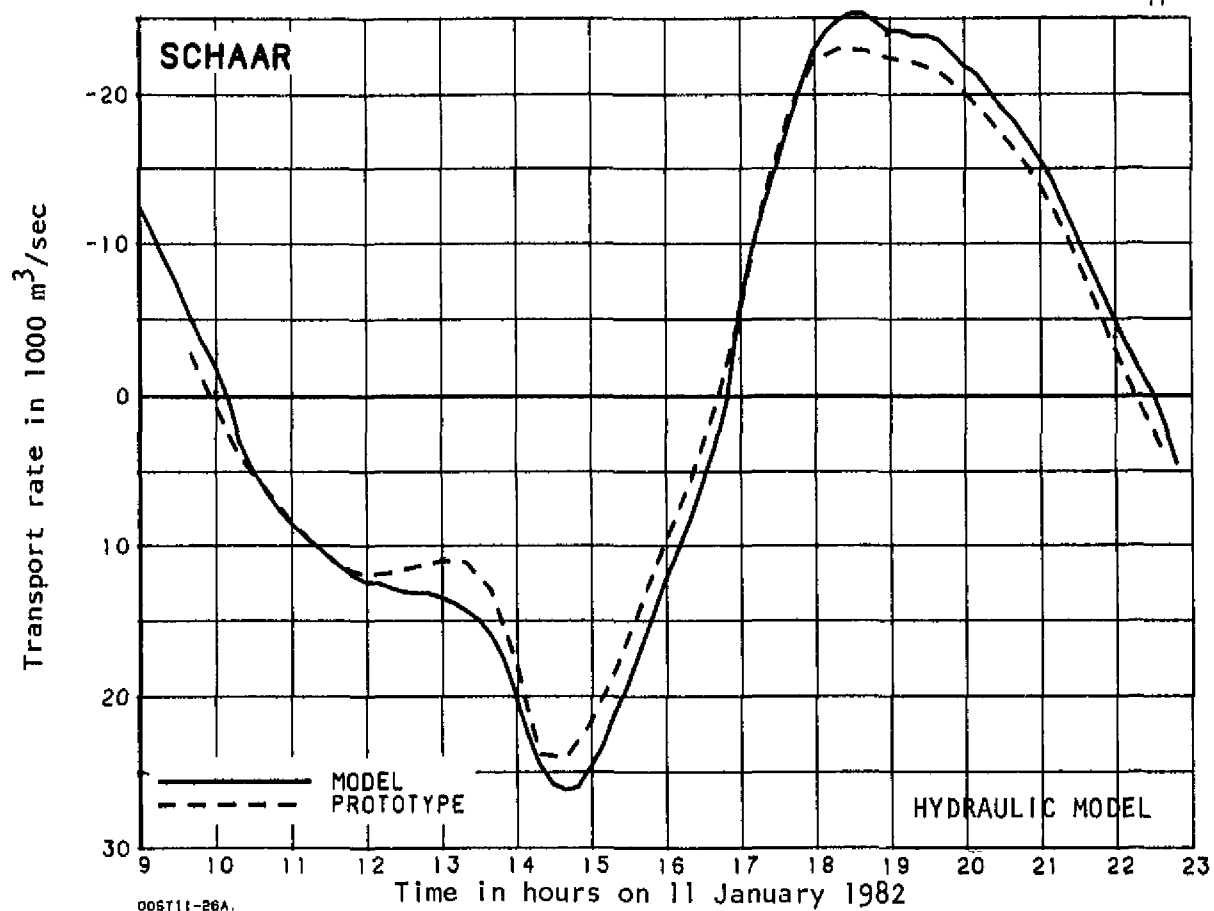
Fig. C.13—Water level at Rak Zuid in the hydraulic model (top graph) and the computational model with variable density (bottom graph) compared to the observed water level

Appendix D
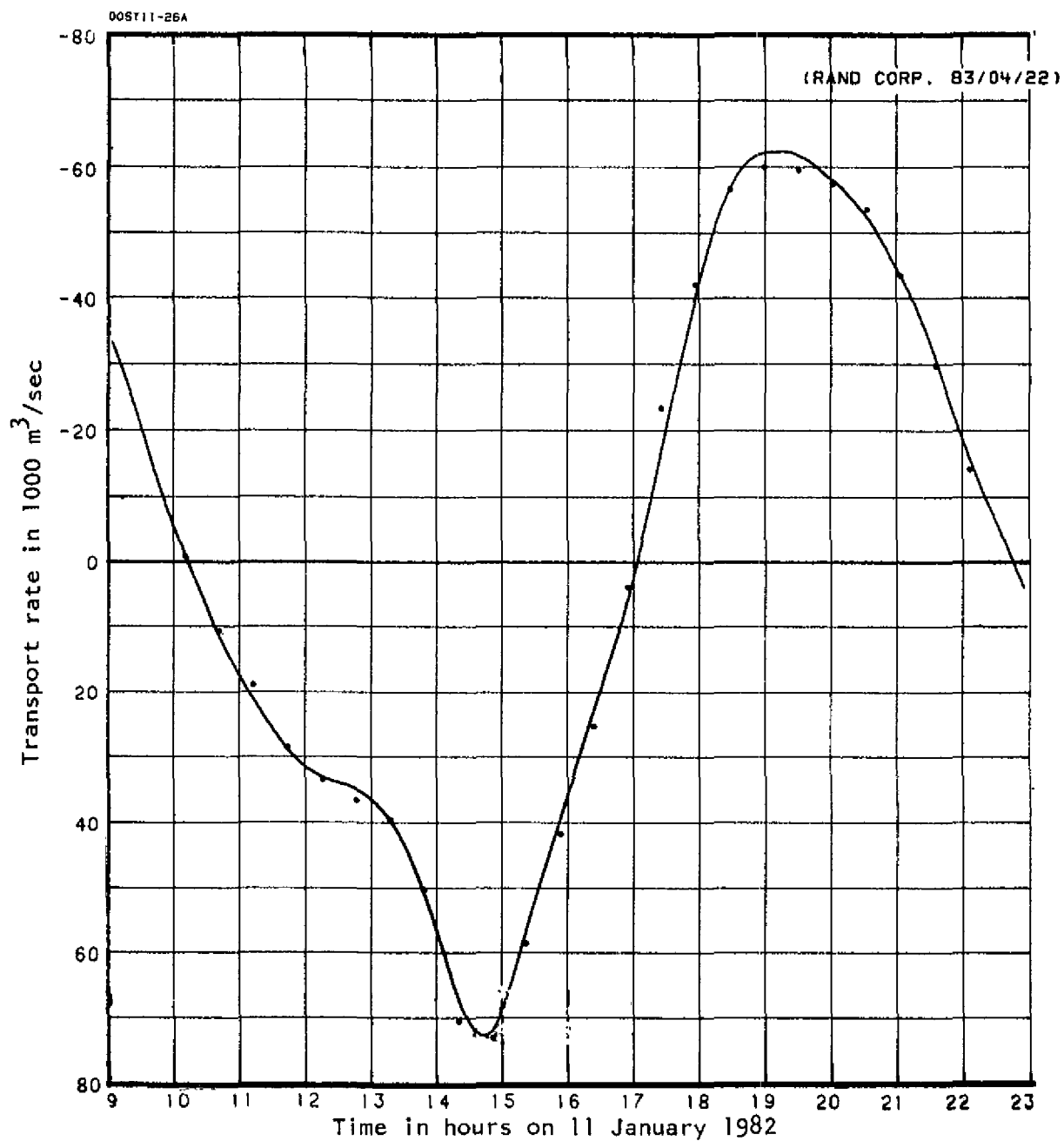
TRANSPORT RATES THROUGH THE
HAMMEN, SCHAAR, AND ROOMPOT
(Verification simulation)

The graphs in this appendix are the same graphs as shown in Fig. 18 but they are presented on a larger scale. The results of this verification simulation with variable density should be compared with those in Appendix B.
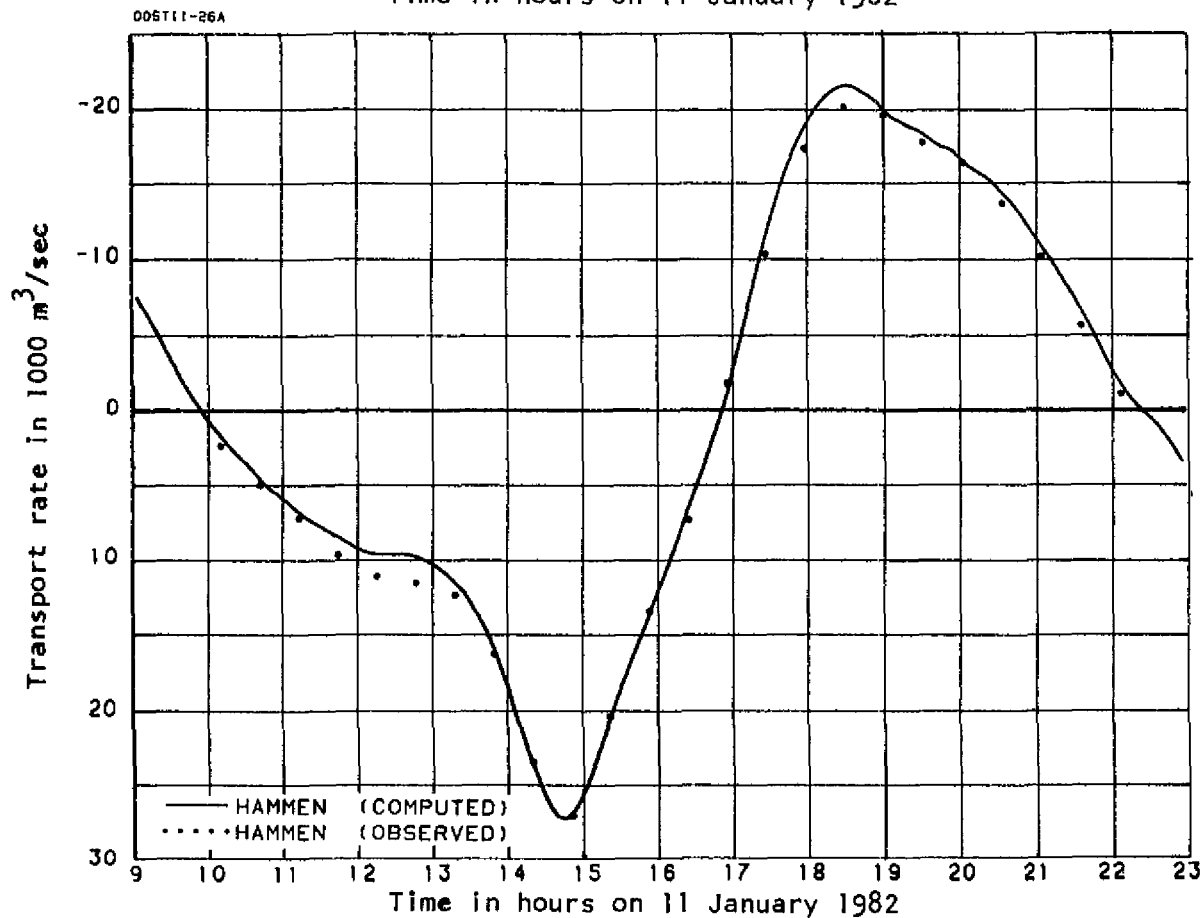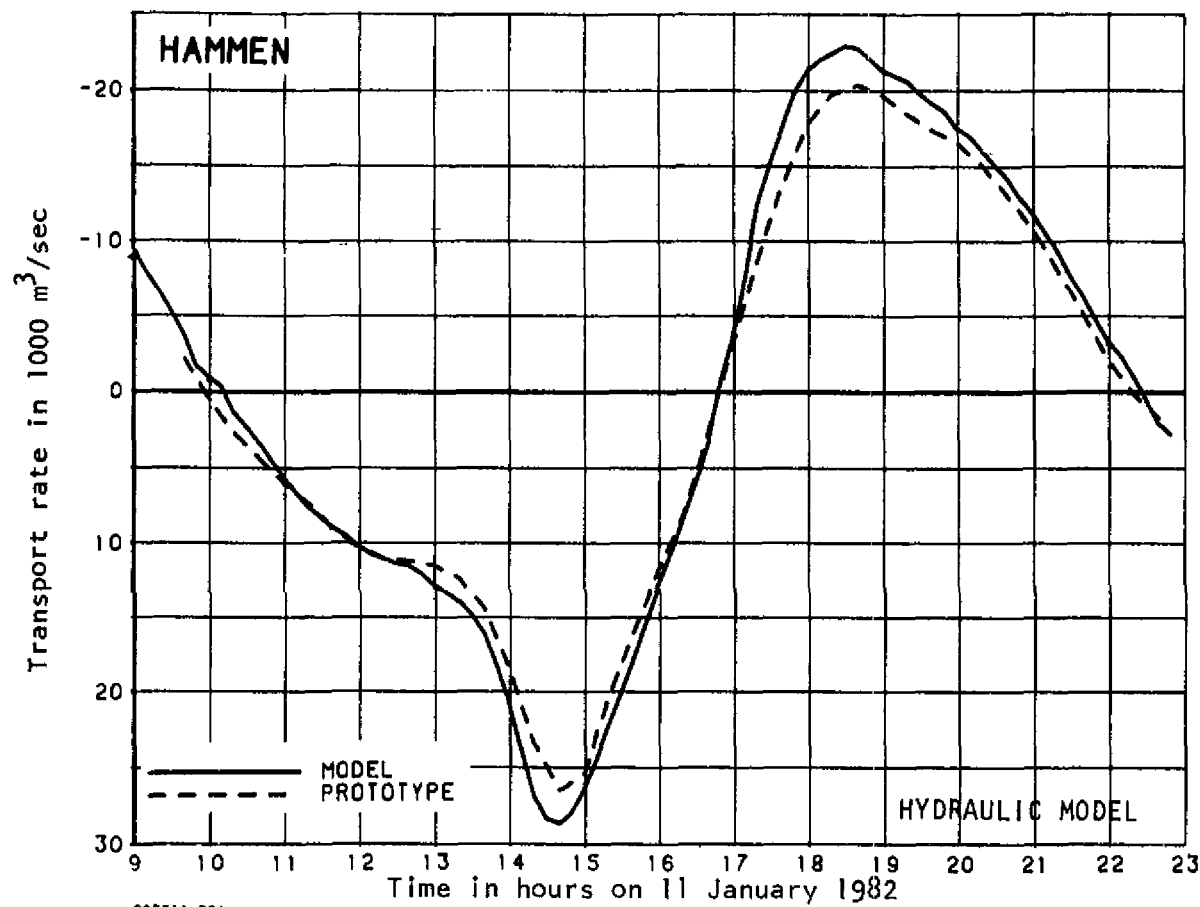
Fig. D.1—Transport rate through the Hammen in the hydraulic model (top graph) and in the computational model with variable density (bottom graph) compared to the observed transport rate

Fig. D.2—Transport rate through the Schaar in the hydraulic model (top graph) and in the computational model with variable density (bottom graph) compared to the observed transport rate

Fig. D.3—Transport rate through the Roompot in the computational model with variable density compared to the observed transport rate

Appendix E

OBSERVED AND COMPUTED TIDE AND TIDAL COMPONENTS
(Verification simulation)

In this appendix, the observed and computed tidal records for each station are shown. Also shown are the observed and computed tidal components for the semidiurnal tide, the quarter-diurnal tide, the sixth-diurnal tide, the eighth-diurnal tide, and the tenth-diurnal tide. The last four tidal components are shown on a scale ten times as large as the one used for the tide and the semidiurnal tidal component.

The overtides are generally quite strong in the sixth-diurnal component at Markiezaat-Buiten; it is nearly 30 cm, and the tenth-diurnal component has an amplitude of about 8 cm.

Considerable phase differences exist between some of the stations. For example, the sixth-diurnal tide at Philipsdam W is about 180° out of phase with the tide at Colijnsplaat and Zeelandbrug-Noord.
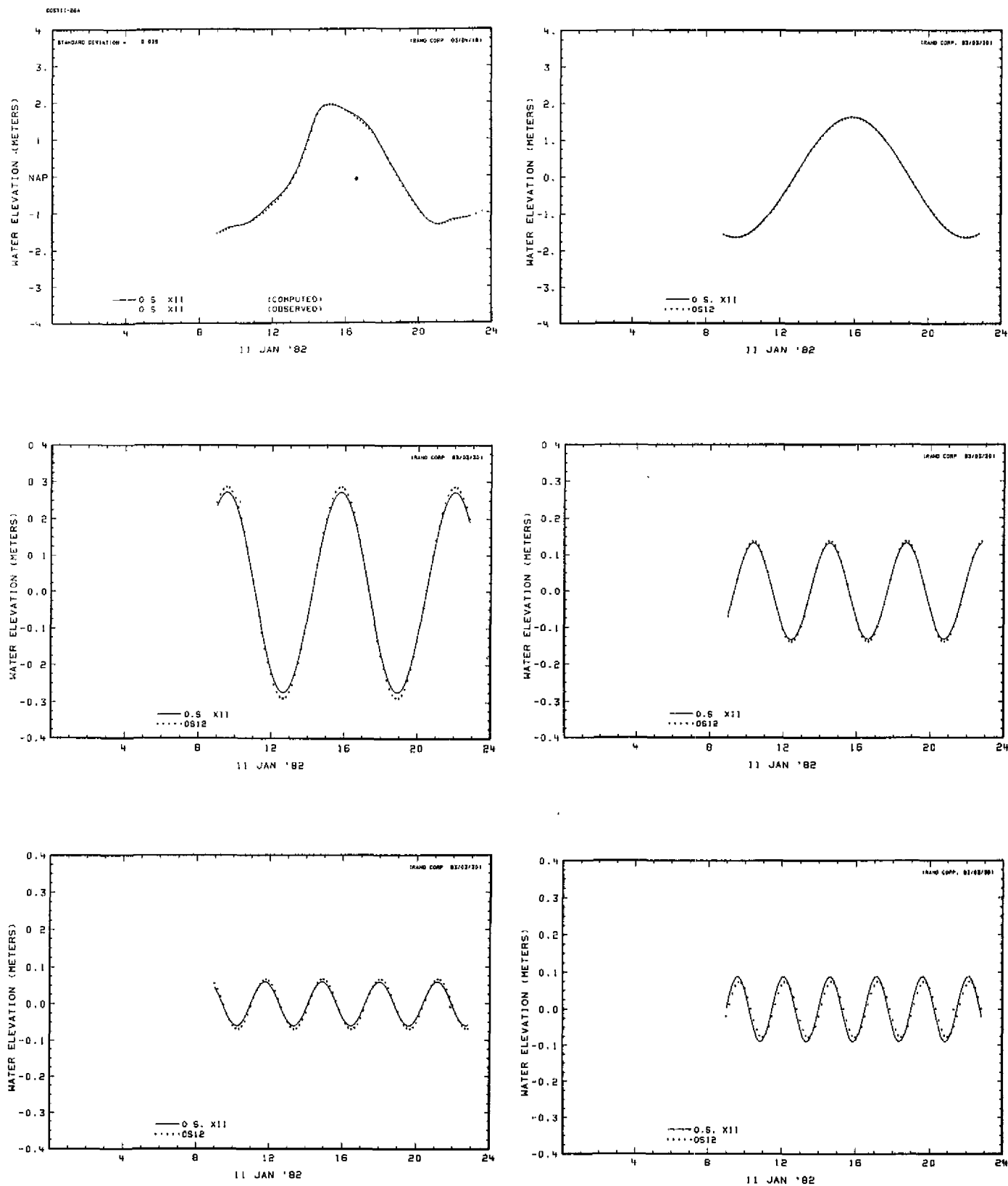
Fig. E.1—Observed and computed tides and tidal components at OS12: (a) composite tide, (b) semidiurnal tide, (c) quarter-diurnal tide, (d) sixth-diurnal tide, (e) eighth-diurnal tide, (f) tenth-diurnal tide
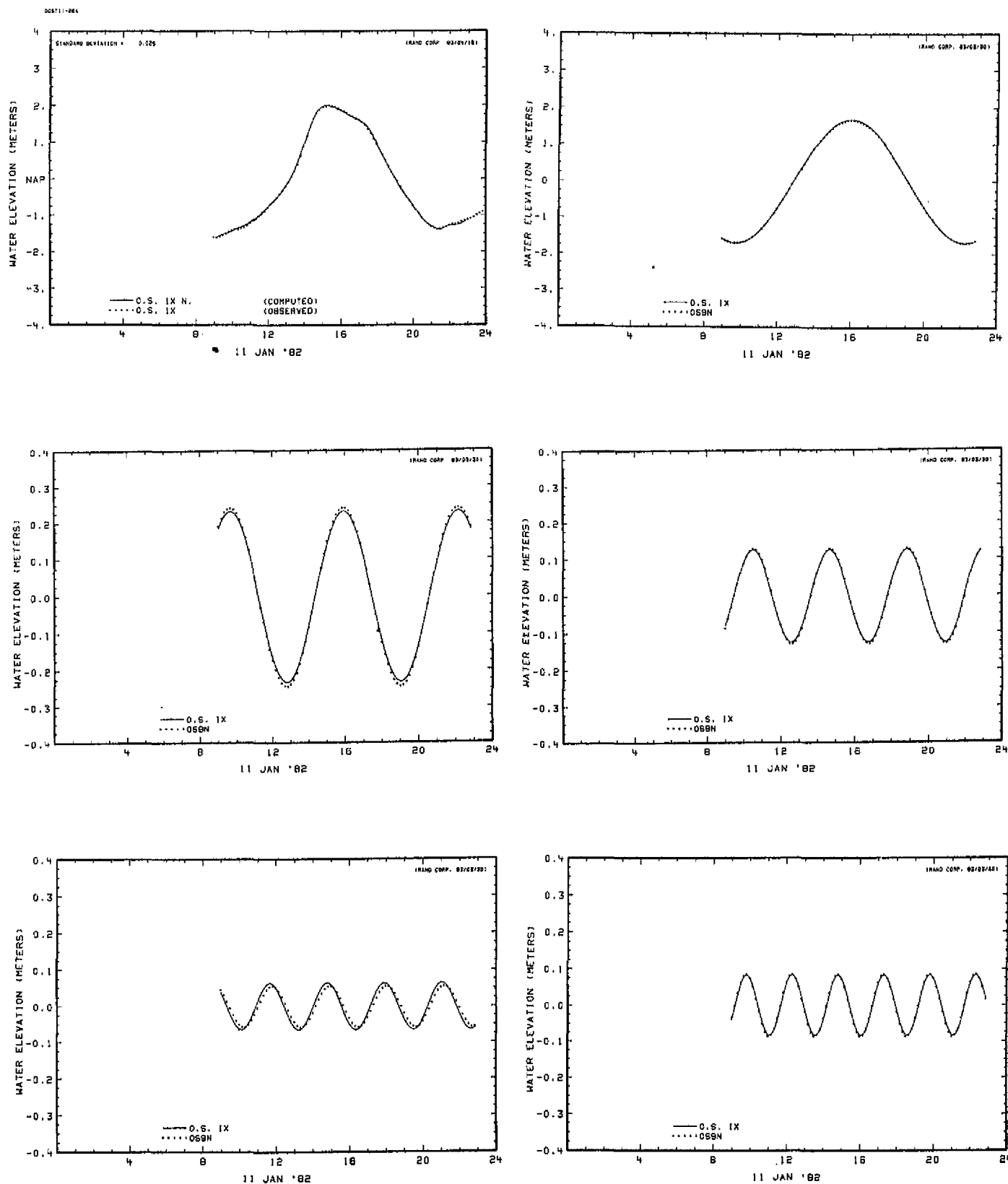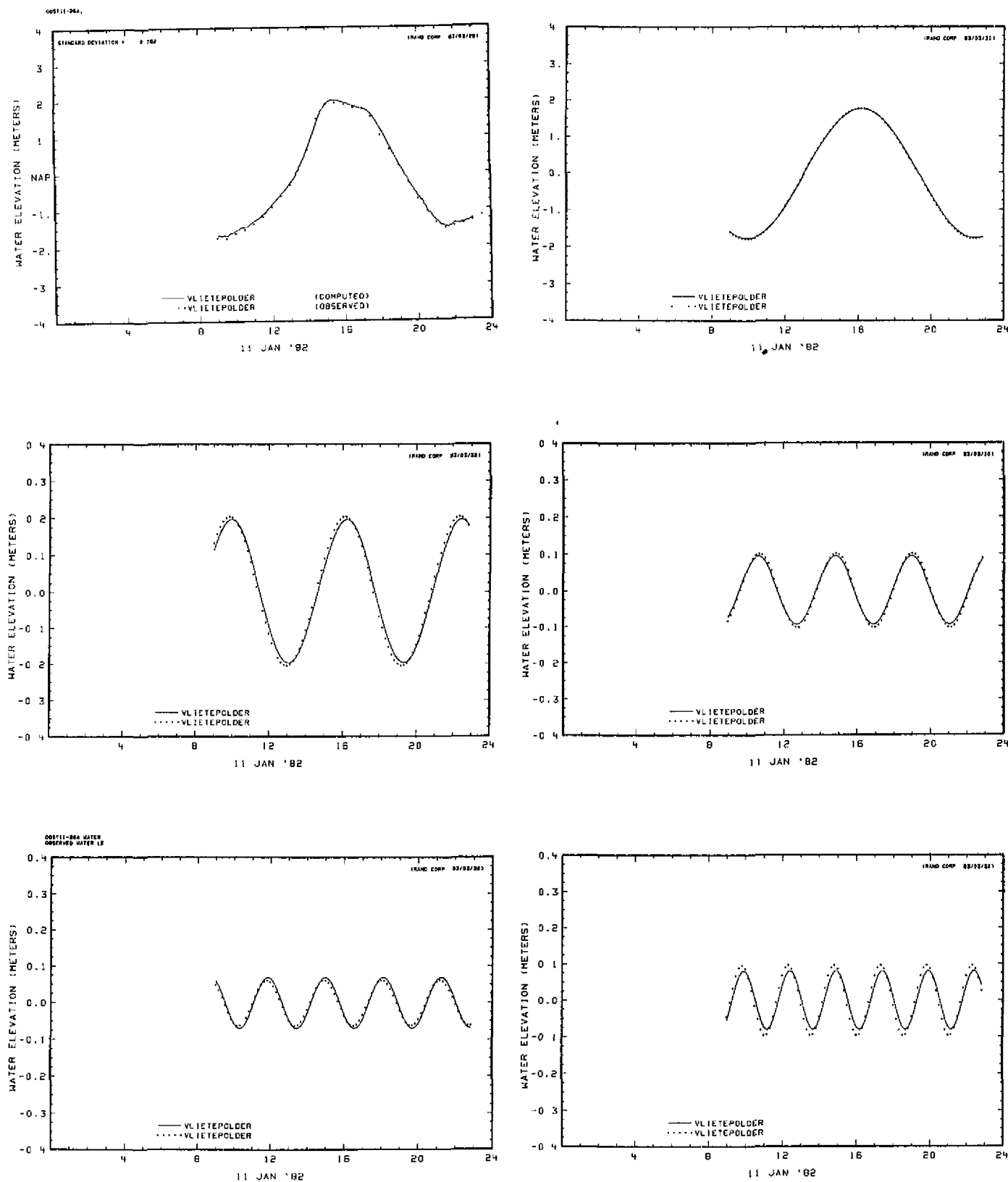
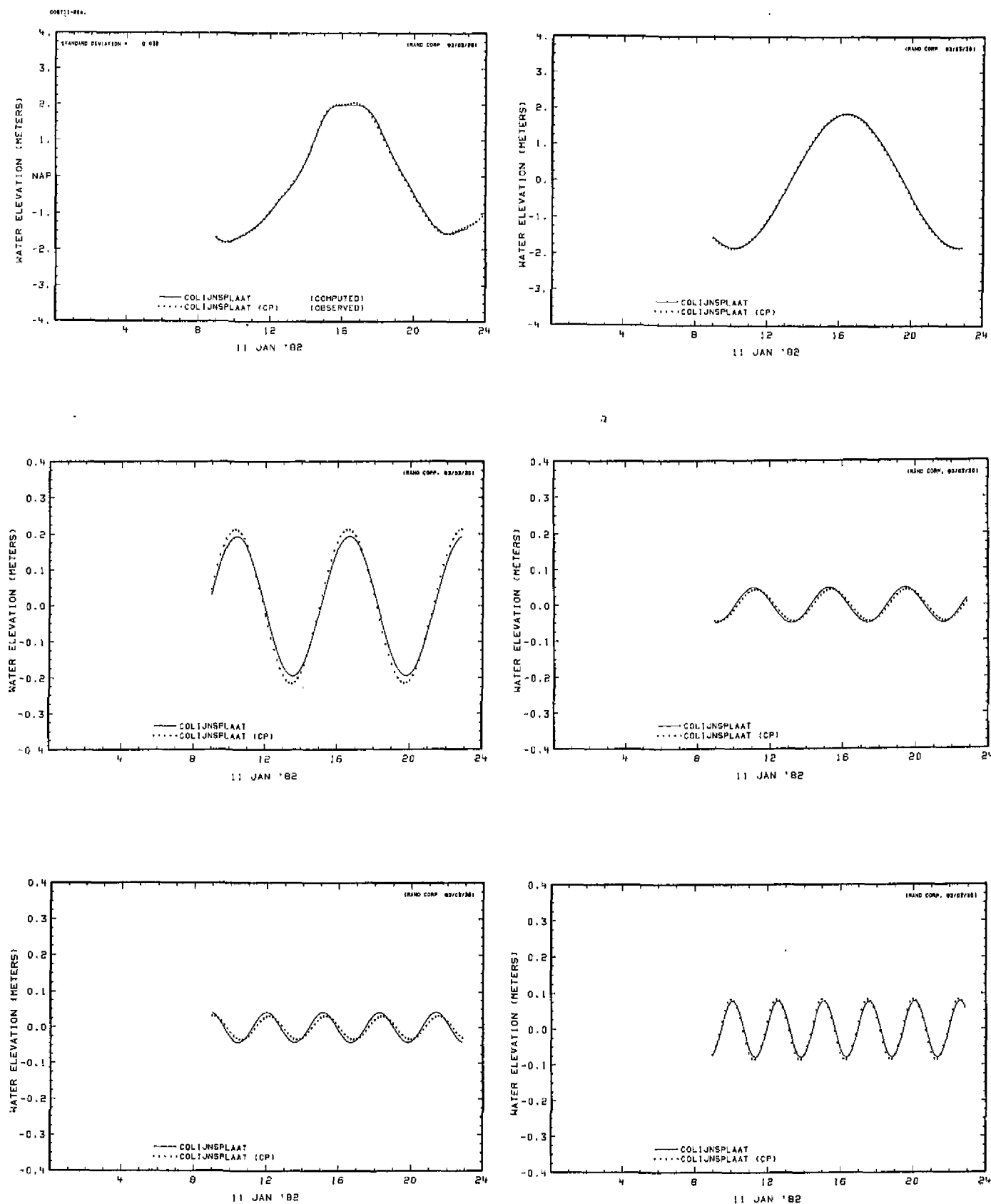Fig. E.2—Observed and computed tides and tidal components at OS9: (a) composite tide,
(b) semidiurnal tide, (c) quarter-diurnal tide, (d) sixth-diurnal tide, (e) eighth-
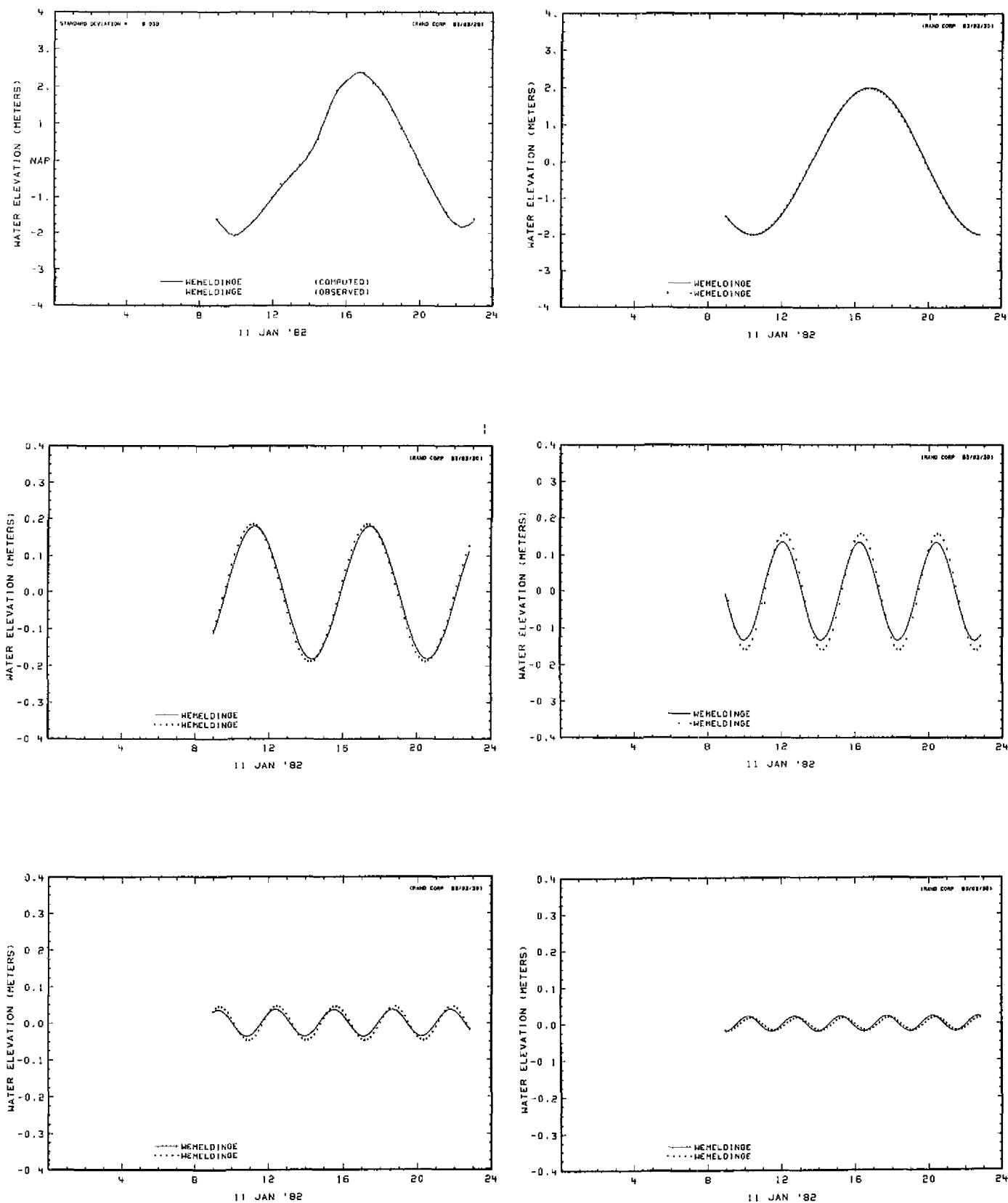diurnal tide, (f) tenth-diurnal tide

Fig. E.3—Observed and computed tides and tidal components at Vlietepolder:
(a) composite tide, (b) semidiurnal tide, (c) quarter-diurnal tide, (d) sixth-
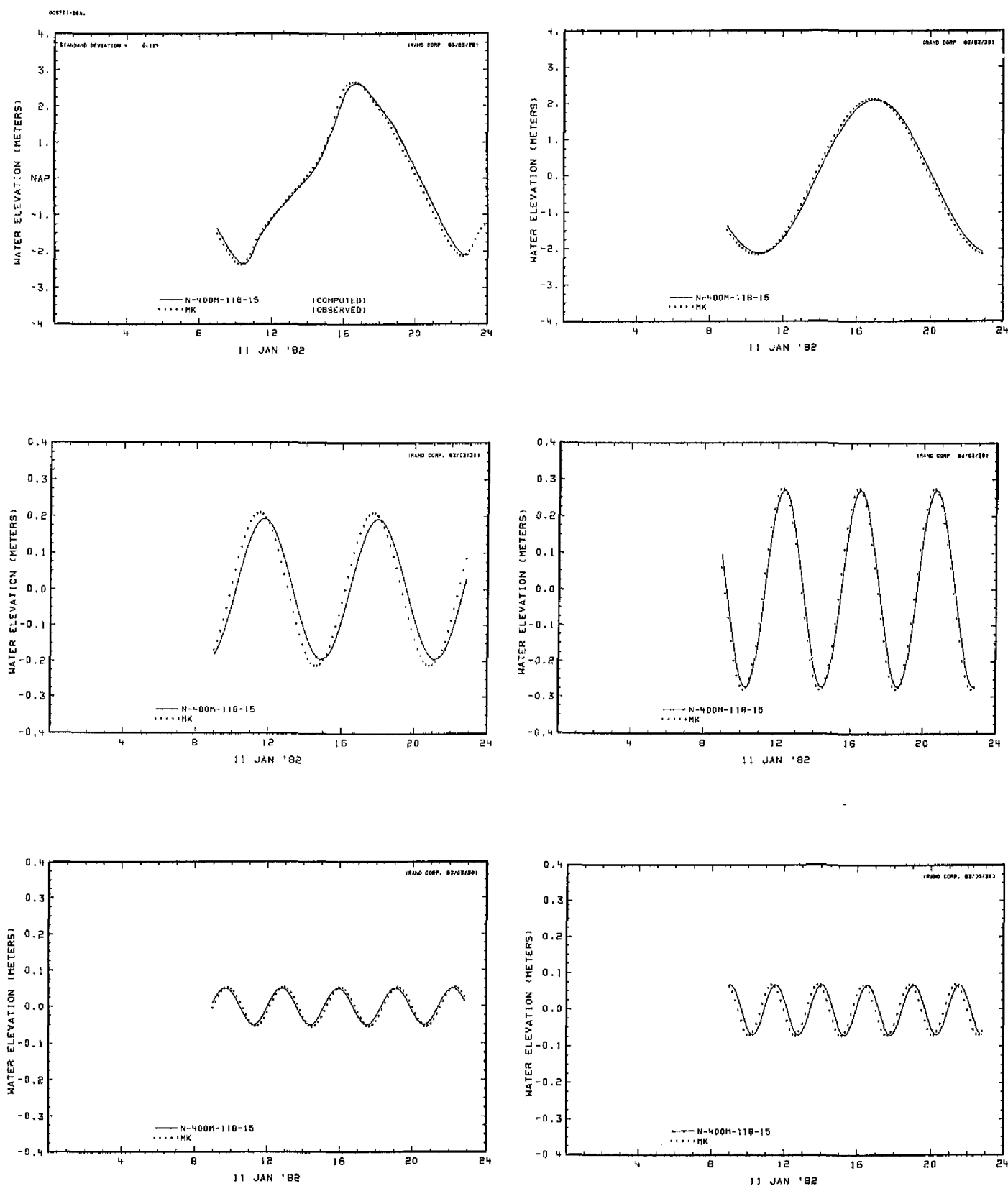diurnal tide, (e) eighth-diurnal tide, (f) tenth-diurnal tide

Fig. E.4—Observed and computed tides and tidal components at Colijnsplaat:
(a) composite tide, (b) semidiurnal tide, (c) quarter-diurnal tide, (d) sixth-
diurnal tide, (e) eighth-diurnal tide, (f) tenth-diurnal tide

Fig. E.5—Observed and computed tides and tidal components at Wemeldinge:
(a) composite tide, (b) semidiurnal tide, (c) quarter-diurnal tide, (d) sixth-
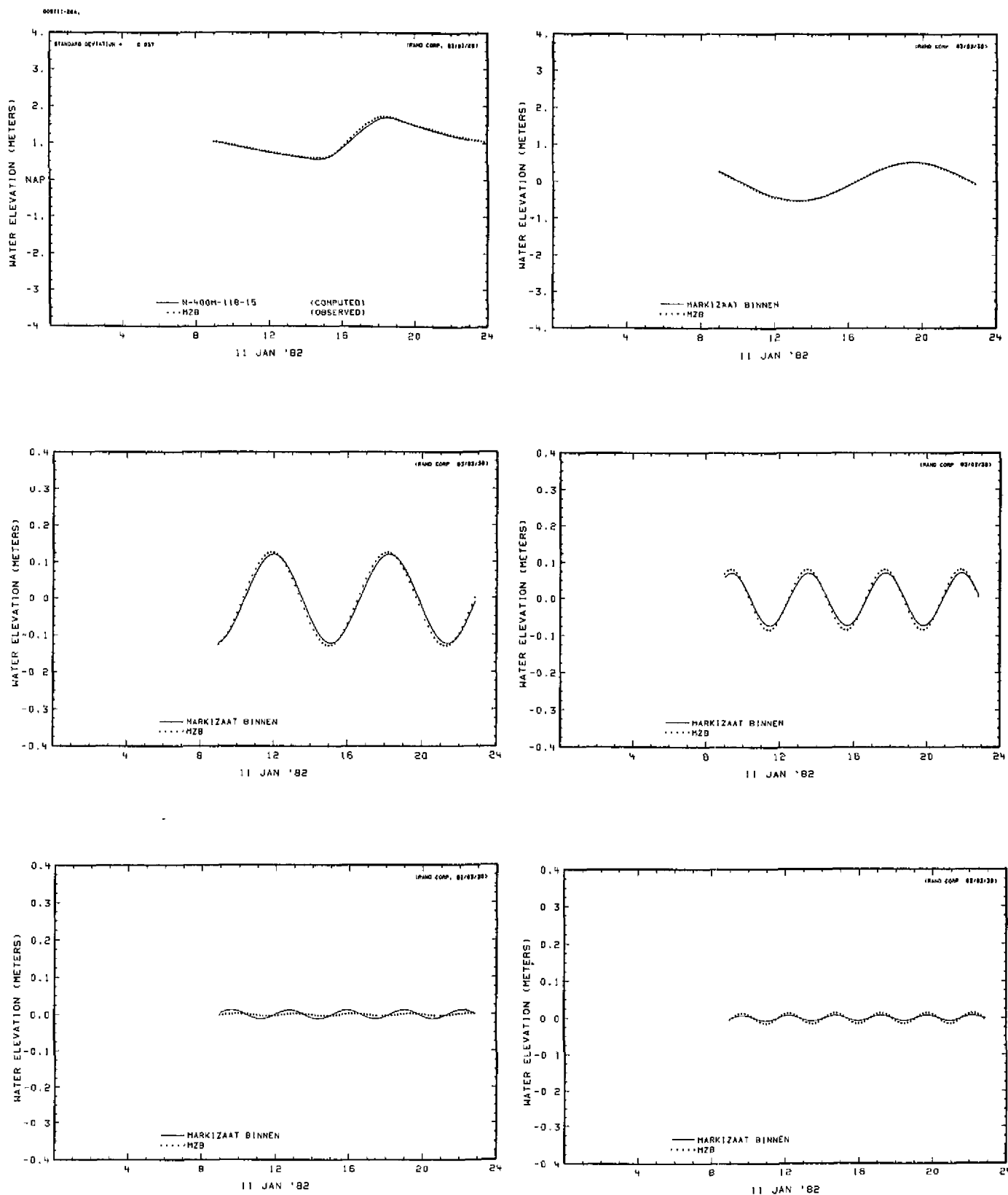diurnal tide, (e) eighth-diurnal tide, (f) tenth-diurnal tide

Fig. E.6—Observed and computed tides and tidal components at Markiezaat-Buiten:
(a) composite tide, (b) semidiurnal tide, (c) quarter-diurnal tide, (d) sixth-
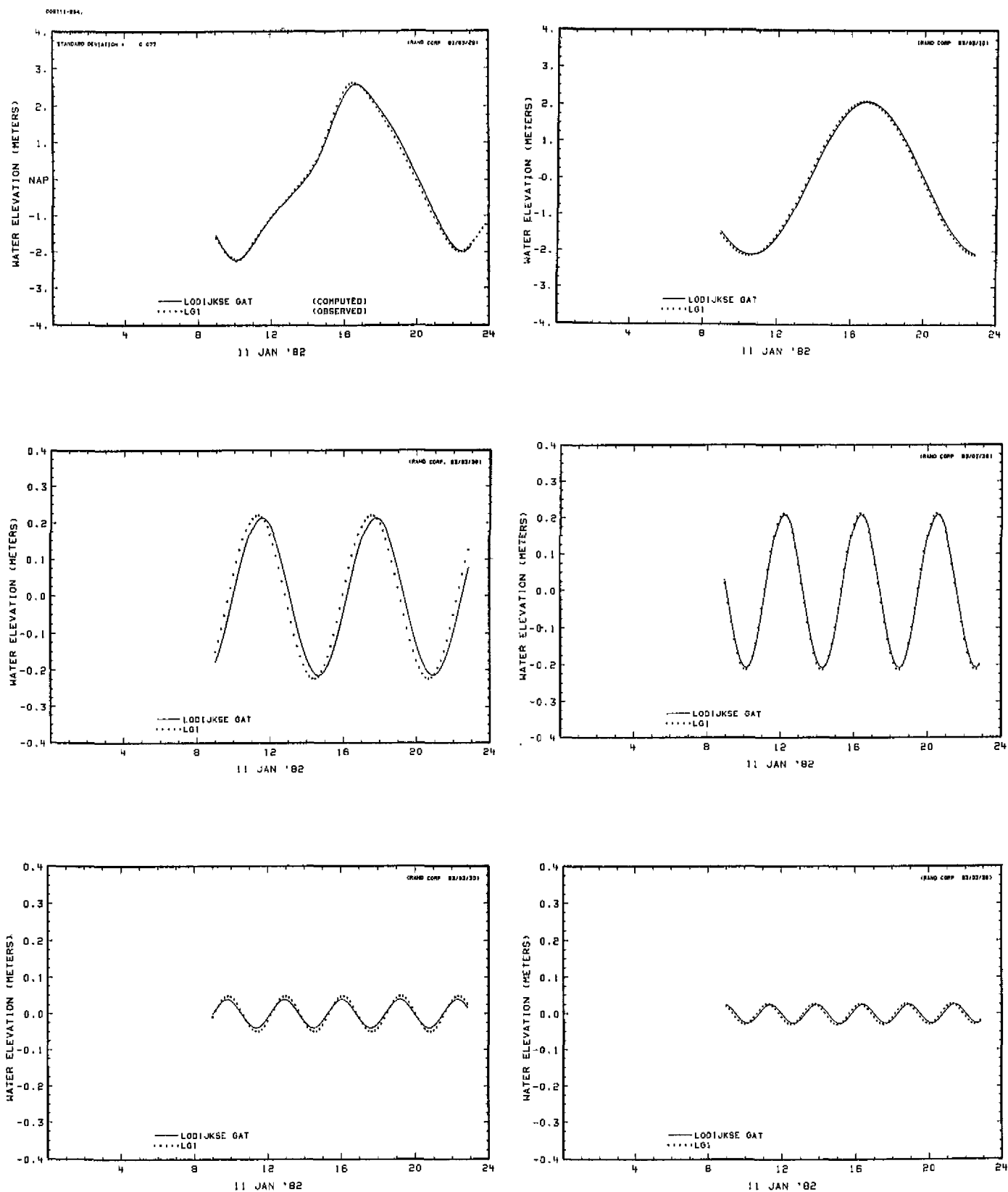diurnal tide, (e) eighth-diurnal tide, (f) tenth-diurnal tide

Fig. E.7—Observed and computed tides and tidal components at Markiezaat-Binnen:
(a) composite tide, (b) semidiurnal tide, (c) quarter-diurnal tide, (d) sixth-
diurnal tide, (e) eighth-diurnal tide, (f) tenth-diurnal tide

Fig. E.8—Observed and computed tides and tidal components at Lodijkse Gat:
(a) composite tide, (b) semidiurnal tide, (c) quarter-diurnal tide, (d) sixth-
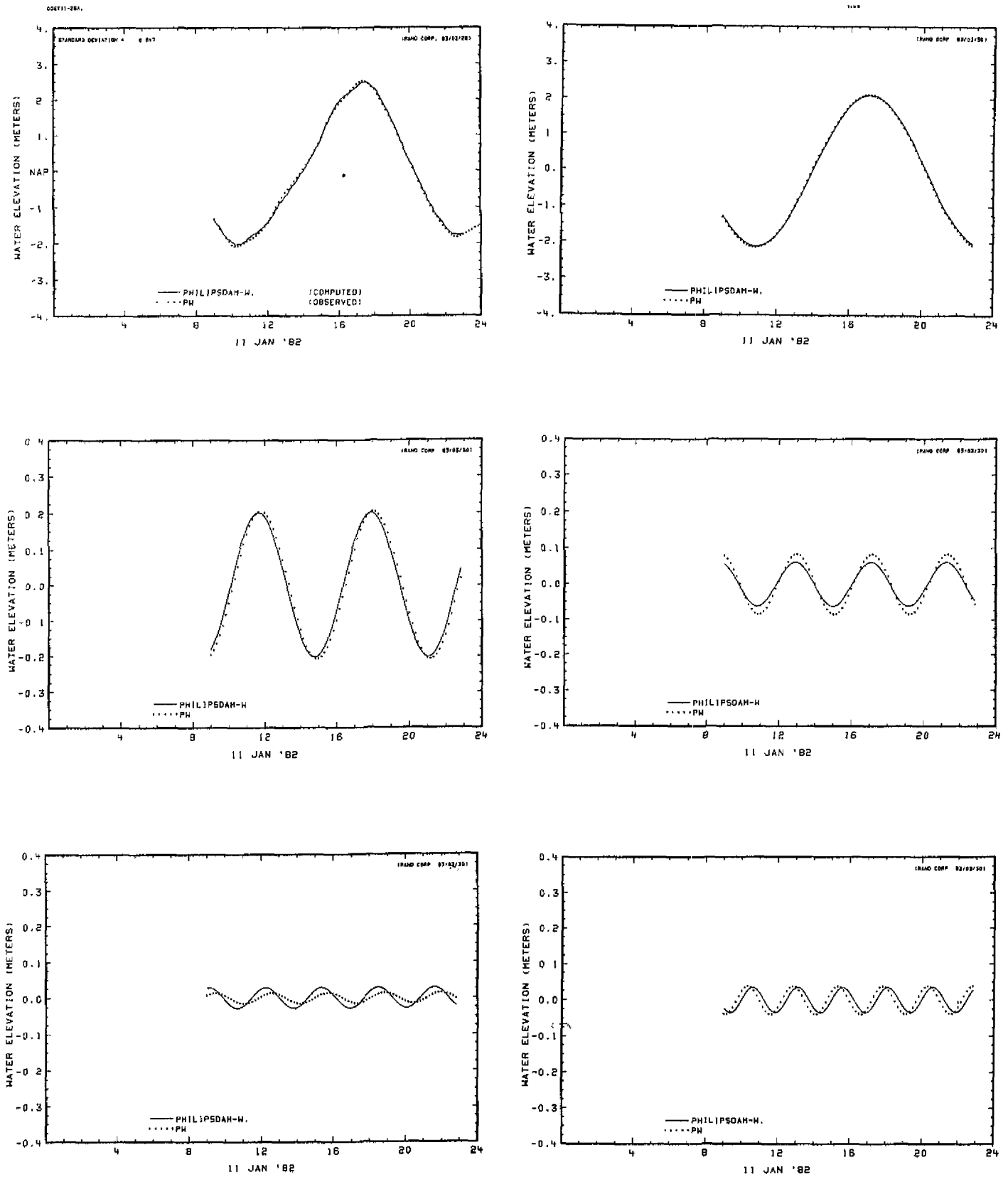diurnal tide, (e) eighth-diurnal tide, (f) tenth-diurnal tide

Fig. E.9—Observed and computed tides and tidal components at Philipsdam-West:
(a) composite tide, (b) semidiurnal tide, (c) quarter-diurnal tide, (d) sixth-
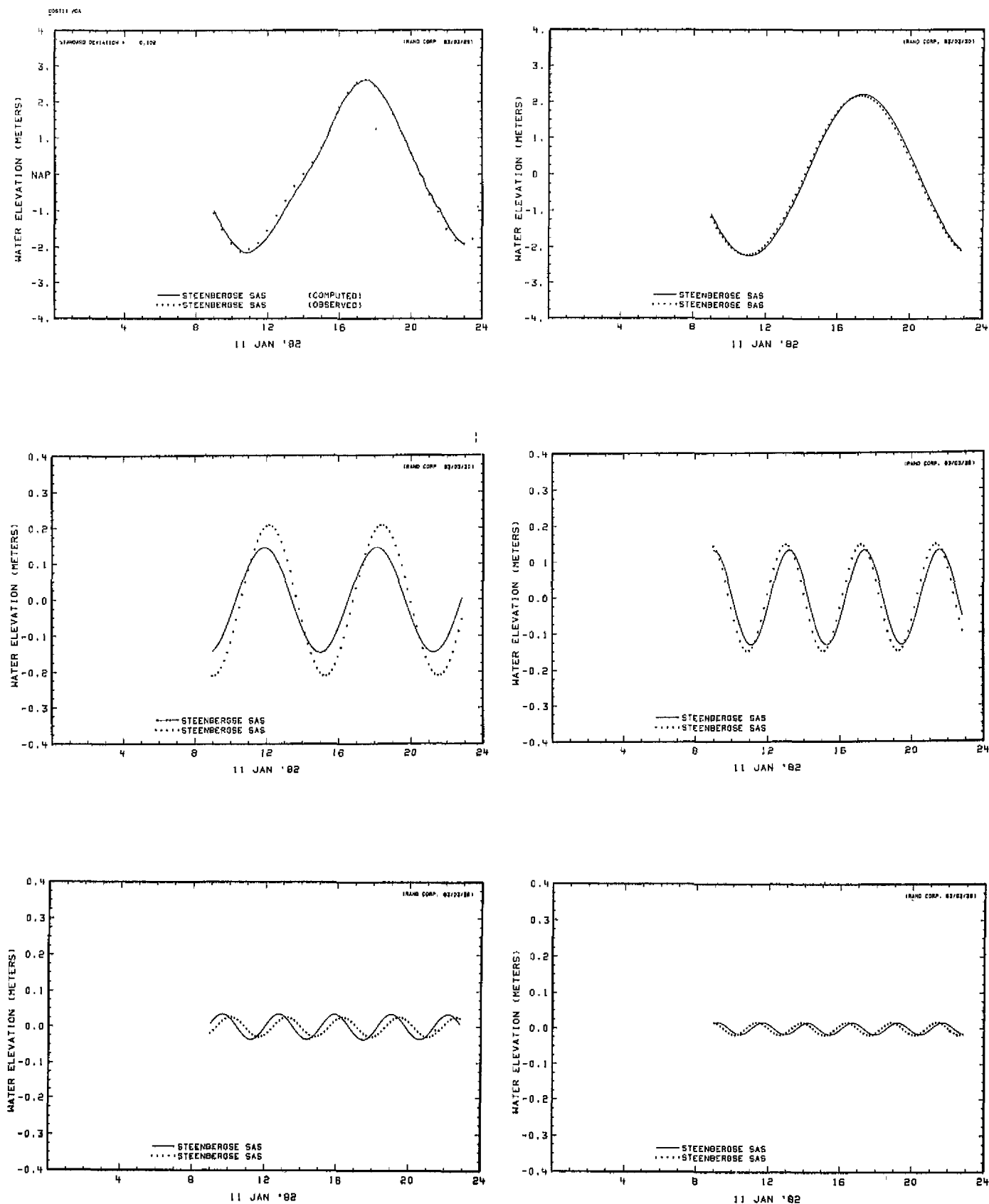diurnal tide, (e) eighth-diurnal tide, (f) tenth-diurnal tide

Fig. E.10—Observed and computed tides and tidal components at Steenbergse Sas:
(a) composite tide, (b) semidiurnal tide, (c) quarter-diurnal tide, (d) sixth-
diurnal tide, (e) eighth-diurnal tide, (f) tenth-diurnal tide
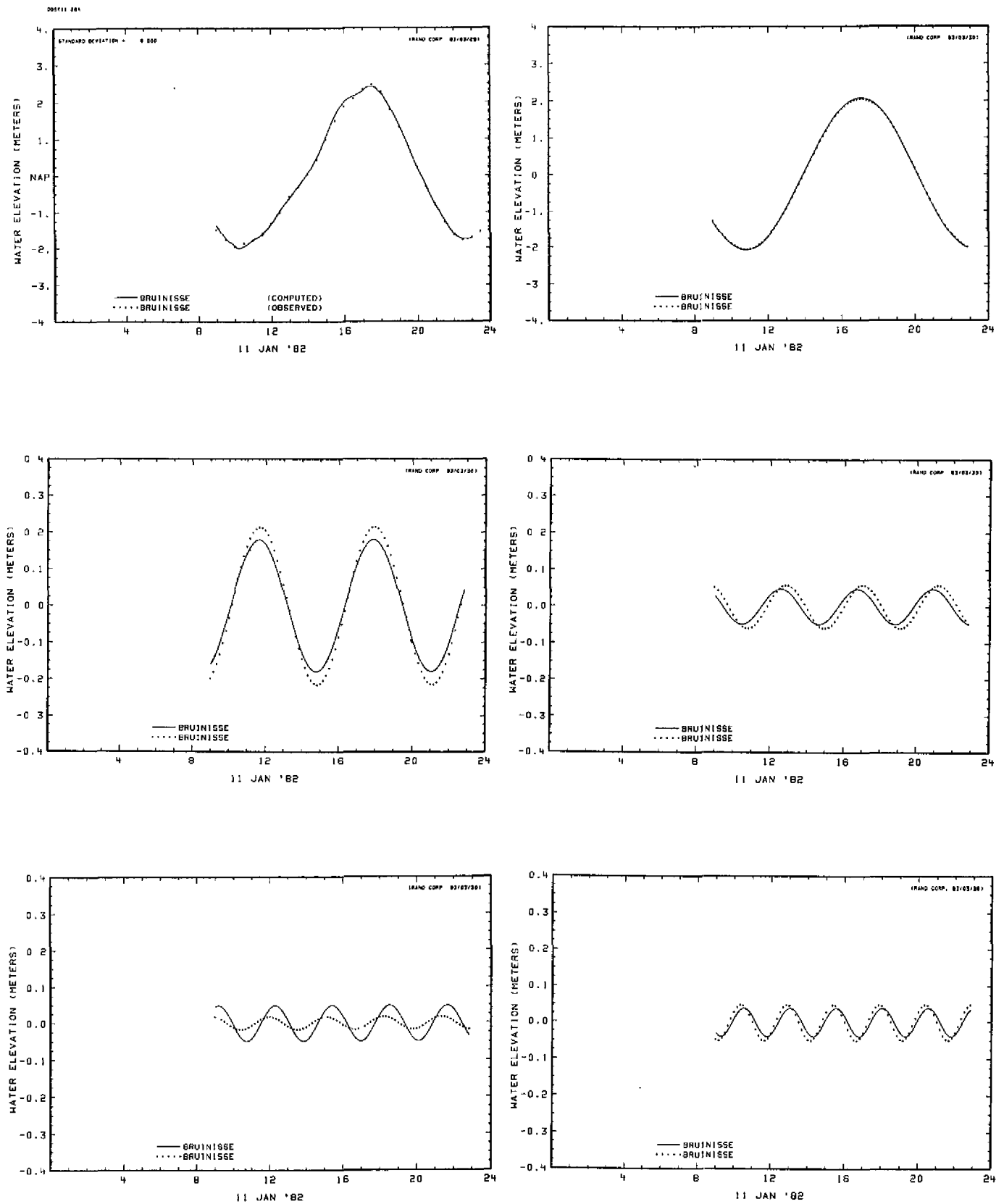
Fig. E.11—Observed and computed tides and tidal components at Bruinisse:
(a) composite tide, (b) semidiurnal tide, (c) quarter-diurnal tide, (d) sixth-
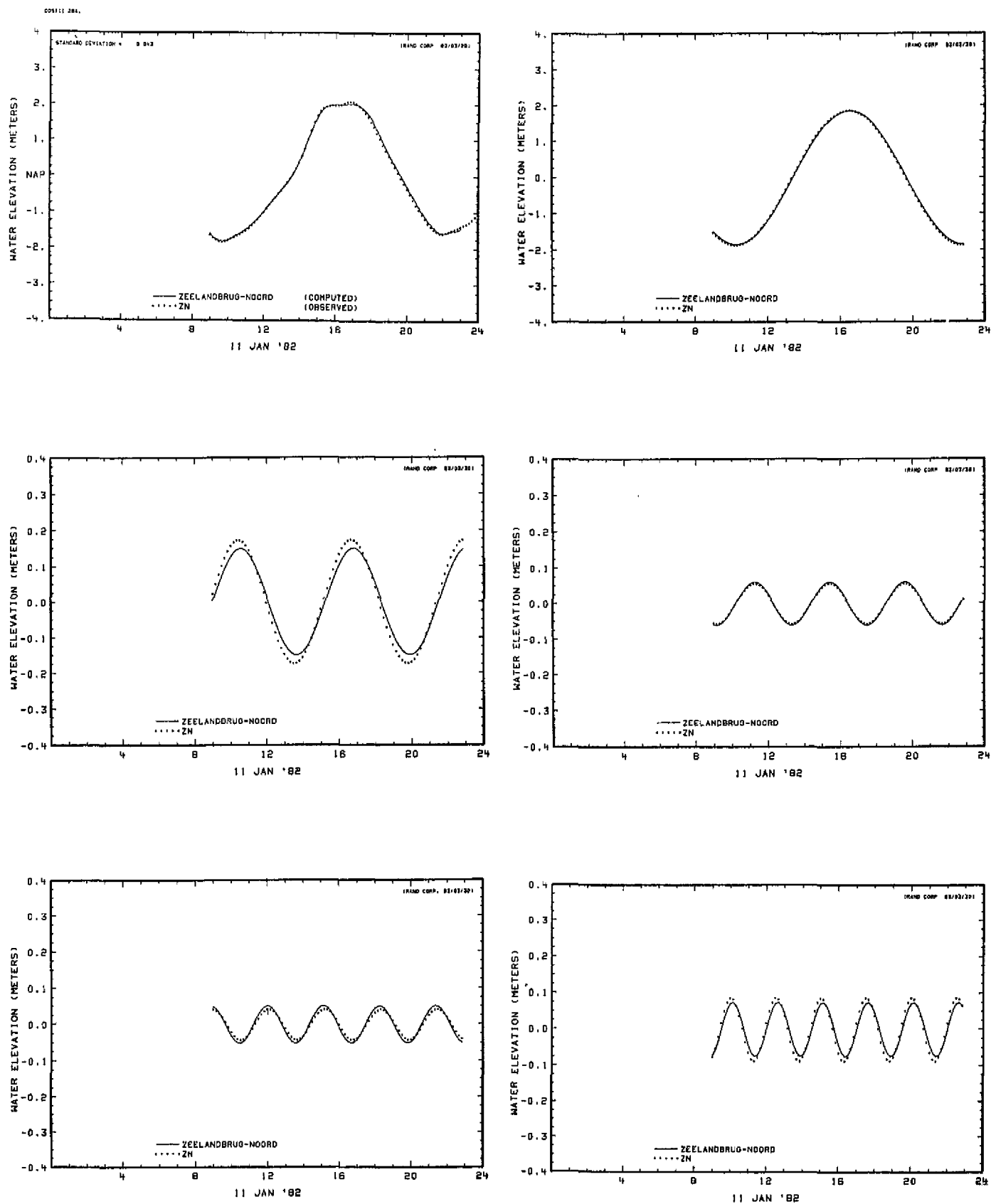diurnal tide, (e) eighth-diurnal tide, (f) tenth-diurnal tide

Fig. E.12—Observed and computed tides and tidal components at Zeelandbrug-N:
(a) composite tide, (b) semidiurnal tide, (c) quarter-diurnal tide, (d) sixth-
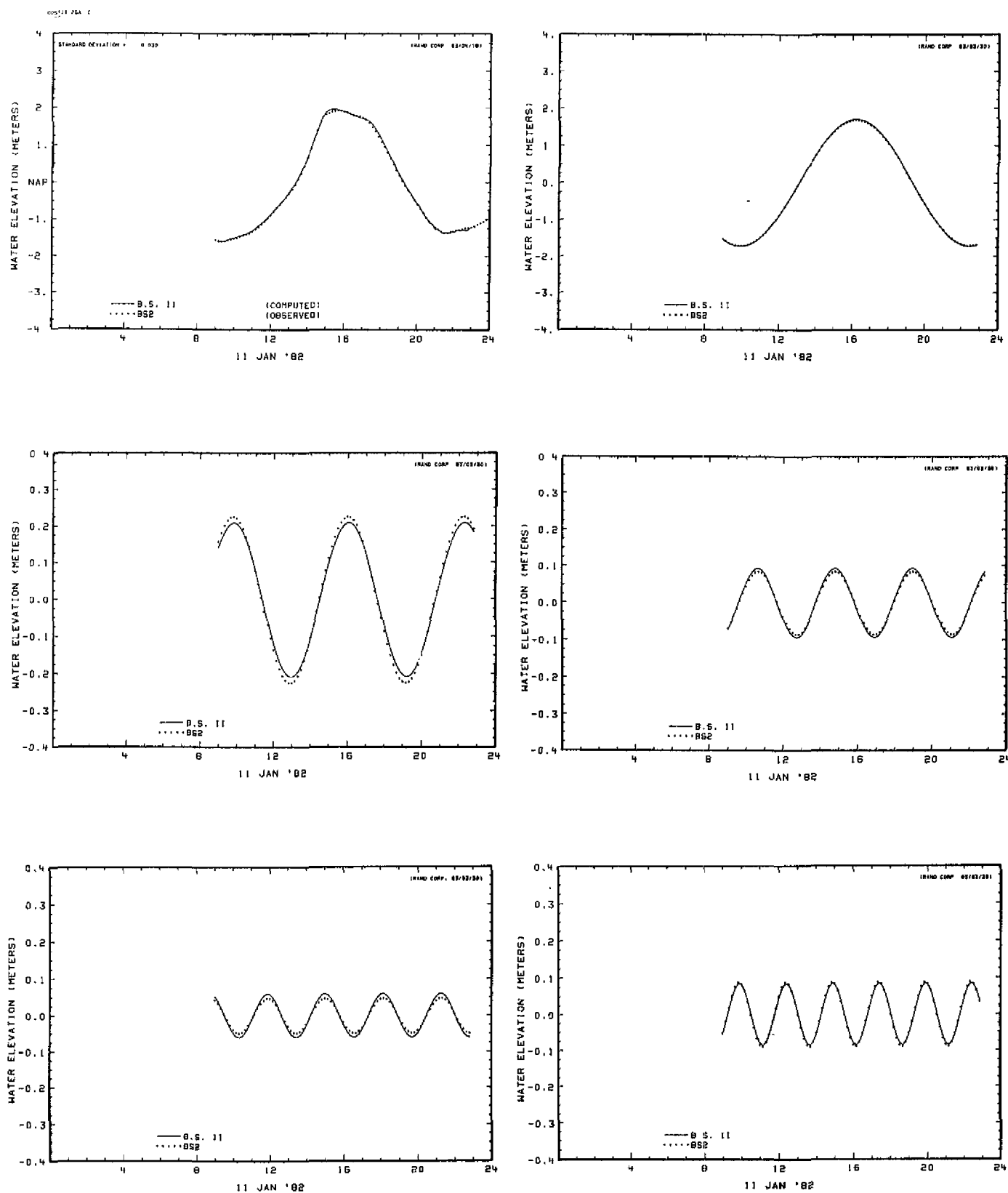diurnal tide, (e) eighth-diurnal tide, (f) tenth-diurnal tide

Fig. E.13—Observed and computed tides and tidal components at BS2: (a) composite tide,
(b) semidiurnal tide, (c) quarter-diurnal tide, (d) sixth-diurnal tide, (e) eighth-
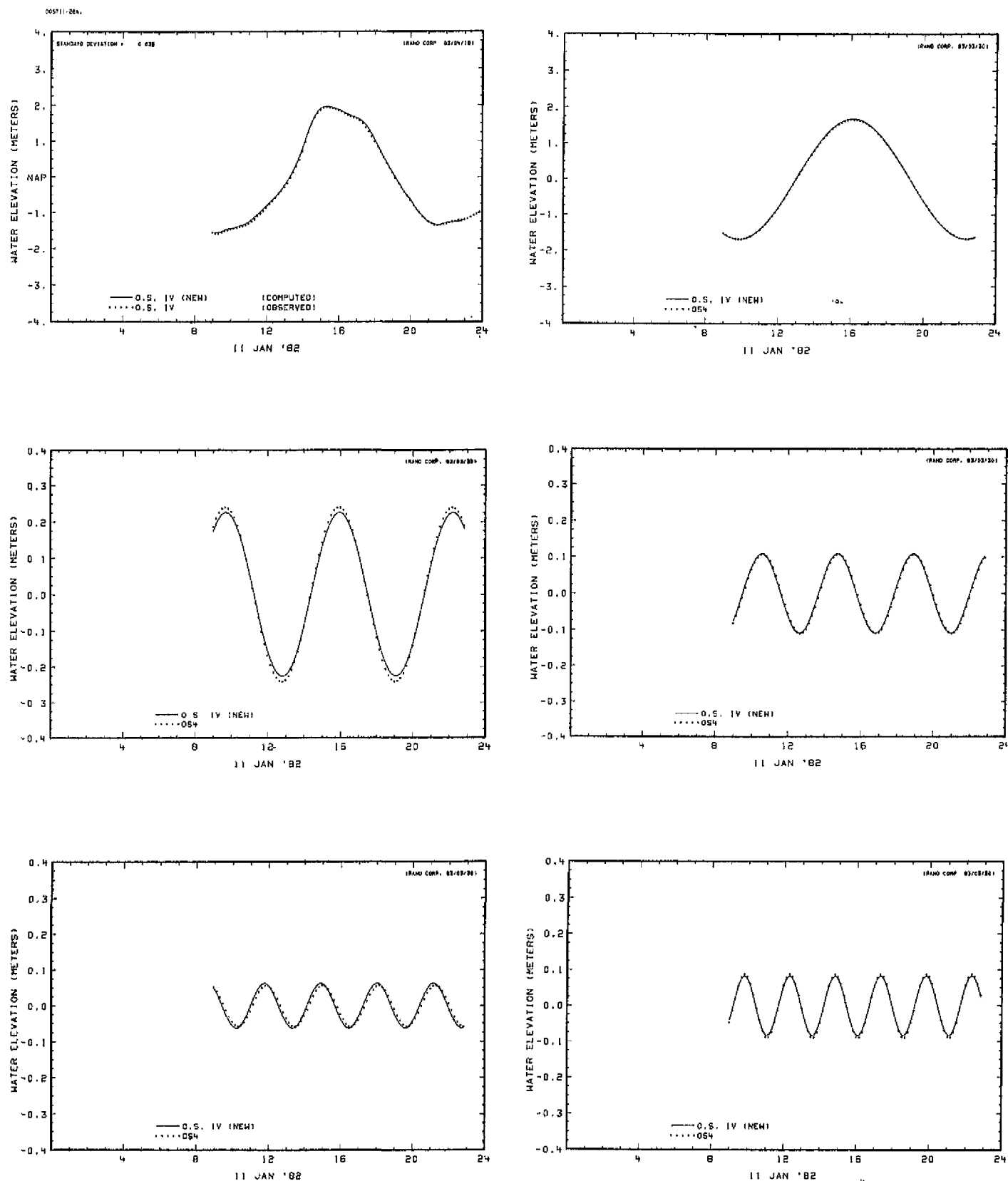diurnal tide, (f) tenth-diurnal tide

Fig. E.14—Observed and computed tides and tidal components at OS4: (a) composite tide,
(b) semidiurnal tide, (c) quarter-diurnal tide, (d) sixth-diurnal tide, (e) eighth-
diurnal tide, (f) tenth-diurnal tide

Appendix F

COMPUTED SALINITY DISTRIBUTIONS FOR THE VERIFICATION SIMULATION

The set of hourly charts in this appendix shows the salinity iso-contours. The lowest contour value is 16 kg/m^3 and is indicated by index (1) and occurs only near the Volkerak in the northeast corner of the model area. The contour interval is set at 2 kg/m^3 with the highest contour line at 30 kg/m^3, which has an index of (9). However, a contour line at 29 kg/m^3 with index (8) is also included as the movement of this line through the tidal cycle shows interesting processes.

The dots on the graphs indicate that at the plotting time in the simulation, the computational point participated in all computation (wet point). In the graphs some current vectors are also shown to correlate the water movements with the configuration of the contour line.
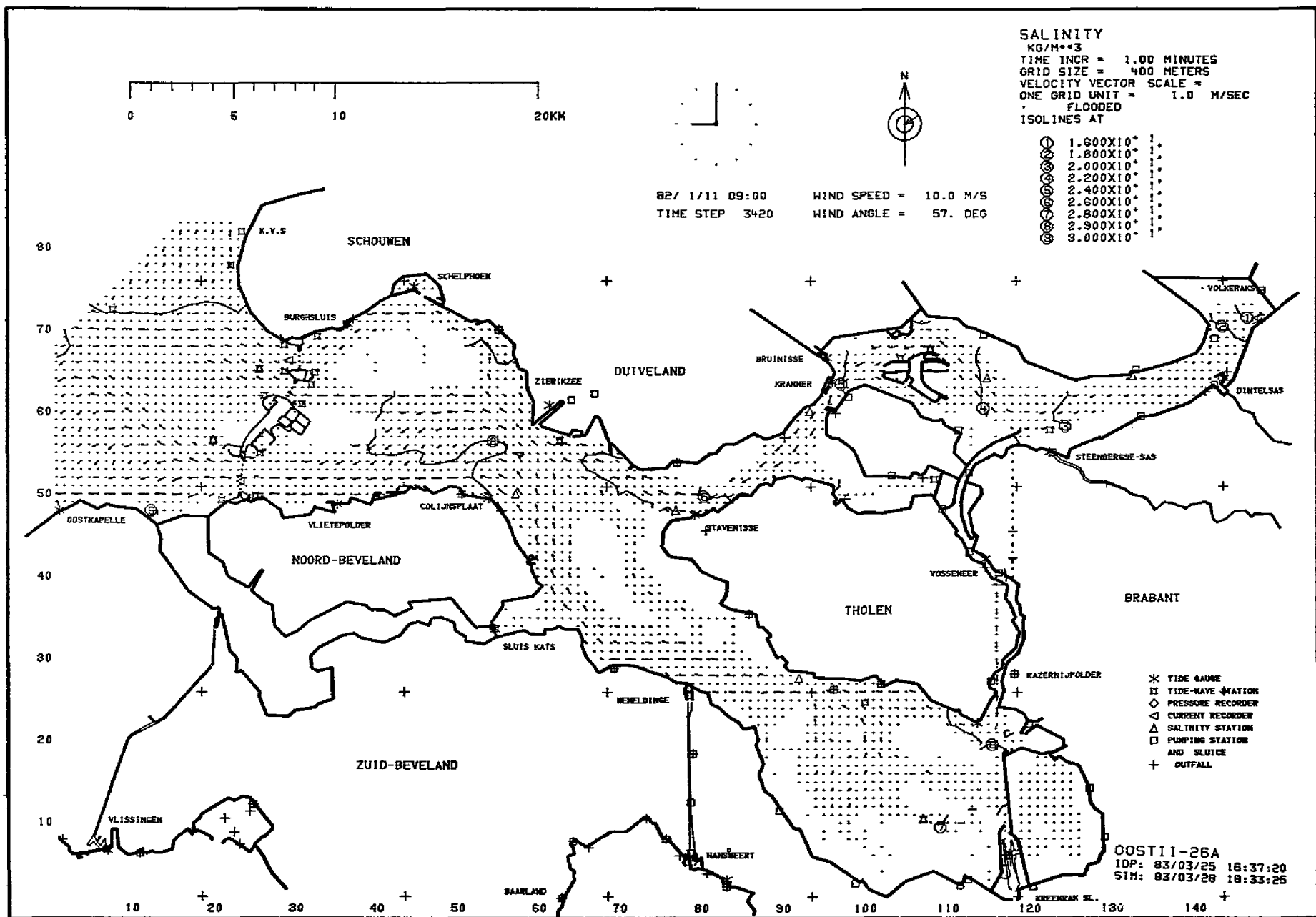
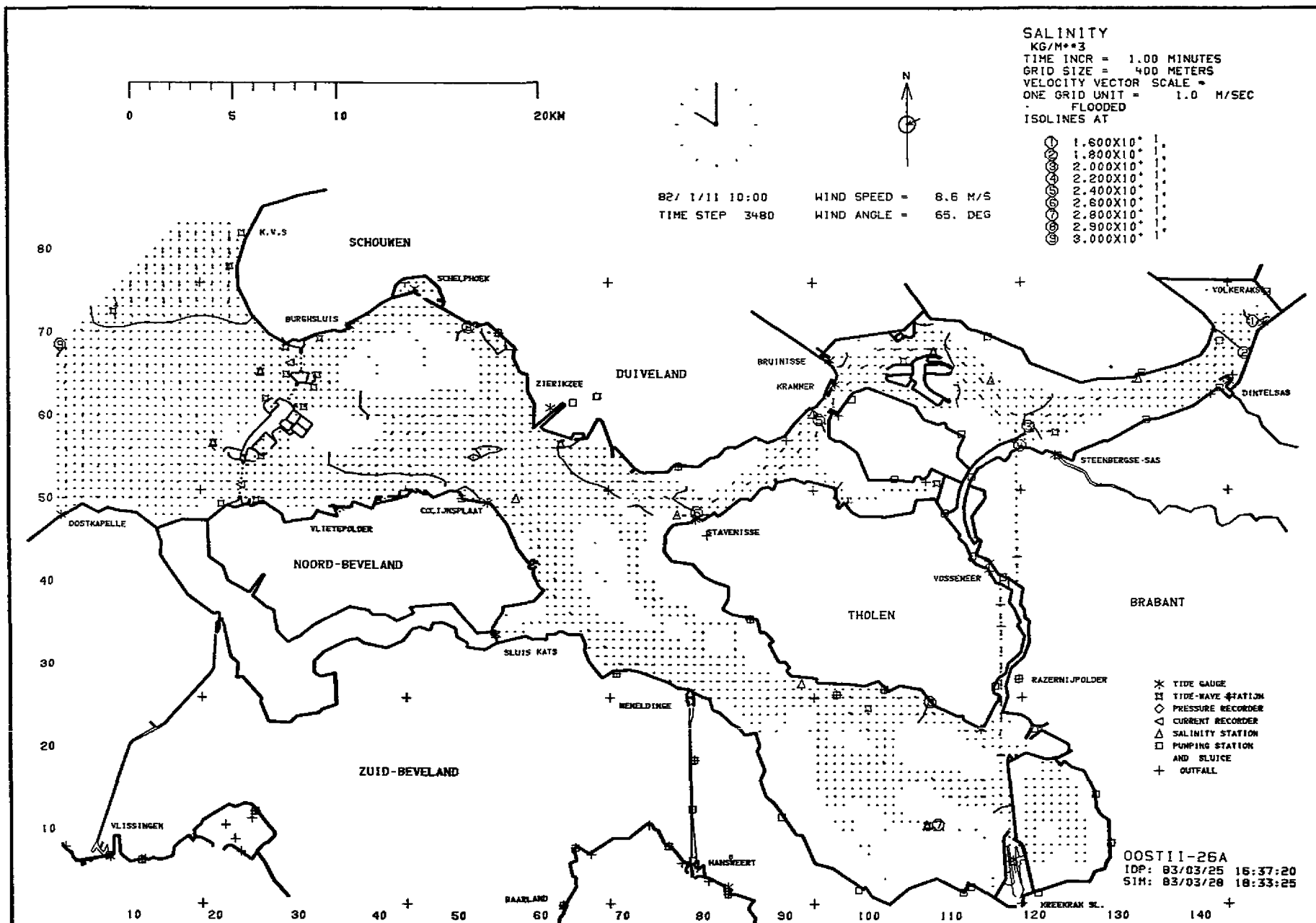Fig. F.1—Computed salinity distributions of the verification simulation at 9:00 hours on 11 January 1982

Fig. F.2—Computed salinity distributions of the verification simulation at 10:00 hours on 11 January 1982
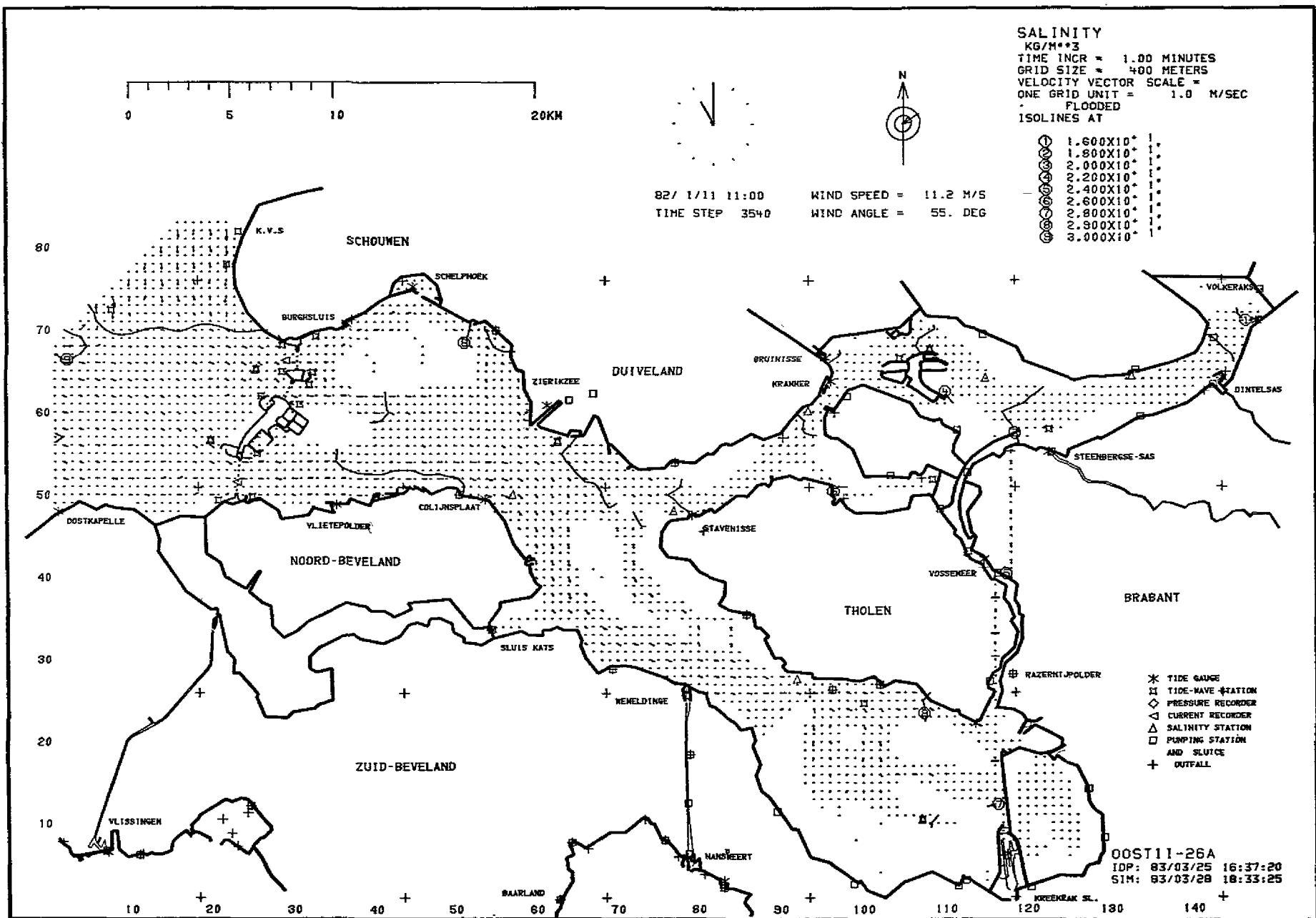
Fig. F.3—Computed salinity distributions of the verification simulation at 11:00 hours on 11 January 1982
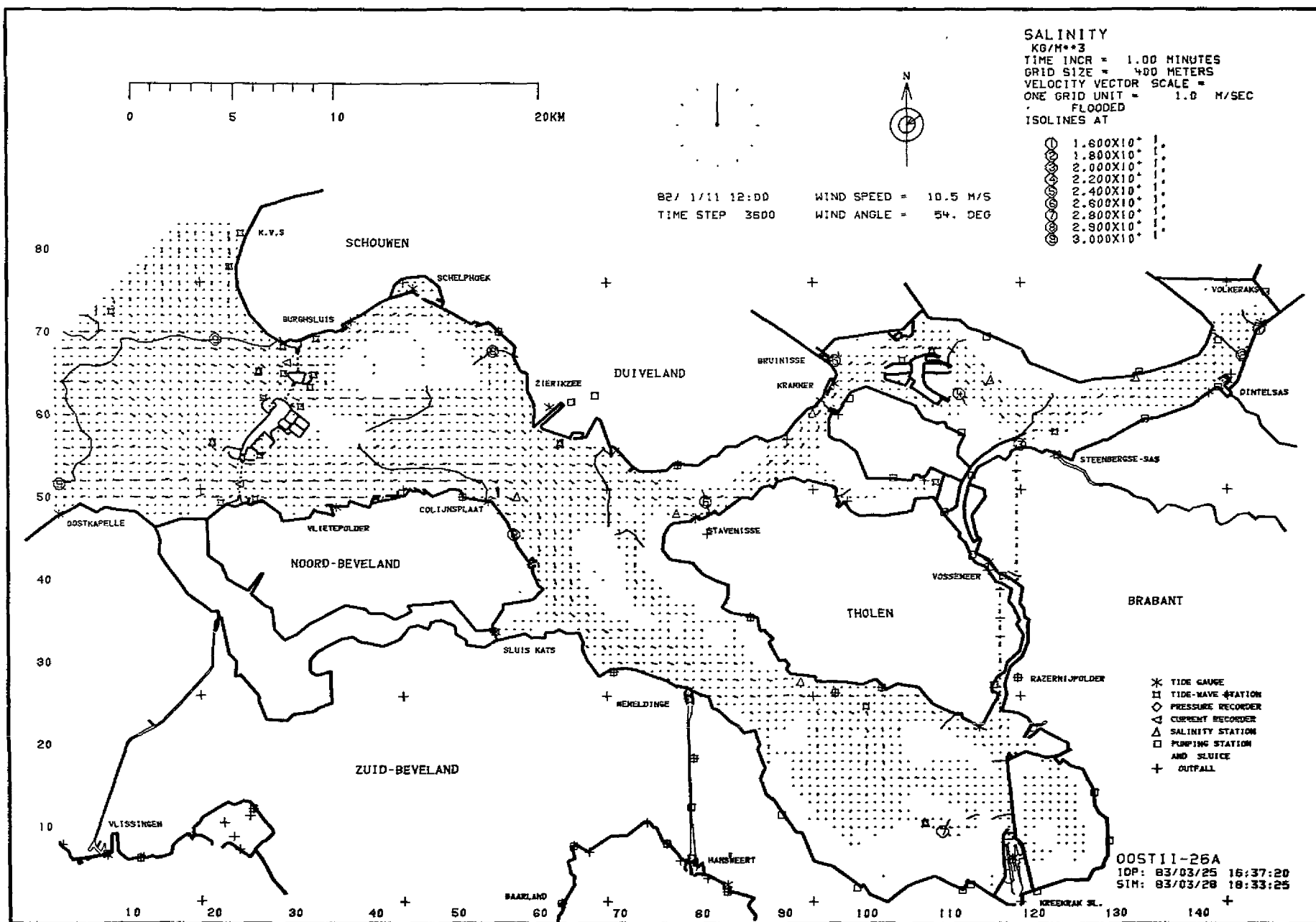
SALINITY
KG/M**3
TIME INCR = 1.00 MINUTES
GRID SIZE = 400 METERS
VELOCITY VECTOR SCALE =
ONE GRID UNIT = 1.0 M/SEC
· FLOODED
ISOLINES AT

① 1.600X10⁺
② 1.800X10⁺
③ 2.000X10⁺
④ 2.200X10⁺
⑤ 2.400X10⁺
⑥ 2.600X10⁺
⑦ 2.800X10⁺
⑧ 2.900X10⁺
⑨ 3.000X10⁺

82/ 1/11 12:00   WIND SPEED = 10.5 M/S
TIME STEP 3600   WIND ANGLE = 54. DEG

N

SCHOUWEN
K.V.S
SCHELPHOEK
BURGHSLUIS
ZIERIKZEE
DUIVELAND
BRUINISSE
KRAMMER
VOLKERAKS
DINTELSAS
STEENBERGSE-SAS
OOSTKAPELLE
VLIETEPOLDER
COLIJNSPLAAT
STAVENISSE
NOORD-BEVELAND
VOSSEMEER
THOLEN
BRABANT
SLUIS KATS
RAZERNIJPOLDER
WEMELDINGE
ZUID-BEVELAND
VLISSINGEN
HANSWEERT
BAARLAND
KREEKRAK SL.

※ TIDE GAUGE
Ⅱ TIDE-WAVE STATION
◇ PRESSURE RECORDER
◁ CURRENT RECORDER
△ SALINITY STATION
□ PUMPING STATION
   AND SLUICE
+ OUTFALL

OOSTII-26A
IOP: 83/03/25 16:37:20
SIM: 83/03/28 18:33:25

0 5 10 20KM

Fig. F.4—Computed salinity distributions of the verification simulation at 12:00 hours on 11 January 1982
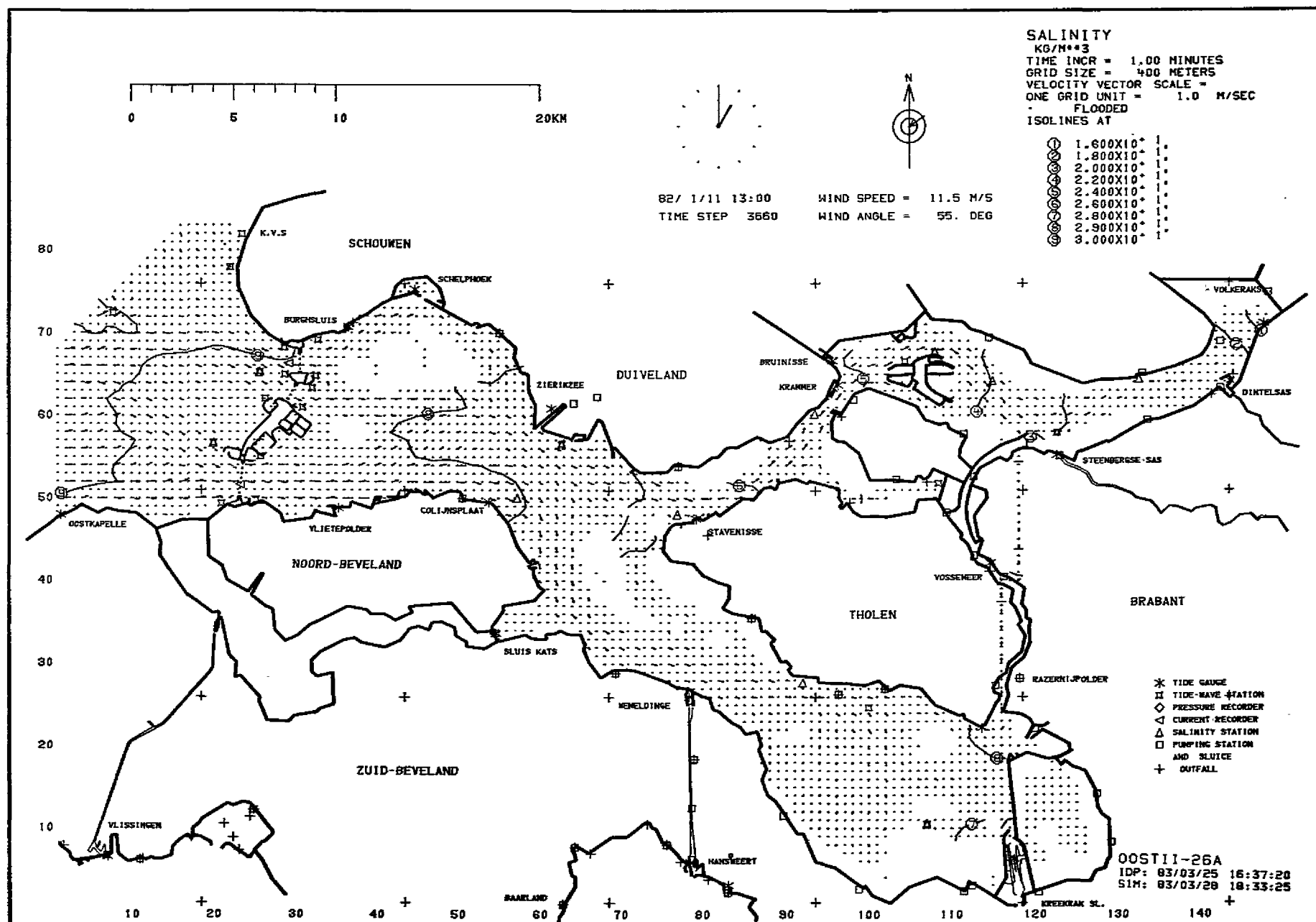
Fig. F.5—Computed salinity distributions of the verification simulation at 13:00 hours on 11 January 1982
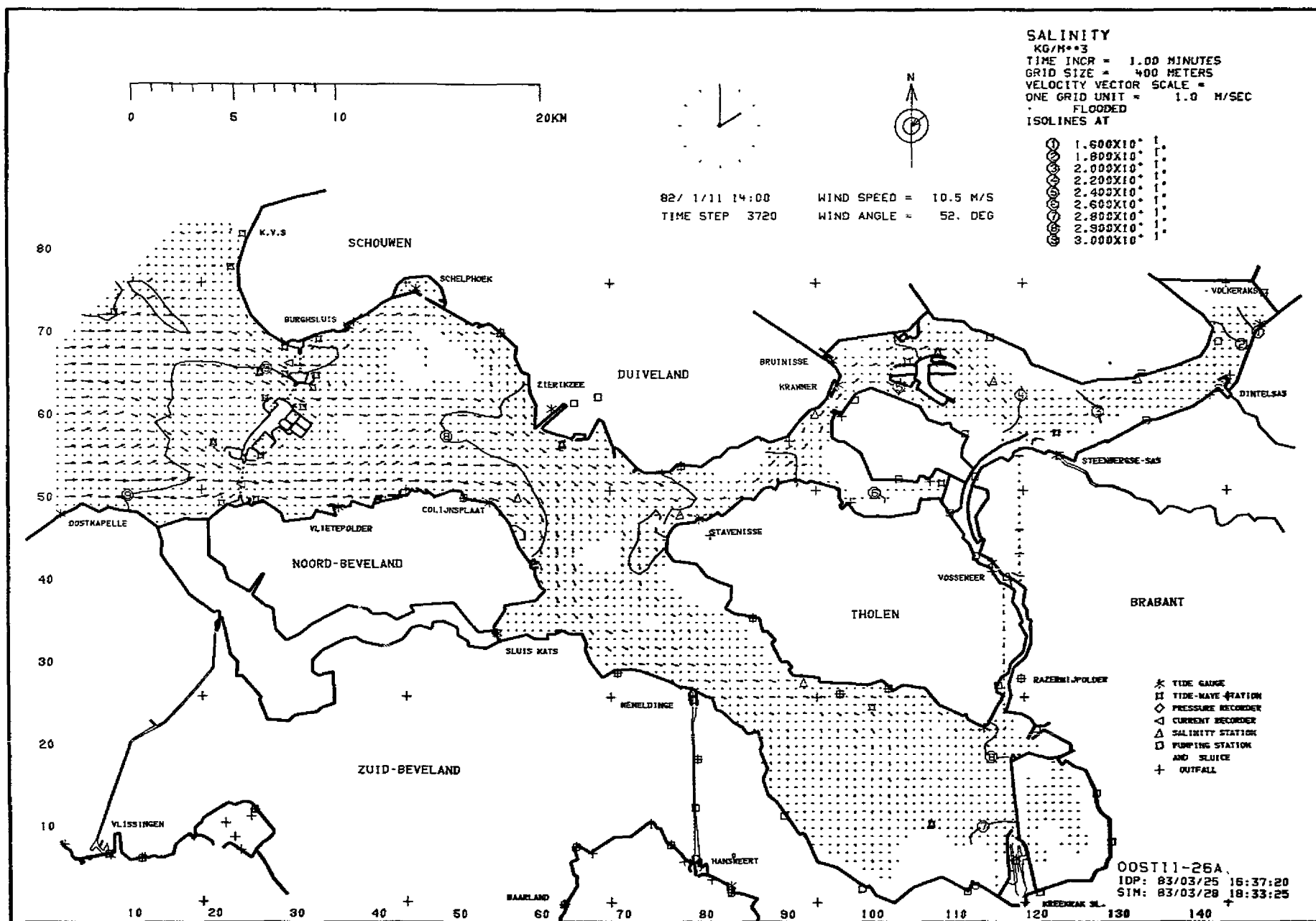
Fig. F.6—Computed salinity distributions of the verification simulation at 14:00 hours on 11 January 1982
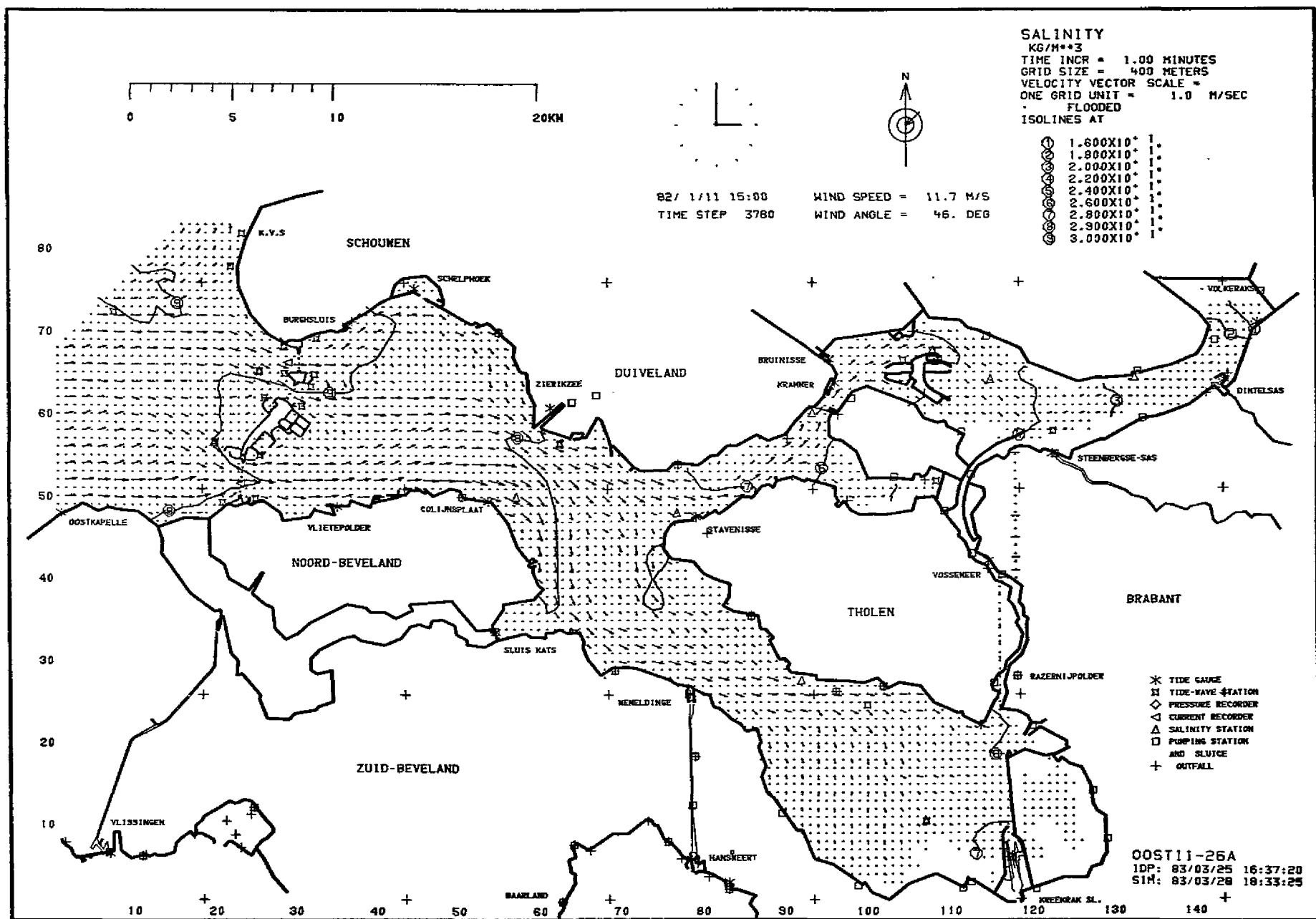
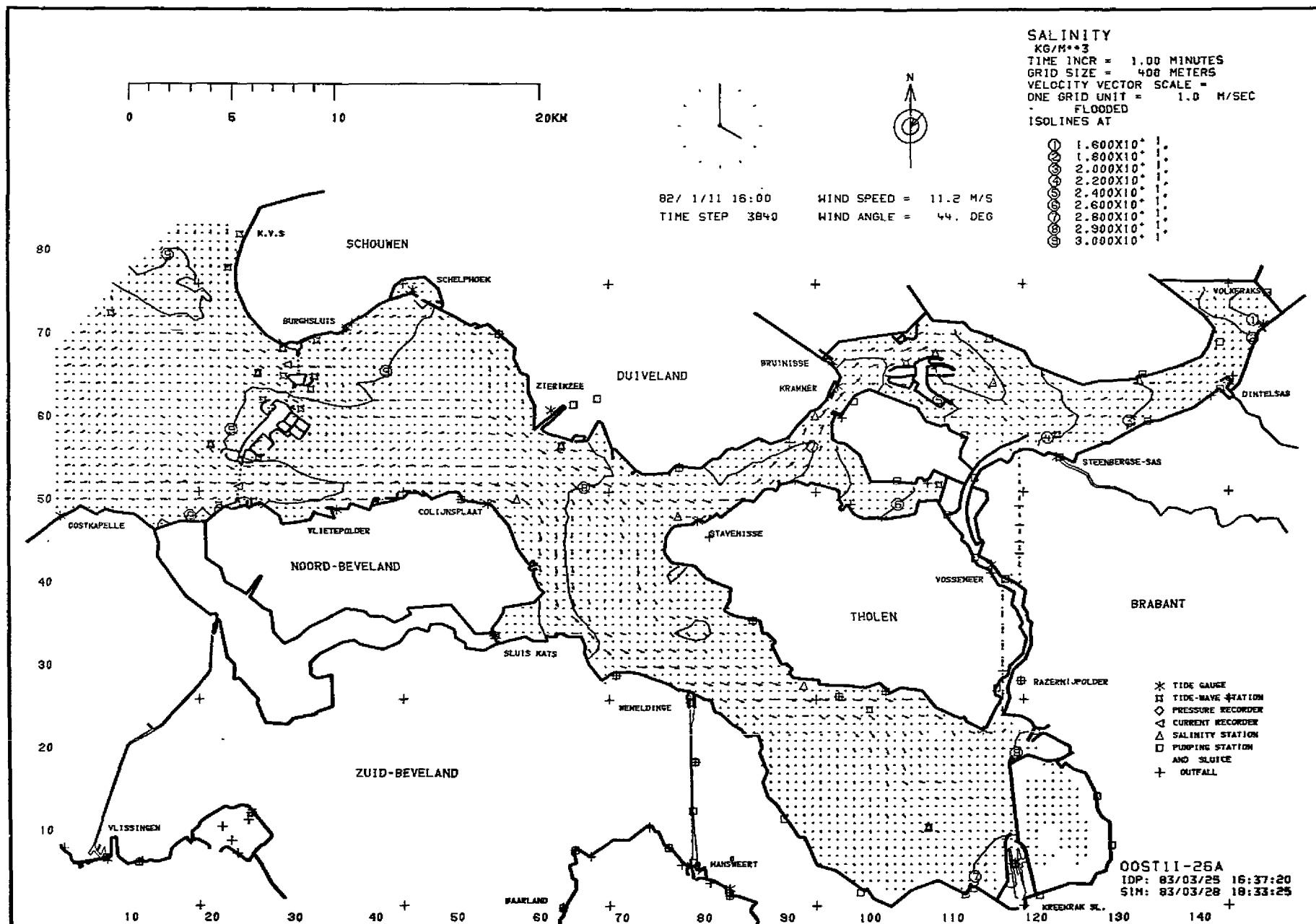Fig. F.7—Computed salinity distributions of the verification simulation at 15:00 hours on 11 January 1982

Fig. F.8—Computed salinity distributions of the verification simulation at 16:00 hours on 11 January 1982
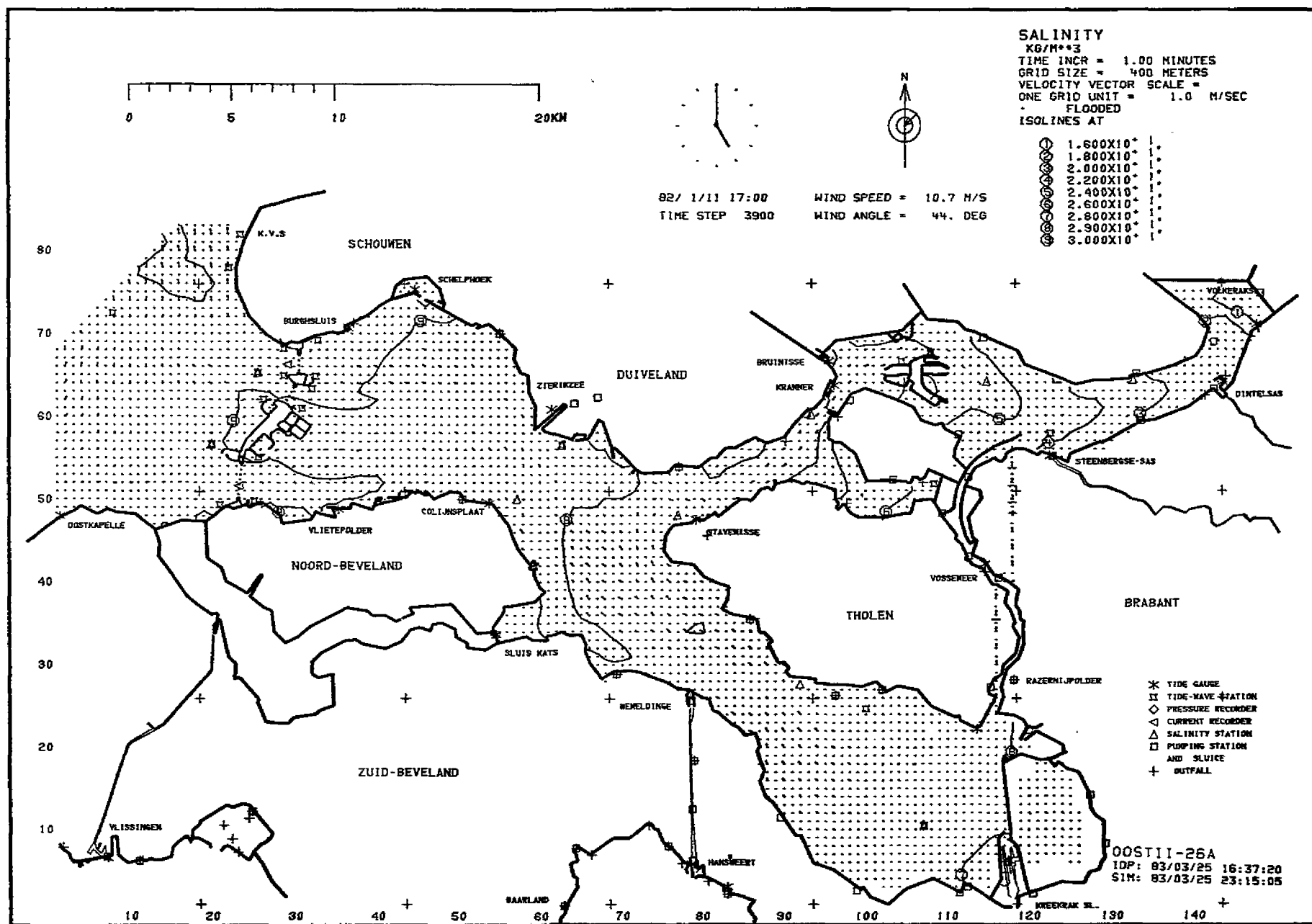
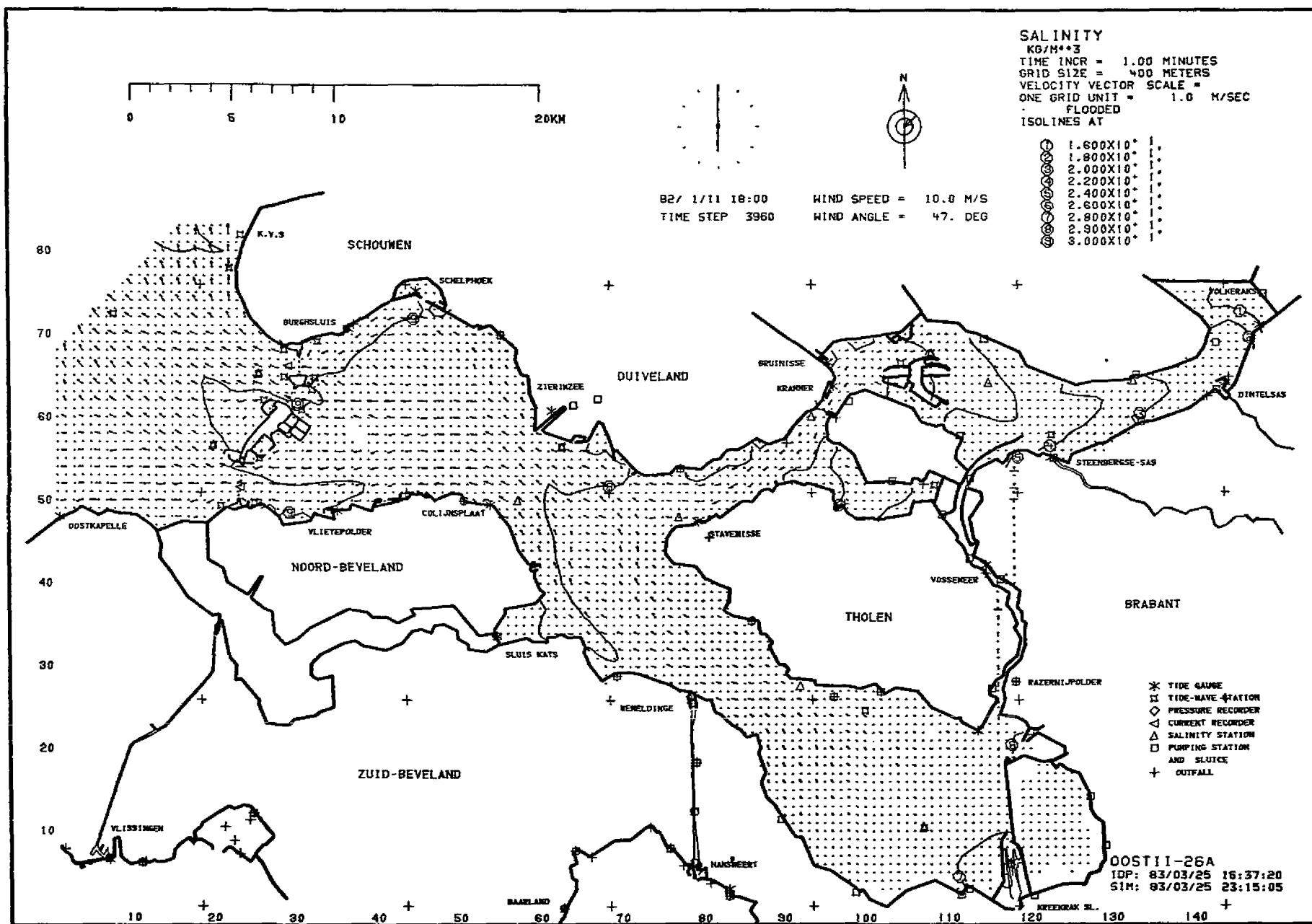Fig. F.9—Computed salinity distributions of the verification simulation at 17:00 hours on 11 January 1982

Fig. F.10—Computed salinity distributions of the verification simulation at 18:00 hours on 11 January 1982
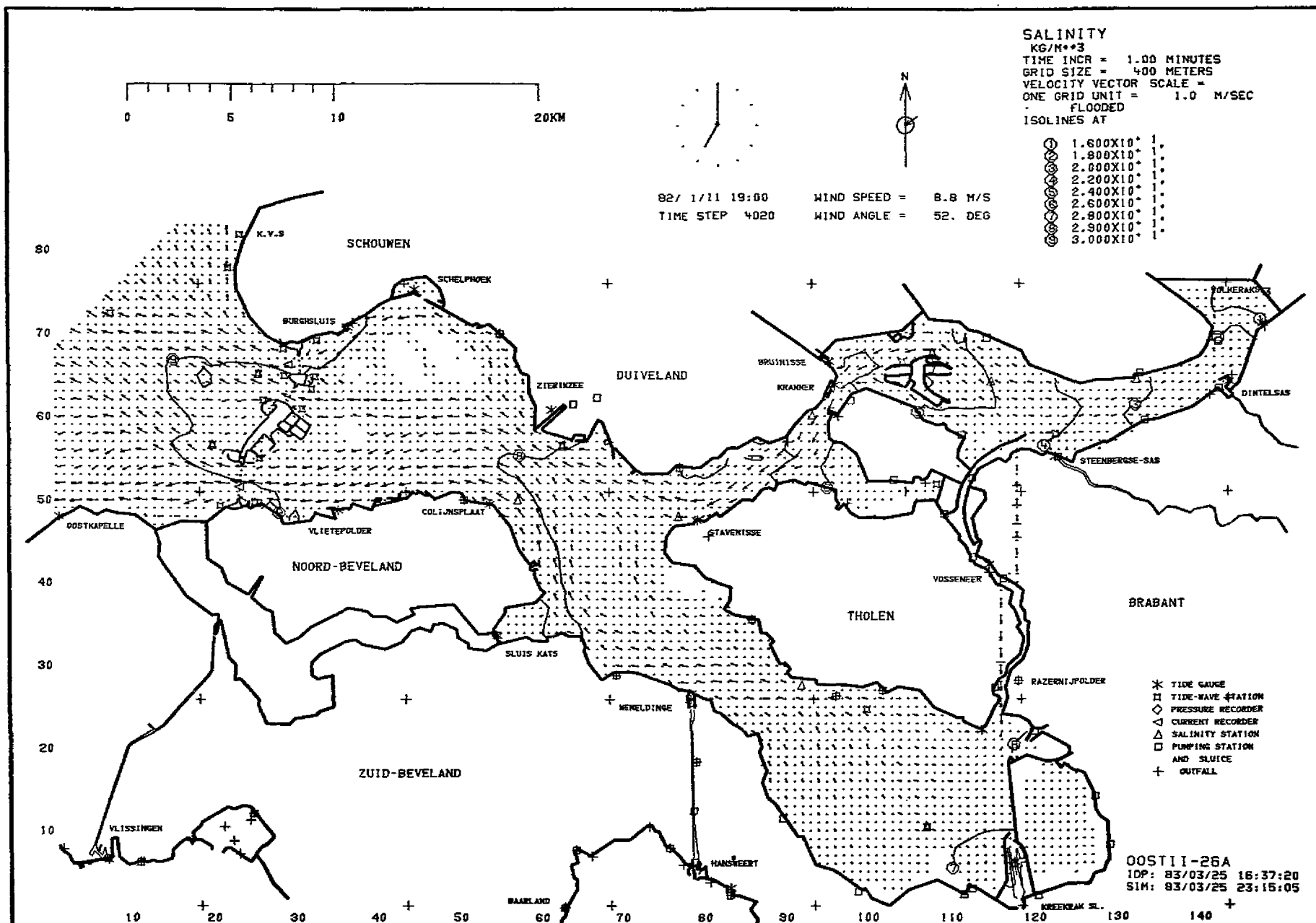
Fig. F.11—Computed salinity distributions of the verification simulation at 19:00 hours on 11 January 1982

Fig. F.12—Computed salinity distributions of the verification simulation at 20:00 hours on 11 January 1982

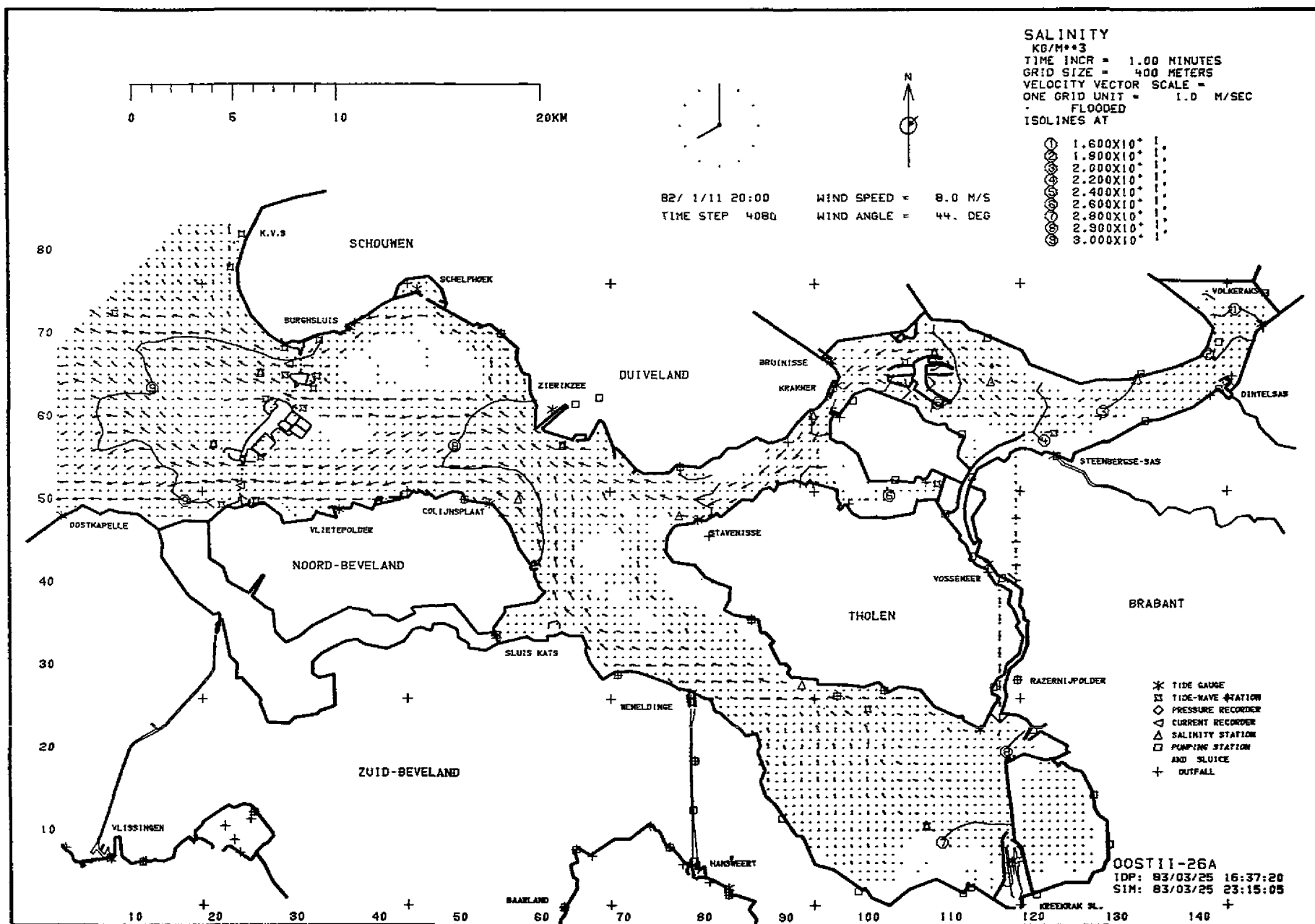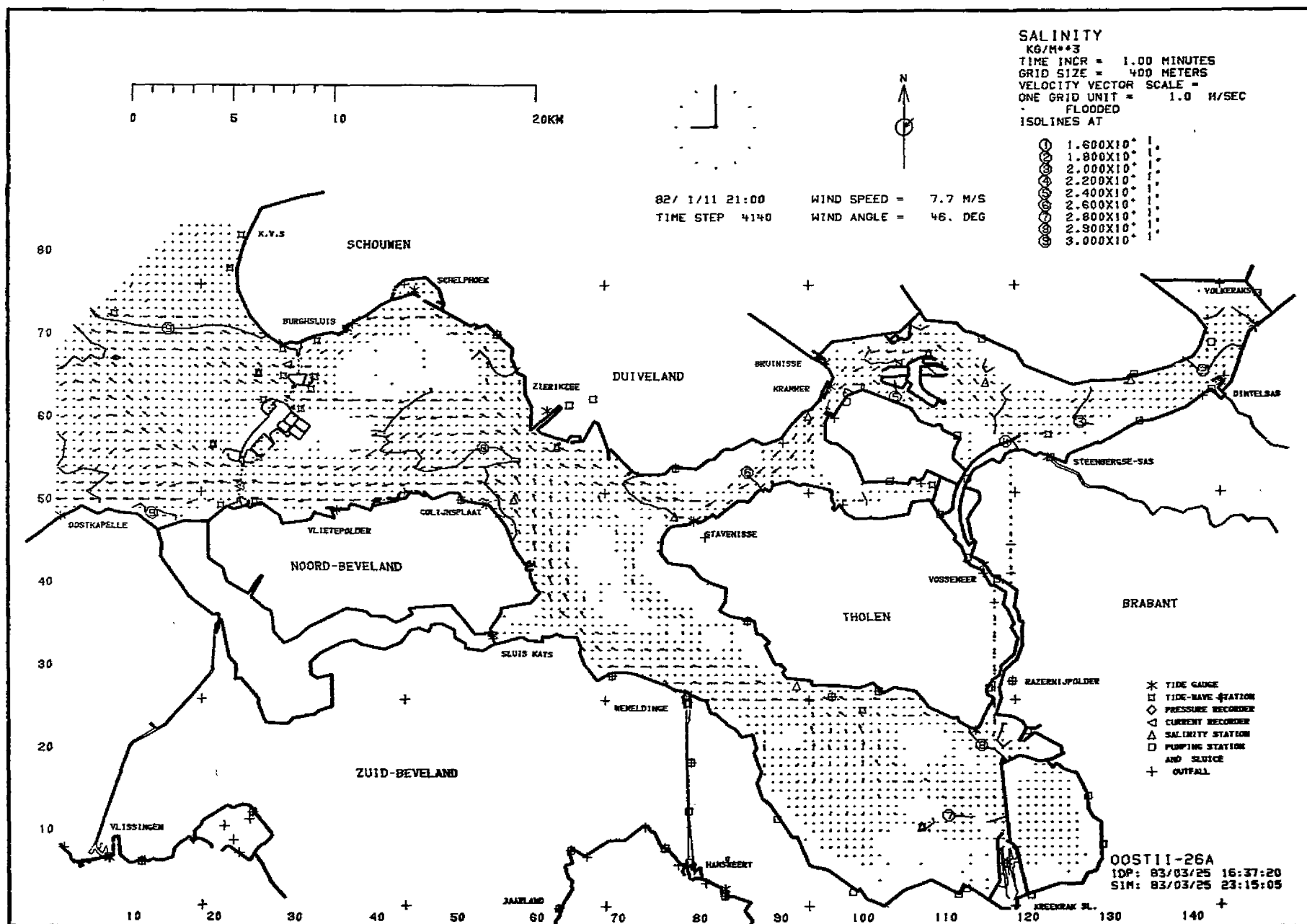Fig. F.13—Computed salinity distributions of the verification simulation at 21:00 hours on 11 January 1982
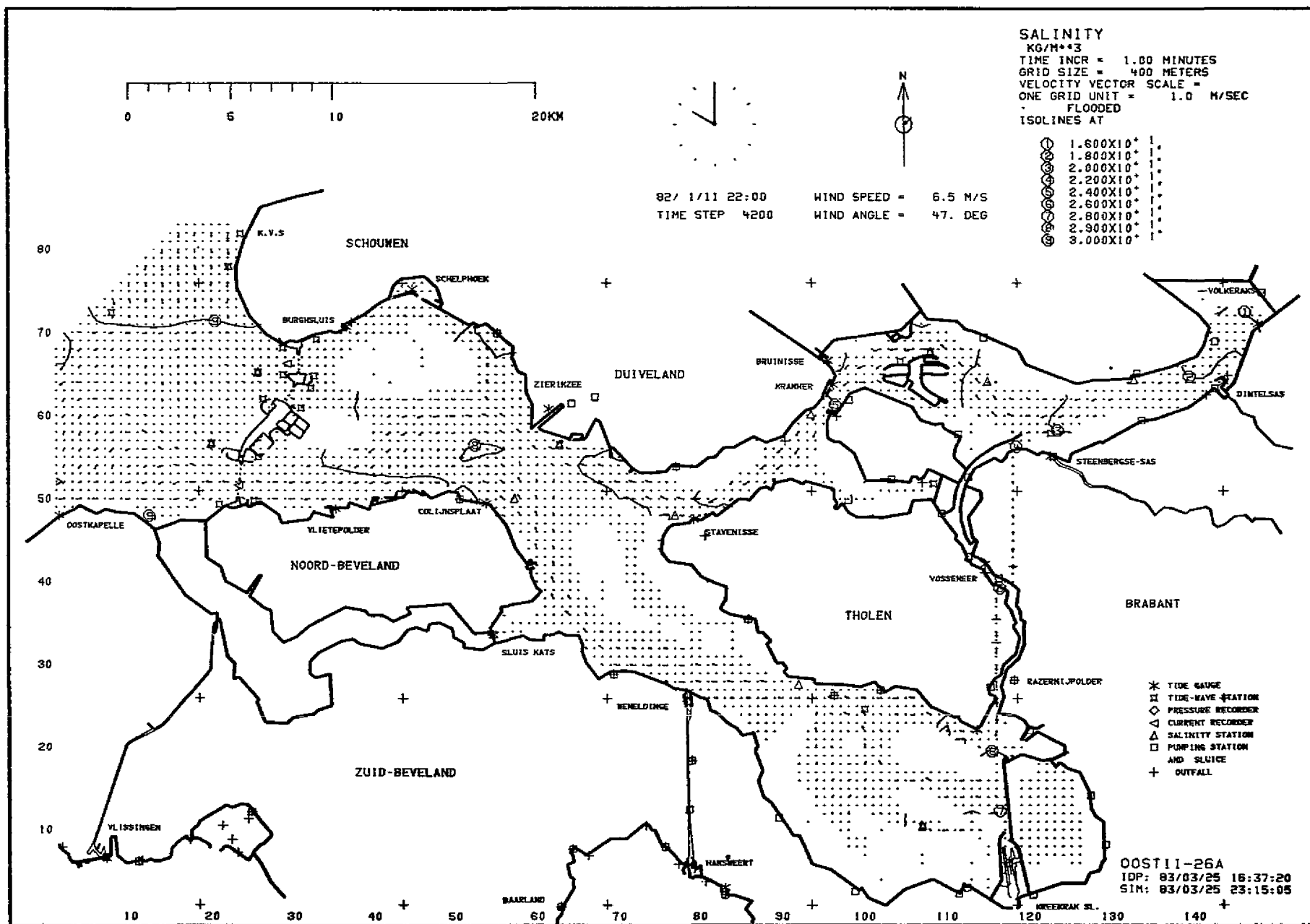
Fig. F.14—Computed salinity distributions of the verification simulation at 22:00 hours on 11 January 1982
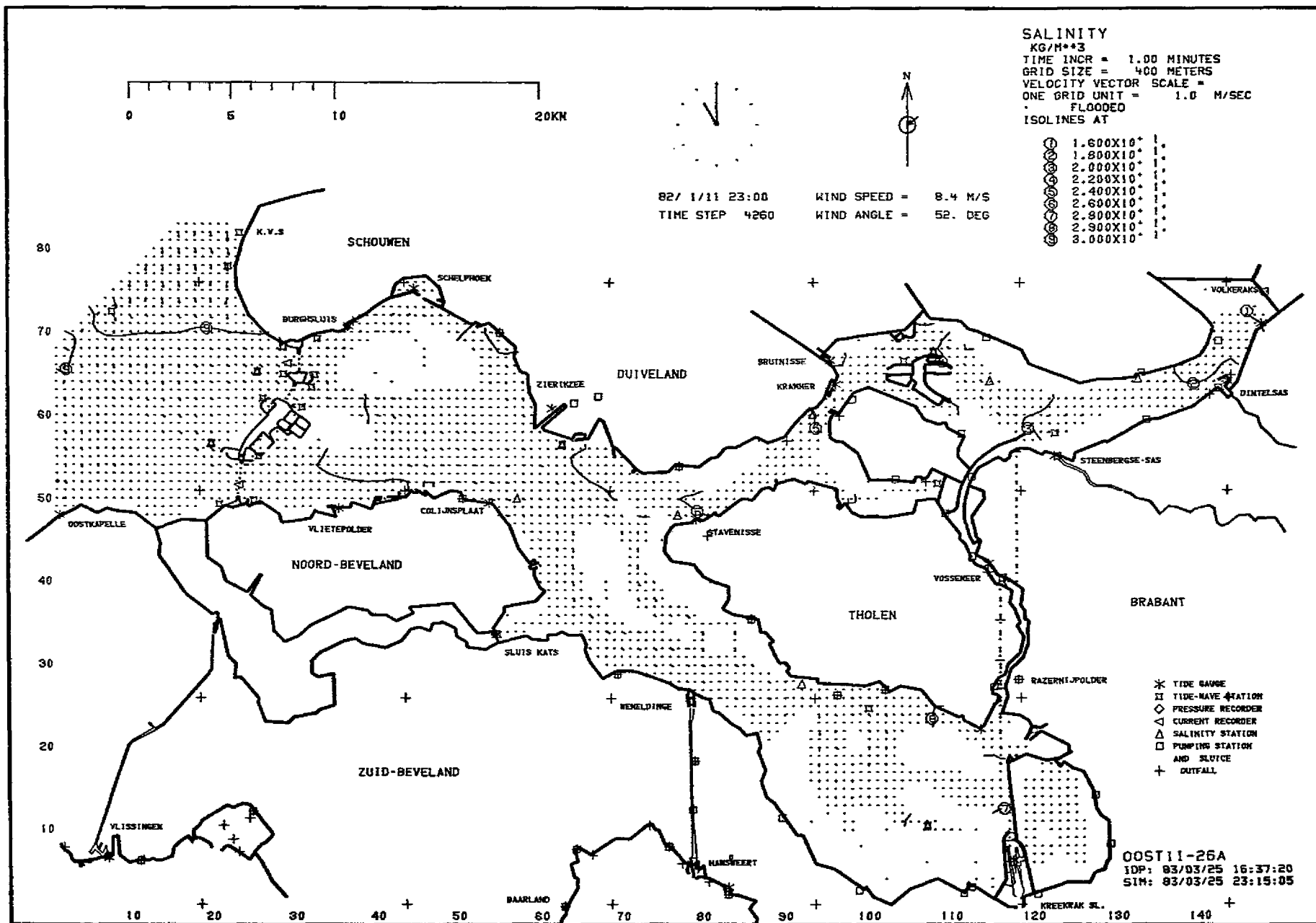
Fig. F.15—Computed salinity distributions of the verification simulation at 23:00 hours on 11 January 1982

Appendix G

COMPUTED VELOCITY FIELDS OF THE
VERIFICATION SIMULATION

This set of hourly graphs shows the velocity fields during the computation. The velocity vector length is linearly related to the magnitude of the velocity. If the velocity is 1 m/sec, then the vector length equals the distance between the grid points.

The contour lines are the iso-contours for the velocity. The different contour values are shown in the right top part of the figure. No index is added as these clobber the figure considerably and the value can easily be found by counting the number of lines between the shore and the one of interest.

The results of this simulation can be compared with those of the O-OOST-II model in Fig. 14.

Fig. G.1—Computed velocities of the verification simulation at 9:00 hours on 11 January 1982

Fig. G.2—Computed velocities of the verification simulation at 10:00 hours on 11 January 1982

Fig. G.3—Computed velocities of the verification simulation at 11:00 hours on 11 January 1982

VELOCITIES
TIME INCR = 1.00 MINUTES
GRID SIZE = 400 METERS
VELOCITY VECTOR SCALE =
ONE GRID UNIT = 1.0 M/SEC
ISOLINES AT

① 1.000X10⁻¹
② 2.500X10⁻¹
③ 5.000X10⁻¹
④ 7.500X10⁻¹
⑤ 1.000X10⁺⁰
⑥ 1.250X10⁺⁰
⑦ 1.500X10⁺⁰
⑧ 2.000X10⁺⁰

82/ 1/11 12:00   WIND SPEED = 10.5 M/S
TIME STEP 3600   WIND ANGLE = 54. DEG

OOSTII-26A
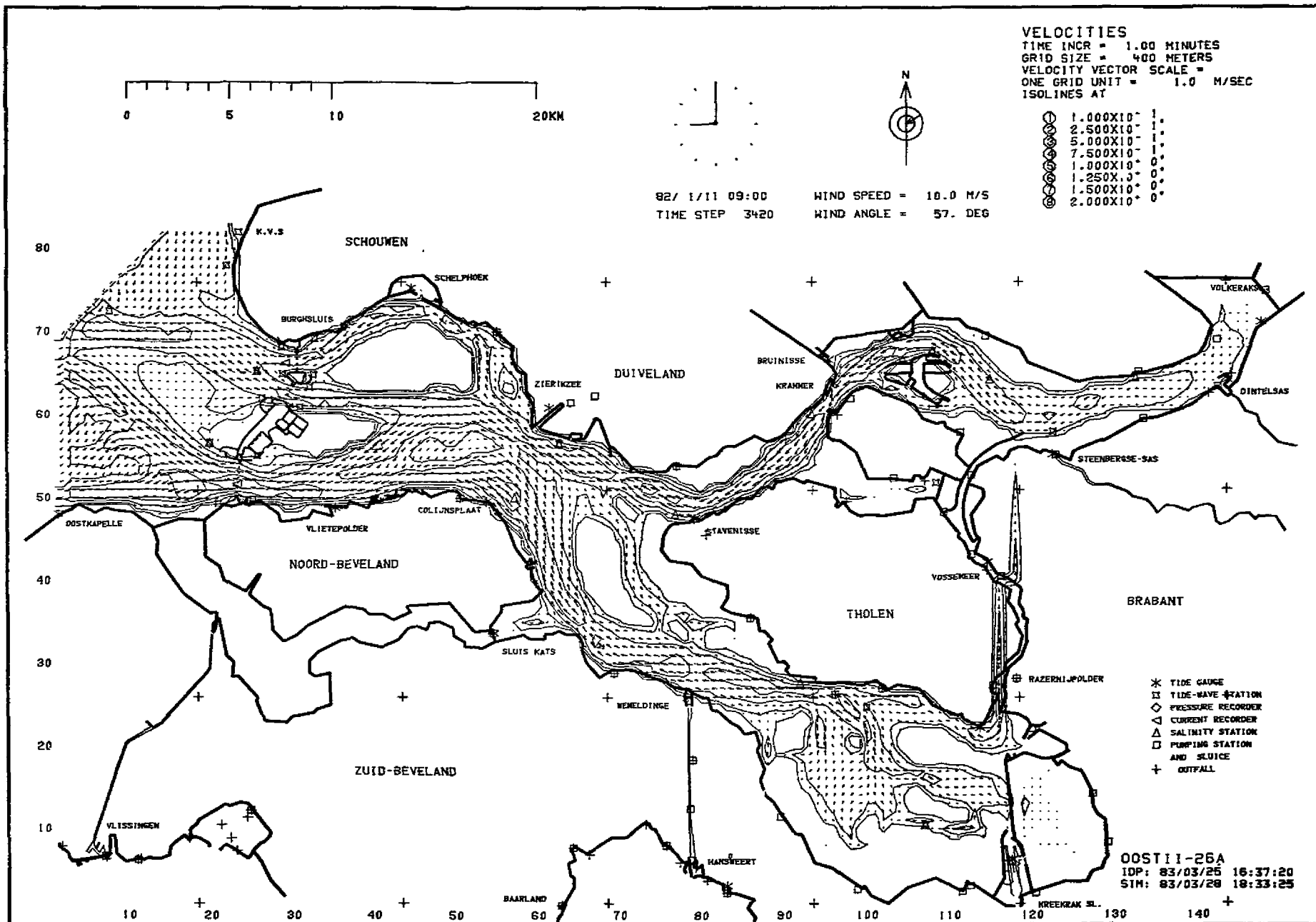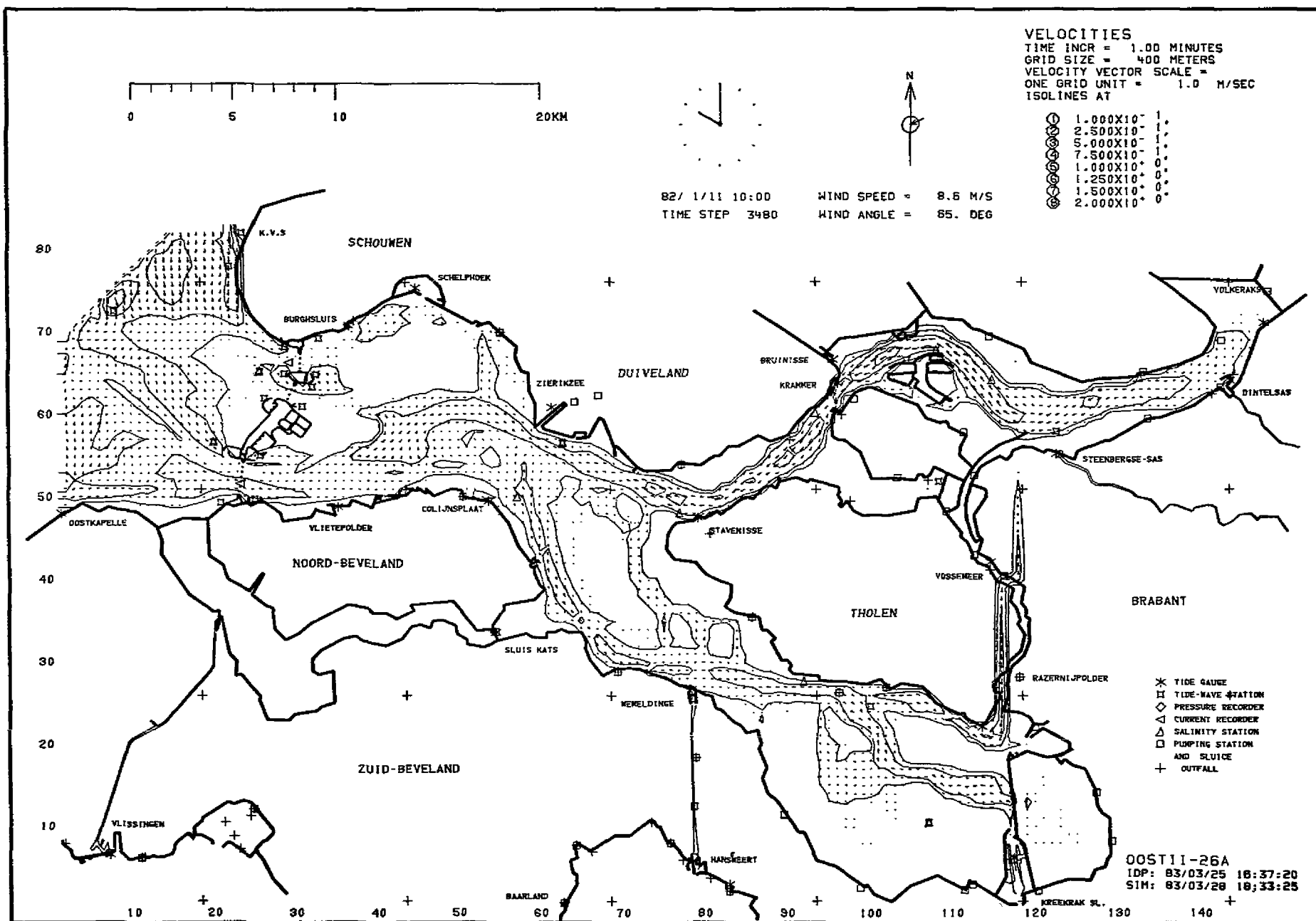IDP: 83/03/25 16:37:20
SIM: 83/03/28 18:33:25

Fig. G.4—Computed velocities of the verification simulation at 12:00 hours on 11 January 1982

Fig. G.5—Computed velocities of the verification simulation at 13:00 hours on 11 January 1982
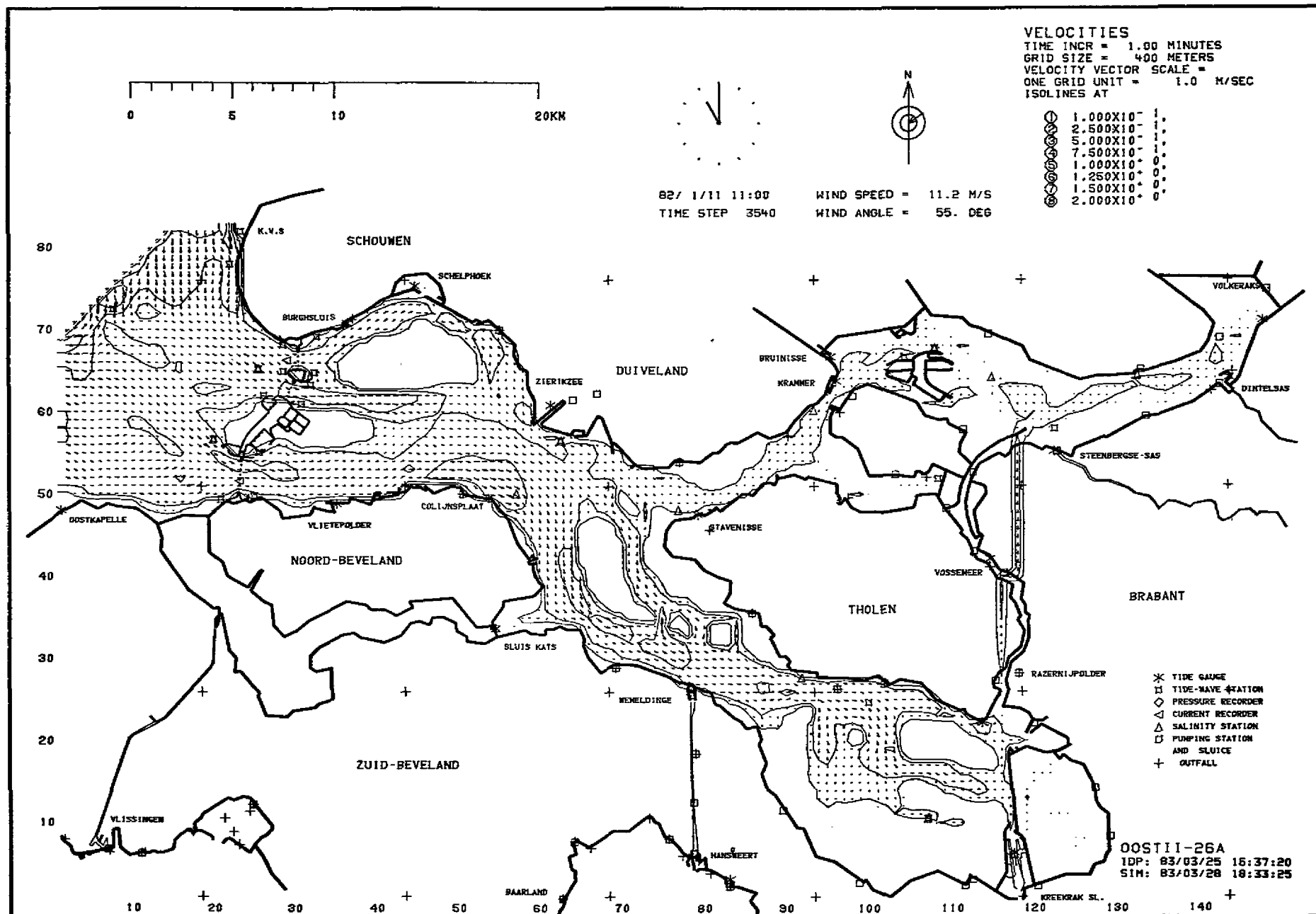
Fig. G.6—Computed velocities of the verification simulation at 14:00 hours on 11 January 1982

Fig. G.7—Computed velocities of the verification simulation at 15:00 hours on 11 January 1982
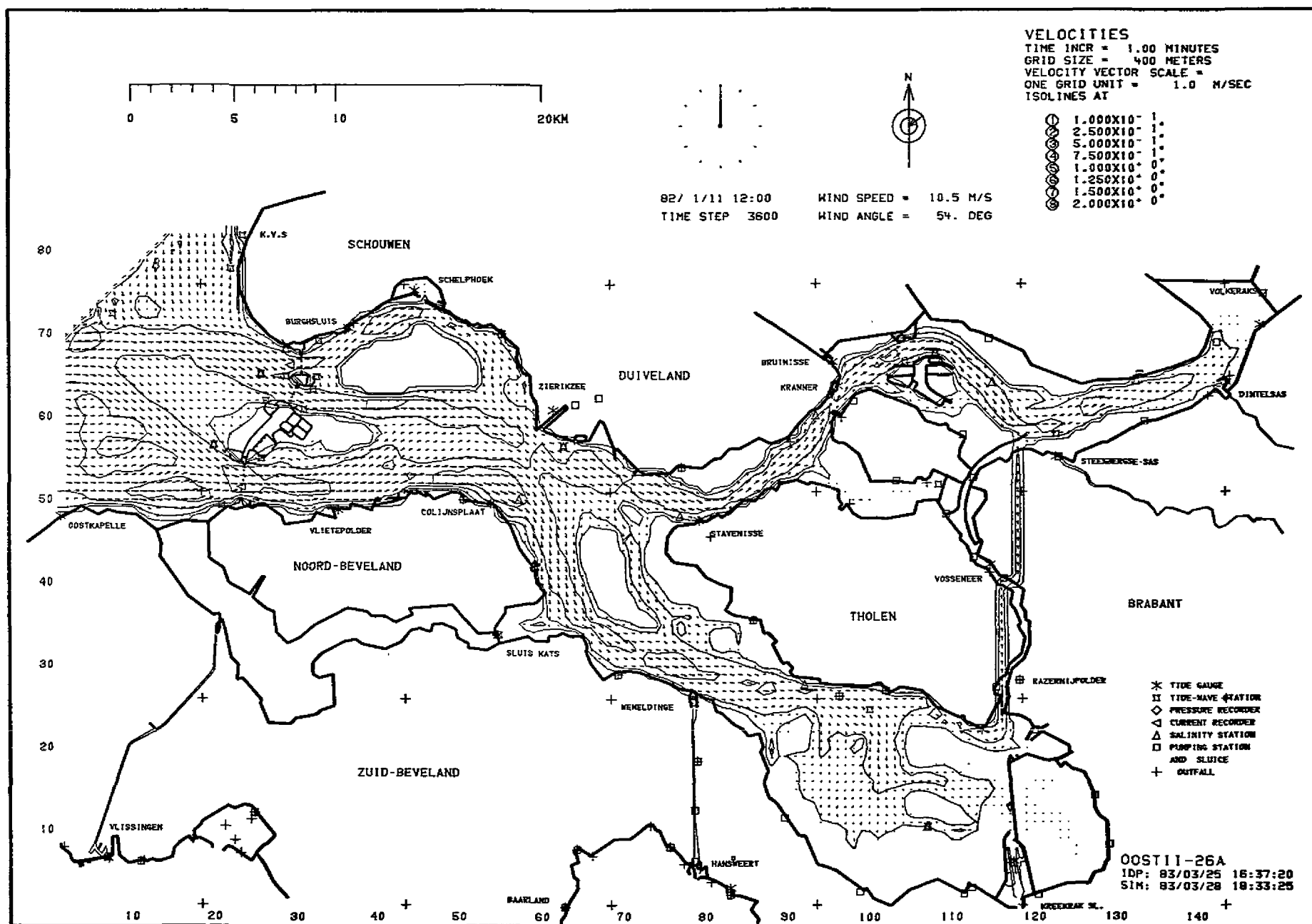
Fig. G.8—Computed velocities of the verification simulation at 16:00 hours on 11 January 1982

Fig. G.9—Computed velocities of the verification simulation at 17:00 hours on 11 January 1982

Fig. G.10—Computed velocities of the verification simulation at 18:00 hours on 11 January 1982
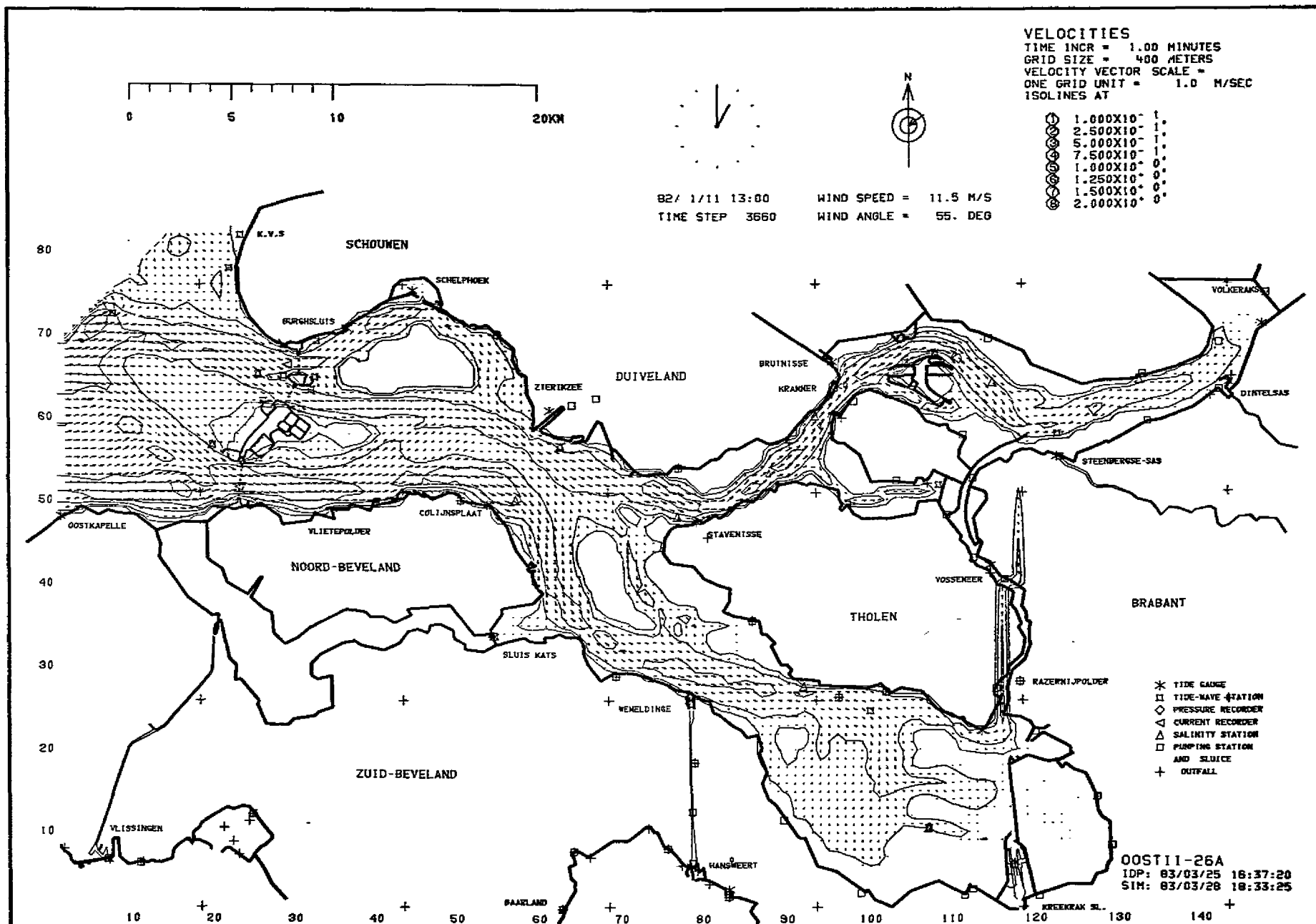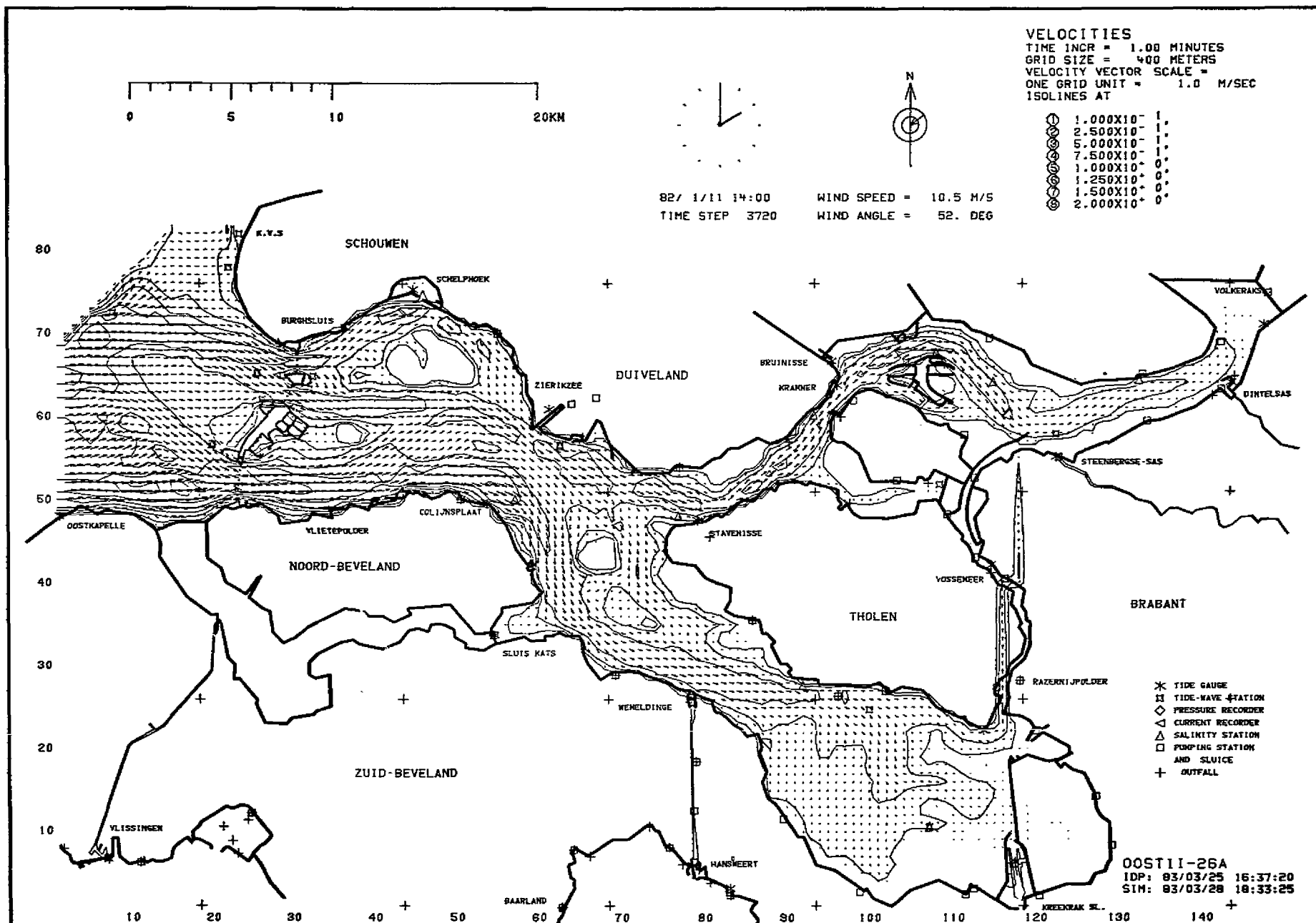
Fig. G.11—Computed velocities of the verification simulation at 19:00 hours on 11 January 1982
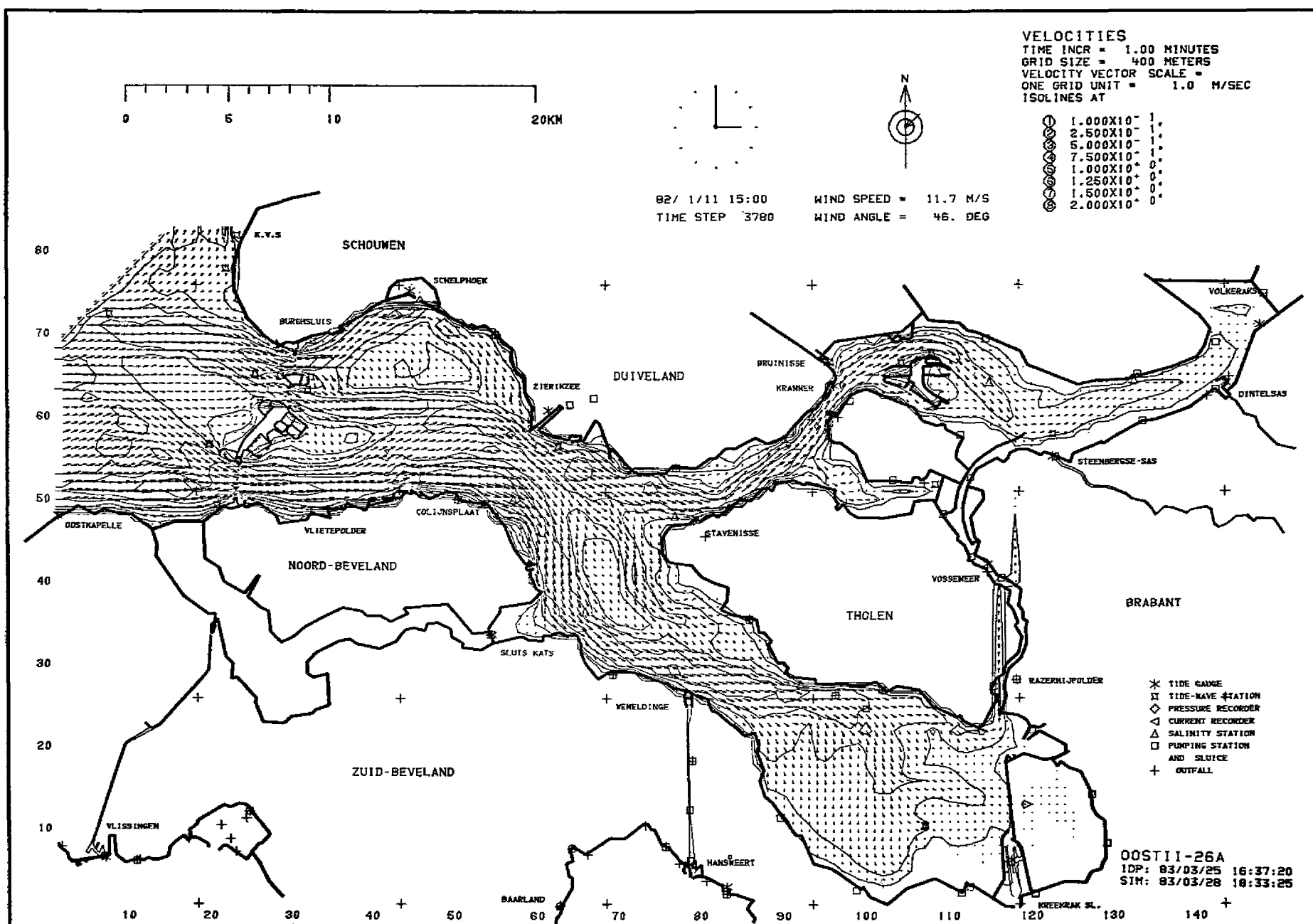
VELOCITIES
TIME INCR = 1.00 MINUTES
GRID SIZE = 400 METERS
VELOCITY VECTOR SCALE =
ONE GRID UNIT = 1.0 M/SEC
ISOLINES AT

1. 1.000X10⁻ 1:
2. 2.500X10⁻ 1:
3. 5.000X10⁻ 1:
4. 7.500X10⁻ 1:
5. 1.000X10⁺ 0:
6. 1.250X10⁺ 0:
7. 1.500X10⁺ 0:
8. 2.000X10⁺ 0:

82/ 1/11 20:00   WIND SPEED = 8.0 M/S
TIME STEP 4080   WIND ANGLE = 44. DEG

N

SCHOUWEN
K.V.9
SCHELPHOEK
BURGHSLUIS
ZIERIKZEE
DUIVELAND
BRUINISSE
KRAMMER
ROLKERAK
DINTELSAS
STEENBERGSE-SAS
OOSTKAPELLE
VLIETEPOLDER
COLIJNSPLAAT
STAVENISSE
NOORD-BEVELAND
VOSSEMEER
THOLEN
BRABANT
SLUIS KATS
RAZERNIJPOLDER
WEMELDINGE
ZUID-BEVELAND
VLISSINGEN
HANSWEERT
BAARLAND
KREEKRAK SL.

* TIDE GAUGE
Ⅱ TIDE-WAVE STATION
◇ PRESSURE RECORDER
◁ CURRENT RECORDER
△ SALINITY STATION
□ PUMPING STATION
  AND SLUICE
+ OUTFALL

OOSTII-26A
IDP: 83/03/25 16:37:20
SIM: 83/03/25 23:15:05

0 5 10 20KM

Fig. G.12—Computed velocities of the verification simulation at 20:00 hours on 11 January 1982
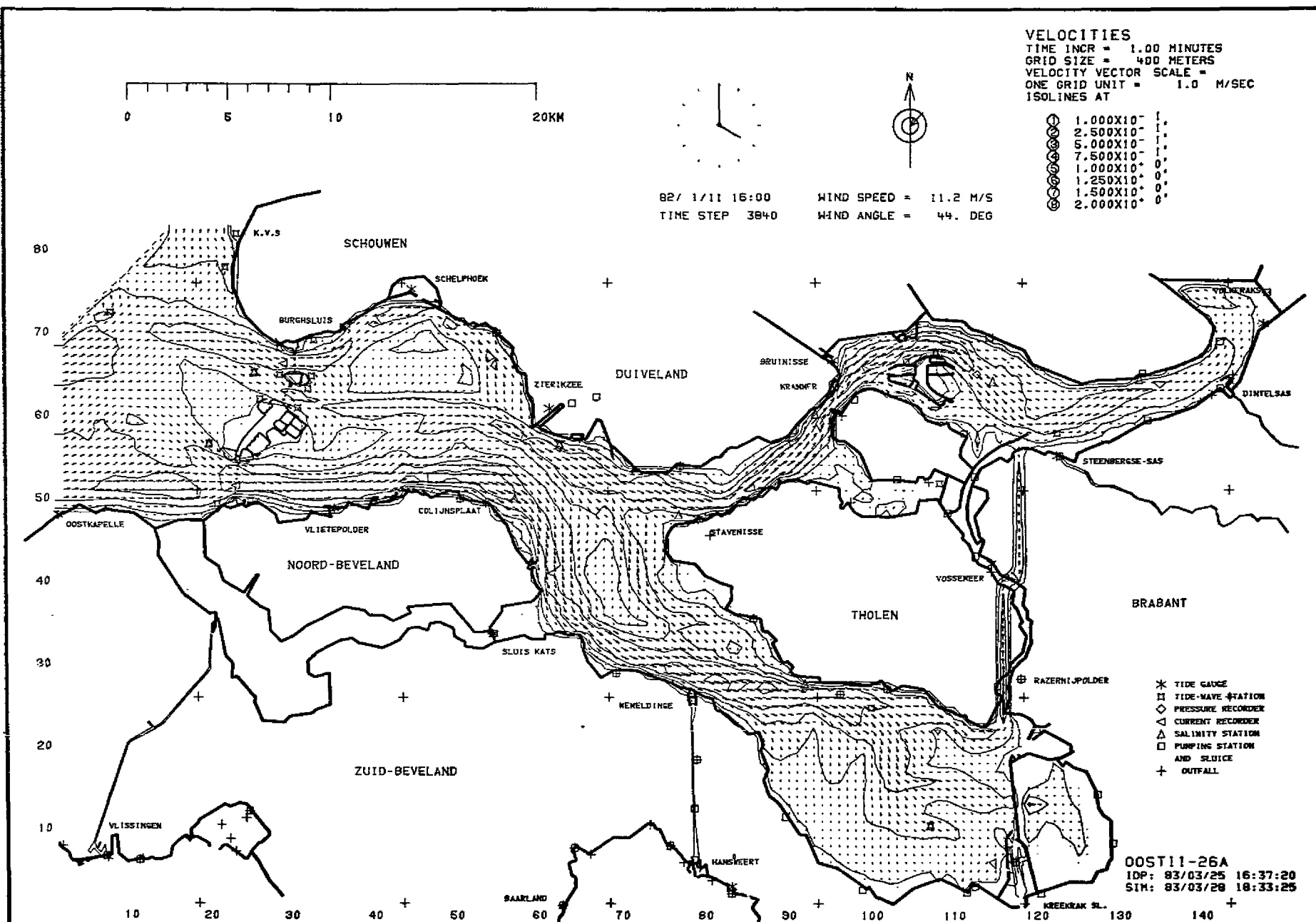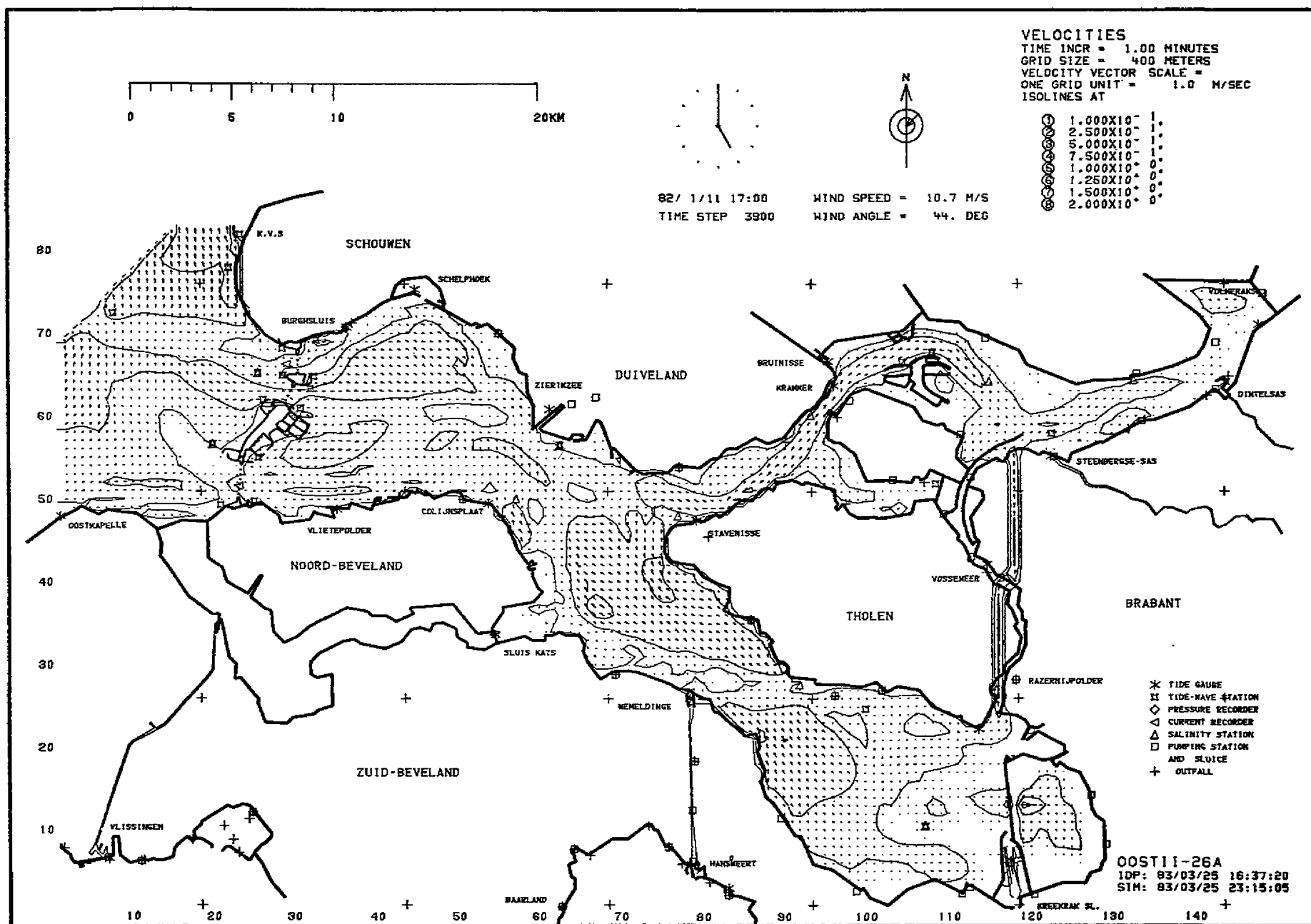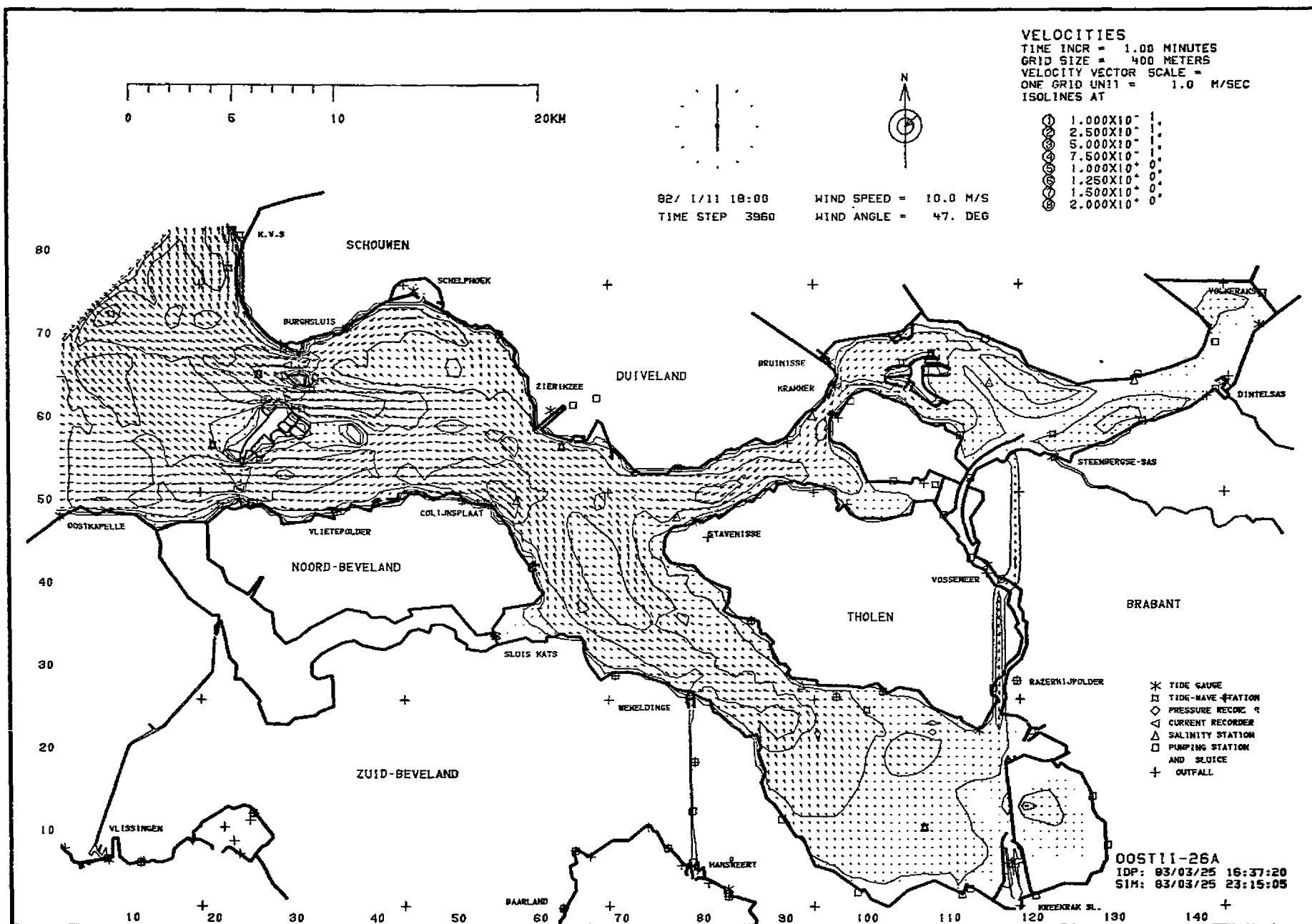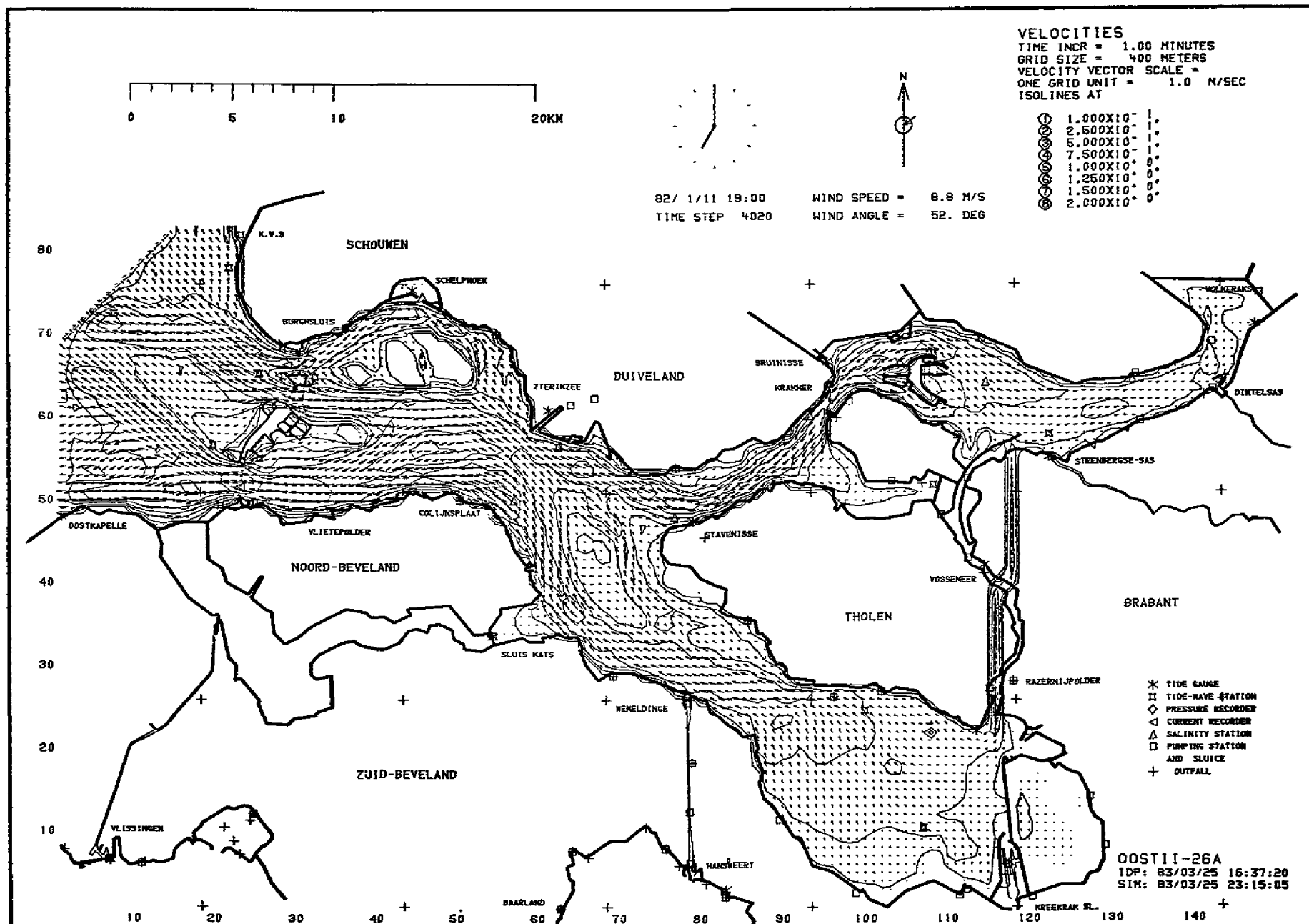
Fig. G.13—Computed velocities of the verification simulation at 21:00 hours on 11 January 1982
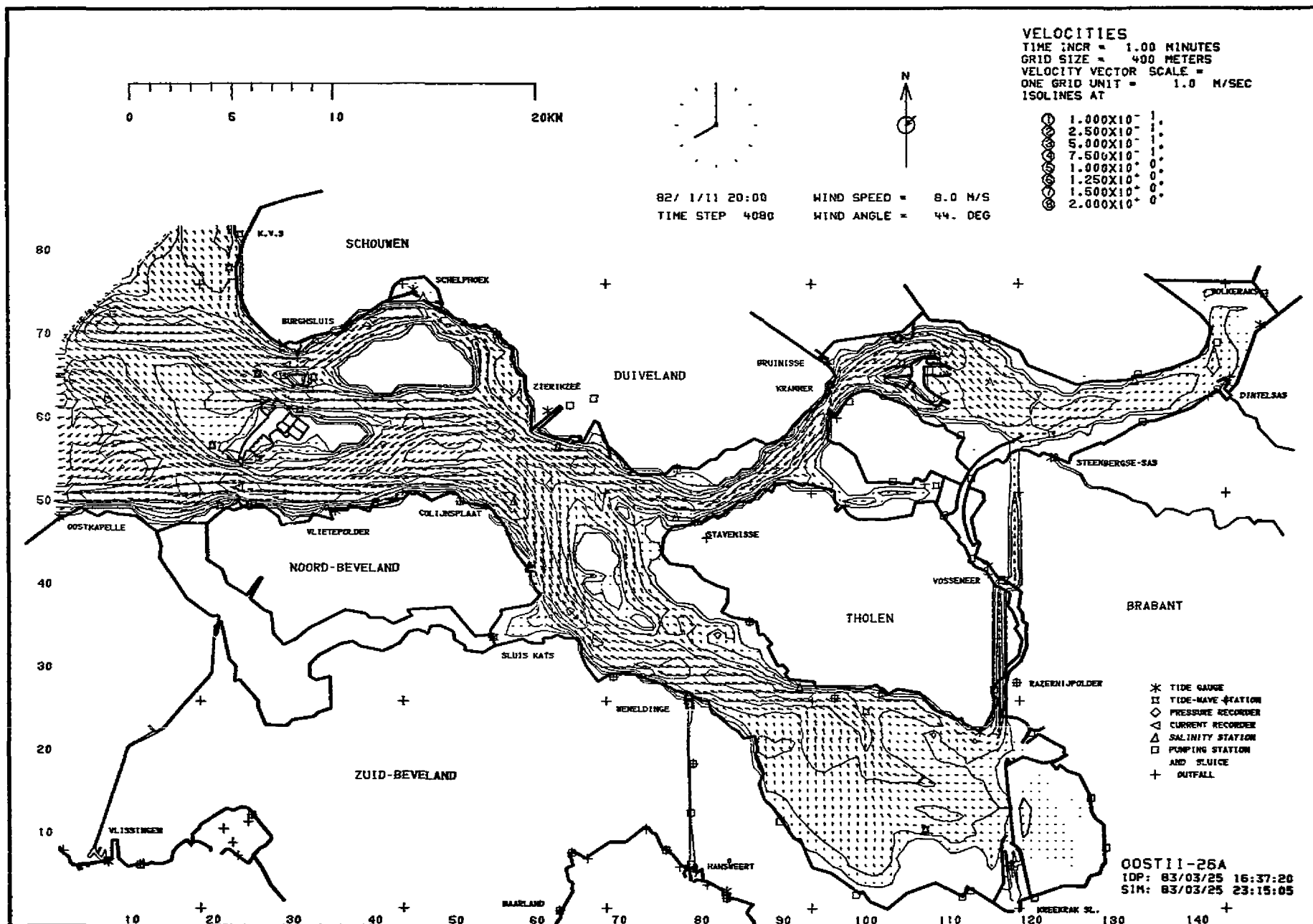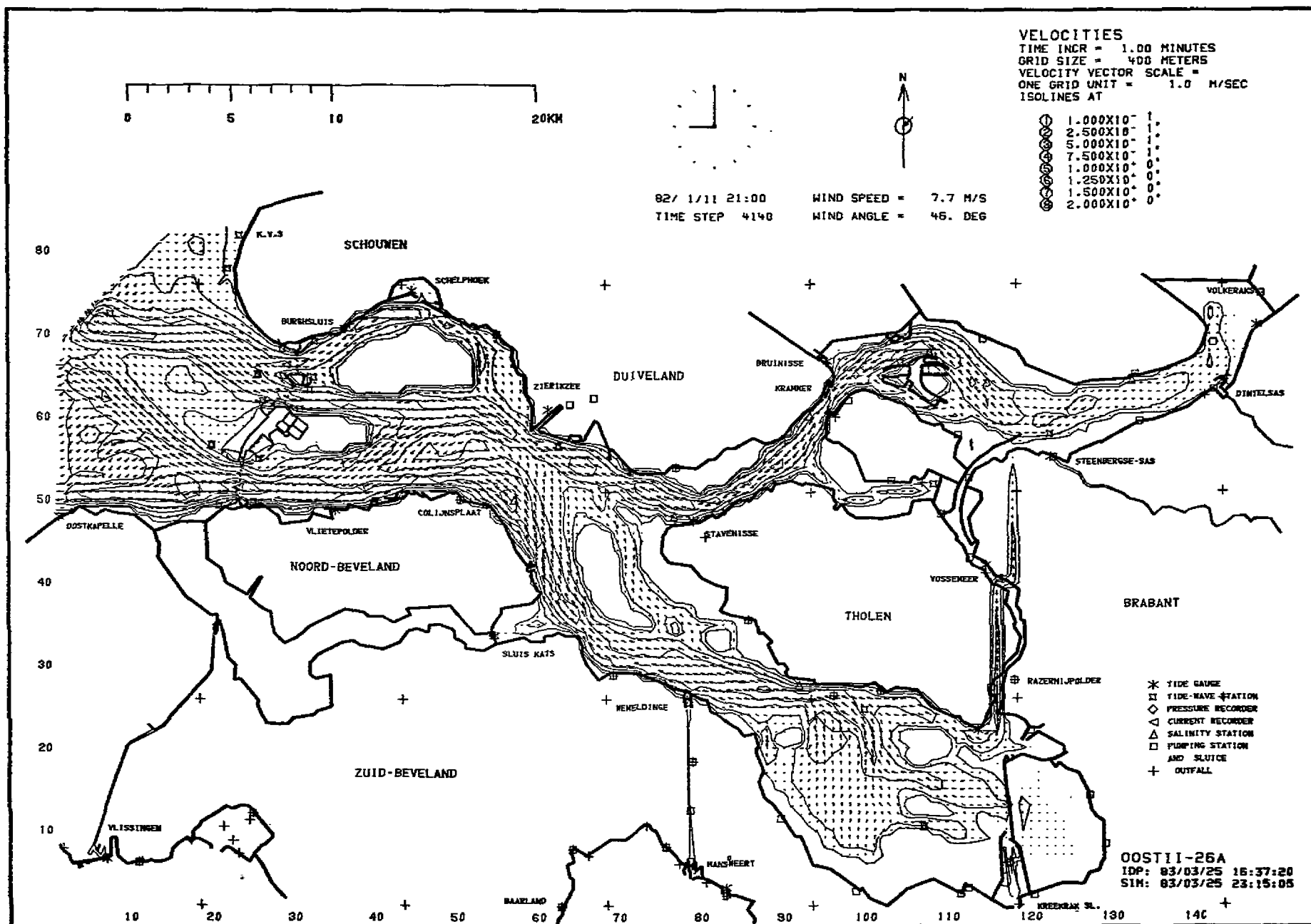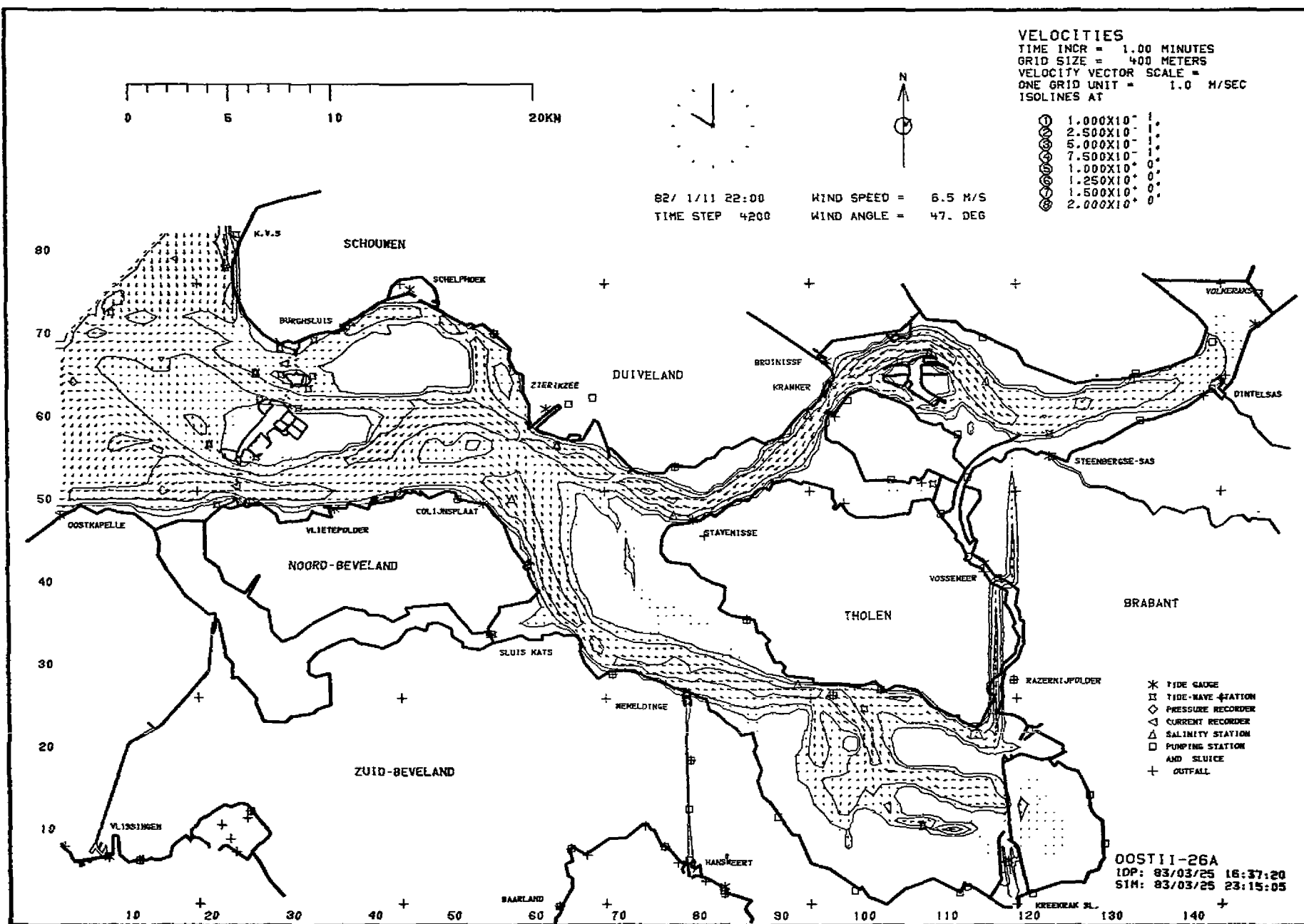
Fig. G.14—Computed velocities of the verification simulation at 22:00 hours on 11 January 1982
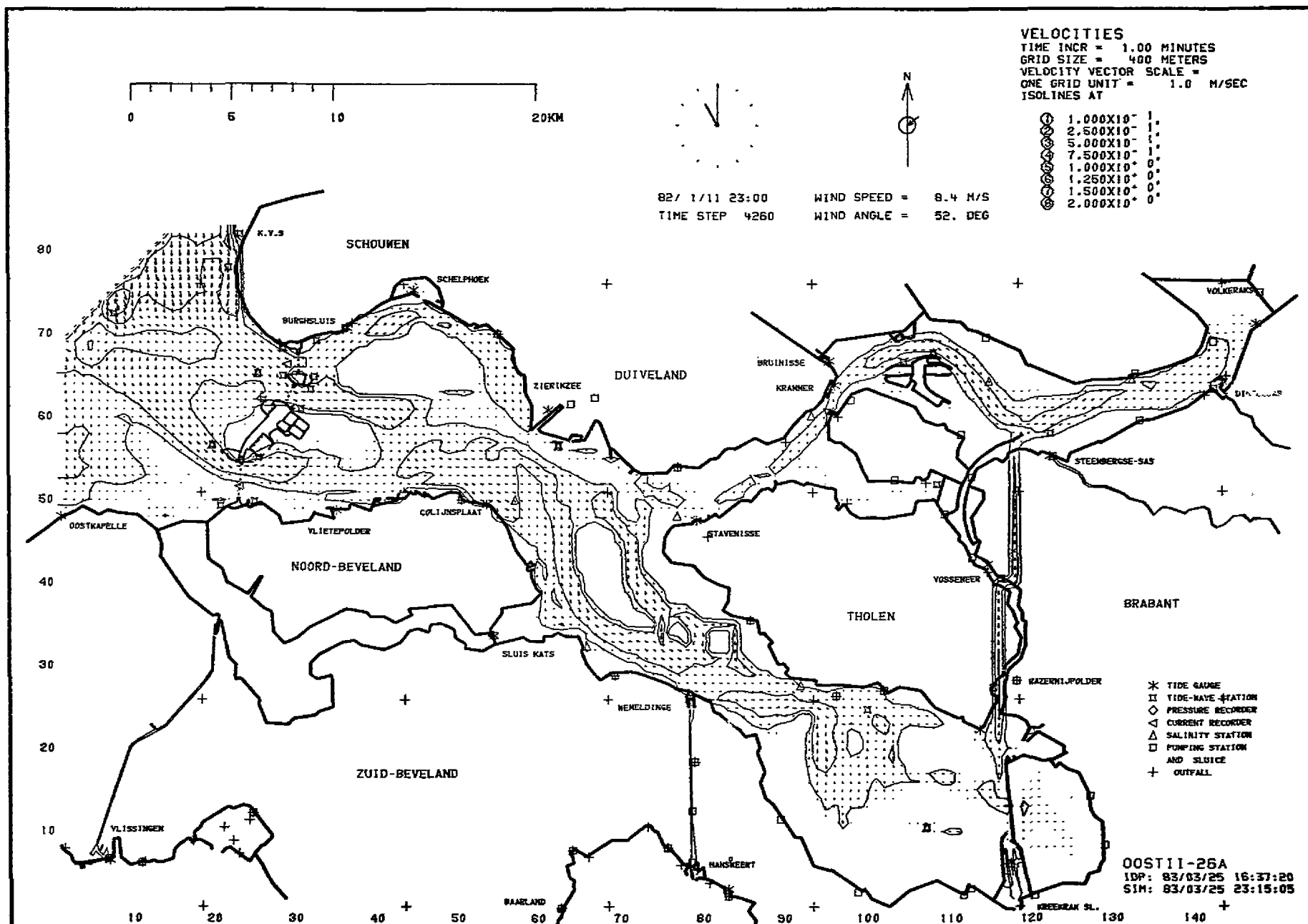
Fig. G.15—Computed velocities of the verification simulation at 23:00 hours on 11 January 1982

REFERENCES

1. Stroband, H. J., and N. J. van Wijngaarden, *Modelling of the Oosterschelde Estuary by a Hydraulic Model and a Mathematical Model*, Proceedings XVII Int. Assoc. of Hydraulic Research Congress, Baden-Baden, 1977.

2. Perrels, P.A.J., and M. Karelse, "A Two-Dimensional, Laterally Averaged Model for Salt Intrusion in Estuaries," in Hugo B. Fischer (ed.), *Transport Models for Inland and Coastal Waters*, Proceedings of a Symposium on Predictive Ability, Academic Press, Inc., New York, 1981, pp. 483–534.

3. Leendertse, J. J., A. Langerak, M.A.M. de Ras, "Two-Dimensional Tidal Models for the Delta Works," in Hugo B. Fischer (ed.), *Transport Models for Inland and Coastal Waters*, Proceedings of a Symposium on Predictive Ability, Academic Press, Inc., New York, 1981, pp. 408–450.

4. Leendertse, J. J., *SIMSYS2D: A Two-Dimensional Flow and Water Quality System*, Proceedings of the Seminar on Two-Dimensional Flow Modeling, Hydrologic Engineering Center, Davis, California, July 1981. Also, The Rand Corporation, P-6646, July 1981.

5. Leendertse, J. J., and E. C. Gritton, *A Water-Quality Simulation Model for Well Mixed Estuaries and Coastal Seas: Vol. II, Computation Procedures*, The New York City-Rand Institute, R-708-NYC, July 1971.

6. Grammeltvedt, Arne, "A Survey of Finite-Difference Schemes for the Primitive Equations for a Barotropic Fluid," *Monthly Weather Review*, Vol. 97, No. 5, 1969.

7. Leendertse, J. J., and Shiao-Kung Liu, "Sensitivity of Parameters and Approximations in Models of Tidal Propagation and Circulation," Proceedings of the Eighteenth Conference on Coastal Engineering, American Society of Civil Engineers, New York, 1983.

8. Eckert, C., "The Equation of State of Water and Sea Water at Low Temperatures and Pressures," *Am. Jour. of Sci.*, Vol. 256, 1958, pp. 240–250.

9. Abraham, G., *An Internally Generated Estuarine Turbulence*, Proceedings of the Second International Symposium on Stratified Flows, The Norwegian Institute of Technology, Trondheim, Norway, 24–27 June 1980. Also, Publication 247, Delft Hydraulics Laboratorium, Delft, December 1980.

10. Voogt, J., and A. Roos, "Effects on Tidal Regime," *Hydraulic Aspects of Coastal Structures*, Part I, Delft University Press, Delft, 1980.

11. Rijkswaterstaat, Deltadienst, De Morfologische Ontwikkeling in de Oosterschelde en het aangrenzende kustgebied bij aanleg van een stormvloedkering in de mond. Unpublished report W-75.067, 1975 (Dutch text).

12. Jenkins, G. M., and D. G. Watts, *Spectral Analysis and Its Applications*, Holden-Day Publishing Co., San Francisco, 1969.

13. Liu, Shiao-Kung, *Stochastic Analysis and Control of Urban Estuarine Water-Quality Systems: Vol. I – Estimation and Prediction*, The New York City-Rand Institute, R-1622-NYC, December 1974.

14. Delft Hydraulics Laboratory, Getijmodel Oosterschelde, Reproductie Prototype-Getij, 11 January 1982, M01855 band 4, Juni 1982 (Dutch text).

15. Delft Hydraulics Laboratory, Getijmodel Oosterschelde, Instellen Getij, 4 September 1975, M-1000-14, September 1980 (Dutch text).

16. Stelling, G., personal communication, September 1983.